UNIVERSITY OF COPENHAGEN
FACULTY OF HEALTH AND MEDICAL SCIENCES

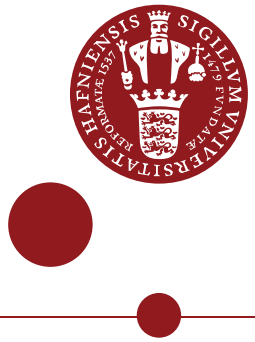

PhD Thesis

João Henrique Fróis Lameiras Campagnolo

Neural Correlates of Stress Resilience in Zebrafish Larvae

Supervisor: Florence Kermen

Date: 14 November 2025

Name of department:	Department of Neuroscience
Author(s):	João Henrique Fróis Lameiras Campagnolo
Title and subtitle:	Neural Correlates of Stress Resilience in Zebrafish Larvae
Topic description:	This study defines resilience in larval zebrafish as post-stress return to baseline and maps brain recovery, describing neural correlates of resilience.
Supervisor:	Florence Kermen
Date:	14 November 2025

TABLE OF CONTENTS

SUMMARY (English)

Stress is a real or perceived threat that triggers coordinated physiological and behavioral responses. Although adaptive in the short term, prolonged or poorly regulated activation increases risk for anxiety-like disorders and depression. Resilience, the ability to regain adaptive function after challenge, varies widely across individuals. This thesis established a standardized behavioral assay in larval zebrafish and mapped brain-wide activity patterns that distinguish resilient from vulnerable animals during early recovery.

The assay comprised three phases: baseline, acute stress exposure, and recovery. Resilience was quantified as locomotor rebound, defined as the change in swimming speed from baseline to recovery. This segregated resilient trajectories (rapid return to pre-stress movement) from vulnerable trajectories (sustained hypoactivity or immobility). Higher rebound scores indicate greater resilience. Population means declined with stronger stressors, yet separation persisted. Classification was consistent across lines and stressor types. Larval labels showed partial stability and predicted greater challenge-evoked exploration in juveniles, but could not do so without a brief pre-test perturbation.

To identify neural correlates, whole-brain activity during recovery was mapped with pERK immunohistochemistry and analyzed using voxel- and region-level statistics and network-level summaries. Resilience was associated with elevated activity in subsets of the caudal hypothalamus, paraventricular organ, and ventral telencephalon/diencephalon, and with greater engagement of premotor brainstem outputs, including the nucleus of the medial longitudinal fasciculus and reticulospinal neurons. Network summaries indicated condition-specific reweighting, with relatively stronger long-range forebrain-hindbrain interactions in resilient graphs.

These findings establish a quantitative framework that links behavior to brain-wide activity in larval zebrafish to study individual differences in stress coping. Results indicate that recovery from acute stress involves coordinated engagement of hypothalamic and premotor brainstem circuits that promote behavioral rebound. The framework identifies candidate nodes and interactions for causal testing and translational work on enhancing resilience.

RESUMÉ (Dansk)

Stress er en reel eller opfattet trussel, der udløser koordinerede fysiologiske og adfærdsmæssige reaktioner. Selvom stress er adaptivt på kort sigt, øger langvarig eller dårligt reguleret aktivering risikoen for angstlignende lidelser og depression. Resiliens, evnen til at genvinde adaptiv funktion efter en udfordring, varierer meget fra person til person. Denne afhandling etablerede en standardiseret adfærdsanalyse hos zebrafiskelarver og kortlagde aktivitetsmønstre i hele hjernen, der adskiller resiliente dyr fra sårbare dyr under den tidlige restitution.

Analysen bestod af tre faser: baseline, akut stressekspонering og restitution. Resiliens blev kvantificeret som lokomotorisk rebound, defineret som ændringen i svømmehastighed fra baseline til restitution. Dette adskilte resiliente forløb (hurtig tilbagevenden til bevægelse før stress) fra sårbare forløb (vedvarende hypoaktivitet eller immobilitet). Højere rebound-scores indikerer større resiliens. Populationsgennemsnittene faldt med stærkere stressfaktorer, men adskillelsen varede ved. Klassificeringen var konsistent på tværs af linjer og stressfaktortyper. Larve-mærkninger viste delvis stabilitet og forudsagde større udfordringsfremkaldt udforskning hos ungdyr, men kunne ikke gøre dette uden en kort forstyrrelse før testen.

For at identificere neurale korrelater blev hele hjernens aktivitet under restitution kortlagt med pERK-immunhistokemi og analyseret ved hjælp af voxel- og regionsniveau-statistikker og netværksniveau-opsummeringer. Modstandsdygtighed var forbundet med forhøjet aktivitet i undergrupper af den kaudale hypothalamus, det paraventrikulære organ og det ventrale telencephalon/diencephalon og med større engagement af præmotoriske hjernestammeoutput, herunder kernen i den mediale longitudinale fasciculus og retikulospinale neuroner. Netværksoversigter indikerede tilstandsspecifik omvægtning med relativt stærkere langdistanceinteraktioner mellem forhjerne og baghjerne i modstandsdygtige grafer.

Disse fund etablerer en kvantitativ ramme, der knytter adfærd til hjerneaktivitet hos zebrafiskelarver for at undersøge individuelle forskelle i stresshåndtering. Resultaterne indikerer, at recovery fra akut stress involverer koordineret engagement af hypothalamiske og præmotoriske hjernestamme-kredsløb, der fremmer adfærdsmæssig rebound. Rammen identificerer kandidatknudepunkter og interaktioner til kausal testning og translationelt arbejde med at forbedre resiliens.

LIST OF PUBLICATIONS

This thesis is based on the work presented in the following manuscripts:

I. **Campagnolo, J. H.**, Ahmad, E., Selvan, R. & Kermen, F. (in preparation). Behavioral quantification of stress resilience in larval zebrafish.

Referred to in this thesis as **Manuscript I**.

II. **Campagnolo, J. H.**, Korn, J., Rigola, L. P., Selvan, R. & Kermen, F. (in preparation). Neural correlates of interindividual variability in rebound from acute stress in the zebrafish.

Referred to in this thesis as **Manuscript II**.

The manuscripts are attached as appendices at the end of the thesis.
Both are in preparation for submission to peer-reviewed journals and form the core scientific contributions of this PhD project.

LIST OF ABBREVIATIONS

Physiological and endocrine terms

Abbreviation	Definition
ACTH	Adrenocorticotropic hormone
AFW	Artificial fish water
CRH	Corticotropin-releasing hormone
dpf	Days post-fertilization
GC	Glucocorticoid(s)
HPA	Hypothalamic-pituitary-adrenal (axis)
HPI	Hypothalamic-pituitary-interrenal (axis)
HPA/HPI	Shorthand for the mammalian HPA and teleost HPI axes
MRs/GRs	Mineralocorticoid and glucocorticoid receptors

Brain regions and circuits

Abbreviation	Definition
BNST	Bed nucleus of the stria terminalis
BLA	Basolateral amygdala
CeA	Central amygdala
CH	Caudal hypothalamus
IL	Infralimbic prefrontal cortex
LC	Locus coeruleus
MLR	Mesencephalic locomotor region
NAc	Nucleus accumbens
NPO	Neurosecretory preoptic area
NTS	Nucleus of the solitary tract
nMLF	Nucleus of the medial longitudinal fasciculus
OB	Olfactory bulb
PAG	Periaqueductal gray
PL	Prelimbic prefrontal cortex
POA	Preoptic area
PVN	Paraventricular nucleus (of the hypothalamus)
RSNs	Reticulospinal neurons

TS	Torus semicircularis
VTA	Ventral tegmental area
PVO-Vmat2	Paraventricular organ, Vmat2-positive cluster

Molecular markers and transporters

Abbreviation	**Definition**
Gad1b	Glutamate decarboxylase 1b
Glyt2	Glycine transporter 2
HDAC	Histone deacetylase
IEG	Immediate early gene
pERK	Phosphorylated extracellular signal-regulated kinase
tERK	Total extracellular signal-regulated kinase
VMAT	Vesicular monoamine transporter
Vmat2	Vesicular monoamine transporter 2
Vglut2	Vesicular glutamate transporter 2

Imaging and whole-brain mapping

Abbreviation	**Definition**
CMTK	Computational Morphometry Toolkit
EEG	Electroencephalography
fMRI	Functional magnetic resonance imaging
HCR	Hybridization chain reaction
iDISCO	Immunolabeling-enabled three-dimensional imaging of solvent-cleared organs
LSM	Laser scanning microscope (e.g. Zeiss LSM 700)

Reagents and solutions

Abbreviation	**Definition**
PBS	Phosphate-buffered saline
PBT	PBS with Triton X-100 (PBST; phosphate-buffered saline with Triton)
LED	Light-emitting diode

Transgenic lines

Abbreviation	Definition
elavl3:GCaMP6s	Tg(elavl3:GCaMP6s) zebrafish line expressing GCaMP6s under the elavl3 promoter

INTRODUCTION

1. Stress and Stress Resilience

1.1. Core definitions and scope

Stress is defined as a real or perceived threat to well-being or an actual or anticipated disruption of the body's stable internal state (homeostasis). The resulting coordinated physiological and behavioral adjustments are collectively termed allostasis, signifying the process of achieving stability through active, dynamic change via the release of chemical mediators (McEwen, 2002; Sterling and Eyer, 1988). The primary hormonal response in vertebrates is the activation of the hypothalamic-pituitary-adrenal (HPA) axis, or its fish analogue, the hypothalamic-pituitary-interrenal (HPI) axis, culminating in the systemic release of glucocorticoid hormones (cortisol in fish and humans; Fig. 1). This acute response is essential for survival, mediating rapid defensive reactions such as the "fight-or-flight" response.

Individuals within a population exhibit substantial variability in the magnitude and duration of these acute responses (Beery and Kaufer, 2014; Henckens et al., 2016; Krishnan et al., 2007; Vindas et al., 2017; Zou et al., 2020). While transient activation is adaptive, inadequate recovery or repeated activation can disrupt feedback control. When allostatic systems are engaged too frequently or fail to terminate efficiently, cumulative physiological strain, termed allostatic load, develops, reflecting wear on both peripheral and central regulatory mechanisms (McEwen, 2007). Such chronic dysregulation increases vulnerability to stress-related psychopathology, including Major Depressive Disorder and Post-Traumatic Stress Disorder (Holsboer and Ising, 2008; Kalisch et al., 2017; Lupien et al., 2009). Understanding how individuals recover from acute stress therefore provides a mechanistic entry point for identifying resilience factors that prevent this transition from adaptive to maladaptive states.

1.2. Coping styles and individual variability across vertebrates

Individual variability in response to environmental challenges is characterized by stress coping styles, which are defined as stable, trait-like patterns of correlated behavioral and physiological responses consistently expressed across time and contexts in many taxa (Baker et al., 2018; Coppens et al., 2010; Koolhaas et al., 2010; Rajput et al., 2022). This differentiation is commonly summarized along a proactive-reactive axis (also termed bold-shy in some literature).

The proactive coping style is characterized by active engagement with stressors, often involving high aggression, boldness, risk-taking, active avoidance, and exploration of novel environments.

Proactive individuals tend to rely on intrinsic routines, exhibiting relatively low behavioral flexibility and feed-forward control (Coppens et al., 2010; Øverli et al., 2007; Winberg et al., 2016). Physiologically, this style is associated with a high sympathetic response and a modest glucocorticoid response to acute challenges (Koolhaas et al., 1999; Winberg and Thörnqvist, 2016). Conversely, the reactive coping style involves cautious, inhibited responses and greater sensitivity to external environmental cues, demonstrating high behavioral flexibility. This pattern correlates with high HPA/HPI axis reactivity and elevated glucocorticoid levels following acute stress exposure. For instance, reactive fish lines show a faster cortisol release rate during the rising phase of the endocrine response than proactive lines (Wong et al., 2019).

It is essential to differentiate the stable coping style (trait) from the transient coping state triggered by a specific challenge. The coping style biases the probability of entering particular states but does not uniquely determine them (Coppens et al., 2010; Koolhaas et al., 2010, 1999). A coping state is an acute control mode that directs the expression of behavioral strategies. Active states preferentially yield flight, active avoidance, or exploratory behavior, whereas passive states favor risk assessment and behavioral inhibition, such as freezing (Andalman et al., 2019; Hagenaars et al., 2014). State sequences and switches vary with controllability: low control promotes transitions toward passive responses (Maier and Watkins, 2010). When faced with an inescapable aversive stimulus, individuals often shift from an initial active state with escape attempts to a passive state with reduced mobility as the threat is re-evaluated (Andalman et al., 2019; Hagenaars et al., 2014). This duality between stable characteristics and flexible strategic engagement is crucial for adaptation.

Building on these inter-individual differences in coping and post-challenge reorganization, the following section defines resilience as the restoration of adaptive function after a standardized challenge.

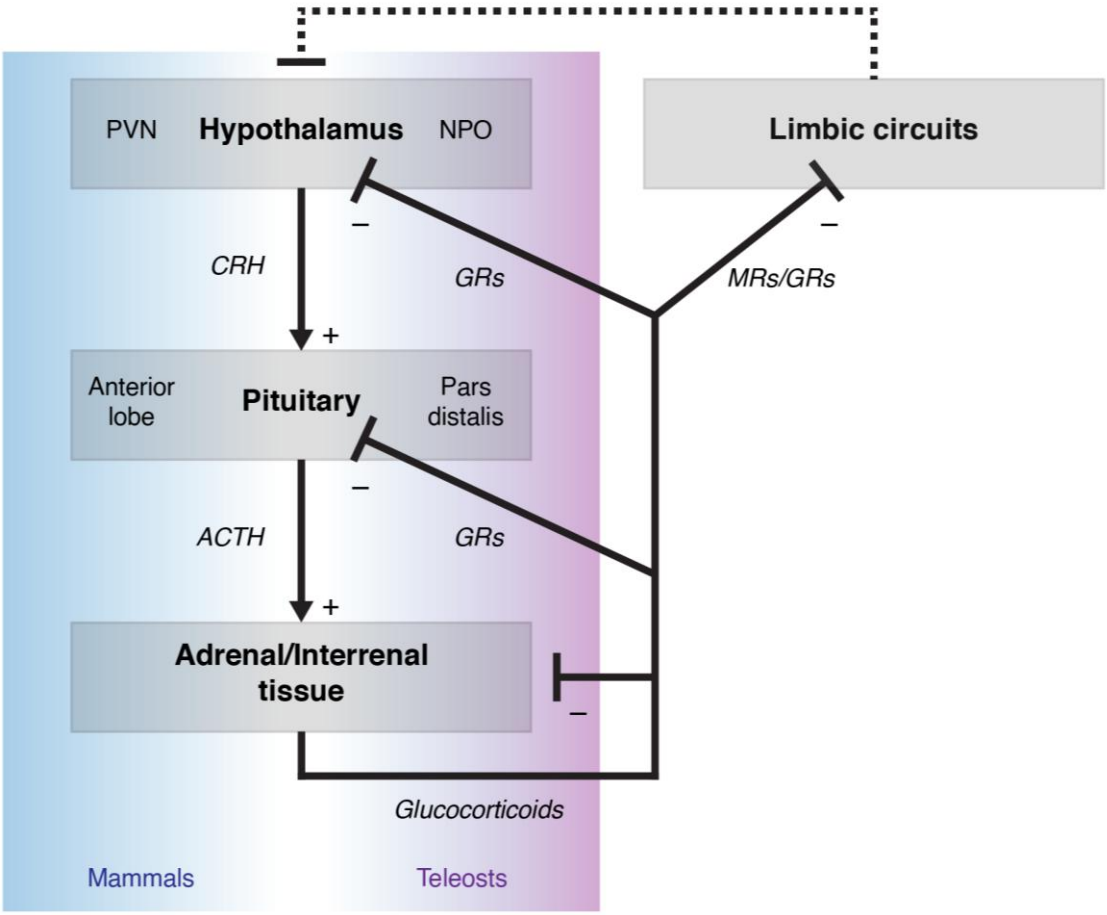

Figure 1. Schematic overview of HPA/HPI axis homologies and limbic feedback.

Schematic overview of the hypothalamic-pituitary-adrenal/interrenal (HPA/HPI) axis in mammals (blue shading) and teleosts (purple shading), emphasizing homologous nodes and glucocorticoid feedback. In mammals, corticotropin-releasing hormone (CRH) is released from paraventricular nucleus (PVN) neurons in the hypothalamus and stimulates adrenocorticotropic hormone (ACTH) secretion from the anterior pituitary lobe, which in turn drives glucocorticoid release from adrenal tissue. In teleosts, neurosecretory cells in the neurosecretory preoptic area (NPO) project to the pars distalis of the pituitary, which controls glucocorticoid secretion from interrenal tissue. Glucocorticoids act via mineralocorticoid and glucocorticoid receptors (MRs/GRs) in limbic circuits and GRs in the hypothalamus and pituitary to provide negative feedback, thereby constraining axis activity and closing the homeostatic loop. Solid arrows indicate excitatory drive, T-shaped lines denote inhibitory feedback, and shading highlights the correspondence between mammalian and teleost components.

1.3. A definition of resilience

Resilience, in systems terms, is the capacity of a dynamic system to withstand disruption and return toward its operating regime (Southwick et al., 2014). In biobehavioral and clinical contexts, it refers to an active process in which neurobiological and psychological mechanisms support the maintenance or restoration of adaptive function after adversity, rather than a mere absence of symptoms (Feder et al., 2009; Scott J Russo et al., 2012). Consistent with outcome-based accounts, resilience is defined from post-challenge functioning and is frequently the modal trajectory following potentially traumatic events (Bonanno et al., 2011; Kalisch et al., 2017). It is dynamic

and context-dependent - not a fixed trait - and should be distinguished from resistance, which refers to minimal disruption during exposure (Rutter, 2012).

Two principles are especially relevant for what follows. First, resilient outcomes reflect adaptive changes that restore function after disruption - they are not simply passive resistance (Nestler and Russo, 2024). At the neurobiological level, this is expressed as coordinated regulation within stress-regulatory circuits and effector systems that support efficient behavioral reorganization and physiological recovery (Cathomas et al., 2019). Second, the experience of behavioral control over an aversive event promotes adaptive responding and guards against passivity, a general principle observed across vertebrates and relevant to how stress is appraised and acted upon in experimental settings (Amat et al., 2005; Baratta et al., 2023). In physiological terms, effective adaptation also entails the timely termination of stress responses, limiting the accumulation of allostatic load over repeated or prolonged challenges (Charney, 2004).

Within this framing, stress resilience denotes either a stable, healthy trajectory or a rapid recovery after an initial disturbance, whereas stress vulnerability/susceptibility reflects protracted or incomplete restoration (Swaminathan et al., 2023). Outcomes are domain- and time-scale-specific: an individual may show resilience in some behavioral or physiological domains, but not others, and trajectories can change across development or with repeated exposure. This conceptualization sets expectations for the remainder of this thesis.

2. Defining Resilience in Animal Models

2.1. What constitutes a “resilience model”

A resilience model exposes subjects to a controlled adverse event and classifies individuals by their post-challenge functioning (Kalisch et al., 2017). The defining feature is heterogeneous outcomes under standardized exposure: only a subset develops sustained behavioral or physiological disruption, whereas others maintain or restore adaptive function. This segregation, observed even in inbred lines, indicates that outcomes reflect interactions among genetic background, prior history, and context rather than genetics alone (Krishnan et al., 2007). Resilience is evaluated by how well one functions after the challenge, rather than by the magnitude of the acute response.

Several design axes organize these models.

1. *Temporal profile*

   Along the temporal axis, stress-resilience paradigms can be framed as acute, chronic, or developmental (Albayrak et al., 2024; McEwen, 2000; Musazzi et al., 2018, 2017). Acute

paradigms involve single or brief exposures that perturb behavior and physiology over minutes to hours. Chronic paradigms impose repeated or prolonged demand, yielding longer-lasting adaptations or dysregulation. Developmental paradigms confine perturbations to sensitive early windows, with outcomes that are read later in life. Together, these distinctions map onto well-described short- versus long-term stress effects and the developmental programming of stress systems.

2. *Approach*

Stress resilience paradigms can be implemented through environmental or behavioral manipulations, genetic interventions, or selective breeding (Feder et al., 2009; Patchev and Patchev, 2006). Environmental and behavioral approaches use social, physical, or ethological stressors (e.g., social defeat, restraint, variable schedules). Genetic interventions introduce targeted mutations or transgenes that modify stress circuits or neuromodulatory systems, offering high mechanistic access at the cost of generalization (Cryan and Holmes, 2005). Selective breeding yields lines that diverge in coping style or endocrine reactivity (e.g., Roman high/low avoidance rats; high- vs low-responder lines), providing stable phenotypes that facilitate comparative work but can narrow external validity (Steimer and Driscoll, 2003). Each approach trades off ecological realism, mechanistic access, and generalization in different proportions (Golden et al., 2011; Willner, 2016).

3. *Construct*

A paradigm's construct refers to controllability and/or the predictability of the stressors. Prior exposure to controllable stress confers "immunization" against later uncontrollable stress of matched load, attenuating escape failures, prolongations of latency, and endocrine consequences at assessment (Amat et al., 2006, 2005).

Controllability. Refers to whether the subject can influence the onset, offset, or intensity of the stressor. Prior exposure to controllable stress confers "immunization" against later uncontrollable stress of matched load, attenuating escape failures, prolongations of latency, and endocrine consequences at assessment (Amat et al., 2006, 2005).

Predictability. Refers to temporal or cue-based expectancy. Holding intensity and duration constant, predictable stressors (those signaled by reliable cues or schedules) produce outcomes that differ from unpredictable stressors, which lack consistent warning or timing.

Unpredictability typically amplifies uncertainty and alters learning about threat, shifting both behavioral readouts and physiological set points (Kearton et al., 2020).

4. *Social Domain*

   The domain specifies the class of function probed at assessment and is independent of the induction paradigm. Social readouts require reference to conspecifics (e.g., cohesion or approach toward conspecifics in zebrafish shoaling or social-preference assays; (Miller and Gerlai, 2007)). Non-social readouts quantify exploration, risk assessment, arousal, or sensorimotor responses in the absence of conspecifics (e.g., open-field exploration in rodents) (Prut and Belzung, 2003). Locomotor indices and endocrine measures (cortisol in teleosts, corticosterone in most rodents) can accompany either domain as species-appropriate adjuncts and do not define the domain itself (Bonga, 1997).

In the context of these designs, one can define *induction* as the exposure protocol that elicits the challenge, and *assessment* as the post-challenge window during which outcomes are measured. Keeping these phases analytically distinct clarifies whether outcome heterogeneity reflects sensitivity to induction, recovery efficiency, or both.

2.2. Canonical mammalian paradigms of stress resilience

With these orthogonal axes and induction-assessment definitions in place, the next step is to examine canonical mammalian paradigms as specific combinations of temporal profile, approach, construct, and domain. Each employs a standardized induction and a defined assessment window, and classifies individuals after exposure based on recovery. This survey highlights how different paradigms are distributed across axes and the kinds of resilient outcomes they address.

Chronic social defeat stress models sustained psychosocial adversity (Golden et al., 2011; Wang et al., 2021). During daily resident-intruder encounters, a smaller focal animal is attacked until defeated and then re-exposed to the aggressor across sessions, resulting in repeated social subordination. Assessment uses a social interaction test that quantifies approach toward an unfamiliar conspecific. Outcomes diverge: susceptible animals avoid social contact, whereas resilient animals maintain a social approach relative to controls. Advantages include strong construct and face validity for psychosocial load and a clear social domain readout. Limitations include a historical bias toward male cohorts, which variants partially address through female procedures (Harris et al., 2018), vicarious defeat without direct contact (Sial et al., 2016), and social instability designs that perturb hierarchies (Koert et al., 2021).

Controllability paradigms isolate the role of control over an aversive event. In triadic designs, one group receives escapable stress, a yoked group receives physically matched inescapable stress, and a control group is unstressed (Drugan et al., 1997; Maier and Seligman, 2016). Assessment in a new context where escape is possible measures latencies and failures to escape. Prior uncontrollable exposure leads to passivity at assessment, whereas prior controllable exposure prevents it. The model cleanly tests the construct of control and demonstrates behavioral immunization, though it emphasizes a specific avoidance domain and requires careful matching of shock or constraint parameters (Amat et al., 2006, 2005).

Chronic unpredictable stress, also termed chronic mild or variable stress, sustains demand by varying the timing and modality of low-to-moderate stressors to prevent habituation (Willner, 2016). Assessment centers on reward processing, complemented by conflict-based exploration. As with social defeat, individuals diverge: susceptible animals show persistent anhedonia, whereas resilient animals preserve reward sensitivity despite comparable exposure. The non-social design facilitates the inclusion of both sexes under similar conditions (Hodes et al., 2015), and provides a construct complementary to defeat and controllability.

Developmental manipulations test timing effects during sensitive periods. Inductions include altered maternal care, limited bedding and nesting, or unstable rearing contexts in early life. Assessment in adolescence or adulthood measures endocrine reactivity and behavioral organization across social and non-social domains. Many protocols increase vulnerability to later challenges by elevating HPA reactivity and disrupting recovery (Kestering-Ferreira et al., 2021; Walker et al., 2017; Wang et al., 2020), while brief, manageable early challenges can inoculate against subsequent stressors (Lyons and Parker, 2007; Meaney, 2001). The approach captures developmental programming of resilience but varies across laboratories and requires careful control of rearing conditions.

Acute trauma-like stressors model single high-impact events with strong ethological or clinical face validity (Goswami et al., 2013; Lisieski et al., 2018; Verbitsky et al., 2020). Inductions include single prolonged stress, restraint or immobilization, and predator odor. Assessment covers fear learning and extinction, acoustic startle response, sleep-wake organization, and endocrine recovery. Within cohorts, some individuals exhibit persistent hyperarousal or impaired extinction, while others return to baseline. This approach offers precise timing and clear links to traumatic exposure, though it may not capture the cumulative aspects of chronic stress.

Together, these mammalian paradigms offer complementary construct anchors for resilience: social defeat foregrounds post-challenge social function under psychosocial load, controllability paradigms demonstrate that opportunities to act on the stressor recruit protective mechanisms,

chronic unpredictable stress emphasizes reward processing under sustained uncertainty, developmental manipulations show how early experience biases adult appraisal and recovery, and acute trauma-like exposure demonstrates that a single event can yield heterogeneous trajectories.

2.3. Zebrafish landscape: adult and larval

Teleost models follow the induction-assessment logic used for mammals: a standardized challenge triggers a temporary disturbance, outcomes are quantified during a specific recovery period, and labels are assigned based on post-challenge function. The teleost HPI axis is the functional equivalent of the mammalian HPA axis, enabling direct translation of exposure methods and readouts. Additionally, zebrafish offer optical access and high throughput, improving the timing between the challenge and the measurement. Teleost stress-resilience paradigms can be described using the four orthogonal axes defined earlier: temporal profile, approach, structure, and domain. The measurement level (behavioral, endocrine, neural) is considered an analytic attribute that can be combined with any of these axes.

Chronic psychosocial load maps only partially onto teleosts. There is no broadly standardized chronic social-defeat protocol in zebrafish, although repeated defeat variants have been reported and are increasingly used in research settings (Lai et al., 2023; Nakajo et al., 2020). Perturbation of social state typically relies on social isolation or instability and on brief antagonistic encounters that produce winner-loser outcomes. Assessment emphasizes shoaling metrics and social-preference or interaction assays, with novel tank or open field used as auxiliary readouts of exploratory behavior during recovery (Facciol and Gerlai, 2020; Fontana et al., 2022; A. M. Stewart et al., 2012). In larvae, robust social preference emerges only after early development, with reliable assays from about the third week post-fertilization, which limits direct analogues of chronic defeat at earlier stages (Dreosti et al., 2015).

Chronic unpredictable stress employs multi-week schedules of mild, varied challenges in adults (Demin et al., 2021, 2020; Piato et al., 2011), with shorter adaptations in juveniles (Golla et al., 2020; Wu et al., 2023). Readouts include the novel tank, light-dark, open field, and age-appropriate social assays, typically administered after a delay to minimize acute carryover. These are conflict-based exploration tasks in which animals weigh innate avoidance of exposed locations against exploratory drive. In zebrafish, avoidance is expressed as bottom-dwelling and delayed entries to the upper water column in the novel tank, preference for the dark compartment in the light-dark assay (scototaxis), and reduced center occupancy or increased wall-hugging (thigmotaxis) in open field (Johnson et al., 2023; Kysil et al., 2017; Maximino et al., 2010; Stewart et al., 2010). Recovery is evaluated longitudinally as the return of these indices toward baseline rather than the

magnitude of acute reactivity. This separation of induction from assessment reduces motor confounds and isolates recovery dynamics.

Developmental manipulations model early-life stress and stress inoculation by delivering brief, age-specific perturbations with outcomes read at juvenile or adult stages (Castillo-Ramírez et al., 2024a; Chin et al., 2022). Implementations include unpredictable mild stress at larval stages, osmotic challenge, and maternal or embryonic glucocorticoid elevation (Alderman and Bernier, 2009; Best et al., 2017; Graves et al., 2023). Assessment tracks how baseline-anchored behavioral ranges shift with developmental history, focusing on exploratory recovery, avoidance performance where applicable, and cortisol regulation rather than acute arousal.

Structure-focused designs manipulate controllability. In adults, two-way active avoidance in shuttle-box apparatuses (Xu et al., 2007) and single-trial inhibitory avoidance (Blank et al., 2009; Manuel et al., 2014) quantify acquisition and expression of control. In larvae, pre-exposure to inescapable stimulation induces helplessness-like deficits that persist into subsequent avoidance and approach behaviors (Lee et al., 2010). Assessment focuses on recovery of goal-directed responding after exposure, including escape latency, proportion of successful avoidances, and failure rate. When protocols incorporate a recovery phase, exploratory behavior can serve as an auxiliary readout. Outcome labels are assigned based on recovery efficiency under matched load rather than on behavior during uncontrollable exposure.

Within the acute class, two induction families are common in zebrafish: ethological or psychological threat, such as conspecific alarm substances or predator cues, and environmental or physiological challenges, such as osmotic, pH or temperature shifts, illumination changes, or brief confinement. The latter family is particularly relevant to this thesis.

Acute ethological threat includes conspecific alarm substances and predator cues, which rapidly induce defensive states in adults (Baker and Wong, 2019; Gerlai et al., 2009; Speedie and Gerlai, 2008). Behavior is sampled immediately after exposure and over defined windows from minutes to hours. Shoaling and social-preference assays index social normalization, whereas novel tank and open field capture exploration rebound (Fontana et al., 2022; Miller and Gerlai, 2007; A. Stewart et al., 2012; A. M. Stewart et al., 2012). Resilient outcomes are operationalized as timely return toward baseline in vertical position, center occupancy, and exploration rate; susceptible outcomes show protracted immobility, thigmotaxis, or fragmented locomotion.

Acute environmental challenges provide precise, time-locked induction in larvae and juveniles. Brief, fixed-dose immersions in hyperosmotic media or solutions altering pH, and physical challenges such as netting, swirling, or high-throughput water-vortex flow, deliver standardized, non-social, inescapable exposures that engage the HPI axis with dose-graded glucocorticoid output

(Castillo-Ramírez et al., 2024b; Lee et al., 2019; Philippe et al., 2023; Shvartsburd and Vijayan, 2025; Swaminathan et al., 2023; Yeh et al., 2013). Stress-resilience classification follows two behavioral schemes in these assays: a baseline-anchored approach that scores each fish by the rate and extent of return to its own pre-stress baseline (Tudorache et al., 2015; Yuan et al., 2018), and a control-referenced approach that scores each fish relative to the concurrently measured distribution of unexposed controls (Swaminathan et al., 2023). Locomotor features (e.g., total distance, swimming speed, and idle time) and bout kinematics (e.g., bout rate, bout duration) further characterize the recovery profile (Marques et al., 2018).

Endocrine classification parallels the behavioral schemes by quantifying recovery kinetics of whole-body cortisol. Typical indices include peak amplitude, time-to-peak, time-to-half-baseline, recovery slope, decay constant, and area under the curve. In larvae, acute osmotic or physical challenges produce peaks within 5-10 minutes, followed by decay over tens of minutes (Castillo-Ramírez et al., 2024b; Yeh et al., 2013), whereas adults after net-handling return toward baseline on the order of an hour (Ramsay et al., 2009). Some studies integrate behavioral and endocrine recovery to profile faster-recovering versus slower-recovering individuals (Tudorache et al., 2015).

3. Neural Substrates of Stress Resilience

3.1. Stress axis and acute threat processing

Acute threat engages a conserved neuroendocrine cascade in which hypothalamic corticotropin-releasing hormone (CRH) drives pituitary adrenocorticotropic hormone (ACTH) and glucocorticoid (GC) secretion via the HPA axis in mammals (Scott J. Russo et al., 2012) and the homologous HPI axis in teleosts (Bonga, 1997). Resilience in this framework is defined by two temporal signatures: rapid, proportional activation during exposure and efficient termination during recovery (Castillo-Ramírez et al., 2024b). Sympathetic catecholamine release provides the earliest systemic support, while GCs set the slower hormonal envelope that constrains energy allocation, modulates inflammation, and tunes neural excitability (Herman et al., 2016; Joëls and de Kloet, 1992). Prolonged or poorly terminated responses accumulate allostatic load (McEwen, 2007), so the emphasis here is on mechanisms that accelerate return to baseline.

Initiation arises with the release of CRH from neurons in the paraventricular nucleus in mammals, or the homologous nucleus preopticus in zebrafish (Herget et al., 2014; Herman et al., 2016; Herman and Tasker, 2016). CRH stimulates pituitary ACTH, which then drives adrenal (or interrenal in fish) glucocorticoid secretion, with a characteristic minutes-scale lag between ACTH

and the peak corticosterone or cortisol (Butt et al., 2020; Castillo-Ramírez et al., 2024b; de Abreu et al., 2021; Joëls et al., 2018). In teleosts, which lack aldosterone, cortisol serves both glucocorticoid and mineralocorticoid roles, and mineralocorticoid receptors can also be engaged by 11-deoxycorticosterone (DOC; Takahashi and Sakamoto, 2013). Glucocorticoids act on both mineralocorticoid and glucocorticoid receptors: high-affinity MR shapes basal tone, whereas GR is recruited as concentrations rise to provide negative feedback and terminate the response (de Kloet, 2022; de Kloet et al., 1998; Myers et al., 2012). Disruption of receptor signaling prolongs hormone elevation and delays normalization of behavior and physiology, as shown in zebrafish lacking functional GR (Ziv et al., 2013).

Larval zebrafish provide tractable recovery kinetics (Yeh et al., 2013). The HPI axis is competent within the first post-hatching days (Lee et al., 2024), acute stressors drive a cortisol peak within minutes, and levels typically return toward baseline within 30-40 minutes under standard conditions (Castillo-Ramírez et al., 2024b). After normalization, a short refractory period reduces responsiveness to a second challenge, consistent with fast GR-dependent feedback (Castillo-Ramírez et al., 2024a). Local pre-receptor metabolism contributes to termination: 11β-hydroxysteroid dehydrogenase converts cortisol to cortisone in zebrafish, with robust brain expression and stress-regulated activity (Alderman and Vijayan, 2012). Genetic or pharmacologic reduction of this pathway prolongs the decline to baseline (Theodoridi et al., 2021). These dynamics make larvae suitable for time-locked sampling of neuroendocrine recovery and for comparing individuals that diverge in rebound despite similar exposure peaks.

3.2. Macrocircuitry

While the neuroendocrine axis provides systemic mediators, the individual variability in stress response is ultimately governed by the specific neural circuits that detect, evaluate, and control the threat signal (Tovote et al., 2015; see Fig. 2 for corticolimbic and brainstem examples). Across the brain, many regions exhibit robust patterns of stress exposure, but only a few prospectively predict rebound. The emphasis in this section is therefore on circuit motifs that actively promote recovery.

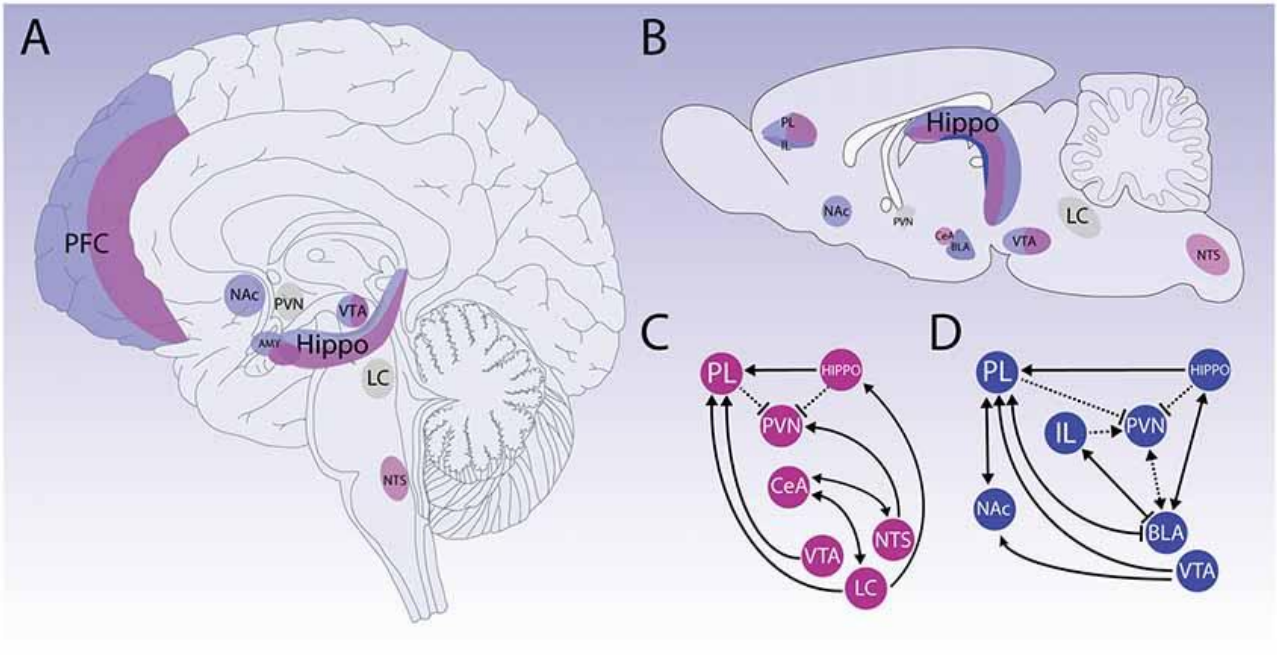

Figure 2. Corticolimbic and brainstem circuits recruited by physical and psychological stressors.

Schematic overview of key brain regions involved in stress processing in humans (A) and rodents (B), and of the main network motifs engaged by predominantly physical (C, magenta) versus psychological (D, blue) stressors. Physical stressors rely more strongly on brainstem and hypothalamic structures such as the nucleus of the solitary tract (NTS), locus coeruleus (LC) and paraventricular nucleus of the hypothalamus (PVN), with additional input from prelimbic prefrontal cortex (PL) and central amygdala (CeA). Psychological or anticipatory stressors place greater weight on corticolimbic and reward-related circuits, including PL and infralimbic (IL) prefrontal cortex, basolateral amygdala (BLA), hippocampus, nucleus accumbens (NAc), and ventral tegmental area (VTA), which together shape appraisal and top-down control over PVN and downstream autonomic outputs. Gray-shaded PVN and LC indicate common effector nodes across stressor classes. Adapted from Godoy et al., (2018), Frontiers in Behavioral Neuroscience, CC BY 4.0.

3.2.1. Threat valuation and controllability: prefrontal-limbic-brainstem interfaces

Distal or predictable threats activate medial prefrontal and hippocampal systems for contextual appraisal and planning, while proximal or inescapable threats shift control toward midbrain and pontine regions that mediate reflexive responses (Maren et al., 2013; Mobbs et al., 2007). Controllability is crucial - under similar physical load, escapable and yoked inescapable stressors produce comparable endocrine peaks during exposure, yet prior or concurrent control recruits medial prefrontal outputs that suppress dorsal raphe nucleus activation and prevent prolonged passive coping (Amat et al., 2005). Causal interventions support this pattern: transient prefrontal inactivation during controllable stress eliminates protection, and targeted prefrontal activation restores active responses under otherwise uncontrollable conditions (Amat et al., 2006; Warden et al., 2012). Lasting protection across subsequent exposures reflects prelimbic prefrontal control over the dorsal raphe circuit, consistent with circuit-specific plasticity in this pathway (Amat et al., 2006; Baratta et al., 2023; Christianson et al., 2014).

Although teleosts lack a laminated prefrontal cortex, control of monoaminergic nuclei can be routed through forebrain and diencephalic hubs. In zebrafish, the ventral habenula-raphe pathway modulates serotonergic output and defensive behaviors, indicating that raphe gating is conserved but can be achieved through alternative routes (Amo et al., 2014; Andalman et al., 2019).

3.2.2. BNST and sustained threat: setting the baseline for rebound

The bed nucleus of the stria terminalis (BNST) integrates prolonged, uncertain threat and interfaces with hypothalamic and brainstem effectors (Avery et al., 2016). During exposure, BNST activity sustains vigilance and autonomic adjustments, and during recovery, down-scaling is hypothesized to permit re-engagement (Goode et al., 2019; Lebow and Chen, 2016). Projections to hypothalamic and brainstem nuclei allow BNST to modulate HPA/HPI tone and autonomic outflow (Forray and Gysling, 2004). In some paradigms, CRFR2-positive posterior BNST subcircuits have been implicated in faster endocrine and behavioral recovery, consistent with a recovery-gating role (Henckens et al., 2017). In zebrafish, ventral telencephalic and preoptic regions with BNST-like connectivity couple valuation to endocrine and autonomic controllers, offering a tractable test of whether dampening sustained-threat signals accelerates rebound (Corradi et al., 2022; Lal and Kawakami, 2022; Porter and Mueller, 2020).

3.2.3. LC-noradrenaline: arousal offset and network reset

Locus coeruleus noradrenergic neurons broadcast arousal signals that modulate network gain and behavioral mode (Aston-Jones and Cohen, 2005). Stress elevates LC activity and catecholamine release in prefrontal and amygdala circuits, biasing action selection (Arnsten, 2015; Giustino et al., 2020; Privitera et al., 2024). Recovery likely benefits from reducing LC output and restoring prefrontal network integrity (Giovannitti et al., 2015; Wang et al., 2007). α2A-agonists suppress LC-NE drive and can strengthen prefrontal connectivity, facilitating autonomic normalization (Arnsten and Jin, 2012; Marwaha et al., 1983; Pineda et al., 1997). In zebrafish, a conserved LC and NE-dependent arousal supports the idea that adjusting LC-NE tone aids the transition from immobility to re-engagement, although recovery-phase dynamics remain to be tested directly (PoKay M. Ma, 1994; Pokay M. Ma, 1994; Singh et al., 2015).

3.2.4. PAG columns: switching action modes

Columnar organization within the periaqueductal gray (PAG) aligns with defensive modes: activation of dorsal/lateral columns promotes active escape, whereas ventrolateral columns favor passive responses, including freezing (Dampney, 2018). During exposure, PAG recruitment varies with threat demands, and freezing and flight circuits can oppose each other to permit rapid

switching (Franklin, 2019; Tovote et al., 2016). After offset, movement re-initiation likely reflects decreased ventrolateral drive and recruitment of dorsal/lateral circuits. The PAG receives inputs from the central amygdala and the bed nucleus of the stria terminalis and projects to medullary premotor nuclei, situating it between valuation and execution (Holstege et al., 1985).

Teleosts possess a midbrain griseum centrale (GC), a periventricular column proposed to correspond to the mammalian PAG based on its position and connectivity with hypothalamus, pallium, raphe, and the interpeduncular nucleus (Okamoto et al., 2012). However, whether it exhibits mammal-like columnar specialization and descending premotor outputs remains incompletely resolved in fish (Olson et al., 2017).

3.2.5. Habenula-IPN-raphe: updating aversive prediction to permit recovery

The habenula provides a conserved valuation hub that shapes monoaminergic output (Hikosaka et al., 2008). In zebrafish and mammals, habenular microcircuits regulate raphe activity through the interpeduncular nucleus and encode aversive prediction, or expectation signals that update with learning (Amo et al., 2014; Kobayashi et al., 2013; Matsumoto and Hikosaka, 2007; McLaughlin et al., 2017). In zebrafish, ventral habenula activity signals expected danger and modulates the raphe inferior (the homolog of the mammalian median raphe). Moreover, activation of the left dorsal habenula to the interpeduncular pathway has been shown to speed up the return to swimming after a shock, while disruption of this pathway prolongs immobility (Duboué et al., 2017). These effects appear context and developmental stage-dependent (Agetsuma et al., 2010). This subcortical route complements cortical and basal ganglia influences over the raphe and offers a candidate mechanism for control during recovery that is anatomically conserved (Kobayashi et al., 2013; Rolls, 2017).

3.2.6. Tectum/superior colliculus to premotor brainstem: executing re-engagement

Successful recovery requires a valuation that permits re-engagement and premotor commands that implement it. In teleosts, the optic tectum relays salience and orienting signals to the nucleus of the medial longitudinal fasciculus and to identified reticulospinal neurons (RSNs) that project to the spinal cord (Gahtan et al., 2005). The mesencephalic locomotor region (MLR) recruits V2a reticulospinal populations to initiate forward locomotion and shape steering, placing MLR-RSN coupling as a primary start and kinematics controller in zebrafish (Carbo-Tano et al., 2023). Direct, time-resolved mapping of recovery-phase tectal drive is limited, but available evidence supports a plausible route in which restored tectal and MLR engagement re-enable orienting and forward swim after stressor offset. Disruption of tectal recipients in the nMLF impairs prey capture, and MLR manipulations alter locomotor initiation, consistent with a causal role for these nodes in re-

entry to ongoing behavior (Carbo-Tano et al., 2023; Gahtan et al., 2005). In mammals, the superior colliculus issues commands to premotor nuclei in the medulla oblongata and interfaces with mesencephalic locomotor circuits, supporting context-dependent transitions from immobility to movement during orienting and defensive behaviors (Caggiano et al., 2018; Capelli et al., 2017; Lynch et al., 2022; Wolf et al., 2015).

3.2.7. Cross-species synthesis and predictions

Two principles emerge. First, descending control from valuation networks to monoaminergic and premotor effectors constrains the persistence of defensive states once threat probability falls (Agetsuma et al., 2010; Corradi et al., 2022; Forray and Gysling, 2004; Warden et al., 2012). This control can be cortical via prefrontal-raphe pathways, subcortical via habenula-interpeduncular-raphe, or forebrain-hypothalamic via BNST and preoptic regulators of endocrine and autonomic output. In each case, the recovery-linked pattern is an active configuration rather than the absence of exposure-related activity. Second, re-engagement of ongoing behavior likely involves a shift in locus coeruleus-noradrenergic activity from high-arousal modes toward moderate tonic firing that supports task engagement (Aston-Jones and Cohen, 2005), together with the recruitment of brainstem premotor assemblies that initiate exploratory locomotion and other context-appropriate actions (Caggiano et al., 2018; Leiras et al., 2022). Work across mammals and zebrafish highlights PAG interfaces with the mesencephalic locomotor region and reticulospinal pools that couple midbrain locomotor commands to spinal locomotor networks, including central pattern generators (Caggiano et al., 2018; Capelli et al., 2017; Carbo-Tano et al., 2023; Leiras et al., 2022).

3.3. Cellular and molecular programs

The circuit-level flow of information, from forebrain appraisal to brainstem action selection, is fundamentally reliant on the integrated output of individual neurons, requiring an examination of the cellular and molecular mechanisms that support resilience. To avoid veering too much from the scope of this thesis, a multilevel summary of these mechanisms is provided here.

3.3.1. Endocrine receptor signaling and kinetics

Glucocorticoid actions during recovery depend on how MR and GR are occupied over time: high-affinity MRs are engaged near basal concentrations, GRs are progressively recruited as levels rise, and pulsatile hormone release drives brief bouts of GR-dependent transcription rather than a sustained “on” state (de Kloet, 2022; de Kloet et al., 1998; Lightman and Conway-Campbell, 2024; Myers et al., 2012). Fast non-genomic glucocorticoid signaling, dynamic changes in corticosteroid-binding globulin, and activity-dependent FKBP5 induction modulate receptor

sensitivity on seconds-to-hours timescales, transiently altering how strongly feedback is expressed (Binder, 2009; Haller et al., 2008; Lee et al., 2023; Lewis and Elder, 2014). In teleosts, cortisol acts via both MR and GR, with additional tuning by alternative ligands and 11β-HSD2-mediated metabolism, so recovery reflects the combined effects of receptor balance, pulsatility, and local ligand access (Alderman and Vijayan, 2012; Takahashi and Sakamoto, 2013).

3.3.2. Synaptic and circuit recalibration

At the synaptic and circuit levels, recovery involves dampening residual arousal and restoring firing patterns that remain flexible but controllable. Inhibitory gain via α2-containing $GABA_A$ receptors in stress-linked networks promotes resilience-like behavior, while homeostatic mechanisms such as synaptic scaling and intrinsic plasticity stabilize activity by adjusting synaptic and intrinsic gains without imposing new stimulus-specific structure (Benham et al., 2021; Debanne et al., 2019; Turrigiano, 2012). Neurotrophic signaling through BDNF-TrkB supports dendritic and spine maintenance and underlies plasticity that helps circuits re-engage after perturbation, so inhibitory control, homeostatic stabilization, and trophic support jointly shape how quickly workable network dynamics are re-established (Zagrebelsky et al., 2020).

3.3.3. Gene-regulatory programs, proteostasis, and neuromodulators

On slower timescales, resilient versus susceptible outcomes are associated with distinct region-specific transcriptional modules and integrated stress-response dynamics rather than simple mirror-image gene expression, with prefrontal networks and relief of eIF2α-ATF4-mediated translational braking emerging as key determinants of recovery (Bagot et al., 2016; Costa-Mattioli et al., 2009; Lorsch et al., 2019; Pakos-Zebrucka et al., 2016; Sidrauski et al., 2013). Glial and vascular adaptations, including blood-brain barrier and endothelial signatures, further differentiate resilient from susceptible animals in chronic stress models, indicating that the neurovascular state participates in long-term resolution (Dion-Albert et al., 2022; Lehmann et al., 2018). Superimposed on these molecular and vascular changes, neuromodulatory systems such as prefrontal α2A-noradrenergic signaling, neuropeptide Y, locus-coeruleus galanin, and reduced orexin tone bias cortical-subcortical networks toward restored function rather than persistent hyperarousal (Grafe et al., 2018; Morgan et al., 2000; Seutin et al., 1989; Tillage et al., 2020; Wang et al., 2007).

3.4 Epigenetics

Enduring protection against subsequent stressors relies not only on transient transcriptional responses but also on the stabilization of gene-regulatory states through epigenetic mechanisms

that establish and preserve recovery ranges over time. Because the thesis focuses on standardized induction, behavioral recovery, and whole-brain activity, the discussion of epigenetic mechanisms remains brief and directs readers to the listed reviews for depth. Two levels are considered here: developmental programming, which inscribes durable set-point shifts during sensitive windows, and acute-to-subacute consolidation, in which activity-linked chromatin and transcriptional gating stabilize adaptations across the recovery epoch.

3.4.1. Developmental programming

Early-life adversity is linked to lasting epigenetic changes in stress-axis and plasticity genes, with DNA methylation shifts at loci like NR3C1 and, in specific models, CRH and related regulators. These changes are associated with altered HPA feedback and behavioral set-points in a region- and cell-type-specific manner (Bakusic et al., 2020; Rahman and McGowan, 2022). Genotype-environment interactions at FKBP5 serve as a clear example: risk haplotypes exhibit adversity-related demethylation at glucocorticoid-responsive elements, enhanced inducible FKBP5 expression, and altered GR signaling, consistent with programmed changes in feedback sensitivity (Klengel et al., 2013; Zannas et al., 2016). Zebrafish models extend these principles, as conserved stress-axis orthologues and defined developmental windows allow early glucocorticoid disruptions to be linked to long-lasting changes in HPI-axis function and behavior (Eachus et al., 2024, 2021).

3.4.2. Acute-to-subacute consolidation

After acute stress or other significant experiences, activity-regulated transcription shifts from a rapid wave of immediate-early genes to slower chromatin remodeling. This process is driven by calcium/MAPK-CREB signaling with CBP/p300 recruitment and associated increases in enhancer acetylation, and histone acetylation can support consolidation, aligning with the effects of HDAC inhibitors on memory and stress-related plasticity (Peixoto and Abel, 2013; Vecsey et al., 2007; Yap and Greenberg, 2018). These transcriptional programs are highly stimulus- and cell-type-specific rather than universal. Additionally, ultradian glucocorticoid pulses introduce temporal structure by causing cyclical GR binding to chromatin and pulsatile transcription (Conway-Campbell et al., 2010; Stavreva et al., 2009; Tyssowski et al., 2018). Together, these mechanisms illustrate how activity patterns over exposure time and hormone fluctuations can influence recovery trajectories, without implying a one-to-one correspondence between any specific epigenetic marker and behavioral outcome.

4. Whole-Brain Perspectives and Mapping Toolkits

4.1. Why brain-wide approaches are needed

Resilience is increasingly understood as a systems property: adaptive outcomes after stress arise from coordinated regulation across distributed cortical-subcortical networks rather than isolated regional responses (Kalisch et al., 2015; Scott J Russo et al., 2012). This view is supported by conceptual and empirical syntheses showing that emotion and stress control are implemented by functionally integrated circuits spanning appraisal, neuromodulatory, and premotor systems, which argues against single-region accounts (Hermans et al., 2014; Pessoa, 2017). Whole-brain analyses are therefore needed not only to characterize responses during stress exposure but also to resolve configurations that predict recovery, as large-scale network topology shifts with stress and can reconfigure as arousal subsides (Hermans et al., 2011; Lupinsky et al., 2025). Within this framework, functional-connectivity and graph-theoretic descriptions of integration and segregation offer principled metrics to quantify coordination and information flow, while acknowledging the need for careful interpretation (Bassett and Sporns, 2017; Palma-Espinosa et al., 2025). Together, these considerations motivate brain-wide, temporally grounded measurements to distinguish exposure-locked activity from recovery-linked network states that support a return to adaptive function.

4.2. Stress resilience mapping toolkits

Whole-brain mapping of stress resilience relies on two complementary imaging methods: static snapshots that locate recent activity at cellular resolution in fixed tissue, and dynamic recordings that track distributed population dynamics across exposure and recovery epochs.

4.2.1. Static modalities

Static approaches capture recent activity at cellular resolution by fixing tissue after a defined interval and labeling activity proxies across the entire brain. They offer anatomical completeness and quantitative cell counting but reflect time-integrated signals and therefore depend on precise control of labeling windows. Across species, IEG mapping combined with solvent clearing and light-sheet imaging (e.g., iDISCO+/ClearMap) provides whole-brain, atlas-registered cell counts after defined experiences, typically reflecting activity over tens of minutes (Chung et al., 2013; Minatohara et al., 2016; Renier et al., 2016).

In zebrafish larvae, the pERK/tERK ratio provides a rapid activity snapshot with a minutes-scale integration window (last ~5-10 min before termination), making strict time-locking and fast fixation essential when targeting recovery epochs (Pantoja et al., 2020; Randlett et al., 2015).

Alternative static readouts include brain-wide IEG labeling (immunolabeling or HCR RNA-FISH: slower kinetics, tens of minutes to hours) and phospho-S6 as a translational-engagement marker (Corrales Parada et al., 2024; Diekmann et al., 2015; Watanabe et al., 2024). Genetically encoded integrators such as CaMPARI1/2 and related variants add a user-defined window: brief 405-nm illumination permanently photoconverts active cells for *ex vivo* readout at cellular resolution (Edwards et al., 2020; Moeyaert et al., 2018).

4.2.2. Dynamic modalities

Dynamic approaches measure time-resolved population activity across large portions of the brain. These methods reveal trajectories and inter-regional coordination during behavior, sacrificing some cellular specificity or naturalism for temporal coverage and allowing explicit separation of induction and recovery phases. In humans, fMRI is the primary whole-brain dynamic tool; community standards from the Human Connectome Project provide widely adopted acquisition and "minimal preprocessing" pipelines that enable reproducible connectivity and network analyses (Glasser et al., 2013; Van Essen et al., 2013). EEG/MEG often complements fMRI by providing better temporal resolution (He and Liu, 2008). In rodents, awake fMRI has advanced rapidly (Klohs et al., 2025; Mandino et al., 2023), while mesoscale widefield calcium imaging provides bilateral, cortex-wide dynamics at high frame rates (Ren and Komiyama, 2021). Functional ultrasound extends coverage to deep structures with favorable spatiotemporal trade-offs (Deffieux et al., 2021), and optogenetics-fMRI links causal perturbations to brain-wide hemodynamic responses (Lin et al., 2016). Together, these modalities map large-scale reconfiguration with different balances of spatial resolution, cellular specificity, and behavioral freedom.

In zebrafish larvae, optical access allows for near-cellular-resolution, brain-wide recordings *in vivo*. Light-sheet calcium imaging can capture most neurons across the larval brain during behavior or fictive paradigms, with different variations supporting stabilized, head-embedded, or closed-loop preparations (Ahrens et al., 2013; Naumann et al., 2016; Vladimirov et al., 2014). Complementary volumetric techniques include light-field microscopy for rapid 3D imaging (Prevedel et al., 2014) and two-photon imaging for targeted circuits (Portugues et al., 2014). Specialized setups have incorporated vestibular stimulation (Migault et al., 2018) and can allow for freely swimming whole-brain recordings (Cong et al., 2017). Each method balances optical stability and coverage with naturalism and speed, but collectively they provide dynamic, brain-wide views capable of distinguishing induction from recovery.

5. Why Larval Zebrafish for Resilience?

Larval zebrafish offer an unusual blend of systems-level access and experimental scale that suits resilience research. Importantly, the HPI axis develops and becomes stress-responsive early: transcriptional components are present by ~3 dpf, acute challenges elicit measurable whole-body cortisol increases from ~3-4 dpf, and robust responses are observed by 5-6 dpf (Alsop and Vijayan, 2008; Lee et al., 2024; Yeh et al., 2013; Fig. 3). Optical transparency and compact brain size permit near-cellular-resolution, brain-wide recordings (Hasani et al., 2023; Loring et al., 2020) and atlas-registered activity mapping (Légaré et al., 2023), enabling circuit-level hypotheses to be tested across induction and recovery epochs (e.g., light-sheet whole-brain calcium imaging, pERK/IEG atlas mapping). High fecundity, rapid external development, and standardized husbandry reduce costs and logistical barriers, while mature genetic and transgenic toolkits and plate-based pharmacology support causal and screening workflows at a population scale. These properties are broadly documented in recent "zebrafishology" and methods reviews, as well as in seminal demonstrations of whole-brain imaging and atlas pipelines (Bedell et al., 2025; Loring et al., 2020; Ochenkowska et al., 2022; Randlett et al., 2015). Finally, several studies indicate that individual differences in behavior show measurable repeatability from early life, making larvae a tractable stage for probing how variation in recovery emerges and stabilizes (Fitzgerald et al., 2019). Together, these features recommend larvae as a high-leverage vertebrate model for unbiased discovery of brain-wide substrates and modulators of stress recovery.

A parallel need exists for rigorous, quantitative behavioral phenotyping that can distinguish recovery from initial reactivity and remain robust across batches and contexts. Community guidelines and reproducibility reviews increasingly emphasize clear assay definitions, standardized rearing and recording conditions, and transparent reporting, with preregistered analyses encouraged where feasible to improve comparability across laboratories and life stages (Bedell et al., 2025; Petersen et al., 2022; S. de Abreu et al., 2024). Within this framework, larval assays benefit from high-throughput video tracking and bout-level kinematics, which support baseline-anchored measures such as rebound magnitude or decay-to-baseline estimates and multi-feature behavioral profiles rather than single indices (Marques et al., 2018; Orger and Polavieja, 2015; Tudorache et al., 2015). Endocrine time courses provide an external clock for aligning behavioral and neural readouts over minutes-to-hours windows, as stress-induced cortisol peaks and recovery are relatively stereotyped in larvae (Marco et al., 2014; Yeh et al., 2013). Coping-style and individual-difference paradigms in larval zebrafish already classify phenotypes based on recovery relative to within-subject baselines (Tudorache et al., 2015) or concurrent controls (Swaminathan et al., 2023), illustrating how resilience-like dimensions can be operationalized.

Methodologically, these developments point toward pipelines that marry standardized behavioral acquisition with open, computational feature extraction and validation across days and cohorts (Dommanget-Kott et al., 2024; Gerlai, 2019; Hageter et al., 2025).

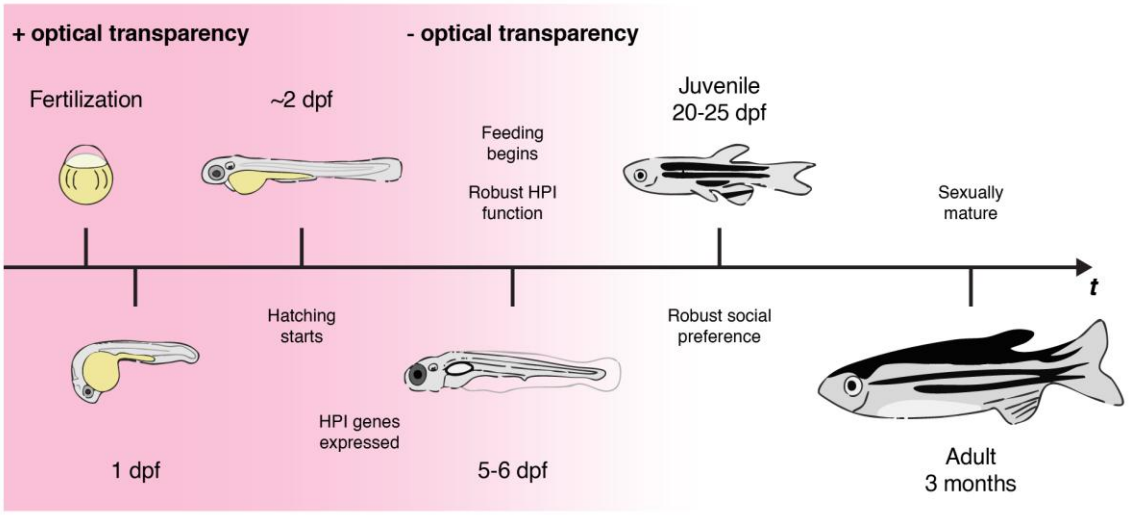

Figure 3. Developmental timeline in zebrafish.

Schematic of key stages from fertilization to adulthood with the early window of high optical transparency (pink, ~0-6 dpf) indicated. Milestones shown: fertilization; ~1 dpf embryo; hatching onset at ~2-3 dpf; free-swimming larva at 5-6 dpf when first feeding begins and the HPI axis shows robust stress responsiveness; juvenile at ~20-25 dpf when social preference is reliably expressed; and sexually mature adult (~3 months). Abbreviations: dpf, days post-fertilization. Drawings adapted from (Hasani et al., 2023).

AIMS

The main objective of this project was to establish a durable behavioral-neural framework for studying stress resilience in larval zebrafish. This framework was developed by measuring resilience as locomotor recovery after acute stress, using a score calculated relative to each individual's pre-challenge activity to minimize confounding variability. This established inter-individual variability in recovery was then used to perform unbiased whole-brain activity mapping (using pERK) and network analysis, aiming to identify the neural circuits and functional connectivity patterns that support resilient recovery.

Aim 1: Establish a behavioral assay and a quantitative resilience score that reliably separates stress-resilient from stress-susceptible larvae

Aim 1 addressed the behavioral construct. The main goal was to develop a high-throughput behavioral assay designed to quantify stress resilience by assessing locomotor rebound following acute challenge. This approach aimed to derive a quantitative resilience score that could reliably distinguish between resilient and vulnerable phenotypes. A key requirement was creating a metric that evaluated stress resilience independently of the larva's initial locomotor activity, thereby minimizing confounding variability. The study planned to examine the robustness of the resilience phenotypes across different transgenic lines and assess how the score varied with different stressor types and intensities. Lastly, the stability of individual resilience classifications was to be evaluated longitudinally throughout mid-larval and juvenile developmental stages.

Aim 2: Describe the brain-wide structural and functional adaptations that underlie resilient recovery

Aim 2 focused on the neural substrates of the behavioral phenotypes identified in Aim 1. The main goal was to use an unbiased whole-brain imaging approach to map neural signatures that distinguish resilient from vulnerable larval zebrafish after an acute challenge. The initial goal was to identify the specific brain regions activated solely by the stressor, thereby defining the stress exposure network. Next, the objective was to use multivariate analysis to identify consistent regional activity patterns that distinguish the resilient and vulnerable groups. Based on findings in conserved vertebrate systems, the project aimed to investigate the potential role of monoaminergic centers in the hypothalamus and telencephalon. Additionally, objectives included determining whether brainstem premotor systems were differentially engaged in the resilient phenotype, which was already defined by locomotor re-engagement. Lastly, the study intended to assess the

functional connectivity structure within these networks and determine the temporal dynamics of activity during early recovery.

By centering questions on what constitutes recovery, how broadly the construct generalizes, and which circuit adaptations represent it, the thesis aimed to establish a durable behavioral-neural framework for studying stress resilience in developing vertebrates and to delimit the conditions under which it offers predictive and mechanistic insights.

METHODS

1. Overview and structure of methods

This thesis integrates behavioral, imaging, and computational approaches to investigate the neural correlates of stress resilience in larval zebrafish (*Danio rerio*). The work comprises two primary manuscripts, each contributing complementary datasets and analyses. **Manuscript I** introduces a within-animal, baseline-anchored framework to quantify stress resilience as locomotor rebound after an acute challenge. **Manuscript II** extends this framework to the neural level, combining whole-brain phosphorylated ERK (pERK) activity mapping with statistical and network analyses to identify circuit correlates of resilience.

All experiments were conducted between 2022 and 2024 at the Department of Neuroscience, University of Copenhagen, under the license issued by the Danish Animal Experiments Inspectorate (license 2023-15-0201-01493). Experimental procedures, imaging pipelines, and analytical workflows are described in detail in the corresponding manuscripts appended to this thesis (Appendix: **I** and **II**). To avoid redundancy, the present section provides a concise overview of the core experimental tools, behavioral paradigms, imaging procedures, and computational analyses used throughout the thesis.

2. Animal husbandry and experimental design

Larval zebrafish (*Danio rerio*) of the nacre (mitfa$^{-/-}$) background were used in all experiments unless stated otherwise (Lister et al., 1999). Breeding adults were maintained under standard aquaculture conditions on a recirculating system (Techniplast, 28.4 °C, 400 µS cm^{-1} conductivity, pH 7.4, 14:10 h light/dark cycle). Embryos were obtained by natural spawning and reared in Petri dishes containing artificial fish water (AFW; 0.06 g L^{-1} marine salt in reverse-osmosis water). Larvae were maintained at 28 °C in incubators under identical light/dark cycles, with daily water renewal and once-daily feeding (shrimp larval diet, 5-50 µm particle size) starting at 5 days post-fertilization (dpf).

Experimental cohorts were generated from multiple breeding batches to ensure reproducibility across independent biological replicates. The main experimental designs followed a developmental timeline in which behavioral resilience was first quantified at 6 dpf, then longitudinally retested at 14 dpf, and finally validated in juveniles (30/31 dpf). Neural imaging experiments were conducted on separate cohorts exposed to identical stress-resilience assays and

euthanized at defined post-recovery time points (5 min or 10 min) for whole-brain pERK/tERK immunohistochemistry.

All procedures complied with European Directive 2010/63/EU on the protection of animals used for scientific purposes. Larvae were tested individually under temperature-controlled conditions and randomly assigned to experimental groups. Each experimental replicate was defined as an independent block conducted on a separate day using distinct clutches, identical apparatus, and fixed acquisition parameters.

3. Stress resilience assays

Stress resilience was quantified using a three-phase behavioral paradigm designed to measure locomotor rebound following an acute stressor. The assay was performed between 13:00 and 18:00 in darkness inside a temperature-controlled enclosure maintained at 28 ± 0.5 °C. Individual larvae were transferred with cut-tip pipettes into custom 24-well plates (12.8 x 8.6 x 1.8 cm) rendered opaque with acetone and fitted with nylon mesh bottoms (300 µm pore size) to allow rapid fluid exchange. The plate was inserted into a custom acrylic holder equipped with a silicone tubing system that enabled simultaneous draining and refilling of all wells. Each well contained artificial fish water (AFW) at a depth of 1.2 cm (Fig. 4).

The assay consisted of three consecutive stages: a baseline period of 30 minutes in AFW, a 10-minute stressor exposure, and a recovery period in AFW lasting 5-60 minutes, depending on the experiment. The stressor consisted of either 250 mM NaCl (osmotic stress) or acidified AFW (pH 4.0-5.5). Solutions were pre-warmed to 28 °C and introduced by draining and replacing the well contents manually through the tubing system.

Behavioral recordings were acquired with a monochrome camera (Mako U-319B, Allied Vision) equipped with a 35 mm Fujinon HF35SA-1 lens positioned above the multi-well plate. Infrared illumination was delivered via a flexible LED strip, with an opaque acrylic diffuser placed beneath the wells. Videos were recorded at 10 frames per second using a custom Python acquisition script. Larval trajectories were extracted from downsampled videos (2 Hz) using DeepLabCut (ResNet-50 architecture trained on custom annotations; Mathis et al., 2018). Eye positions were tracked and post-processed to correct detection artifacts using a dedicated graphical user interface. From the resulting trajectories, the following kinematic and spatial features were computed: swimming speed, acceleration, angular velocity, angular acceleration, movement duration, idle time, number of swim bursts, number of sharp turns, and distance to well center.

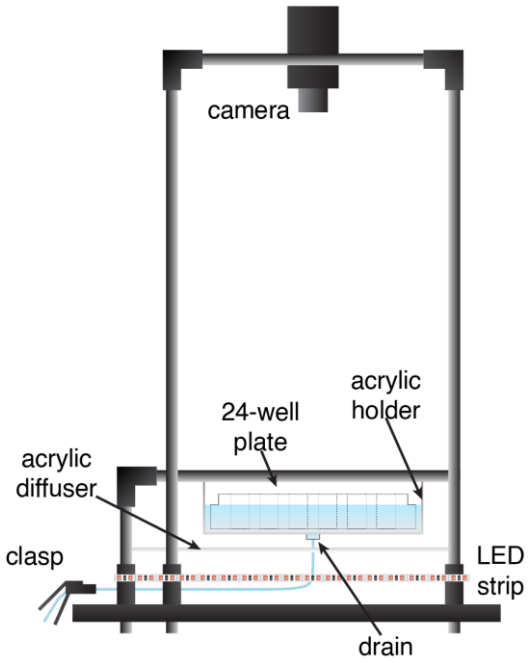

Figure 4. Schematic of the custom behavioral arena used to assess stress resilience in zebrafish larvae.
Individual larvae were housed in mesh-bottom wells of a modified 24-well plate, inserted into a custom acrylic holder. The arena was illuminated from below using an infrared LED strip and an opaque acrylic diffuser and imaged from above with a high-speed camera. A manual clasp allowed rapid draining and replacement of the medium without disturbing the plate, enabling fast transitions between assay phases.

For each larva, resilience was quantified by comparing mean swimming speed during the final 20 minutes of the baseline phase ($Speed_{baseline}$) with the first 5 minutes of recovery ($Speed_{recovery}$) according to:

$$\text{Resilience Score} = \frac{\text{Speed}_{\text{recovery}} - \text{Speed}_{\text{baseline}}}{\text{Speed}_{\text{baseline}}} \quad (1)$$

To convert the continuous resilience score into categorical labels, Gaussian mixture models (GMMs; K = 2-10) were fit to the pooled score distribution and used AIC/BIC to guide model complexity. A 7-component GMM was adopted for density visualization to avoid underfitting the pronounced right tail. Operational cut-points were set to contrast the distribution's extremes while maintaining sample sizes: scores ≤ -0.5 were labeled *vulnerable*, scores > -0.1 *resilient*, intermediate values unlabeled; extreme outliers (score > 5) were excluded. Full diagnostics (AIC/BIC curves; mixture components) are provided with **Manuscript I**.

4. Longitudinal stress resilience assays and novel tank tests

4.1. Longitudinal stress-resilience assay (6 to 14 dpf)

To evaluate the stability of stress-resilience classifications across development, larvae were re-assayed one week after initial testing. At 6 dpf, larvae were first exposed to the standard stress-resilience assay and assigned Control, Resilient, or Vulnerable labels based on their individual resilience scores. Within 24 hours, fish from each label were redistributed into separate 90-mm Petri dishes (6-7 larvae per dish) containing 50 mL of artificial fish water. Dishes were maintained at 28 °C under a 14:10 h light/dark cycle, with daily water renewal and identical feeding conditions.

At 14 dpf, fish were tested again using the same three-phase assay and identical acquisition parameters. Each recording session included approximately equal numbers of fish from each group randomized across wells. Behavioral features and resilience scores were computed using the same procedures as at 6 dpf. Group comparisons were performed both at cohort level to assess label stability and recovery of the resilience distribution.

4.2. Novel tank test at the juvenile stage (30 dpf)

To determine whether early-life resilience labels predict later behavioral responses, cohorts labeled at 6 dpf were reared to approximately one month of age (30-31 dpf) and tested in the novel tank test (NTT). At 7 dpf, larvae from each label (control, resilient, vulnerable) were transferred to group tanks containing 20-30 fish per cohort and maintained under standard aquaculture conditions until testing.

On the experimental day, juveniles were randomly assigned to a stressed or unstressed condition. Stressed cohorts were exposed to 250 mM NaCl for 10 minutes immediately before testing, while unstressed cohorts were kept in artificial fish water. After a 5-minute recovery period in 13 mL tubes containing 10 mL of AFW, fish were individually transferred to the test tanks.

The NTT apparatus consisted of six transparent tanks (12 x 10 x 1.5 cm) arranged in a rack (66 × 40 cm) and backlit with uniform LED illumination. Each tank was filled with 100 mL of AFW. Video recordings were acquired at 2 frames per second using a Mako 319 camera (Allied Vision) controlled by Pylon Viewer.

Behavioral trajectories were processed in DeepLabCut (Mathis et al., 2018) using custom labels. From each trajectory, the following metrics were extracted: vertical position (percent tank height), distance to surface, distance to walls, swimming speed, idle time, swim bursts, time in the top

third, and time near walls. Each feature was summarized as the mean value across the first six minutes following tank entry.

Differences between groups were evaluated using nonparametric statistics (Kruskal-Wallis omnibus tests with Dunn post hoc comparisons and Holm correction). In all analyses, behavioral separation between resilience groups was observed only in the stressed condition, consistent with resilience-specific differences emerging under challenge.

5. Immunohistochemistry and confocal imaging

Whole-brain neural activity was quantified using immunohistochemistry against pERK and total ERK (tERK), a method adapted from (Randlett et al., 2015). The pERK/tERK ratio provides a proxy for recent neuronal activation at cellular resolution.

5.1. Experimental cohorts and fixation

Larvae used for imaging were collected from the stress-resilience assay at 6 dpf. Stressed cohorts were exposed to 250 mM NaCl for 10 minutes, followed by a recovery period in artificial fish water lasting either 5 or 10 minutes. Control cohorts remained in artificial fish water for the entire 45-minute assay. Immediately after the designated recovery time, larvae were euthanized by rapid immersion in ice-cold water and fixed overnight at 4 °C in 10% neutral-buffered formalin. Samples were then rinsed three times in PBS containing 0.25% Triton X-100 (PBT) and stored in PBT at 4 °C until immunostaining.

5.2. Immunostaining protocol

Samples were permeabilized in 0.05% EDTA-Trypsin on ice for 45 minutes, blocked in serum-containing buffer, and incubated at 4 °C for three nights with primary antibodies against pERK and tERK (rabbit anti-pERK and mouse anti-tERK; 1:600). After three washes in PBT, larvae were incubated overnight at 4 °C with secondary antibodies (Alexa Fluor 488 goat anti-rabbit and Alexa Fluor 633 goat anti-mouse; 1:600). Following secondary incubation, samples were washed three times in PBT and stored at 4 °C until imaging. All experimental groups were processed in parallel using identical reagent batches and incubation times to minimize variability.

5.3. Confocal imaging

Stained larvae were mounted upright in 2% low-melting-point agarose within silicone ring spacers on glass slides. Whole-brain confocal images were acquired on a Zeiss LSM 700 microscope equipped with a 20x water-immersion objective. Each larva was imaged in two overlapping stacks, one covering the forebrain and midbrain and the other the hindbrain and anterior spinal cord.

Images were acquired at 0.33 x 0.33 x 1.00 μm (x, y, z) voxel resolution with consistent laser power, gain, and offset settings across animals within a replicate.

5.4. Image registration and signal normalization

Acquired image stacks were stitched into single 3D volumes and resampled to isotropic voxel resolution. The tERK channel served as the anatomical reference for alignment. Each brain was registered to the Z-Brain atlas (Randlett et al., 2015) using the Computational Morphometry Toolkit (CMTK) with parameters optimized for larval zebrafish brains. To improve anatomical precision, replicate-specific templates were generated by averaging a subset of well-registered scans and used as refined targets for a second registration pass.

After registration, voxel intensities were capped at the 99th percentile (plus an extra 5%) to reduce outlier influence and normalized across samples. pERK/tERK ratios were computed voxel-wise and used for subsequent voxel-level and region-level analyses.

Subsequent analyses used a neuron-focused subset of Z-Brain regions: from 294 atlas labels, peripheral ganglia were removed and entries that were non-parenchymal, fiber-dominated, lumen, meningeal, or vascular were excluded based on rule-based name filters, resulting in 218 regions for further analysis.

6. Depictions of neural substrates of stress resilience

6.1. PLS-DA region-set definition

Partial Least Squares Discriminant Analysis (PLS-DA) was run separately per replicate on z-scored regional pERK/tERK profiles. For each component, regions were ranked by absolute loading, the top 50 per replicate were selected, and only regions that appeared in the top 50 of both replicates with matching loading signs were kept. The resulting consensus sets define the *stress exposure* (PLS Component 1) and *stress resilience* (PLS Component 2) substrates used for downstream connectivity and graph analyses.

6.2. Functional connectivity and graph-theoretic analysis

Regional pERK/tERK values were z-scored within each fish and then combined by cohort to calculate group-level Pearson correlations across regions. To ensure robust coupling, only edges with $|r| \geq 0.40$ were kept (results are qualitatively similar for 0.35-0.45), and the same backbone was used for mesoscale and graph analyses. For mesoscale summaries, regions were mapped onto four brain macro-divisions (Telencephalon/Diencephalon/Mesencephalon/Rhombencephalon), correlations within each division pair were averaged using Fisher-z means, and contrasts were

defined as Stressed-Control for the Stress-Exposure set and Resilient-Vulnerable for the Stress-Resilience set. Thresholded matrices were treated as undirected, unweighted graphs. Computed metrics were density, global efficiency, Louvain modularity, and mean clustering (via the NetworkX library). Uncertainty was estimated via a 1000 fish-level bootstrap, recalculating correlations, graphs, and metrics for each resample. Degree-preserving Maslov-Sneppen rewires served as null models for small-worldness comparisons (efficiency ~ null; clustering > null). Node centrality was summarized using Katz centrality on group graphs. Additional details and robustness checks are available in **Manuscript II**.

7. Data availability and reproducibility

All experimental procedures, analysis scripts, and figure-generation code used in this thesis are available upon reasonable request. Raw and processed datasets are stored on institutional servers at the Department of Neuroscience, University of Copenhagen, and archived in compliance with institutional data management policies.

The behavioral and imaging analyses were implemented in Python using fully scripted and version-controlled workflows. Processing steps, from data curation and preprocessing to dimensionality reduction and network analysis, were implemented using modular code repositories, ensuring the reproducibility of all results. Statistical analyses, figure scripts, and configuration files are maintained in Git-managed directories, enabling direct re-execution of analyses from raw data to final figures.

All experiments adhered to standard operating procedures and were performed using fixed acquisition parameters within each replicate. Imaging, registration, and computational analyses followed established frameworks with consistent calibration and quality-control steps across datasets.

SUMMARY RESULTS AND DISCUSSION

The following sections provide a summary of the main results obtained during the PhD project, rather than a figure-by-figure repetition of the attached manuscripts. The focus is on the core findings that emerged across projects: (i) the development and characterization of a standardized behavioral assay and quantitative resilience score that separate stress-resilient from stress-vulnerable larval zebrafish, and (ii) the identification of brain-wide activity patterns and network organization associated with stress exposure and resilient recovery.

To avoid redundancy and respect authorship and copyright considerations, detailed methodological descriptions, full statistical outputs, and complete figure sets are not reproduced here. Instead, the summary emphasizes the most critical results for understanding the thesis's main goals and situating the work within the current state of the art. Readers are referred to Manuscripts **I** and **II**, included at the end of the thesis, for comprehensive accounts of the experimental design, analyses, and supplementary findings.

1. Behavioral quantification of stress resilience in larval zebrafish

1.1. A baseline-anchored Resilience Score for individual recovery

A central objective of the thesis was to obtain a principled behavioral measure of stress resilience that explicitly accounted for the stark inter-individual variability in spontaneous locomotion observed in larval zebrafish (Ingebretson and Masino, 2013; MacPhail et al., 2009). Current larval tests usually judge coping or resilience based on speed-related metrics sampled during recovery from stress, either by ranking individuals based on post-stress activity compared to the group or by referencing performance to unexposed controls (Swaminathan et al., 2023; Tudorache et al., 2015). Since baseline locomotor activity varies with genetic background, development, internal state, and environmental conditions (Andalman et al., 2019; Farrell et al., 2011), such approaches risked conflating trait-like differences in spontaneous movement with true variation in recovery from stress.

To address this limitation, the present work introduced a baseline-anchored stress resilience score (hereafter referred to as *resilience score*, for brevity) that quantified recovery as the relative change in swimming speed from each larva's own baseline to the early post-stress recovery window. By expressing recovery as a proportional rebound toward the pre-challenge state, this score treated resilience as a property of within-individual regulation rather than just a ranking of absolute post-stress speeds. In this approach, resilient outcomes corresponded to rapid restoration of baseline-

anchored locomotor activity after exposure, while vulnerable outcomes reflected prolonged suppression or incomplete rebound under matched challenge conditions.

This baseline normalization offered several conceptual advantages over prior approaches. First, it minimized the influence of developmental or strain-dependent differences in spontaneous locomotion, enabling comparisons of resilience across cohorts, transgenic lines, and experimental rounds without assuming identical baseline activity distributions. And, second, it aligned the behavioral definition of resilience with outcome-based frameworks in the broader stress literature, in which resilience is defined from post-challenge functioning relative to pre-challenge status rather than from the magnitude of acute reactivity alone (Charney, 2004; Kalisch et al., 2015; McEwen, 2007).

Within this framework, the three-phase assay (baseline, acute stress exposure, and recovery; Fig. 5A-B) primarily served to anchor the resilience score in a controlled context where exposure was standardized but outcomes varied. The emphasis was not on the characteristics of behavior during the stressor, but on how rapidly and to what extent individuals re-entered their own locomotor operating range once the challenge terminated (Kalisch et al., 2017). This design positioned the assay as a generalizable platform for resilience phenotyping that could be combined with whole-brain activity mapping, endocrine measurements, or pharmacological manipulations. In particular, it provided a direct link between individual recovery profiles and brain-wide pERK signatures and network organization examined in Manuscript **II**.

1.2. Distinct resilient and vulnerable recovery trajectories

Having defined a baseline-anchored resilience score that quantifies recovery at the individual level, the next step was to determine whether this continuous measure supported meaningful categorical distinctions between resilient and vulnerable trajectories. The distribution of resilience scores across assays was not unimodal but instead showed evidence of multiple modes, suggesting that larvae did not form a single continuum of recovery but clustered into partially discrete behavioral subsets. Rather than imposing a single cut-off relative to control animals, as is common in rodent and zebrafish literature (Golden et al., 2011; Krishnan et al., 2007; Swaminathan et al., 2023; Willmore et al., 2022), thresholds were chosen to isolate contrasting recovery profiles. Larvae with strongly negative scores (≤ -0.5) were labeled as vulnerable, reflecting persistent suppression of movement after stress. In contrast, larvae with higher scores (> 0.1) were labeled as resilient, reflecting rapid return toward their own baseline operating range (Fig. 5B). This conservative strategy retained approximately the top $\approx 20\%$ of the distribution as resilient and $\approx$

65% as vulnerable, leaving intermediate cases unlabeled, to maximize behavioral coherence within each group and thereby increase sensitivity for downstream analyses (Jacobs and Ryu, 2023). With these thresholds in place, resilient and vulnerable larvae could be compared across the three assay stages. Both groups displayed similar dynamics during baseline, with an initial decline in swimming speed followed by stabilization, consistent with habituation to the recording environment (Fig. 5B-C). During hyperosmotic exposure, average speed increased modestly and to a comparable extent in both groups. Thus, neither spontaneous locomotion nor immediate reactivity to the stressor distinguished resilient from vulnerable larvae. Divergence emerged only after stressor removal. In the early recovery window, resilient larvae exhibited a pronounced rebound in locomotion, rapidly approaching or surpassing their baseline speed, whereas vulnerable larvae maintained reduced activity and in many cases near-immobility.

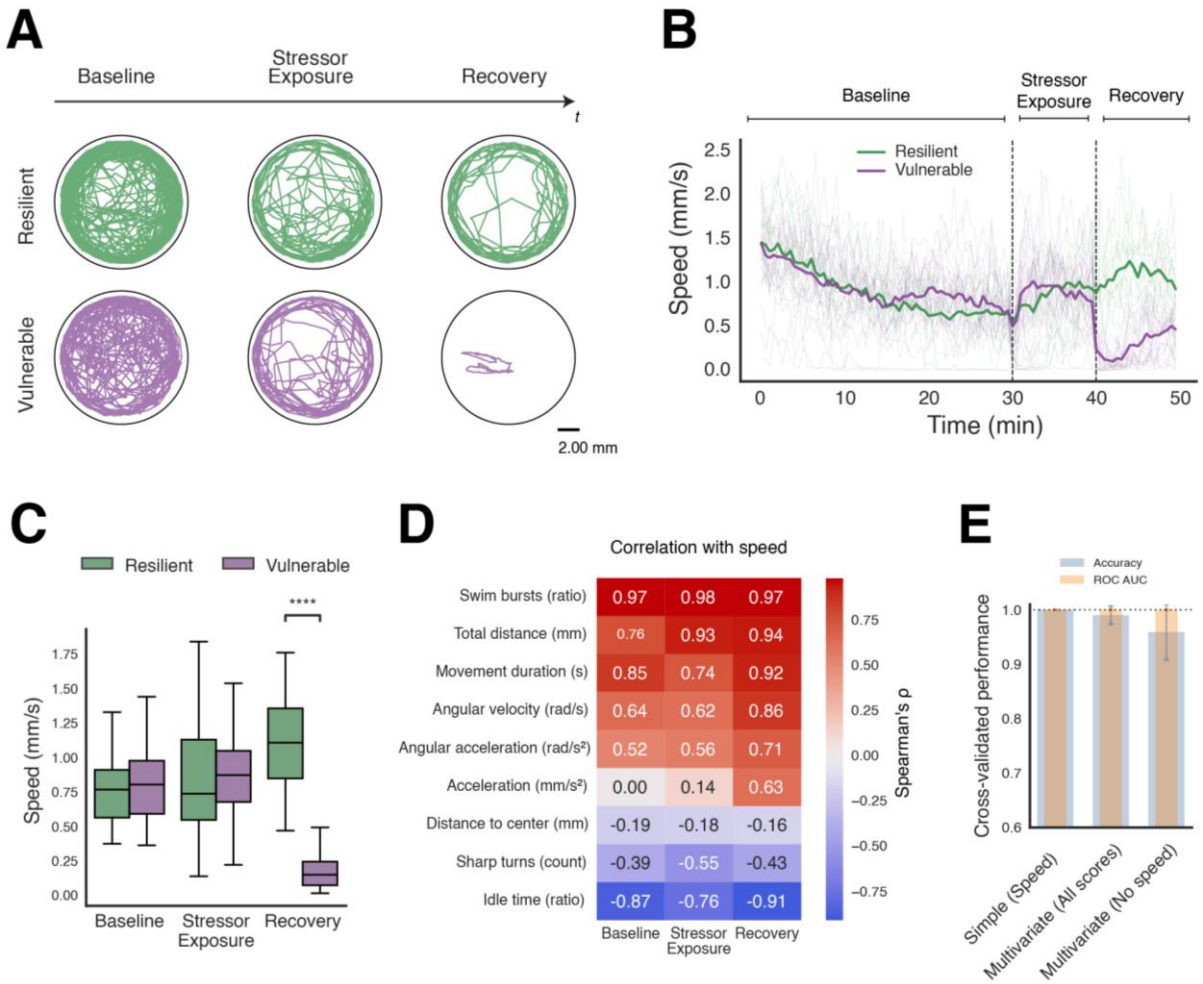

Figure 5. Stress-resilience assay design and behavioral readouts.

A. *Example trajectories for larvae classified as resilient (R; green) or vulnerable (V; purple) across assay stages: baseline (0-30 min), stressor exposure (30-40 min; 250 mM NaCl), and recovery (≥40 min).* ***B.*** *Swimming speed*

(mm/s) during the assay for resilient (green) and vulnerable (purple); thin lines are individual larvae, thick lines are group means. ***C.*** *Mean swimming speed (mm/s) per group within each stage (same animals as in B). Within-stage group differences: Welch's t-test at stressor exposure; Mann-Whitney U at baseline and recovery. Significance shown in the figure: **** $p < 0.0001$.* ***D.*** *Spearman correlations between swimming speed and other behavioral metrics across stages (baseline 10-30 min, stressor 30-40 min, recovery 40-45 min; same animals as in C).* ***E.*** *Cross-validated classification of resilient versus vulnerable from baseline-recovery behavioral scores. Shown are a single-feature reference model using Speed ("Simple: Speed") and two multivariate logistic models ("Multivariate: All scores" and "Multivariate: No speed"). Bars show mean balanced accuracy (blue) and ROC AUC (orange); error bars are SD across GroupKFold splits by assay. Sample sizes. R = 25; V = 52; total n = 77.*

This contrast extended to other behavioral metrics, as many are inherently linked to speed. Nevertheless, this begged the question of whether focusing on speed as the primary metric would omit relevant information or materially alter group assignments. Correlation analyses revealed that most behavioral features were tightly coupled to speed across all assay stages: distance traveled, movement duration, swim bursts, and angular velocity covaried positively with speed, whereas idle time was strongly negatively associated (Fig. 5D). Principal component analysis showed that a single latent component accounted for more than half of the variance. Moreover, when multivariate classifiers were trained on baseline-to-recovery change scores derived from all behavioral metrics to predict the speed-based labels, performance approached ceiling, and even models that excluded speed retained near-perfect accuracy (Fig. 5E). These findings suggest that the remaining metrics mainly reflect the classification derived from speed, providing limited independent criterion variance. Therefore, speed was kept as a simple and biologically interpretable summary of the main recovery dimension.

To further rule out trivial explanations related to physical impairment, a longer assay with 45 minutes of recovery was conducted. In this setup, resilient and vulnerable larvae once again showed a clear difference during the initial post-stress period, with vulnerable fish displaying sustained reduction in movement over the first 10-15 minutes (Fig. 6A-B). However, with additional time both groups gradually matched each other's swimming speeds, and no persistent activity deficit was observed in the vulnerable group. This delayed recovery suggests that irreversible saltwater damage or major motor impairment is unlikely to be the cause of vulnerability. Instead, it supports the interpretation that resilient and vulnerable phenotypes mainly differ in the timing and regulation of recovery, rather than in their overall ability to return to baseline locomotor activity.

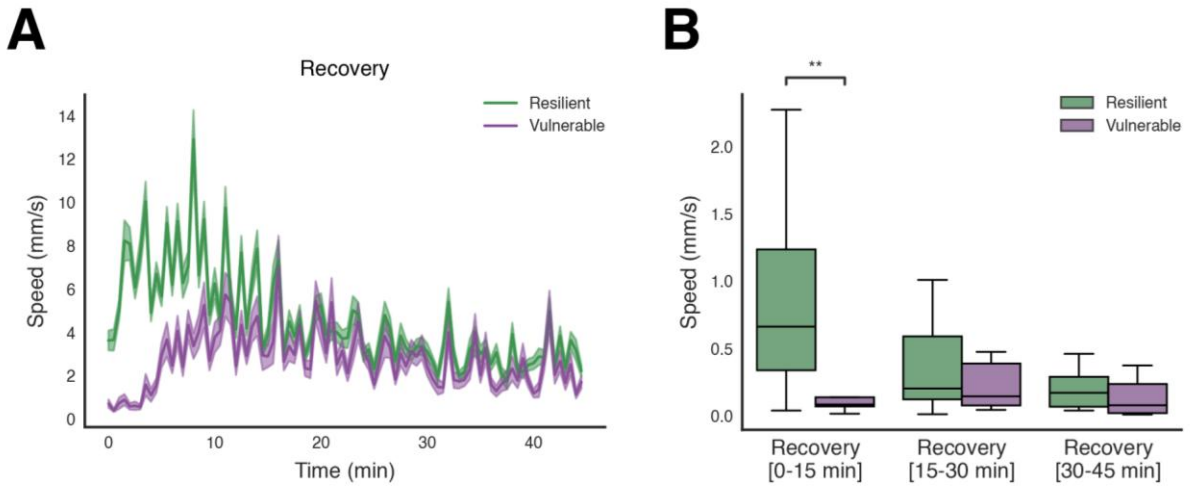

Figure 6. Extended recovery dynamics.

A. *Speed during the extended recovery (0-45 min) for resilient (R; green) and vulnerable (V; purple); mean ± SEM.* ***B.*** *Boxplots of per-fish mean speed across recovery windows (0-15, 15-30, 30-45 min). Within-window group differences tested with Student's t (0-15 min) and Mann-Whitney U (15-30 and 30-45 min). Significance shown in the figure: ** $p < 0.01$. Sample sizes. Panels A-B (same animals as Figure 1C-E): R = 25; V = 52; total = 77. Panels C-D: R = 28; V = 13.*

1.3. Robustness across genotypes, stressor types, and intensities

Once a baseline-anchored resilience score and distinct recovery trajectories had been established, the question arose whether this metric provided a stable basis for comparing resilience across genetic backgrounds and experimental conditions. The assay was designed primarily for use in unpigmented larvae amenable to whole-brain imaging, and initial tests therefore focused on nacre and Tg(elavl3:GCaMP6s) fish on a nacre background. Resilience score distributions and the proportions of resilient and vulnerable individuals were comparable across these lines, indicating that the index captured individual differences in recovery without being strongly biased by this transgenic manipulation (Fig. 7A-B). These findings are consistent with previous work reporting similar resilience-like measures across wildtype AB and Tüpfel longfin strains (Swaminathan et al., 2023), and suggest that, at least under the relatively strong osmotic challenge used here, the assay is robust to moderate genetic variation. At the same time, strain-dependent differences in stress reactivity and sensitivity have been documented in zebrafish (Gorissen et al., 2015; Vignet et al., 2013), and the lack of detectable variation in the present context may partly reflect ceiling effects imposed by the high-intensity stressor. The current results, therefore, support the use of the resilience score for comparing nacre-based lines, while leaving open the possibility that lower-intensity challenges or additional backgrounds would reveal more pronounced strain-specific modulation.

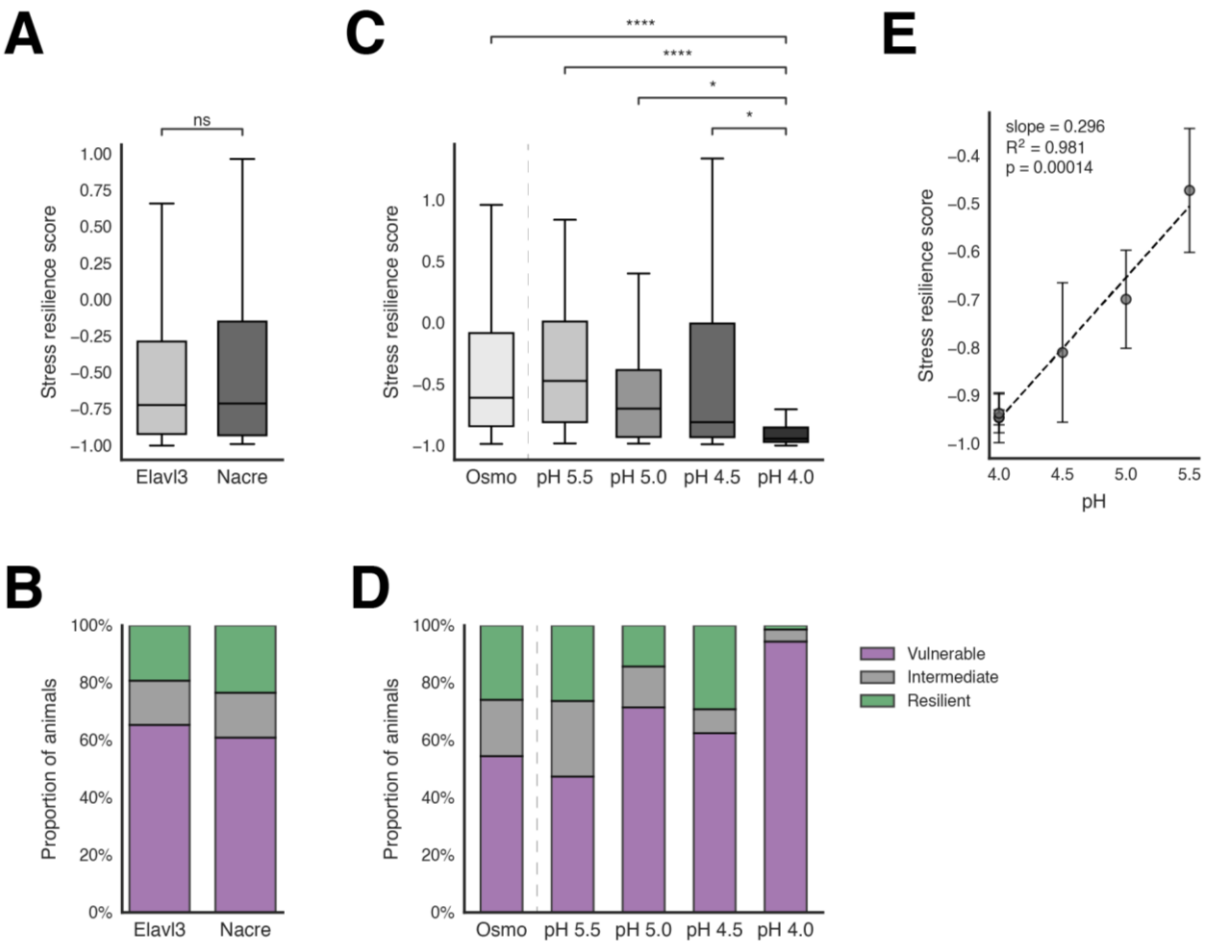

Figure 7. Consistency of the resilience score across zebrafish transgenic lines and stressors.

A. *Distribution of resilience scores by strain under an osmotic stressor (250 mM NaCl): Tg(elavl3:GCaMP6s) vs nacre. Mann-Whitney U with Holm correction; rank-biserial r reported.* ***B.*** *Proportions of vulnerable, intermediate, and resilient classifications by strain (totals as in A).* ***C.*** *Resilience scores in nacre under different stressors: osmotic (250 mM NaCl) and acid (pH 5.5, 5.0, 4.5, 4.0). Kruskal-Wallis omnibus; Dunn post-hoc with Holm adjustment (brackets show adjusted p). Significance shown in the figure: * $p < 0.05$; **** $p < 0.0001$.* ***D.*** *Proportions of vulnerable, intermediate, and resilient classifications by stressor (totals as in C).* ***E.*** *Resilience score vs pH (assay-level median ± SEM) with linear fit (slope, R^2, and p shown on plot). Sample sizes. Panels A-B: Tg(elavl3:GCaMP6s) n = 260; nacre n = 64. Panels C-D (nacre): Osmotic n = 189; pH 5.5 n = 19; pH 5.0 n = 21; pH 4.5 n = 24; pH 4.0 n = 71. Panel E: assay-level medians from the acid-stressor conditions in C-D.*

The resilience score also provided a quantitative readout of how behavioral recovery scaled with stressor characteristics (Fig. 7C-E). When larvae were exposed to graded levels of acute osmotic stress, resilience score distributions shifted systematically with increasing intensity (Yeh et al., 2013). Mild stress conditions yielded average scores and proportions of resilient and vulnerable larvae like those observed in the standard 250 mM saltwater assay, whereas stronger challenges produced lower mean scores and a higher fraction of vulnerable individuals. In other words, as the

stressor became more severe, fewer fish achieved rapid baseline-anchored rebound, and more exhibited prolonged suppression of locomotion. This parametric relationship between challenge level and resilience capacity aligns with previous observations that longer or more intense stress exposures reduce the proportion of resilient animals in both zebrafish and mammalian paradigms (Cheng et al., 2022; Swaminathan et al., 2023), and is consistent with allostatic frameworks in which resilience is constrained by the cumulative load imposed by the stressor.

1.4. Developmental progression and predictive value of early resilience labels

The resilience score and related recovery trajectories were next analyzed across development to determine whether early-life classifications captured transient states or more stable traits (Fig. 8A). When the same cohorts were reassessed at 14 dpf using the same saltwater challenge and baseline-anchored recovery metric, the overall distribution of resilience scores shifted downward, with most larvae now falling into the vulnerable range (Fig. 8B-C). This indicated a general age-related decline in rapid locomotor rebound rather than a simple reshuffling of individuals between categories. Within this compressed distribution, however, the groups defined at 6 dpf maintained a clear order: batches initially labeled as resilient remained, on average, higher-scoring than age-matched controls and tended to outperform previously vulnerable batches. Similarly, at the individual level, stress resilience scores normalized against the control population indicated that larvae from resilient batches remained more resilient than those from vulnerable batches (Fig. 8D). The attenuated separation at 14 dpf may reflect a behavioral transition in which coping-related systems are being reorganized: around this period, zebrafish show emerging social preference, shifts in dark-light behavior, and changing responsivity to challenges (Dreosti et al., 2015; Varga et al., 2020). A non-mutually exclusive explanation is cumulative husbandry load: routine handling elevates whole-body cortisol, housing density can act as a low-grade stressor, and time-of-day or feeding schedules measurably shift larval locomotor readouts, which could compress recovery phenotypes if not tightly standardized and logged (Andersson et al., 2022; Ramsay et al., 2009; S. de Abreu et al., 2024).

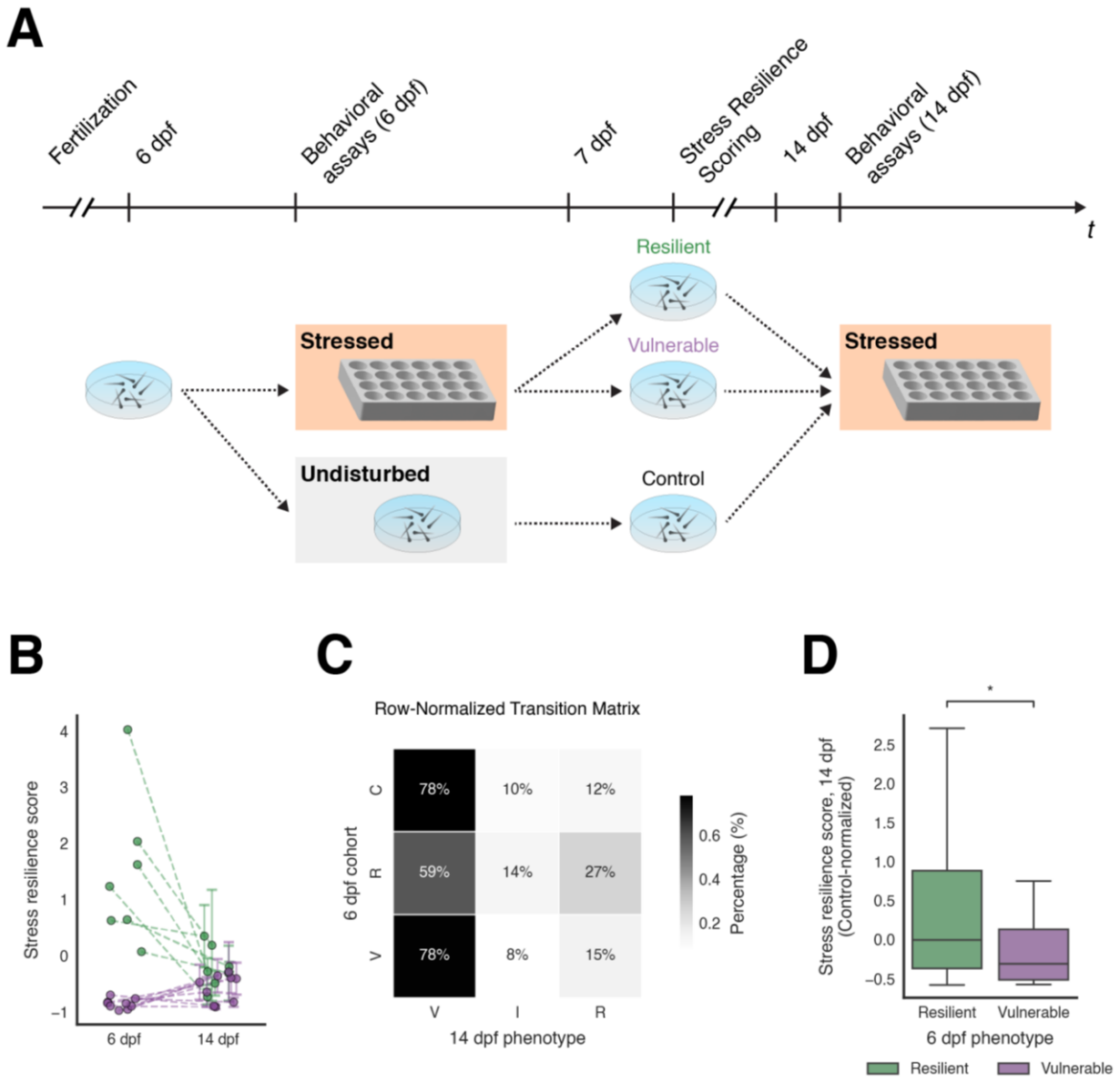

Figure 8. Consistency of stress resilience phenotypes during early larval development

A. *Experimental design. Larvae classified at 6 dpf as resilient (R), vulnerable (V), or undisturbed controls (C) were raised in Petri dishes and re-assayed at 14 dpf.* ***B.*** *Cohort-level stress-resilience scores from 6 to 14 dpf. Each line links one 6 dpf cohort to its 14 dpf outcome (R, green; V, purple). Left dots are 6 dpf cohort medians; right dots are 14 dpf cohort means ± SEM; slight horizontal jitter reduces overlap. Scores are z-scored to the 14 dpf control distribution.* ***C.*** *Transition matrix from 6 dpf cohorts (rows) to 14 dpf phenotypes: control (C), resilient (R), intermediate (I), vulnerable (V). Cells show row-normalized percentages.* ***D.*** *14 dpf resilience scores grouped by 6 dpf origin (z-scored to the 14 dpf control distribution). Groups compared with one-sided Mann-Whitney U (R > V). Significance shown in the figure: * $p < 0.05$. Sample sizes. Panel B: R = 38, V = 40 (cohort pairs: R, k = 7; V, k = 9). Panels C-D: C = 93, R = 38, V = 40.*

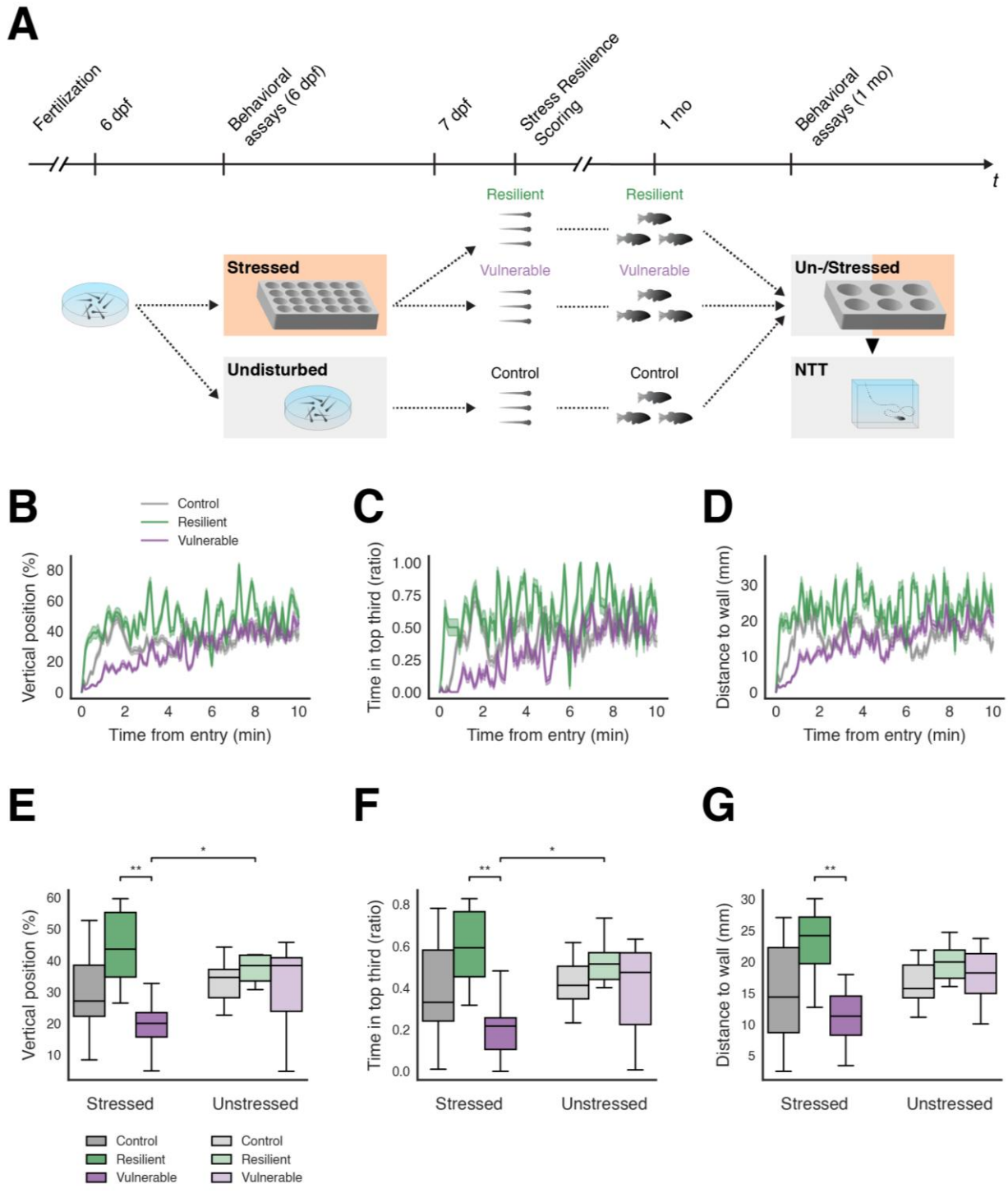

Figure 9. Anxiety-like responses of resilient and vulnerable groups in the novel tank test

A. *Experimental design. Larvae labelled at 6 dpf as control (C), resilient (R), or vulnerable (V) were reared ~1 month, assigned to stressed (S; 10-min 250 mM NaCl) or unstressed (U; 10-min AFW) cohorts, rested 5 min, and tested in the novel tank test.* ***B-D.*** *Time course for vertical position (% tank height; B), time in top third (ratio, C), and distance to nearest wall (mm, D) over 0-10 min from entry for S-C, S-R and S-V fish; lines show group means ± SEM over 5 second bins.* ***E-G.*** *Boxplots summarizing vertical position (% tank height) per group, computed as each fish's mean over 0-6 min from its own tank entry, split by Stressed vs Unstressed conditions. Within-group differences used*

*Kruskal-Wallis omnibus with Dunn post-hoc and Holm adjustment (brackets show adjusted p). Significance shown in the figure: * $p < 0.05$; ** $p < 0.01$. Sample sizes. S-C = 13, S-R = 6, S-V = 10, U-C = 13, U-R = 6, U-V = 9.*

To determine whether larval resilience classifications have predictive value beyond the early larval stage, individuals labeled as resilient, vulnerable, or control at 6 dpf were reared to one month and evaluated in a NTT under baseline and post-stress conditions (Fig. 9A). In the absence of an acute challenge, juveniles from all three groups exhibited similar anxiety-like behaviors, with comparable vertical distributions and proximity to the tank walls. Therefore, early resilience labels did not result in noticeable differences in baseline exploratory drive or anxiety-like measures in this assay. In contrast, when the novel tank was introduced immediately after acute saltwater exposure, juveniles classified as resilient at 6 dpf showed a more exploratory profile than their vulnerable siblings, with controls generally falling between the two. Resilient fish entered and occupied higher regions of the water column earlier in the session (Fig. 9B, E), spending more time in the upper third portion of the tank (Fig. 9C, F), and swam farther from the walls (Fig. 9D, G). In contrast, vulnerable fish ascended more slowly and stayed closer to the boundaries before gradually converging later in the test.

Together, these developmental observations suggest that the larval resilience phenotype captures more than a transient response to a single stressor. Despite an overall decline in resilience at 14 dpf and reduced separability at this transitional stage, larvae initially classified as resilient tend to retain relatively higher resilience scores across early development and later adopt a more proactive, challenge-evoked exploratory strategy as juveniles. Conversely, vulnerable larvae do not differ markedly in baseline anxiety-like behavior but appear less inclined to engage with a novel environment immediately after stress. This pattern is consistent with the idea that early individual differences in recovery from acute challenges foreshadow longer-term coping styles, and supports the use of the larval assay as a developmental entry point for studying how resilience and vulnerability trajectories emerge and are maintained over time (Fitzgerald et al., 2019; Swaminathan et al., 2023; Tudorache et al., 2015).

2. Brain-wide neural and network correlates of active resilience

2.1. A stress exposure network engaging sensory and HPI-axis regions

The second main objective of the thesis was to leverage the newly developed stress resilience scores to identify the neural substrates engaged by acute stress and to distinguish these generalized stress responses from resilience-specific signatures. To this effect, 6 dpf larvae were exposed to the same three-phase protocol used to define resilience classes, with 250 mM NaCl serving as the

stressor medium. Immediately after 5- or 10-minute recovery windows, larvae were euthanized, fixed, and processed for whole-mount immunohistochemistry against pERK and total ERK (tERK), followed by confocal imaging of the entire brain volume (Fig. 10A). Brain-wide pERK/tERK ratios were then extracted and registered to the Z-Brain atlas template, enabling voxel-wise and region-wise comparisons across conditions (Randlett et al., 2015). The two time points were chosen to sample the early rise/decay regime of pERK, which in larval zebrafish peaks within 2-5 min after brief stimulation and declines toward baseline by 30 min, providing an initial view of decay kinetics relevant to resilience-linked shutdown.

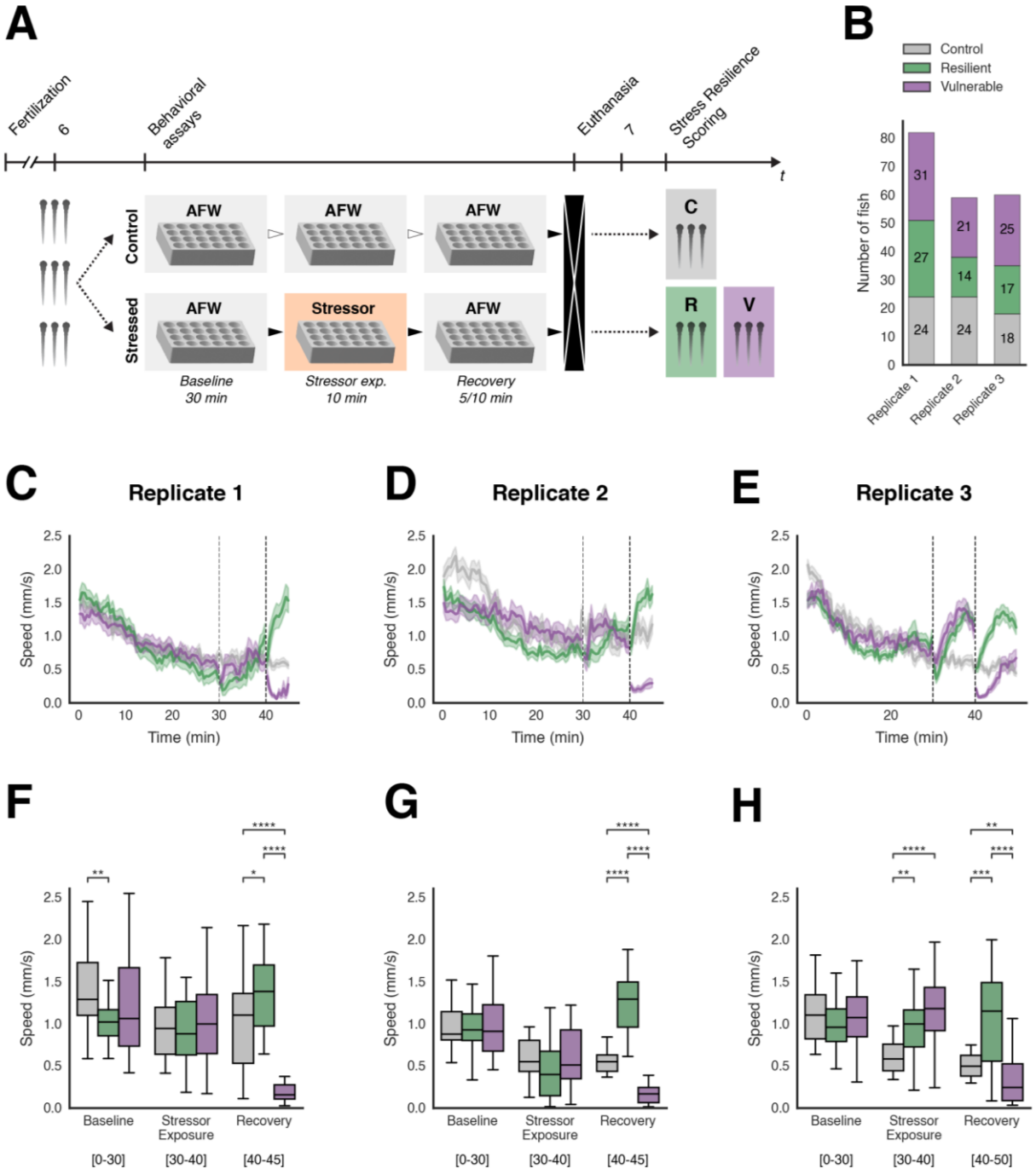

Figure 10: A stress recovery assay separates stress-resilient and -vulnerable zebrafish larvae.

A. *Experimental workflow. Larvae undergo a three-phase assay: Baseline (30 min in artificial freshwater, AFW), Stressor exposure (10 min in 250 mM NaCl), and Recovery (5 or 10 min in AFW). In parallel, control fish remain undisturbed in AFW for 45 min. After the assay, all fish are euthanized and the following morning, categorized as resilient or vulnerable based on locomotor rebound during recovery; brains are then processed for ex vivo pERK immunohistochemistry. Time in days post-fertilization (dpf).* ***B.*** *Numbers of animals per experimental replicate stacked by resilience class. Replicate 1: control, n=24; resilient, n=27; vulnerable, n=31; Replicate 2: control, n=24; resilient, n=14; vulnerable, n=21.* ***C-E.*** *Time-binned average swimming speed (mm/s) across assay phases for replicate 1 (C), replicate 2 (D), and replicate 3 (E). Vertical dashed lines mark the boundaries between the assay phases (baseline, 0-30 min; stressor exposure 30-40 min; recovery, 40-45 min for replicates 1 and 2, 40-50min for replicate 3).* ***F-H****. Swimming speed (mm/s) across assay phases for each replicate (F, replicate 1; G, replicate 2; H. replicate 3). Within each phase, groups were compared with a Kruskal-Wallis test; when significant, pairwise Mann-Whitney U tests with Benjamini-Hochberg FDR correction were applied. Significance: *p < 0.05; **p < 0.01; ***p*

*< 0.001; ***p < 0.0001. Sample sizes: replicate 1 (control, n=24; resilient, n=27; vulnerable, n=31), replicate 2 (control, n=24; resilient, n=14; vulnerable, n=21), replicate 3 (control, n=18; resilient, n=17; vulnerable, n=25).*

Across both 5 min recovery datasets (termed replicates 1 and 2), voxel-wise contrasts between stressed larvae (resilient or vulnerable groups) and unstressed controls revealed a reproducible stress-exposure network with elevated pERK/tERK in forebrain and diencephalic territories implicated in sensory detection and endocrine signaling (Fig. 11A-B). Hyperosmotic challenge was accompanied by robust activation of the olfactory bulbs and the posterior dorsomedial pallium, as well as the preoptic and hypothalamic nuclei and the habenulae; convergence across biological replicates indicates a common response to saltwater exposure rather than resilience-specific modulation.

The regional profile of this network aligns with established osmotic-stress processing in larvae: saltwater at comparable concentrations drives avoidance via olfactory detection of sodium and chloride, and elevates whole-body cortisol (Herrera et al., 2021; Vom Berg-Maurer et al., 2016; Yeh et al., 2013). Accordingly, preoptic neuroendocrine territories and the habenula-olfactory axis are strongly recruited (Alsop and Vijayan, 2008; Yeh et al., 2013). The right habenula's olfactory inputs in zebrafish provide an anatomically plausible route by which odorant cues couple to aversive avoidance and HPI engagement (Kermen et al., 2013).

2.2. Resilience-specific engagement of premotor brainstem circuits

Next, we contrasted pERK levels within the exposed cohort to isolate recovery-linked differences (resilient vs vulnerable; Fig. 11C; Fig. 12A-B). At 5 min post-offset, resilient larvae showed higher pERK in the caudal hypothalamus (CH) and paraventricular organ. In the brainstem, resilient animals also exhibited stronger signals in the ventrolateral stripe of serotonergic neurons in the rhombencephalon, as well as in descending premotor nodes - reticulospinal clusters (RoM1, RoV3, RoM2) and the nucleus of the medial longitudinal fasciculus (nMLF) - with additional increases in hindbrain Gad1b^{+} and Glyt2^{+} inhibitory clusters. Identified reticulospinal neurons, including RoV3/MiV2, causally contribute to turning and early bout initiation (Huang et al., 2013; Liu and Fetcho, 1999), while the nMLF gates posture/steering and modulates swim speed and locomotor commands (Severi et al., 2014; Thiele et al., 2014). Hypothalamic monoaminergic populations can acutely promote swimming and bias stimulus-evoked behaviors in larvae, consistent with the observed CH/paraventricular engagement (Barrios et al., 2020; Wee et al., 2019). Taken together, these patterns point to earlier recruitment of hypothalamic control, monoaminergic arousal circuitry, descending command systems, and local inhibitory gain during the rebound phase in

resilient fish, while recognizing that not all clusters meet identical thresholds across replicates and time points.

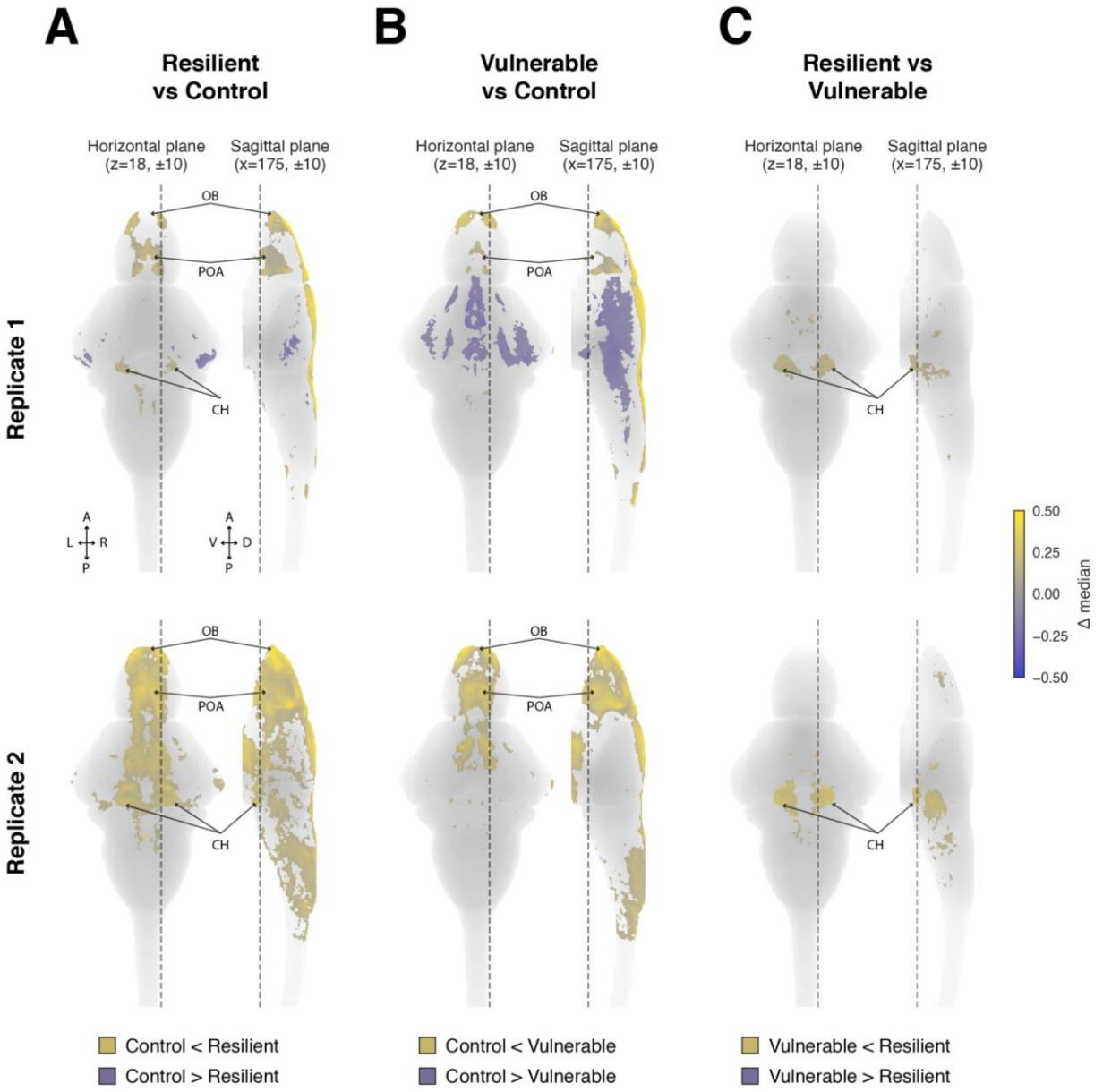

Figure 11: Brain-wide differences in neural activity between resilience groups

Maps of pairwise significant differences in pERK levels between resilience groups. Horizontal (left panels) and sagittal (right panels) projections are shown, with replicate 1 at the top and 2 at the bottom. ***A****. Significant differences between the resilient and control groups.* ***B****. Significant differences between vulnerable and control groups.* ***C****. Significant differences between resilient and vulnerable groups. Colors indicate the median difference between groups in each comparison. Slices are averaged over ±10 slices around the specified planes (horizontal: z=18; sagittal: x=175). OB: olfactory bulbs; POA: preoptic area; CH: caudal hypothalamus. Replicate 1 (control, n=21; resilient, n=22; vulnerable, n=31); replicate 2 (control, n=21; resilient, n=12; vulnerable, n=20).*

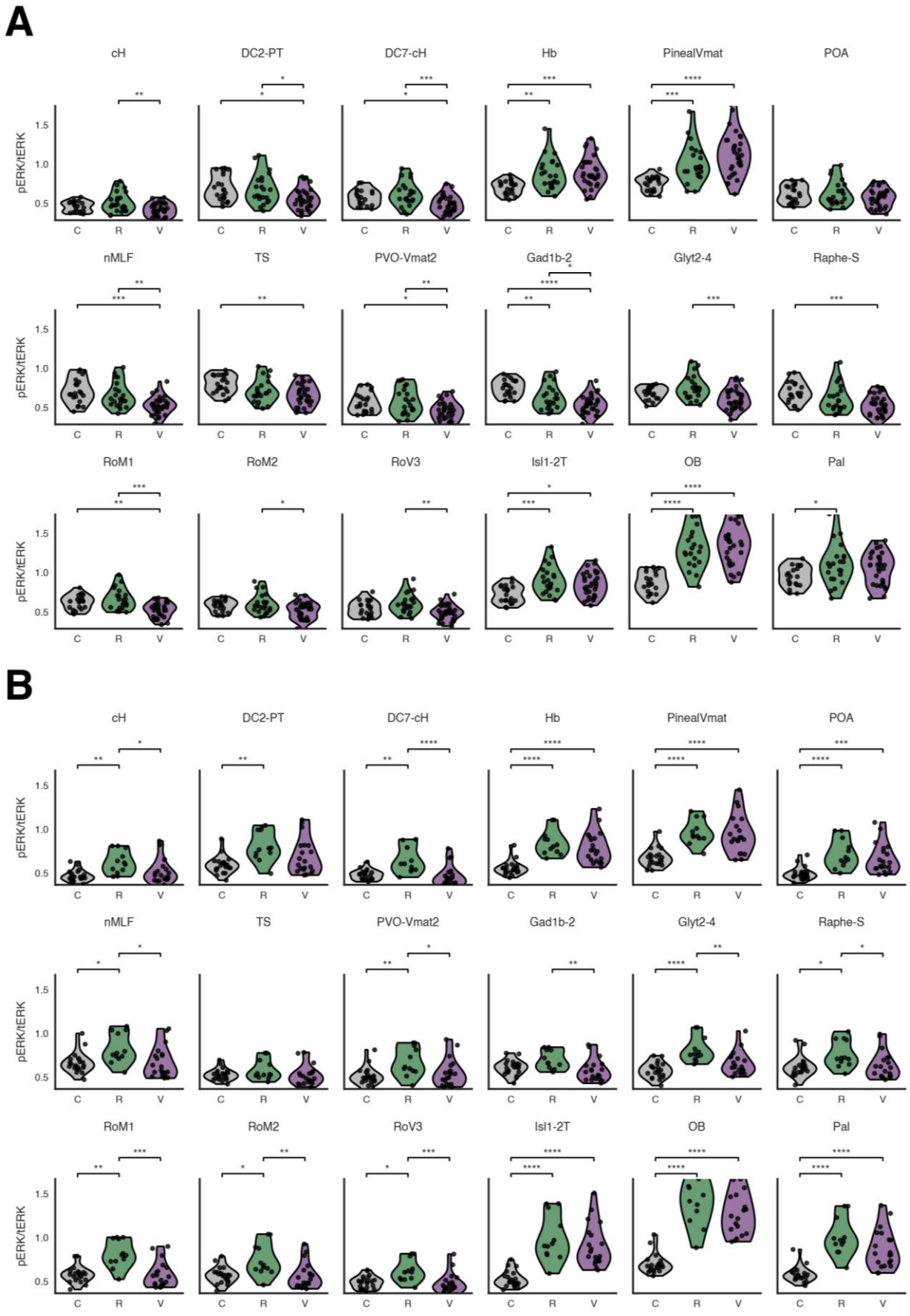

Figure 12: Regional pERK/tERK differences across stress-resilience groups (5 minutes recovery).

A-B. *Violin plots show the distribution of the median pERK/tERK ratio per fish for selected Z-Brain regions in Replicate 1 (A) and Replicate 2 (B). Points are individual fish; violins depict kernel density. Groups: control (C, grey), resilient (R, green), vulnerable (V, purple). Horizontal brackets indicate pairwise group comparisons with Holm-adjusted p values; asterisks denote significance (p < 0.05 *, < 0.01 **, < 0.001 ***, < 0.0001 ****). Included regions are: CH, caudal hypothalamus; DC2-PT, dopaminergic cluster 2 (posterior tuberculum); DC7-cH, dopaminergic cluster 7 (caudal hypothalamus); Hb, habenulae; PinealVmat, pineal Vmat2 cluster; POA, preoptic area; nMLF, nucleus of the medial longitudinal fasciculus; TS, torus semicircularis; PVO-Vmat2, paraventricular organ Vmat2 cluster; Gad1b-2, Gad1b cluster 2; Glyt2-4, Glyt2 cluster 4; Raphe-S, superior raphe; RoM1/2 and RoV3, reticulospinal neurons of medial (M) and ventral (V) nuclei; Isl1-2T, telencephalic Isl1 cluster 2; OB, olfactory bulb; Pal, pallium. Replicate 1 (control, n=21; resilient, n=22; vulnerable, n=31); replicate 2 (control, n=21; resilient, n=12; vulnerable, n=20); replicate 3 (control, n=18; resilient, n=17; vulnerable, n=25).*

2.3. Dopaminergic correlates and translational links to mesolimbic systems

The voxel-wise contrasts and single-region comparisons discussed above identified several candidate regions associated with acute stress exposure and early recovery. However, they also revealed many spatially scattered differences that were difficult to interpret coherently. To create a more concise and anatomically meaningful representation of how regional activity patterns differentiate the experimental groups, regional pERK/tERK profiles were analyzed using Partial Least Squares Discriminant Analysis (PLS-DA). This method explicitly maximizes separation between predefined classes while retaining a linear relationship between regional activity and latent components.

For each 5-minute recovery dataset, PLS-DA was applied to within-fish z-scored regional pERK/tERK matrices to emphasize relative regional profiles over global intensity differences. In both biological replicates, the resulting embedding showed the same structure: the first component separated saltwater-exposed larvae (resilient and vulnerable combined) from unstressed controls, whereas the second component separated resilient from vulnerable fish along an orthogonal axis, with high cross-validated performance and permutation nulls failing to reproduce the observed separation (Fig. 13A-B). Component 1 was therefore interpreted as a *stress exposure* axis and Component 2 as a *stress resilience* axis. To link these latent dimensions to anatomically defined substrates, regions were ranked by absolute loading for each replicate, the top 50 contributors were extracted, and consensus sets were defined by retaining only regions that appeared in the top 50 of both replicates with the same loading sign. This yielded 21-region (Fig. 13C) and 25-region (Fig. 13D) consensus sets for the stress exposure and resilience components, respectively, providing replicate-robust region lists for downstream connectivity and graph-theoretical analyses while preserving transparent mapping between components and their underlying regional activity patterns.

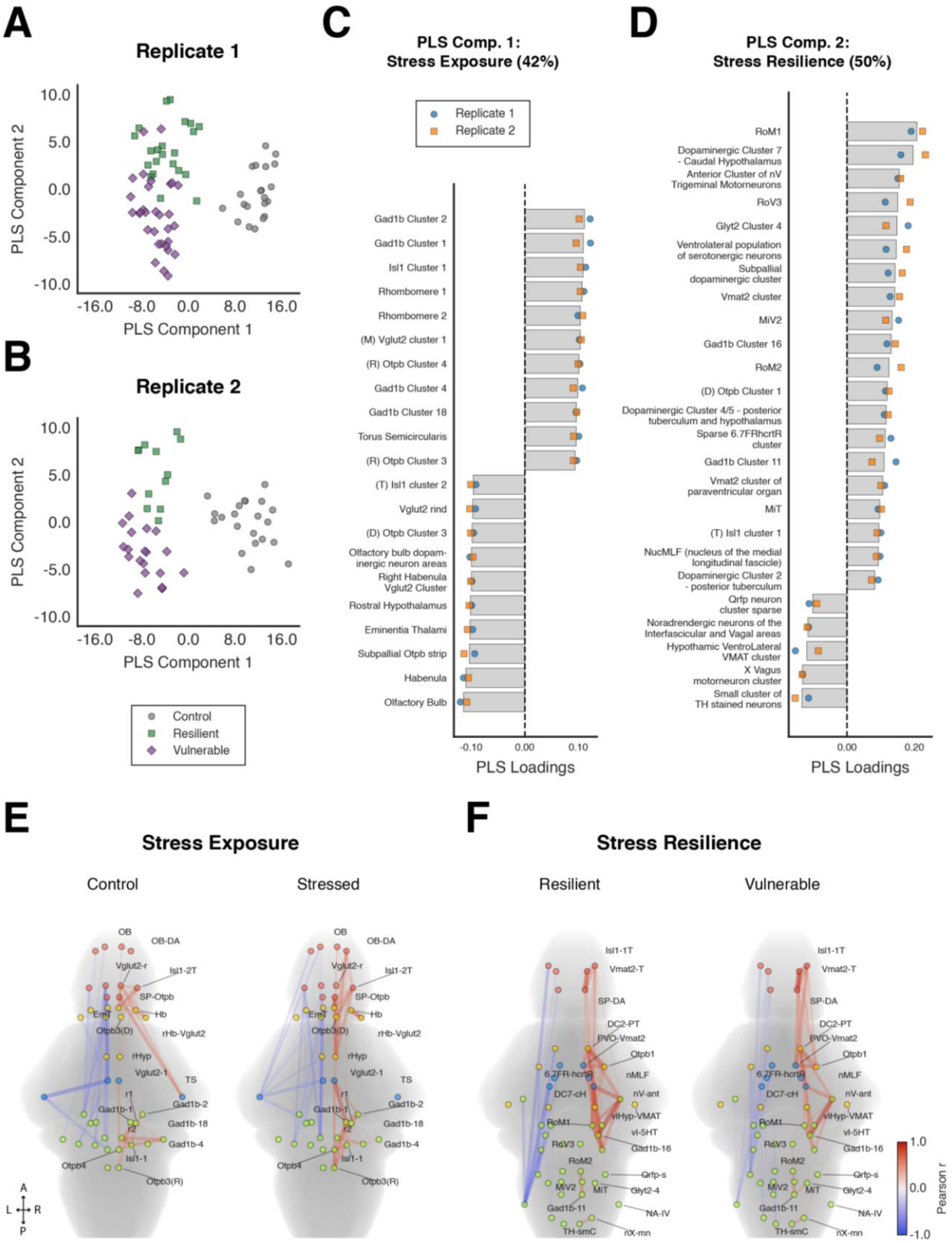

Figure 13: Partial Least Squares Discriminant Analysis (PLS-DA) embedding and region loadings across experimental replicates.

A-B. *PLS-DA embeddings by experimental replicate using region-level ERK ratios across 218 filtered Z-Brain regions* (Randlett et al., 2015). *A, Replicate 1. B, Replicate 2. Each point is a single fish, colored and shaped by group (control:*

gray circles; resilient: green squares; vulnerable: purple diamonds). Axes show PLS Components 1 and 2. ***C-D.*** *Consensus region sets for each PLS component. For each replicate, the top 50 regions by absolute loading were identified for the component. Regions were retained only if they (i) appeared in the top-50 of both replicates and (ii) had the same loading sign in both replicates. C, PLS Component 1 - Stress Exposure (21 regions). D, PLS Component 2 - Stress Resilience (25 regions). Percentages above each panel indicate the proportion of overlapping regions between replicates out of the top 50 contributors. Bars show the average loading across both replicates for each overlapping region (dashed line at 0). Overlaid markers denote per-replicate loadings for the same region (Replicate 1: blue circles; Replicate 2: orange squares).* ***E-F.*** *Anatomical projections of functional connectivity networks derived from the consensus region sets. E, Component 1 - Stress exposure network: correlations shown separately for control and stressed (resilient + vulnerable combined) groups. F, Component 2 - Stress resilience network: correlations shown separately for resilient and vulnerable groups. Each dot represents the centroid of a brain region. Edges represent strong functional connectivity between pairs of brain regions (only strong positive or negative Pearson correlations with* $|r| \geq 0.40$ *are displayed). Negative correlations are shown on the left half of the brain in blue; positive correlations are shown on the right in red. The thickness of edges is proportional to the* $|r|$ *value. Region abbreviations for E-F follow Supplementary Table 1. Replicate 1 (control, n=21; resilient, n=22; vulnerable, n=31); replicate 2 (control, n=21; resilient, n=12; vulnerable, n=20).*

Consistent with the univariate contrasts described earlier, the stress exposure component was dominated by sensory and hypothalamic elements of the osmotic-stress response. Regions with negative loadings on Component 1, corresponding to higher relative activation in stressed fish, included the olfactory bulbs, right habenula, rostral hypothalamus, and Otpb and Vglut2^{+} clusters in preoptic and forebrain areas. Positive loadings, indicating higher relative activity in controls, were enriched for Gad1b-positive inhibitory populations, Isl1-expressing motor and hypothalamic groups, rhombomeric segments, and the torus semicircularis. In contrast, the resilience component primarily recruited posterior brainstem and hypothalamic territories, together with dopaminergic populations in the caudal hypothalamus and posterior tuberculum, as well as additional telencephalic dopaminergic clusters. Most regions in this resilience consensus set carried positive loadings, indicating greater relative activity in resilient than in vulnerable fish. These included reticulospinal nodes such as the nMLF, RoM1, RoM2, RoV3, and MiT, glycinergic and GABAergic hindbrain clusters (e.g., Glyt2 Cluster 4, Gad1b Clusters 11 and 16), and dopaminergic clusters in the CH (Cluster 7) and posterior tuberculum (Clusters 2 and 4/5).

Thus, PLS-DA multivariate analysis highlighted a dopaminergic-noradrenergic opponency that dovetails with broader vertebrate resilience models. On the resilience axis, telencephalic and diencephalic dopaminergic clusters, particularly in the CH and posterior tuberculum, emerge among the most discriminative regions, with higher relative activity in resilient fish. This pattern is reminiscent of the mammalian mesolimbic system, where ventral tegmental area-nucleus accumbens circuits promote active coping and stress resilience (Cao et al., 2010; Chaudhury et al.,

2013; Friedman et al., 2016; Krishnan et al., 2007). Although zebrafish lack midbrain dopaminergic neurons, ventral telencephalic and diencephalic dopaminergic groups have been proposed as functional analogues in social and motivational contexts (Geng and Peterson, 2019), and their association here with resilient rebound suggests that dopamine's role in facilitating adaptive responses to stress may be conserved across vertebrates. Conversely, the resilience component assigned higher loadings to a noradrenergic region of the medulla oblongata in vulnerable animals, a territory previously shown to respond robustly to aversive experiences such as repeated swim failures or acoustic/vestibular stimuli and to bias behavior toward suppression via activation of adjacent radial glia (Chen et al., 2024; Mu et al., 2019; Orts-Del'Immagine et al., 2022). Taken together, these multivariate patterns support a model in which resilient trajectories are characterized by preferential engagement of hypothalamic and telencephalic dopaminergic circuits coupled to premotor brainstem centers. In contrast, vulnerable trajectories recruit medullary noradrenergic systems linked to sustained immobility, thereby embedding the zebrafish findings within a cross-species framework of approach-versus-withdrawal-oriented stress responses.

2.4. Network architecture and hypothalamic-brainstem coupling in resilience

To move beyond region-by-region effects, regional pERK/tERK values within the PLS-DA-derived stress exposure and resilience consensus sets were used to construct functional connectivity graphs, with edges defined as strong pairwise correlations ($|r| \geq 0.40$) between regions (Fig. 13E-F). For each component and phenotype, these graphs were summarized using standard graph-theoretical measures, and their topologies were compared with degree-preserving random null networks to assess whether they exhibited small-world organization. Across both the stress exposure and resilience components, control, stressed, resilient, and vulnerable graphs showed comparable density and global efficiency, with clustering coefficients systematically higher than in their randomized counterparts and global efficiency of similar magnitude (Fig. 14A-B, E-F). Thus, at the chosen backbone threshold, all groups combined random-like efficiency with elevated local clustering, consistent with the small-world architecture commonly observed in activity-derived brain graphs (Betzel, 2020; Terstege et al., 2022).

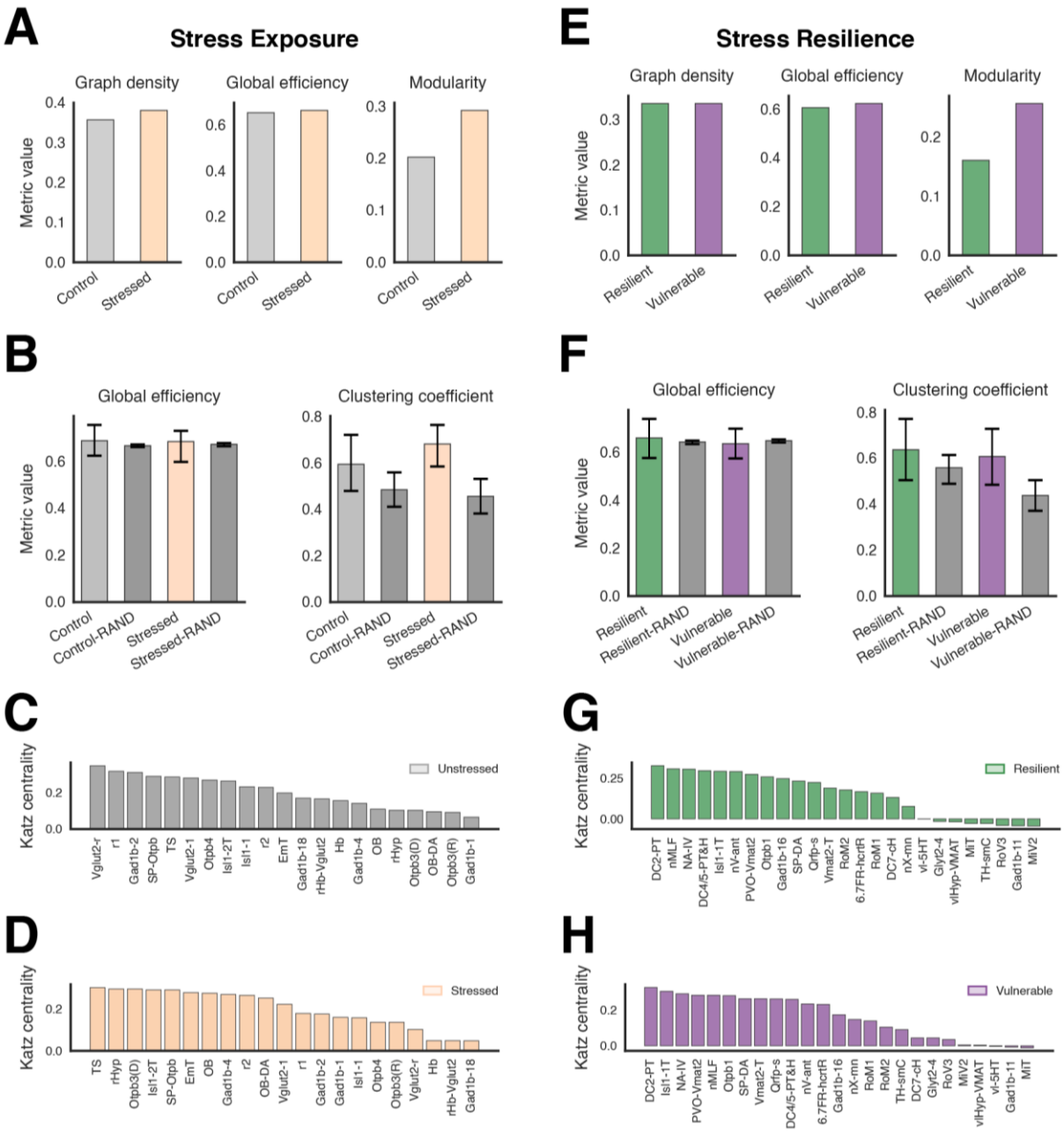

Figure 14: Graph-theoretic organization and hub structure of stress exposure and stress resilience networks. ***A,E.*** *Global graph metrics for empirical stress exposure (A) and stress resilience (E) networks. Bars show graph density, global efficiency, and modularity for the control and stressed group-level graphs.* ***B,F.*** *Small-worldness of the stress exposure network (B) and the stress resilience network (F). Bars show global efficiency (left) and mean clustering coefficient (right) for empirical network bootstraps and their degree-preserving random counterparts ("RAND") for each group. Random networks were generated by rewiring the empirical adjacency matrix while preserving the degree distribution; bars show means across randomizations with 95% confidence intervals.* ***C-D, G-H.*** *Katz centrality profiles for the stress exposure network. Bars show Katz centrality values for individual regions in the control (C) and stressed (D), resilient (G), and vulnerable (H) group-level graphs, ranked from highest to lowest within each group. Region labels follow the abbreviations in Supplementary Table 1. All networks were constructed from group-level Pearson correlation matrices of z-scored pERK/tERK values within the PLS-DA-defined stress*

exposure (Component 1) and stress resilience (Component 2) region sets (Fig. 3C-D). Adjacency matrices were thresholded at $|r| \geq 0.40$ and treated as undirected, unweighted graphs. Sample sizes: stress exposure network (control, n=42, stressed, n=85); stress resilience network (resilient, n=34; vulnerable, n=51).

In the stress-exposure network, saltwater graphs were modestly denser and more modular than controls (Fig. 14A), with Katz centrality shifting toward olfactory and hypothalamic nodes (olfactory bulb, rostral hypothalamus, Otpb^{+} hypothalamic cluster, torus semicircularis) and away from several telencephalic/hindbrain inhibitory nodes and the habenulae - indicating a stress-driven emphasis on olfactory-hypothalamic coordination (Fig. 14C-D). In the resilience network, resilient and vulnerable graphs showed nearly identical density and global efficiency, with somewhat higher modularity in vulnerable graphs (Fig. 14E-F). Hub sets were largely shared and concentrated in hypothalamic/monoaminergic territories, telencephalic dopaminergic/Vmat2 clusters, and premotor brainstem centers (nMLF, reticulospinal nuclei; Fig. 14G-H). Differences between phenotypes were expressed mainly as modest rank shifts within this common hub ensemble rather than wholesale topological reconfiguration, suggesting that resilience reflects a retuning of hub prominence and inter-modular coupling within a conserved scaffold, shifting the system's emphasis from sensory-neuroendocrine coordination during exposure toward hypothalamic/monoaminergic control coupled to premotor execution during recovery.

2.5. Temporal evolution of resilience signatures across early recovery

To examine how resilience-related activity patterns evolve as larvae progress further into recovery, the imaging experiment was repeated in an independent cohort euthanized after 10 min of post-stress recovery, rather than 5 min. Behaviorally, this cohort recapitulated the defining feature of the earlier assays: resilient and vulnerable fish were indistinguishable during baseline and exposure, diverged sharply during the first 5 min of recovery, and then gradually converged as vulnerable fish increased their swimming speed and resilient fish decelerated (Fig. 15A). Whole-brain pERK/tERK maps mirrored this trajectory (Fig. 15B-D). Compared to the 5 min recovery datasets, 10 min maps displayed a broadly similar spatial pattern but with reduced spatial extent and lower signal intensities. Prominent foci in olfactory bulbs, preoptic area, hypothalamus, habenulae, and pineal VMAT-positive clusters remained visible in resilient-control and vulnerable-control contrasts. Still, activity in hypothalamic dopaminergic clusters (posterior tuberculum and caudal hypothalamus), hindbrain premotor and reticulospinal systems (nMLF, RoM/RoV), midbrain sensory relays such as the torus semicircularis, and hindbrain inhibitory/glycinergic pools was markedly attenuated at 10 min. Residual differences were concentrated in anterior forebrain and epithalamic/diencephalic territories, including olfactory and

pallial telencephalon, a telencephalic Isl1 cluster, preoptic-hypothalamic regions, and the habenula-pineal VMAT axis.

Effect-size analyses restricted to the PLS-DA-defined region sets confirmed that the 10 min time point preserved the hierarchical ordering of regions established at 5 min while compressing its amplitude. Along the stress-exposure axis, regional effect sizes at 10 min closely tracked their 5 min ranks, with olfactory bulb and habenular nodes remaining among the strongest stressed-higher regions, but nearly all areas showed reduced magnitude (Fig15E, F). A similar pattern applied to the resilience axis: the ordering of resilience versus vulnerability-related regions remained largely consistent, with key nodes such as an anterior trigeminal motor cluster continuing to be classified as more resilient, while dopaminergic clusters in the caudal hypothalamus showed a marked decrease in effect size (Fig. 15F, H). Overall, these observations indicate that the stress-exposure and resilience networks identified at 5 min do not reorganize into a qualitatively different configuration by 10 min. Instead, they undergo a global attenuation in which the same circuits continue to differentiate groups, but with weaker contrasts as behavior converges. In this framework, the 5 min window captures the peak expression of resilience-related recruitment of hypothalamic monoaminergic and premotor brainstem circuits. In comparison, the 10 min window reflects an ongoing shutdown in which sensory-hypothalamic and resilience-linked signals decay toward a shared baseline.

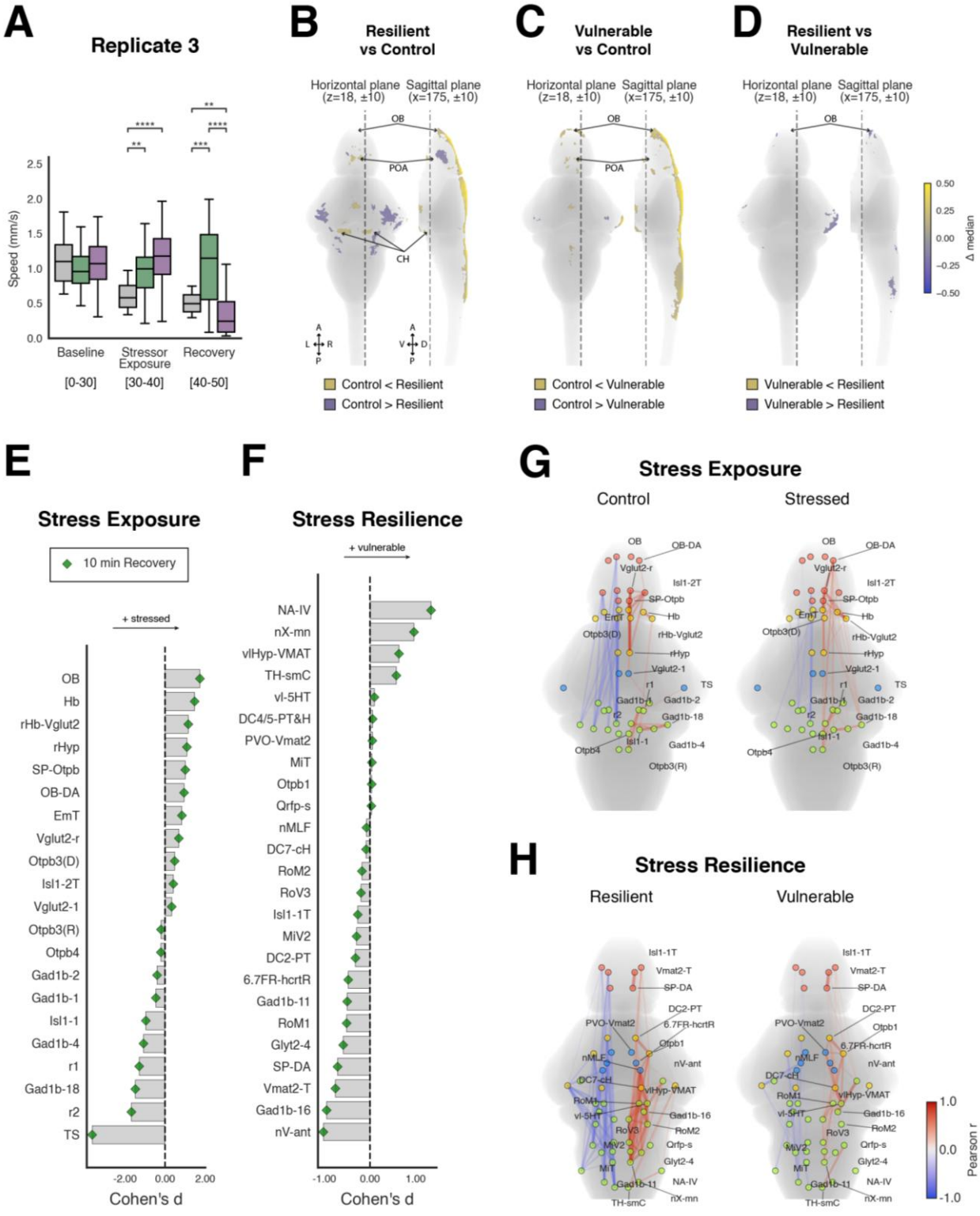

Figure 15: Brain-wide pERK/tERK maps, effect sizes, and connectivity for the 10 min recovery dataset.

A-C. *Projected maps of significant pERK/tERK differences for the 10 min recovery dataset are shown in two orthogonal views (horizontal and sagittal). Colors encode the median difference (Δ median) between the first and second group in each comparison (colorbar, yellow-blue): A, resilient (R) vs control (C; yellow: R > C; blue: C > R), B, vulnerable (V) vs control (yellow: V > C; blue: C > V), C, resilient vs vulnerable (yellow: R > V; blue: V > R). Only voxels that pass multiple-comparison correction are displayed (FDR, q ≤ 0.10).* Slices are averaged over ±10

slices around the indicated planes (horizontal: z=18; sagittal: x=175). ***D-E.*** *Cohen's d effect sizes for the 10 min recovery dataset, computed for the PLS-DA region sets corresponding to each axis.* ***D****, Stress Exposure (PLS Comp. 1) compares control vs stressed with stressed, i.e., resilient + vulnerable combined (d < 0 ⇒ control > stressed; d > 0 ⇒ stressed > control). E, Stress Resilience (PLS Comp. 2) compares resilient vs vulnerable (d < 0 ⇒ resilient > vulnerable; d > 0 ⇒ vulnerable > resilient). Region abbreviations follow Supplementary Table 1. Markers show per-region effect sizes; dashed line at 0.* ***F-G.*** *Anatomical projections of functional connectivity for the 10 min recovery dataset, evaluated within the PLS-DA region sets for Stress Exposure (F, PLS Comp. 1) and Stress Resilience (G, PLS Comp. 2). For each network, correlations are shown for the relevant comparison: control and stressed (resilient + vulnerable combined) in* ***F****, and resilient and vulnerable in G. Nodes are Z-Brain region centroids* (Randlett et al., 2015)*; edges denote pairwise Pearson correlations between region-level ERK values and are colored by correlation. OB: olfactory bulbs; POA: preoptic area; CH: caudal hypothalamus. Region abbreviations for D-G follow Supplementary Table 1. 10 min recovery dataset (control, n=18; resilient, n=17; vulnerable, n=25).*

CONCLUSIONS AND FUTURE PERSPECTIVES

Taken together, the results presented in the previous chapter can be condensed into the following main methodological contributions and empirical findings:

- The thesis establishes a standardized three-phase behavioral assay and a baseline-anchored resilience score that quantify individual recovery from acute osmotic stress in a medium-throughput, comparably scalable format for larval zebrafish.
- The Resilience Score is robust across nacre-derived transgenic lines and scales with challenge severity, with more acidic stressors shifting score distributions toward vulnerability, consistent with load-dependent limits on resilience.
- Extended 45-minute recovery assays demonstrate that resilient and vulnerable larvae converge to similar locomotor output over time, indicating that vulnerability reflects delayed rebound dynamics rather than irreversible damage or impaired swimming capacity.
- Longitudinal testing from 6 to 14 dpf reveals a global age-dependent decline in resilience but preserved relative ordering of cohorts, such that larvae initially classified as resilient retain higher normalized resilience scores than vulnerable cohorts at later larval stages.
- Longitudinal NTTs at one month show that early resilience labels predict a more proactive, challenge-evoked exploratory strategy after acute stress, while baseline anxiety-like behavior remains comparable across resilient, vulnerable, and control juveniles.
- Whole-brain pERK/tERK imaging registered to the Z-Brain atlas (Randlett et al., 2015) identifies a reproducible stress-exposure network where osmotic stress engages an olfactory-habenular-preoptic-hypothalamic axis consistent with salt detection and HPI-axis activation.
- Within this shared exposure framework, resilient animals display stronger recruitment of caudal hypothalamic and paraventricular monoaminergic populations, premotor brainstem centers (nMLF and reticulospinal clusters), and hindbrain inhibitory stripes, while vulnerable animals preferentially recruit medullary noradrenergic regions linked to behavioral suppression.
- Supervised PLS-DA cleanly separates stressed from control larvae along one component and resilient from vulnerable larvae along a second, yielding consensus sets of stress-exposure and resilience regions where telencephalic and diencephalic dopaminergic clusters emerge as key resilience discriminants, and medullary noradrenergic territories as discriminants of vulnerability.

- Functional connectivity graphs built on these region sets show conserved small-world organization across groups, with stress exposure shifting hub centrality toward olfactory and hypothalamic nodes and resilience associated with strengthened integration between hypothalamic/monoaminergic hubs and premotor brainstem centers.
- Temporal comparisons between 5- and 10-minute recovery reveal that stress-exposure and resilience-related spatial hierarchies are preserved but attenuated over time, indicating that resilience signatures correspond to a transient enhancement of activity and coupling in specific circuits superimposed on a more slowly decaying stress-exposure pattern.

These points outline a behavioral and neural framework for quantifying stress resilience in larval zebrafish, connecting baseline-anchored recovery phenotypes to specific hypothalamic, monoaminergic, and premotor circuits embedded in a conserved small-world scaffold. At the same time, they leave several aspects of resilience unresolved, from the causal role of the identified hubs, their endocrine context, to the long-term outcomes of resilient versus vulnerable phenotypes.

I. A priority is to expand the behavioral assay beyond just locomotion to include multi-level phenotyping. The current classification depends on speed-based trajectories, which proved robust but offer only one window onto coping style. Future work could combine the Resilience Score with endocrine and molecular measurements, such as whole-body cortisol, which varies in magnitude and timing across coping styles (Wong et al., 2019), and the expression of resilience-related neuropeptides (e.g., neuropeptide Y, oxytocin, vasopressin), which have been shown to be upregulated in resilient individuals after stress (Swaminathan et al., 2023). Integrating behavioral, endocrine, and transcriptional profiling would help determine whether the identified locomotor classes correspond with broader physiological signatures and could reveal biomarkers that persist beyond the immediate recovery window.

II. A second set of questions relates to causality within the identified circuits. The current analyses are correlational and do not yet determine whether hypothalamic dopaminergic clusters, premotor brainstem centers, or medullary noradrenergic regions are necessary or sufficient for resilient versus vulnerable trajectories. Targeted manipulations using transgenic lines, optogenetic or chemogenetic tools, and pharmacology could test whether boosting CH or posterior tubercular dopaminergic activity, or enhancing reticulospinal/nMLF drive, promotes faster rebound, and whether inhibiting medullary noradrenergic-radial glia pathways mitigates prolonged immobility (Ailani and Deepak, 2017; Barrios et al., 2020; Mu et al., 2019; Wee et al., 2019). Conversely, disrupting

olfactory input or components of the HPI axis would help clarify how sensory detection and endocrine signals interact with these downstream circuits and assess potential confounds related to salt sensing.

III. Third, the developmental and longitudinal aspects of resilience are still only partially explored. The present data suggest that 6 dpf resilience labels can anticipate juvenile stress-evoked behaviors, but do not reveal whether vulnerable larvae are more susceptible to stress-induced pathology later in life. Long-term studies that combine early resilience assessment with chronic unpredictable stress during juvenile stages (Golla et al., 2020; Varga et al., 2020) could determine whether vulnerable trajectories predispose to stronger anxiety-like or depression-like phenotypes, paralleling evidence in mammals showing that reactive coping styles increase risk (Albrechet-Souza and Gilpin, 2019; McIlwrick et al., 2016; Tudorache et al., 2015). Simultaneously, repeated whole-brain imaging (e.g., light-sheet calcium imaging) in identified resilient and vulnerable fish could monitor how network states change over repeated challenges, exploring whether resilience reflects a faster return to a shared attractor state or qualitatively distinct routes back to stable function.

IV. Finally, future paradigms could explicitly embed the larval assay within the construct axes outlined in the introduction by manipulating both controllability, predictability, and the modality of the stressor. Within this same acute environmental framework, one could vary whether and how larvae can influence the onset or offset of hyperosmotic exposure, signal its timing with reliable or unreliable cues, or combine osmotic pulses with other stressor modalities such as pH shifts, temperature changes, confinement, or ethological threat cues. These designs would test whether the hypothalamic-monoaminergic and premotor motifs identified here are generalizable across different stressor classes and experiential setups, or whether distinct circuit configurations support resilience under different combinations of load, controllability, and predictability.

ACKNOWLEDGMENTS

A brief pause from the science talk here to acknowledge those who supported me during this venture (if you are not expecting a mention here, you might want to skip ahead to the manuscripts in the appendix).

Firstly, I must thank Florence for bringing me into her lab. I feel incredibly privileged to have had this opportunity. Joining the lab at its very beginning as the first (and, for a while, only) student has made it especially rewarding to watch it grow into the vibrant group it is now. Thank you, Florence, for having me and for the way you care about your group members.

I am also grateful to Raghav, whose computational perspective helped bridge my early ideas with the lab's biological focus. He was always eager to be involved, consistently welcoming, and generous with his time. I sincerely thank him for his support and dedication throughout this work.

To everyone I crossed paths with in Kermen Lab, it was genuinely a pleasure to work alongside you. In particular, thank you to Emel, Laia, and Jonathan for helping to shape this project. I would also like to extend this gratitude to my colleagues and friends from the Department of Neuroscience, especially those around 24.4. Thank you for indulging my energy drink tasting project, for the reliably chaotic lunch-table discussions, and for the companionship throughout these years.

I am grateful to Benjamin, who supervised my external stay in Tromsø, for welcoming me into his lab. Working with him and the ML group at UiT was a unique and thoroughly enjoyable experience that I will always cherish. I also thank him for nurturing my enthusiasm for graph-based approaches, which has made an imprint on this thesis.

Finally, the most important thank you goes to Em. Meeting her has been the bright point of these years, thanks in no small part to Lucia's matchmaking. Her support, patience, and ability to lift me out of the toughest PhD moments have been invaluable. She has long joked about being my "PhD wife," and with this submission, I am very ready to return to her properly. *Amo-te muito!*

Por fim, com profunda saudade, quero dedicar este trabalho à avó - a "primerira pessoa a segurar-me nos bracos". Não posso deixar de me lembrar de todas as sessões de estudo noturnas, dos cafés com leite às 3h da manhã, das viagens no Smart a conversar e a ouvir fado. Obrigado avó. À minha mãe, ao meu pai e à Camille, ao meu irmão, aos meus primos e aos meus tios queria também deixar um agradecimento, por todo o carinho e ajuda.

REFERENCES

Agetsuma, M., Aizawa, H., Aoki, T., Nakayama, R., Takahoko, M., Goto, M., Sassa, T., Amo, R., Shiraki, T., Kawakami, K., Hosoya, T., Higashijima, S., Okamoto, H., 2010. The habenula is crucial for experience-dependent modification of fear responses in zebrafish. Nat. Neurosci. 13, 1354–1356. https://doi.org/10.1038/nn.2654

Ahrens, M.B., Orger, M.B., Robson, D.N., Li, J.M., Keller, P.J., 2013. Whole-brain functional imaging at cellular resolution using light-sheet microscopy. Nat. Methods 10, 413–420. https://doi.org/10.1038/nmeth.2434

Ailani, D., Deepak, A., 2017. Genetic Studies on Hypothalamus Functions in Zebrafish. No Title.

Albayrak, Z.S., Vaz, A., Bordes, J., Ünlü, S., Sep, M.S.C., Vinkers, C.H., Pinto, L., Yapici-Eser, H., 2024. Translational models of stress and resilience: An applied neuroscience methodology review. Neurosci. Appl. 3, 104064. https://doi.org/10.1016/j.nsa.2024.104064

Albrechet-Souza, L., Gilpin, N.W., 2019. The predator odor avoidance model of post-traumatic stress disorder in rats. Behav. Pharmacol. 30, 105–114. https://doi.org/10.1097/FBP.0000000000000460

Alderman, S.L., Bernier, N.J., 2009. Ontogeny of the corticotropin-releasing factor system in zebrafish. Gen. Comp. Endocrinol. 164, 61–69. https://doi.org/10.1016/j.ygcen.2009.04.007

Alderman, S.L., Vijayan, M.M., 2012. 11β-Hydroxysteroid dehydrogenase type 2 in zebrafish brain: a functional role in hypothalamus-pituitary-interrenal axis regulation. J. Endocrinol. 215, 393–402. https://doi.org/10.1530/JOE-12-0379

Alsop, D., Vijayan, M.M., 2008. Development of the corticosteroid stress axis and receptor expression in zebrafish. Am. J. Physiol.-Regul. Integr. Comp. Physiol. 294, R711–R719. https://doi.org/10.1152/ajpregu.00671.2007

Amat, J., Baratta, M.V., Paul, E., Bland, S.T., Watkins, L.R., Maier, S.F., 2005. Medial prefrontal cortex determines how stressor controllability affects behavior and dorsal raphe nucleus. Nat. Neurosci. 8, 365–371. https://doi.org/10.1038/nn1399

Amat, J., Paul, E., Zarza, C., Watkins, L.R., Maier, S.F., 2006. Previous Experience with Behavioral Control over Stress Blocks the Behavioral and Dorsal Raphe Nucleus Activating Effects of Later Uncontrollable Stress: Role of the Ventral Medial Prefrontal Cortex. J. Neurosci. 26, 13264–13272. https://doi.org/10.1523/JNEUROSCI.3630-06.2006

Amo, R., Fredes, F., Kinoshita, M., Aoki, R., Aizawa, H., Agetsuma, M., Aoki, T., Shiraki, T., Kakinuma, H., Matsuda, M., Yamazaki, M., Takahoko, M., Tsuboi, T., Higashijima, S., Miyasaka, N., Koide, T., Yabuki, Y., Yoshihara, Y., Fukai, T., Okamoto, H., 2014. The Habenulo-Raphe Serotonergic Circuit Encodes an Aversive Expectation Value Essential for Adaptive Active Avoidance of Danger. Neuron 84, 1034–1048. https://doi.org/10.1016/j.neuron.2014.10.035

Andalman, A.S., Burns, V.M., Lovett-Barron, M., Broxton, M., Poole, B., Yang, S.J., Grosenick, L., Lerner, T.N., Chen, R., Benster, T., Mourrain, P., Levoy, M., Rajan, K., Deisseroth, K., 2019. Neuronal dynamics regulating brain and behavioral state transitions. Cell 177, 970-985.e20. https://doi.org/10.1016/j.cell.2019.02.037

Andersson, M., Roques, J.A.C., Aliti, G.M., Ademar, K., Sundh, H., Sundell, K., Ericson, M., Kettunen, P., 2022. Low Holding Densities Increase Stress Response and Aggression in Zebrafish. Biology 11, 725. https://doi.org/10.3390/biology11050725

Arnsten, A.F.T., 2015. Stress weakens prefrontal networks: molecular insults to higher cognition. Nat. Neurosci. 18, 1376–1385. https://doi.org/10.1038/nn.4087

Arnsten, A.F.T., Jin, L.E., 2012. Guanfacine for the Treatment of Cognitive Disorders: A Century of Discoveries at Yale. Yale J. Biol. Med. 85, 45–58.

Aston-Jones, G., Cohen, J.D., 2005. An integrative theory of locus coeruleus-norepinephrine function: adaptive gain and optimal performance. Annu. Rev. Neurosci. 28, 403–450. https://doi.org/10.1146/annurev.neuro.28.061604.135709

Avery, S.N., Clauss, J.A., Blackford, J.U., 2016. The Human BNST: Functional Role in Anxiety and Addiction. Neuropsychopharmacology 41, 126–141. https://doi.org/10.1038/npp.2015.185

Bagot, R.C., Cates, H.M., Purushothaman, I., Lorsch, Z.S., Walker, D.M., Wang, J., Huang, X., Schlüter, O.M., Maze, I., Peña, C.J., Heller, E.A., Issler, O., Wang, M., Song, W., Stein, Jason.L., Liu, X., Doyle, M.A., Scobie, K.N., Sun, H.S., Neve, R.L., Geschwind, D., Dong, Y., Shen, L., Zhang, B., Nestler, E.J., 2016. Circuit-wide Transcriptional Profiling Reveals Brain Region-Specific Gene Networks Regulating Depression Susceptibility. Neuron 90, 969–983. https://doi.org/10.1016/j.neuron.2016.04.015

Baker, M.R., Goodman, A.C., Santo, J.B., Wong, R.Y., 2018. Repeatability and reliability of exploratory behavior in proactive and reactive zebrafish, Danio rerio. Sci. Rep. 8, 12114. https://doi.org/10.1038/s41598-018-30630-3

Baker, M.R., Wong, R.Y., 2019. Contextual fear learning and memory differ between stress coping styles in zebrafish. Sci. Rep. 9, 9935. https://doi.org/10.1038/s41598-019-46319-0

Bakusic, J., Vrieze, E., Ghosh, M., Bekaert, B., Claes, S., Godderis, L., 2020. Increased methylation of NR3C1 and SLC6A4 is associated with blunted cortisol reactivity to stress in major depression. Neurobiol. Stress 13, 100272. https://doi.org/10.1016/j.ynstr.2020.100272

Baratta, M.V., Seligman, M.E.P., Maier, S.F., 2023. From helplessness to controllability: toward a neuroscience of resilience. Front. Psychiatry 14, 1170417. https://doi.org/10.3389/fpsyt.2023.1170417

Barrios, J.P., Wang, W.-C., England, R., Reifenberg, E., Douglass, A.D., 2020. Hypothalamic Dopamine Neurons Control Sensorimotor Behavior by Modulating Brainstem Premotor Nuclei in Zebrafish. Curr. Biol. 30, 4606-4618.e4. https://doi.org/10.1016/j.cub.2020.09.002

Bassett, D.S., Sporns, O., 2017. Network neuroscience. Nat. Neurosci. 20, 353–364. https://doi.org/10.1038/nn.4502

Bedell, V.M., Dubey, P., Lee, H.B., Bailey, D.S., Anderson, J.L., Jamieson-Lucy, A., Xiao, R., Leonard, E.V., Falk, M.J., Pack, M.A., Mullins, M., Farber, S.A., Eckenhoff, R.G., Ekker, S.C., 2025. Zebrafishology, study design guidelines for rigorous and reproducible data using zebrafish. Commun. Biol. 8, 739. https://doi.org/10.1038/s42003-025-07496-z

Beery, A.K., Kaufer, D., 2014. Stress, social behavior, and resilience: Insights from rodents. Neurobiol. Stress 1, 116–127. https://doi.org/10.1016/j.ynstr.2014.10.004

Benham, R.S., Choi, C., Hodgson, N.W., Hewage, N.B., Kastli, R., Donahue, R.J., Muschamp, J.W., Engin, E., Carlezon, W.A., Hensch, T.K., Rudolph, U., 2021. α2-containing γ-aminobutyric acid type A receptors promote stress resiliency in male mice. Neuropsychopharmacology 46, 2197–2206. https://doi.org/10.1038/s41386-021-01144-w

Best, C., Kurrasch, D.M., Vijayan, M.M., 2017. Maternal cortisol stimulates neurogenesis and affects larval behaviour in zebrafish. Sci. Rep. 7, 40905. https://doi.org/10.1038/srep40905

Betzel, R.F., 2020. Organizing principles of whole-brain functional connectivity in zebrafish larvae. Netw. Neurosci. 4, 234–256. https://doi.org/10.1162/netn_a_00121

Binder, E.B., 2009. The role of FKBP5, a co-chaperone of the glucocorticoid receptor in the pathogenesis and therapy of affective and anxiety disorders. Psychoneuroendocrinology, NEUROACTIVE STEROIDS: EFFECTS AND MECHANISMS OF ACTION 34, S186–S195. https://doi.org/10.1016/j.psyneuen.2009.05.021

Blank, M., Guerim, L.D., Cordeiro, R.F., Vianna, M.R.M., 2009. A one-trial inhibitory avoidance task to zebrafish: Rapid acquisition of an NMDA-dependent long-term memory. Neurobiol. Learn. Mem. 92, 529–534. https://doi.org/10.1016/j.nlm.2009.07.001

Bonanno, G.A., Westphal, M., Mancini, A.D., 2011. Resilience to Loss and Potential Trauma. Annu. Rev. Clin. Psychol. 7, 511–535. https://doi.org/10.1146/annurev-clinpsy-032210-104526

Bonga, S.E.W., 1997. The stress response in fish. Physiol. Rev. 77, 591–625. https://doi.org/10.1152/physrev.1997.77.3.591

Butt, M.I., Alzuhayri, N., Amer, L., Riazuddin, M., Aljamei, H., Khan, M.S., Abufarhaneh, M., Alrajhi, E., Alnassar, A., Alahmed, R., Aljayar, D.M.A., Abothenain, F.F., De Vol, E., 2020. Comparing the utility of 30- and 60-minute cortisol levels after the standard short synacthen test to determine adrenal insufficiency. Medicine (Baltimore) 99, e22621. https://doi.org/10.1097/MD.0000000000022621

Caggiano, V., Leiras, R., Goñi-Erro, H., Masini, D., Bellardita, C., Bouvier, J., Caldeira, V., Fisone, G., Kiehn, O., 2018. Midbrain circuits that set locomotor speed and gait selection. Nature 553, 455–460. https://doi.org/10.1038/nature25448

Cao, J.-L., Covington, H.E., Friedman, A.K., Wilkinson, M.B., Walsh, J.J., Cooper, D.C., Nestler, E.J., Han, M.-H., 2010. Mesolimbic Dopamine Neurons in the Brain Reward Circuit Mediate Susceptibility to Social Defeat and Antidepressant Action. J. Neurosci. 30, 16453–16458. https://doi.org/10.1523/JNEUROSCI.3177-10.2010

Capelli, P., Pivetta, C., Soledad Esposito, M., Arber, S., 2017. Locomotor speed control circuits in the caudal brainstem. Nature 551, 373–377. https://doi.org/10.1038/nature24064

Carbo-Tano, M., Lapoix, M., Jia, X., Thouvenin, O., Pascucci, M., Auclair, F., Quan, F.B., Albadri, S., Aguda, V., Farouj, Y., Hillman, E.M.C., Portugues, R., Del Bene, F., Thiele, T.R., Dubuc, R., Wyart, C., 2023. The mesencephalic locomotor region recruits V2a reticulospinal neurons to drive forward locomotion in larval zebrafish. Nat. Neurosci. 26, 1775–1790. https://doi.org/10.1038/s41593-023-01418-0

Castillo-Ramírez, L.A., Herget, U., Ryu, S., De Marco, R.J., 2024a. Early-life challenge enhances cortisol regulation in zebrafish larvae. Biol. Open 13, bio061684. https://doi.org/10.1242/bio.061684

Castillo-Ramírez, L.A., Ryu, S., De Marco, R.J., 2024b. Cortisol dynamics and GR-dependent feedback regulation in zebrafish larvae exposed to repeated stress. Biol. Open 13, bio061683. https://doi.org/10.1242/bio.061683

Cathomas, F., Murrough, J.W., Nestler, E.J., Han, M.-H., Russo, S.J., 2019. Neurobiology of Resilience: Interface Between Mind and Body. Biol. Psychiatry 86, 410–420. https://doi.org/10.1016/j.biopsych.2019.04.011

Charney, D.S., 2004. Psychobiological Mechanisms of Resilience and Vulnerability: Implications for Successful Adaptation to Extreme Stress. Am. J. Psychiatry 161, 195–216. https://doi.org/10.1176/appi.ajp.161.2.195

Chaudhury, D., Walsh, J.J., Friedman, A.K., Juarez, B., Ku, S.M., Koo, J.W., Ferguson, D., Tsai, H.-C., Pomeranz, L., Christoffel, D.J., Nectow, A.R., Ekstrand, M., Domingos, A., Mazei-Robison, M.S., Mouzon, E., Lobo, M.K., Neve, R.L., Friedman, J.M., Russo, S.J., Deisseroth, K., Nestler, E.J., Han, M.-H., 2013. Rapid regulation of depression-related behaviours by control of midbrain dopamine neurons. Nature 493, 532–536. https://doi.org/10.1038/nature11713

Chen, A.B., Duque, M., Wang, V.M., Dhanasekar, M., Mi, X., Rymbek, A., Tocquer, L., Narayan, S., Prober, D., Yu, G., Wyart, C., Engert, F., Ahrens, M.B., 2024. Norepinephrine changes behavioral state via astroglial purinergic signaling. https://doi.org/10.1101/2024.05.23.595576

Cheng, R.-K., Tan, J.X.M., Chua, K.X., Tan, C.J.X., Wee, C.L., 2022. Osmotic Stress Uncovers Correlations and Dissociations Between Larval Zebrafish Anxiety Endophenotypes. Front. Mol. Neurosci. 15, 900223. https://doi.org/10.3389/fnmol.2022.900223

Chin, J.S.R., Phan, T.-A.N., Albert, L.T., Keene, A.C., Duboué, E.R., 2022. Long lasting anxiety following early life stress is dependent on glucocorticoid signaling in zebrafish. Sci. Rep. 12, 12826. https://doi.org/10.1038/s41598-022-16257-5

Christianson, J.P., Flyer-Adams, J.G., Drugan, R.C., Amat, J., Daut, R.A., Foilb, A.R., Watkins, L.R., Maier, S.F., 2014. Learned stressor resistance requires extracellular signal-regulated kinase in the prefrontal cortex. Front. Behav. Neurosci. 8. https://doi.org/10.3389/fnbeh.2014.00348

Chung, K., Wallace, J., Kim, S.-Y., Kalyanasundaram, S., Andalman, A.S., Davidson, T.J., Mirzabekov, J.J., Zalocusky, K.A., Mattis, J., Denisin, A.K., Pak, S., Bernstein, H., Ramakrishnan, C., Grosenick, L., Gradinaru, V., Deisseroth, K., 2013. Structural and molecular interrogation of intact biological systems. Nature 497, 332–337. https://doi.org/10.1038/nature12107

Cong, L., Wang, Z., Chai, Y., Hang, W., Shang, C., Yang, W., Bai, L., Du, J., Wang, K., Wen, Q., 2017. Rapid whole brain imaging of neural activity in freely behaving larval zebrafish (Danio rerio). eLife 6, e28158. https://doi.org/10.7554/eLife.28158

Conway-Campbell, B.L., Sarabdjitsingh, R.A., McKenna, M.A., Pooley, J.R., Kershaw, Y.M., Meijer, O.C., de Kloet, E.R., Lightman, S.L., 2010. Glucocorticoid ultradian rhythmicity directs cyclical gene pulsing of the clock gene period 1 in rat hippocampus. J. Neuroendocrinol. 22, 1093–1100. https://doi.org/10.1111/j.1365-2826.2010.02051.x

Coppens, C.M., de Boer, S.F., Koolhaas, J.M., 2010. Coping styles and behavioural flexibility: towards underlying mechanisms. Philos. Trans. R. Soc. B Biol. Sci. 365, 4021–4028. https://doi.org/10.1098/rstb.2010.0217

Corradi, L., Bruzzone, M., Maschio, M. dal, Sawamiphak, S., Filosa, A., 2022. Hypothalamic Galanin-producing neurons regulate stress in zebrafish through a peptidergic, self-inhibitory loop. Curr. Biol. 32, 1497-1510.e5. https://doi.org/10.1016/j.cub.2022.02.011

Corrales Parada, C.D., Mayer, U., Chagnaud, B.P., 2024. The Dorsal Part of the Anterior Tuberal Nucleus Responds to Auditory Stimulation in Zebrafish (Danio rerio). eNeuro 11, ENEURO.0062-24.2024. https://doi.org/10.1523/ENEURO.0062-24.2024

Costa-Mattioli, M., Sossin, W.S., Klann, E., Sonenberg, N., 2009. Translational control of long-lasting synaptic plasticity and memory. Neuron 61, 10–26. https://doi.org/10.1016/j.neuron.2008.10.055

Cryan, J.F., Holmes, A., 2005. The ascent of mouse: advances in modelling human depression and anxiety. Nat. Rev. Drug Discov. 4, 775–790. https://doi.org/10.1038/nrd1825

Dampney, R., 2018. Emotion and the Cardiovascular System: Postulated Role of Inputs From the Medial Prefrontal Cortex to the Dorsolateral Periaqueductal Gray. Front. Neurosci. 12. https://doi.org/10.3389/fnins.2018.00343

de Abreu, M.S., Demin, K.A., Giacomini, A.C.V.V., Amstislavskaya, T.G., Strekalova, T., Maslov, G.O., Kositsin, Y., Petersen, E.V., Kalueff, A.V., 2021. Understanding how stress responses and stress-related behaviors have evolved in zebrafish and mammals. Neurobiol. Stress 15, 100405. https://doi.org/10.1016/j.ynstr.2021.100405

de Kloet, E.R., 2022. Brain mineralocorticoid and glucocorticoid receptor balance in neuroendocrine regulation and stress-related psychiatric etiopathologies. Curr. Opin. Endocr. Metab. Res. 24, 100352. https://doi.org/10.1016/j.coemr.2022.100352

de Kloet, E.R., Vreugdenhil, E., Oitzl, M.S., Joëls, M., 1998. Brain Corticosteroid Receptor Balance in Health and Disease*. Endocr. Rev. 19, 269–301. https://doi.org/10.1210/edrv.19.3.0331

Debanne, D., Inglebert, Y., Russier, M., 2019. Plasticity of intrinsic neuronal excitability. Curr. Opin. Neurobiol., Neurobiology of Learning and Plasticity 54, 73–82. https://doi.org/10.1016/j.conb.2018.09.001

Deffieux, T., Demené, C., Tanter, M., 2021. Functional Ultrasound Imaging: A New Imaging Modality for Neuroscience. Neuroscience, Brain imaging 474, 110–121. https://doi.org/10.1016/j.neuroscience.2021.03.005

Demin, K.A., Kolesnikova, T.O., Galstyan, D.S., Krotova, N.A., Ilyin, N.P., Derzhavina, K.A., Levchenko, N.A., Strekalova, T., de Abreu, M.S., Petersen, E.V., Seredinskaya, M., Cherneyko, Y.V., Kositsyn, Y.M., Sorokin, D.V., Zabegalov, K.N., Mor, M.S., Efimova, E.V., Kalueff, A.V., 2021. Modulation of behavioral and neurochemical responses of adult zebrafish by fluoxetine, eicosapentaenoic acid and lipopolysaccharide in the prolonged chronic unpredictable stress model. Sci. Rep. 11, 14289. https://doi.org/10.1038/s41598-021-92422-6

Demin, K.A., Lakstygal, A.M., Krotova, N.A., Masharsky, A., Tagawa, N., Chernysh, M.V., Ilyin, N.P., Taranov, A.S., Galstyan, D.S., Derzhavina, K.A., Levchenko, N.A., Kolesnikova, T.O., Mor, M.S., Vasyutina, M.L., Efimova, E.V., Katolikova, N., Prjibelski, A.D., Gainetdinov, R.R., de Abreu, M.S., Amstislavskaya, T.G., Strekalova, T., Kalueff, A.V., 2020. Understanding complex dynamics of behavioral, neurochemical and transcriptomic changes induced by prolonged chronic unpredictable stress in zebrafish. Sci. Rep. 10, 19981. https://doi.org/10.1038/s41598-020-75855-3

Diekmann, H., Kalbhen, P., Fischer, D., 2015. Active mechanistic target of rapamycin plays an ancillary rather than essential role in zebrafish CNS axon regeneration. Front. Cell. Neurosci. 9. https://doi.org/10.3389/fncel.2015.00251

Dion-Albert, L., Cadoret, A., Doney, E., Kaufmann, F.N., Dudek, K.A., Daigle, B., Parise, L.F., Cathomas, F., Samba, N., Hudson, N., Lebel, M., Campbell, M., Turecki, G., Mechawar, N., Menard, C., 2022. Vascular and blood-brain barrier-related changes underlie stress responses and resilience in female mice and depression in human tissue. Nat. Commun. 13, 164. https://doi.org/10.1038/s41467-021-27604-x

Dommanget-Kott, M., Fernandez-de-Cossio-Diaz, J., Coraggioso, M., Bormuth, V., Monasson, R., Debrégeas, G., Cocco, S., 2024. Linking Brain and Behavior States in Zebrafish Larvae Locomotion using Hidden Markov Models. https://doi.org/10.1101/2024.11.22.624881

Dreosti, E., Lopes, G., Kampff, A.R., Wilson, S.W., 2015. Development of social behavior in young zebrafish. Front. Neural Circuits 9, 39. https://doi.org/10.3389/fncir.2015.00039

Drugan, R.C., Basile, A.S., Ha, J.-H., Healy, D., Ferland, R.J., 1997. Analysis of the importance of controllable versus uncontrollable stress on subsequent behavioral and physiological functioning. Brain Res. Protoc. 2, 69–74. https://doi.org/10.1016/S1385-299X(97)00031-7

Duboué, E.R., Hong, E., Eldred, K.C., Halpern, M.E., 2017. Left Habenular Activity Attenuates Fear Responses in Larval Zebrafish. Curr. Biol. 27, 2154-2162.e3. https://doi.org/10.1016/j.cub.2017.06.017

Eachus, H., Choi, M.-K., Ryu, S., 2021. The Effects of Early Life Stress on the Brain and Behaviour: Insights From Zebrafish Models. Front. Cell Dev. Biol. 9, 657591. https://doi.org/10.3389/fcell.2021.657591

Eachus, H., Choi, M.-K., Tochwin, A., Kaspareit, J., Ho, M., Ryu, S., 2024. Elevated glucocorticoid alters the developmental dynamics of hypothalamic neurogenesis in zebrafish. Commun. Biol. 7, 416. https://doi.org/10.1038/s42003-024-06060-5

Edwards, K.A., Hoppa, M.B., Bosco, G., 2020. The Photoconvertible Fluorescent Probe, CaMPARI, Labels Active Neurons in Freely-Moving Intact Adult Fruit Flies. Front. Neural Circuits 14. https://doi.org/10.3389/fncir.2020.00022

Facciol, A., Gerlai, R., 2020. Zebrafish Shoaling, Its Behavioral and Neurobiological Mechanisms, and Its Alteration by Embryonic Alcohol Exposure: A Review. Front. Behav. Neurosci. 14. https://doi.org/10.3389/fnbeh.2020.572175

Farrell, T.C., Cario, C.L., Milanese, C., Vogt, A., Jeong, J.-H., Burton, E.A., 2011. Evaluation of spontaneous propulsive movement as a screening tool to detect rescue of Parkinsonism phenotypes in zebrafish models. Neurobiol. Dis. 44, 9–18. https://doi.org/10.1016/j.nbd.2011.05.016

Feder, A., Nestler, E.J., Charney, D.S., 2009. Psychobiology and molecular genetics of resilience. Nat. Rev. Neurosci. 10, 446–457. https://doi.org/10.1038/nrn2649

Fitzgerald, J.A., Kirla, K.T., Zinner, C.P., vom Berg, C.M., 2019. Emergence of consistent intra-individual locomotor patterns during zebrafish development. Sci. Rep. 9, 13647. https://doi.org/10.1038/s41598-019-49614-y

Fontana, B.D., Alnassar, N., Parker, M.O., 2022. The zebrafish (Danio rerio) anxiety test battery: comparison of behavioral responses in the novel tank diving and light–dark tasks following exposure to anxiogenic and anxiolytic compounds. Psychopharmacology (Berl.) 239, 287–296. https://doi.org/10.1007/s00213-021-05990-w

Forray, M.I., Gysling, K., 2004. Role of noradrenergic projections to the bed nucleus of the stria terminalis in the regulation of the hypothalamic–pituitary–adrenal axis. Brain Res. Rev., Chemical and Electrical Synapses 47, 145–160. https://doi.org/10.1016/j.brainresrev.2004.07.011

Franklin, T.B., 2019. Recent Advancements Surrounding the Role of the Periaqueductal Gray in Predators and Prey. Front. Behav. Neurosci. 13. https://doi.org/10.3389/fnbeh.2019.00060

Friedman, A.K., Juarez, B., Ku, S.M., Zhang, H., Calizo, R.C., Walsh, J.J., Chaudhury, D., Zhang, S., Hawkins, A., Dietz, D.M., Murrough, J.W., Ribadeneira, M., Wong, E.H., Neve, R.L., Han, M.-H., 2016. KCNQ channel openers reverse depressive symptoms via an active resilience mechanism. Nat. Commun. 7, 11671. https://doi.org/10.1038/ncomms11671

Gahtan, E., Tanger, P., Baier, H., 2005. Visual Prey Capture in Larval Zebrafish Is Controlled by Identified Reticulospinal Neurons Downstream of the Tectum. J. Neurosci. 25, 9294–9303. https://doi.org/10.1523/JNEUROSCI.2678-05.2005

Geng, Y., Peterson, R.T., 2019. The zebrafish subcortical social brain as a model for studying social behavior disorders. Dis. Model. Mech. 12, dmm039446. https://doi.org/10.1242/dmm.039446

Gerlai, R., 2019. Reproducibility and replicability in zebrafish behavioral neuroscience research. Pharmacol. Biochem. Behav. 178, 30–38. https://doi.org/10.1016/j.pbb.2018.02.005

Gerlai, R., Fernandes, Y., Pereira, T., 2009. Zebrafish (Danio rerio) responds to the animated image of a predator: Towards the development of an automated aversive task. Behav. Brain Res. 201, 318–324. https://doi.org/10.1016/j.bbr.2009.03.003

Giovannitti, J.A., Thoms, S.M., Crawford, J.J., 2015. Alpha-2 Adrenergic Receptor Agonists: A Review of Current Clinical Applications. Anesth. Prog. 62, 31–38. https://doi.org/10.2344/0003-3006-62.1.31

Giustino, T.F., Ramanathan, K.R., Totty, M.S., Miles, O.W., Maren, S., 2020. Locus Coeruleus Norepinephrine Drives Stress-Induced Increases in Basolateral Amygdala Firing and Impairs Extinction Learning. J. Neurosci. 40, 907–916. https://doi.org/10.1523/JNEUROSCI.1092-19.2019

Glasser, M.F., Sotiropoulos, S.N., Wilson, J.A., Coalson, T.S., Fischl, B., Andersson, J.L., Xu, J., Jbabdi, S., Webster, M., Polimeni, J.R., Van Essen, D.C., Jenkinson, M., WU-Minn HCP Consortium, 2013. The minimal preprocessing pipelines for the Human Connectome Project. NeuroImage 80, 105–124. https://doi.org/10.1016/j.neuroimage.2013.04.127

Godoy, L.D., Rossignoli, M.T., Delfino-Pereira, P., Garcia-Cairasco, N., de Lima Umeoka, E.H., 2018. A Comprehensive Overview on Stress Neurobiology: Basic Concepts and Clinical Implications. Front. Behav. Neurosci. 12. https://doi.org/10.3389/fnbeh.2018.00127

Golden, S.A., Covington, H.E., Berton, O., Russo, S.J., 2011. A standardized protocol for repeated social defeat stress in mice. Nat. Protoc. 6, 1183–1191. https://doi.org/10.1038/nprot.2011.361

Golla, A., Østby, H., Kermen, F., 2020. Chronic unpredictable stress induces anxiety-like behaviors in young zebrafish. Sci. Rep. 10, 10339. https://doi.org/10.1038/s41598-020-67182-4

Goode, T.D., Ressler, R.L., Acca, G.M., Miles, O.W., Maren, S., 2019. Bed nucleus of the stria terminalis regulates fear to unpredictable threat signals. eLife 8, e46525. https://doi.org/10.7554/eLife.46525

Gorissen, M., Manuel, R., Pelgrim, T.N.M., Mes, W., de Wolf, M.J.S., Zethof, J., Flik, G., van den Bos, R., 2015. Differences in inhibitory avoidance, cortisol and brain gene expression in TL and AB zebrafish. Genes Brain Behav. 14, 428–438. https://doi.org/10.1111/gbb.12220

Goswami, S., Rodríguez-Sierra, O., Cascardi, M., Paré, D., 2013. Animal models of post-traumatic stress disorder: face validity. Front. Neurosci. 7, 89. https://doi.org/10.3389/fnins.2013.00089

Grafe, L.A., Eacret, D., Dobkin, J., Bhatnagar, S., 2018. Reduced Orexin System Function Contributes to Resilience to Repeated Social Stress. eNeuro 5, ENEURO.0273-17.2018. https://doi.org/10.1523/ENEURO.0273-17.2018

Graves, C.L., Norloff, E., Thompson, D., Kosyk, O., Sang, Y., Chen, A., Zannas, A.S., Wallet, S.M., 2023. Chronic early life stress alters the neuroimmune profile and functioning of the developing zebrafish gut. Brain Behav. Immun. - Health 31, 100655. https://doi.org/10.1016/j.bbih.2023.100655

Hagenaars, M.A., Oitzl, M., Roelofs, K., 2014. Updating freeze: Aligning animal and human research. Neurosci. Biobehav. Rev. 47, 165–176. https://doi.org/10.1016/j.neubiorev.2014.07.021

Hageter, J., Efromson, J., Alban, B., DelGaudio, A., Saliu, V., Wassef, M., Harfouche, M., Horstick, E.J., 2025. High throughput machine learning pipeline to characterize larval zebrafish motor behavior. bioRxiv 2025.06.17.660164. https://doi.org/10.1101/2025.06.17.660164

Haller, J., Mikics, E., Makara, G.B., 2008. The effects of non-genomic glucocorticoid mechanisms on bodily functions and the central neural system. A critical evaluation of findings. Front. Neuroendocrinol. 29, 273–291. https://doi.org/10.1016/j.yfrne.2007.10.004

Harris, A.Z., Atsak, P., Bretton, Z.H., Holt, E.S., Alam, R., Morton, M.P., Abbas, A.I., Leonardo, E.D., Bolkan, S.S., Hen, R., Gordon, J.A., 2018. A Novel Method for Chronic Social Defeat Stress in Female Mice. Neuropsychopharmacology 43, 1276–1283. https://doi.org/10.1038/npp.2017.259

Hasani, H., Sun, J., Zhu, S.I., Rong, Q., Willomitzer, F., Amor, R., McConnell, G., Cossairt, O., Goodhill, G.J., 2023. Whole-brain imaging of freely-moving zebrafish. Front. Neurosci. 17, 1127574. https://doi.org/10.3389/fnins.2023.1127574

He, B., Liu, Z., 2008. Multimodal Functional Neuroimaging: Integrating Functional MRI and EEG/MEG. IEEE Rev. Biomed. Eng. 1, 23–40. https://doi.org/10.1109/RBME.2008.2008233

Henckens, M.J. a. G., Printz, Y., Shamgar, U., Dine, J., Lebow, M., Drori, Y., Kuehne, C., Kolarz, A., Eder, M., Deussing, J.M., Justice, N.J., Yizhar, O., Chen, A., 2017. CRF receptor type 2 neurons in the posterior bed nucleus of the stria terminalis critically contribute to stress recovery. Mol. Psychiatry 22, 1691–1700. https://doi.org/10.1038/mp.2016.133

Henckens, M.J.A.G., Klumpers, F., Everaerd, D., Kooijman, S.C., van Wingen, G.A., Fernández, G., 2016. Interindividual differences in stress sensitivity: basal and stress-induced cortisol levels differentially predict neural vigilance processing under stress. Soc. Cogn. Affect. Neurosci. 11, 663–673. https://doi.org/10.1093/scan/nsv149

Herget, U., Wolf, A., Wullimann, M.F., Ryu, S., 2014. Molecular neuroanatomy and chemoarchitecture of the neurosecretory preoptic-hypothalamic area in zebrafish larvae. J. Comp. Neurol. 522, 1542–1564. https://doi.org/10.1002/cne.23480

Herman, J.P., McKlveen, J.M., Ghosal, S., Kopp, B., Wulsin, A., Makinson, R., Scheimann, J., Myers, B., 2016. Regulation of the hypothalamic-pituitary-adrenocortical stress response. Compr. Physiol. 6, 603–621. https://doi.org/10.1002/cphy.c150015

Herman, J.P., Tasker, J.G., 2016. Paraventricular Hypothalamic Mechanisms of Chronic Stress Adaptation. Front. Endocrinol. 7, 137. https://doi.org/10.3389/fendo.2016.00137

Hermans, E.J., Henckens, M.J.A.G., Joëls, M., Fernández, G., 2014. Dynamic adaptation of large-scale brain networks in response to acute stressors. Trends Neurosci. 37, 304–314. https://doi.org/10.1016/j.tins.2014.03.006

Hermans, E.J., van Marle, H.J.F., Ossewaarde, L., Henckens, M.J.A.G., Qin, S., van Kesteren, M.T.R., Schoots, V.C., Cousijn, H., Rijpkema, M., Oostenveld, R., Fernández, G., 2011. Stress-related noradrenergic activity prompts large-scale neural network reconfiguration. Science 334, 1151–1153. https://doi.org/10.1126/science.1209603

Herrera, K.J., Panier, T., Guggiana-Nilo, D., Engert, F., 2021. Larval Zebrafish Use Olfactory Detection of Sodium and Chloride to Avoid Salt Water. Curr. Biol. 31, 782-793.e3. https://doi.org/10.1016/j.cub.2020.11.051

Hikosaka, O., Sesack, S.R., Lecourtier, L., Shepard, P.D., 2008. Habenula: Crossroad between the Basal Ganglia and the Limbic System. J. Neurosci. 28, 11825–11829. https://doi.org/10.1523/JNEUROSCI.3463-08.2008

Hodes, G.E., Pfau, M.L., Purushothaman, I., Ahn, H.F., Golden, S.A., Christoffel, D.J., Magida, J., Brancato, A., Takahashi, A., Flanigan, M.E., Ménard, C., Aleyasin, H., Koo, J.W., Lorsch, Z.S., Feng, J., Heshmati, M., Wang, M., Turecki, G., Neve, R., Zhang, B., Shen, L., Nestler, E.J., Russo, S.J., 2015. Sex Differences in Nucleus Accumbens Transcriptome Profiles Associated with Susceptibility versus Resilience to Subchronic Variable Stress. J. Neurosci. 35, 16362–16376. https://doi.org/10.1523/JNEUROSCI.1392-15.2015

Holsboer, F., Ising, M., 2008. Central CRH system in depression and anxiety — Evidence from clinical studies with CRH1 receptor antagonists. Eur. J. Pharmacol., Stress Hormone Actions in Brain, in Health and Disease 583, 350–357. https://doi.org/10.1016/j.ejphar.2007.12.032

Holstege, G., Meiners, L., Tan, K., 1985. Projections of the bed nucleus of the stria terminalis to the mesencephalon, pons, and medulla oblongata in the cat. Exp. Brain Res. 58, 379–391. https://doi.org/10.1007/BF00235319

Huang, K.-H., Ahrens, M.B., Dunn, T.W., Engert, F., 2013. Spinal Projection Neurons Control Turning Behaviors in Zebrafish. Curr. Biol. 23, 1566–1573. https://doi.org/10.1016/j.cub.2013.06.044

Ingebretson, J.J., Masino, M.A., 2013. Quantification of locomotor activity in larval zebrafish: considerations for the design of high-throughput behavioral studies. Front. Neural Circuits 7, 109. https://doi.org/10.3389/fncir.2013.00109

Jacobs, E.A.K., Ryu, S., 2023. Larval zebrafish as a model for studying individual variability in translational neuroscience research. Front. Behav. Neurosci. 17. https://doi.org/10.3389/fnbeh.2023.1143391

Joëls, M., de Kloet, E.R., 1992. Control of neuronal excitability by corticosteroid hormones. Trends Neurosci. 15, 25–30. https://doi.org/10.1016/0166-2236(92)90345-9

Joëls, M., Karst, H., Sarabdjitsingh, R.A., 2018. The stressed brain of humans and rodents. Acta Physiol. Oxf. Engl. 223, e13066. https://doi.org/10.1111/apha.13066

Johnson, A., Loh, E., Verbitsky, R., Slessor, J., Franczak, B.C., Schalomon, M., Hamilton, T.J., 2023. Examining behavioural test sensitivity and locomotor proxies of anxiety-like behaviour in zebrafish. Sci. Rep. 13, 3768. https://doi.org/10.1038/s41598-023-29668-9

Kalisch, R., Baker, D.G., Basten, U., Boks, M.P., Bonanno, G.A., Brummelman, E., Chmitorz, A., Fernàndez, G., Fiebach, C.J., Galatzer-Levy, I., Geuze, E., Groppa, S., Helmreich, I., Hendler, T., Hermans, E.J., Jovanovic, T., Kubiak, T., Lieb, K., Lutz, B., Müller, M.B., Murray, R.J., Nievergelt, C.M., Reif, A., Roelofs, K., Rutten, B.P.F., Sander, D., Schick, A., Tüscher, O., Diest, I.V., Harmelen, A.-L. van, Veer, I.M., Vermetten, E., Vinkers, C.H., Wager, T.D., Walter, H., Wessa, M., Wibral, M., Kleim, B., 2017. The resilience framework as a strategy to combat stress-related disorders. Nat. Hum. Behav. 1, 784–790. https://doi.org/10.1038/s41562-017-0200-8

Kalisch, R., Müller, M.B., Tüscher, O., 2015. A conceptual framework for the neurobiological study of resilience. Behav. Brain Sci. 38, e92. https://doi.org/10.1017/s0140525x1400082x

Kearton, T., Marini, D., Cowley, F., Belson, S., Keshavarzi, H., Mayes, B., Lee, C., 2020. The Influence of Predictability and Controllability on Stress Responses to the Aversive Component of a Virtual Fence. Front. Vet. Sci. 7, 580523. https://doi.org/10.3389/fvets.2020.580523

Kermen, F., Franco, L.M., Wyatt, C., Yaksi, E., 2013. Neural circuits mediating olfactory-driven behavior in fish. Front. Neural Circuits 7, 62. https://doi.org/10.3389/fncir.2013.00062

Kestering-Ferreira, E., Tractenberg, S.G., Lumertz, F.S., Orso, R., Creutzberg, K.C., Wearick-Silva, L.E., Viola, T.W., Grassi-Oliveira, R., 2021. Long-term Effects of Maternal Separation on Anxiety-Like Behavior and Neuroendocrine Parameters in Adult Balb/c Mice. Chronic Stress 5, 24705470211067181. https://doi.org/10.1177/24705470211067181

Klengel, T., Mehta, D., Anacker, C., Rex-Haffner, M., Pruessner, J.C., Pariante, C.M., Pace, T.W.W., Mercer, K.B., Mayberg, H.S., Bradley, B., Nemeroff, C.B., Holsboer, F., Heim, C.M., Ressler, K.J., Rein, T., Binder, E.B., 2013. Allele-specific FKBP5 DNA demethylation mediates gene–childhood trauma interactions. Nat. Neurosci. 16, 33–41. https://doi.org/10.1038/nn.3275

Klohs, J., Chen, W.C., Araki, R., 2025. Advanced preclinical functional magnetic resonance imaging of the brain. Npj Imaging 3, 27. https://doi.org/10.1038/s44303-025-00085-z

Kobayashi, Y., Sano, Y., Vannoni, E., Goto, H., Ikeda, T., Suzuki, H., Oba, A., Kawasaki, H., Kanba, S., Lipp, H.-P., Murphy, N.P., Wolfer, D.P., Itohara, S., 2013. Genetic dissection of medial habenula–interpeduncular nucleus pathway function in mice. Front. Behav. Neurosci. 7. https://doi.org/10.3389/fnbeh.2013.00017

Koert, A., Ploeger, A., Bockting, C.L.H., Schmidt, M.V., Lucassen, P.J., Schrantee, A., Mul, J.D., 2021. The social instability stress paradigm in rat and mouse: A systematic review of protocols, limitations, and recommendations. Neurobiol. Stress 15, 100410. https://doi.org/10.1016/j.ynstr.2021.100410

Koolhaas, J.M., de Boer, S.F., Coppens, C.M., Buwalda, B., 2010. Neuroendocrinology of coping styles: Towards understanding the biology of individual variation. Front. Neuroendocrinol. 31, 307–321. https://doi.org/10.1016/j.yfrne.2010.04.001

Koolhaas, J.M., Korte, S.M., De Boer, S.F., Van Der Vegt, B.J., Van Reenen, C.G., Hopster, H., De Jong, I.C., Ruis, M.A.W., Blokhuis, H.J., 1999. Coping styles in animals: current status in behavior and stress-physiology. Neurosci. Biobehav. Rev. 23, 925–935. https://doi.org/10.1016/S0149-7634(99)00026-3

Krishnan, V., Han, M.-H., Graham, D.L., Berton, O., Renthal, W., Russo, S.J., LaPlant, Q., Graham, A., Lutter, M., Lagace, D.C., Ghose, S., Reister, R., Tannous, P., Green, T.A.,

Neve, R.L., Chakravarty, S., Kumar, A., Eisch, A.J., Self, D.W., Lee, F.S., Tamminga, C.A., Cooper, D.C., Gershenfeld, H.K., Nestler, E.J., 2007. Molecular Adaptations Underlying Susceptibility and Resistance to Social Defeat in Brain Reward Regions. Cell 131, 391–404. https://doi.org/10.1016/j.cell.2007.09.018

Kysil, E.V., Meshalkina, D.A., Frick, E.E., Echevarria, D.J., Rosemberg, D.B., Maximino, C., Lima, M.G., Abreu, M.S., Giacomini, A.C., Barcellos, L.J.G., Song, C., Kalueff, A.V., 2017. Comparative Analyses of Zebrafish Anxiety-Like Behavior Using Conflict-Based Novelty Tests. Zebrafish 14, 197–208. https://doi.org/10.1089/zeb.2016.1415

Lai, N.H.Y., Mohd Zahir, I.A., Liew, A.K.Y., Ogawa, S., Parhar, I., Soga, T., 2023. Teleosts as behaviour test models for social stress. Front. Behav. Neurosci. 17. https://doi.org/10.3389/fnbeh.2023.1205175

Lal, P., Kawakami, K., 2022. Integrated Behavioral, Genetic and Brain Circuit Visualization Methods to Unravel Functional Anatomy of Zebrafish Amygdala. Front. Neuroanat. 16. https://doi.org/10.3389/fnana.2022.837527

Lebow, M.A., Chen, A., 2016. Overshadowed by the amygdala: the bed nucleus of the stria terminalis emerges as key to psychiatric disorders. Mol. Psychiatry 21, 450–463. https://doi.org/10.1038/mp.2016.1

Lee, A., Mathuru, A.S., Teh, C., Kibat, C., Korzh, V., Penney, T.B., Jesuthasan, S., 2010. The Habenula Prevents Helpless Behavior in Larval Zebrafish. Curr. Biol. 20, 2211–2216. https://doi.org/10.1016/j.cub.2010.11.025

Lee, H.B., Schwab, T.L., Sigafoos, A.N., Gauerke, J.L., Krug II, R.G., Serres, M.R., Jacobs, D.C., Cotter, R.P., Das, B., Petersen, M.O., Daby, C.L., Urban, R.M., Berry, B.C., Clark, K.J., 2019. Novel zebrafish behavioral assay to identify modifiers of the rapid, nongenomic stress response. Genes Brain Behav. 18, e12549. https://doi.org/10.1111/gbb.12549

Lee, H.B., Shams, S., Dang Thi, V.H., Boyum, G.E., Modhurima, R., Hall, E.M., Green, I.K., Cervantes, E.M., Miguez, F.E., Clark, K.J., 2024. Key HPI axis receptors facilitate light adaptive behavior in larval zebrafish. Sci. Rep. 14, 7759. https://doi.org/10.1038/s41598-024-57707-6

Lee, J.H., Meyer, E.J., Nenke, M.A., Falhammar, H., Torpy, D.J., 2023. Corticosteroid-binding globulin (CBG): spatiotemporal distribution of cortisol in sepsis. Trends Endocrinol. Metab. TEM 34, 181–190. https://doi.org/10.1016/j.tem.2023.01.002

Légaré, A., Lemieux, M., Desrosiers, P., Koninck, P.D., 2023. Zebrafish brain atlases: a collective effort for a tiny vertebrate brain. Neurophotonics 10, 044409–044409. https://doi.org/10.1117/1.nph.10.4.044409

Lehmann, M.L., Weigel, T.K., Cooper, H.A., Elkahloun, A.G., Kigar, S.L., Herkenham, M., 2018. Decoding microglia responses to psychosocial stress reveals blood-brain barrier breakdown that may drive stress susceptibility. Sci. Rep. 8, 11240. https://doi.org/10.1038/s41598-018-28737-8

Leiras, R., Cregg, J.M., Kiehn, O., 2022. Brainstem Circuits for Locomotion. Annu. Rev. Neurosci. 45, 63–85. https://doi.org/10.1146/annurev-neuro-082321-025137

Lewis, J.G., Elder, P.A., 2014. The reactive centre loop of corticosteroid-binding globulin (CBG) is a protease target for cortisol release. Mol. Cell. Endocrinol. 384, 96–101. https://doi.org/10.1016/j.mce.2014.01.005

Lightman, S.L., Conway-Campbell, B.L., 2024. Circadian and ultradian rhythms: Clinical implications. J. Intern. Med. 296, 121–138. https://doi.org/10.1111/joim.13795

Lin, P., Fang, Z., Liu, J., Lee, J.H., 2016. Optogenetic Functional MRI. J. Vis. Exp. JoVE 53346. https://doi.org/10.3791/53346

Lisieski, M.J., Eagle, A.L., Conti, A.C., Liberzon, I., Perrine, S.A., 2018. Single-Prolonged Stress: A Review of Two Decades of Progress in a Rodent Model of Post-traumatic Stress Disorder. Front. Psychiatry 9, 196. https://doi.org/10.3389/fpsyt.2018.00196

Lister, J.A., Robertson, C.P., Lepage, T., Johnson, S.L., Raible, D.W., 1999. nacre encodes a zebrafish microphthalmia-related protein that regulates neural-crest-derived pigment cell fate. Dev. Camb. Engl. 126, 3757–3767. https://doi.org/10.1242/dev.126.17.3757

Liu, K.S., Fetcho, J.R., 1999. Laser Ablations Reveal Functional Relationships of Segmental Hindbrain Neurons in Zebrafish. Neuron 23, 325–335. https://doi.org/10.1016/s0896-6273(00)80783-7

Loring, M.D., Thomson, E.E., Naumann, E.A., 2020. Whole-brain interactions underlying zebrafish behavior. Curr. Opin. Neurobiol. 65, 88–99. https://doi.org/10.1016/j.conb.2020.09.011

Lorsch, Z.S., Hamilton, P.J., Ramakrishnan, A., Parise, E.M., Salery, M., Wright, W.J., Lepack, A.E., Mews, P., Issler, O., McKenzie, A., Zhou, X., Parise, L.F., Pirpinias, S.T., Torres, I.O., Kronman, H.G., Montgomery, S.E., Loh, Y.-H.E., Labonté, B., Conkey, A., Symonds, A.E., Neve, R.L., Turecki, G., Maze, I., Dong, Y., Zhang, B., Shen, L., Bagot, R.C., Nestler, E.J., 2019. Stress resilience is promoted by a Zfp189-driven transcriptional network in prefrontal cortex. Nat. Neurosci. 22, 1413–1423. https://doi.org/10.1038/s41593-019-0462-8

Lupien, S.J., McEwen, B.S., Gunnar, M.R., Heim, C., 2009. Effects of stress throughout the lifespan on the brain, behaviour and cognition. Nat. Rev. Neurosci. 10, 434–445. https://doi.org/10.1038/nrn2639

Lupinsky, D., Nasseef, M.T., Parent, C., Craig, K., Diorio, J., Zhang, T.-Y., Meaney, M.J., 2025. Resting-state fMRI reveals altered functional connectivity associated with resilience and susceptibility to chronic social defeat stress in mouse brain. Mol. Psychiatry 30, 2943–2954. https://doi.org/10.1038/s41380-025-02897-2

Lynch, E., Dempsey, B., Saleeba, C., Monteiro, E., Turner, A., Burke, P.G.R., Allen, A.M., Dampney, R.A.L., Hildreth, C.M., Cornish, J.L., Goodchild, A.K., McMullan, S., 2022. Descending pathways from the superior colliculus mediating autonomic and respiratory effects associated with orienting behaviour. J. Physiol. 600, 5311–5332. https://doi.org/10.1113/JP283789

Lyons, D.M., Parker, K.J., 2007. Stress inoculation-induced indications of resilience in monkeys. J. Trauma. Stress 20, 423–433. https://doi.org/10.1002/jts.20265

Ma, PoKay M., 1994. Catecholaminergic systems in the zebrafish. II. Projection pathways and pattern of termination of the locus coeruleus. J. Comp. Neurol. 344, 256–269. https://doi.org/10.1002/cne.903440207

Ma, Pokay M., 1994. Catecholaminergic systems in the zebrafish. I. Number, morphology, and histochemical characteristics of neurons in the locus coeruleus. J. Comp. Neurol. 344, 242–255. https://doi.org/10.1002/cne.903440206

MacPhail, R.C., Brooks, J., Hunter, D.L., Padnos, B., Irons, T.D., Padilla, S., 2009. Locomotion in larval zebrafish: Influence of time of day, lighting and ethanol. NeuroToxicology 30, 52–58. https://doi.org/10.1016/j.neuro.2008.09.011

Maier, S.F., Seligman, M.E.P., 2016. Learned Helplessness at Fifty: Insights from Neuroscience. Psychol. Rev. 123, 349–367. https://doi.org/10.1037/rev0000033

Maier, S.F., Watkins, L.R., 2010. Role of the medial prefrontal cortex in coping and resilience. Brain Res. 1355, 52–60. https://doi.org/10.1016/j.brainres.2010.08.039

Mandino, F., Vujic, S., Grandjean, J., Lake, E.M.R., 2023. Where do we stand on fMRI in awake mice? Cereb. Cortex N. Y. NY 34, bhad478. https://doi.org/10.1093/cercor/bhad478

Manuel, R., Gorissen, M., Piza Roca, C., Zethof, J., van de Vis, H., Flik, G., van den Bos, R., 2014. Inhibitory Avoidance Learning in Zebrafish (Danio Rerio): Effects of Shock Intensity and Unraveling Differences in Task Performance. Zebrafish 11, 341–352. https://doi.org/10.1089/zeb.2013.0970

Marco, R.J.D., Groneberg, A.H., Yeh, C.-M., Treviño, M., Ryu, S., 2014. The behavior of larval zebrafish reveals stressor-mediated anorexia during early vertebrate development. Front. Behav. Neurosci. 8, 367. https://doi.org/10.3389/fnbeh.2014.00367

Maren, S., Phan, K.L., Liberzon, I., 2013. The contextual brain: implications for fear conditioning, extinction and psychopathology. Nat. Rev. Neurosci. 14, 417–428. https://doi.org/10.1038/nrn3492

Marques, J.C., Lackner, S., Félix, R., Orger, M.B., 2018. Structure of the Zebrafish Locomotor Repertoire Revealed with Unsupervised Behavioral Clustering. Curr. Biol. 28, 181-195.e5. https://doi.org/10.1016/j.cub.2017.12.002

Marwaha, J., Kehne, J.H., Commissaris, R.L., Lakoski, J., Shaw, W., Davis, M., 1983. Spinal clonidine inhibits neural firing in locus coeruleus. Brain Res. 276, 379–383. https://doi.org/10.1016/0006-8993(83)90752-7

Mathis, A., Mamidanna, P., Cury, K.M., Abe, T., Murthy, V.N., Mathis, M.W., Bethge, M., 2018. DeepLabCut: markerless pose estimation of user-defined body parts with deep learning. Nat. Neurosci. 21, 1281–1289. https://doi.org/10.1038/s41593-018-0209-y

Matsumoto, M., Hikosaka, O., 2007. Lateral habenula as a source of negative reward signals in dopamine neurons. Nature 447, 1111–1115. https://doi.org/10.1038/nature05860

Maximino, C., Marques de Brito, T., Dias, C.A.G. de M., Gouveia, A., Morato, S., 2010. Scototaxis as anxiety-like behavior in fish. Nat. Protoc. 5, 209–216. https://doi.org/10.1038/nprot.2009.225

McEwen, B.S., 2007. Physiology and Neurobiology of Stress and Adaptation: Central Role of the Brain. Physiol. Rev. 87, 873–904. https://doi.org/10.1152/physrev.00041.2006

McEwen, B.S., 2002. Sex, stress and the hippocampus: allostasis, allostatic load and the aging process. Neurobiol. Aging, Brain Aging: Identifying the Brakes and Accelerators 23, 921–939. https://doi.org/10.1016/S0197-4580(02)00027-1

McEwen, B.S., 2000. The neurobiology of stress: from serendipity to clinical relevance1. Brain Res., Towards 2010, A brain Odyssey, The 3rd Brain Research Interactive 886, 172–189. https://doi.org/10.1016/S0006-8993(00)02950-4

McIlwrick, S., Rechenberg, A., Matthes, M., Burgstaller, J., Schwarzbauer, T., Chen, A., Touma, C., 2016. Genetic predisposition for high stress reactivity amplifies effects of early-life adversity. Psychoneuroendocrinology 70, 85–97. https://doi.org/10.1016/j.psyneuen.2016.04.023

McLaughlin, I., Dani, J.A., De Biasi, M., 2017. The medial habenula and interpeduncular nucleus circuitry is critical in addiction, anxiety, and mood regulation. J. Neurochem. 142, 130–143. https://doi.org/10.1111/jnc.14008

Meaney, M.J., 2001. Maternal Care, Gene Expression, and the Transmission of Individual Differences in Stress Reactivity Across Generations. Annu. Rev. Neurosci. 24, 1161–1192. https://doi.org/10.1146/annurev.neuro.24.1.1161

Migault, G., van der Plas, T.L., Trentesaux, H., Panier, T., Candelier, R., Proville, R., Englitz, B., Debrégeas, G., Bormuth, V., 2018. Whole-Brain Calcium Imaging during Physiological Vestibular Stimulation in Larval Zebrafish. Curr. Biol. 28, 3723-3735.e6. https://doi.org/10.1016/j.cub.2018.10.017

Miller, N., Gerlai, R., 2007. Quantification of shoaling behaviour in zebrafish (*Danio rerio*). Behav. Brain Res. 184, 157–166. https://doi.org/10.1016/j.bbr.2007.07.007

Minatohara, K., Akiyoshi, M., Okuno, H., 2016. Role of Immediate-Early Genes in Synaptic Plasticity and Neuronal Ensembles Underlying the Memory Trace. Front. Mol. Neurosci. 8, 78. https://doi.org/10.3389/fnmol.2015.00078

Mobbs, D., Petrovic, P., Marchant, J.L., Hassabis, D., Weiskopf, N., Seymour, B., Dolan, R.J., Frith, C.D., 2007. When fear is near: threat imminence elicits prefrontal-periaqueductal gray shifts in humans. Science 317, 1079–1083. https://doi.org/10.1126/science.1144298

Moeyaert, B., Holt, G., Madangopal, R., Perez-Alvarez, A., Fearey, B.C., Trojanowski, N.F., Ledderose, J., Zolnik, T.A., Das, A., Patel, D., Brown, T.A., Sachdev, R.N.S., Eickholt, B.J., Larkum, M.E., Turrigiano, G.G., Dana, H., Gee, C.E., Oertner, T.G., Hope, B.T., Schreiter, E.R., 2018. Improved methods for marking active neuron populations. Nat. Commun. 9, 4440. https://doi.org/10.1038/s41467-018-06935-2

Morgan, C.A., Wang, S., Southwick, S.M., Rasmusson, A., Hazlett, G., Hauger, R.L., Charney, D.S., 2000. Plasma neuropeptide-Y concentrations in humans exposed to military survival training. Biol. Psychiatry 47, 902–909. https://doi.org/10.1016/s0006-3223(99)00239-5

Mu, Y., Bennett, D.V., Rubinov, M., Narayan, S., Yang, C.-T., Tanimoto, M., Mensh, B.D., Looger, L.L., Ahrens, M.B., 2019. Glia Accumulate Evidence that Actions Are Futile and Suppress Unsuccessful Behavior. Cell 178, 27-43.e19. https://doi.org/10.1016/j.cell.2019.05.050

Musazzi, L., Tornese, P., Sala, N., Popoli, M., 2018. What Acute Stress Protocols Can Tell Us About PTSD and Stress-Related Neuropsychiatric Disorders. Front. Pharmacol. 9, 758. https://doi.org/10.3389/fphar.2018.00758

Musazzi, L., Tornese, P., Sala, N., Popoli, M., 2017. Acute or Chronic? A Stressful Question. Trends Neurosci. 40, 525–535. https://doi.org/10.1016/j.tins.2017.07.002

Myers, B., McKlveen, J.M., Herman, J.P., 2012. Neural Regulation of the Stress Response: The Many Faces of Feedback. Cell. Mol. Neurobiol. 32, 683–694. https://doi.org/10.1007/s10571-012-9801-y

Nakajo, H., Tsuboi, T., Okamoto, H., 2020. The behavioral paradigm to induce repeated social defeats in zebrafish. Neurosci. Res. 161, 24–32. https://doi.org/10.1016/j.neures.2019.11.004

Naumann, E.A., Fitzgerald, J.E., Dunn, T.W., Rihel, J., Sompolinsky, H., Engert, F., 2016. From Whole-Brain Data to Functional Circuit Models: The Zebrafish Optomotor Response. Cell 167, 947-960.e20. https://doi.org/10.1016/j.cell.2016.10.019

Nestler, E.J., Russo, S.J., 2024. Neurobiological basis of stress resilience. Neuron 112, 1911–1929. https://doi.org/10.1016/j.neuron.2024.05.001

Ochenkowska, K., Herold, A., Samarut, É., 2022. Zebrafish Is a Powerful Tool for Precision Medicine Approaches to Neurological Disorders. Front. Mol. Neurosci. 15, 944693. https://doi.org/10.3389/fnmol.2022.944693

Okamoto, H., Agetsuma, M., Aizawa, H., 2012. Genetic dissection of the zebrafish habenula, a possible switching board for selection of behavioral strategy to cope with fear and anxiety. Dev. Neurobiol. 72, 386–394. https://doi.org/10.1002/dneu.20913

Olson, I., Suryanarayana, S.M., Robertson, B., Grillner, S., 2017. Griseum centrale, a homologue of the periaqueductal gray in the lamprey. IBRO Rep. 2, 24–30. https://doi.org/10.1016/j.ibror.2017.01.001

Orger, M.B., Polavieja, G.G. de, 2015. Zebrafish Behavior: Opportunities and Challenges. Annu. Rev. Neurosci. 40, 1–23. https://doi.org/10.1146/annurev-neuro-071714-033857

Orts-Del'Immagine, A., Dhanasekar, M., Lejeune, F.-X., Roussel, J., Wyart, C., 2022. A norepinephrine-dependent glial calcium wave travels in the spinal cord upon acoustovestibular stimuli. Glia 70, 491–507. https://doi.org/10.1002/glia.24118

Øverli, Ø., Sørensen, C., Pulman, K.G.T., Pottinger, T.G., Korzan, W., Summers, C.H., Nilsson, G.E., 2007. Evolutionary background for stress-coping styles: Relationships between physiological, behavioral, and cognitive traits in non-mammalian vertebrates. Neurosci. Biobehav. Rev. 31, 396–412. https://doi.org/10.1016/j.neubiorev.2006.10.006

Pakos-Zebrucka, K., Koryga, I., Mnich, K., Ljujic, M., Samali, A., Gorman, A.M., 2016. The integrated stress response. EMBO Rep. 17, 1374–1395. https://doi.org/10.15252/embr.201642195

Palma-Espinosa, J., Orellana-Villota, S., Coronel-Oliveros, C., Maidana, J.P., Orio, P., 2025. The balance between integration and segregation drives network dynamics maximizing multistability and metastability. Sci. Rep. 15, 18811. https://doi.org/10.1038/s41598-025-01612-z

Pantoja, C., Larsch, J., Laurell, E., Marquart, G., Kunst, M., Baier, H., 2020. Rapid Effects of Selection on Brain-wide Activity and Behavior. Curr. Biol. CB 30, 3647-3656.e3. https://doi.org/10.1016/j.cub.2020.06.086

Patchev, V.K., Patchev, A.V., 2006. Experimental models of stress. Dialogues Clin. Neurosci. 8, 417–432. https://doi.org/10.31887/DCNS.2006.8.4/vpatchev

Peixoto, L., Abel, T., 2013. The Role of Histone Acetylation in Memory Formation and Cognitive Impairments. Neuropsychopharmacology 38, 62–76. https://doi.org/10.1038/npp.2012.86

Pessoa, L., 2017. A Network Model of the Emotional Brain. Trends Cogn. Sci. 21, 357–371. https://doi.org/10.1016/j.tics.2017.03.002

Petersen, B.D., Bertoncello, K.T., Bonan, C.D., 2022. Standardizing Zebrafish Behavioral Paradigms Across Life Stages: An Effort Towards Translational Pharmacology. Front. Pharmacol. 13. https://doi.org/10.3389/fphar.2022.833227

Philippe, C., Vergauwen, L., Huyghe, K., De Boeck, G., Knapen, D., 2023. Chronic handling stress in zebrafish Danio rerio husbandry. J. Fish Biol. 103, 367–377. https://doi.org/10.1111/jfb.15453

Piato, Â.L., Capiotti, K.M., Tamborski, A.R., Oses, J.P., Barcellos, L.J.G., Bogo, M.R., Lara, D.R., Vianna, M.R., Bonan, C.D., 2011. Unpredictable chronic stress model in zebrafish (*Danio rerio*): Behavioral and physiological responses. Prog. Neuropsychopharmacol. Biol. Psychiatry, The Neurobiology of Neurodegenerative Disorder: From Basic to Clinical Research 35, 561–567. https://doi.org/10.1016/j.pnpbp.2010.12.018

Pineda, J., Ruiz-Ortega, J.A., Ugedo, L., 1997. Receptor Reserve and Turnover of *Alpha*-2 Adrenoceptors that Mediate the Clonidine-Induced Inhibition of Rat Locus Coeruleus Neurons *In Vivo*1. J. Pharmacol. Exp. Ther. 281, 690–698. https://doi.org/10.1016/S0022-3565(24)36670-4

Porter, B.A., Mueller, T., 2020. The Zebrafish Amygdaloid Complex – Functional Ground Plan, Molecular Delineation, and Everted Topology. Front. Neurosci. 14, 608. https://doi.org/10.3389/fnins.2020.00608

Portugues, R., Feierstein, C.E., Engert, F., Orger, M.B., 2014. Whole-brain activity maps reveal stereotyped, distributed networks for visuomotor behavior. Neuron 81, 1328–1343. https://doi.org/10.1016/j.neuron.2014.01.019

Prevedel, R., Yoon, Y.-G., Hoffmann, M., Pak, N., Wetzstein, G., Kato, S., Schrödel, T., Raskar, R., Zimmer, M., Boyden, E.S., Vaziri, A., 2014. Simultaneous whole-animal 3D imaging of neuronal activity using light-field microscopy. Nat. Methods 11, 727–730. https://doi.org/10.1038/nmeth.2964

Privitera, M., Von Ziegler, L.M., Floriou-Servou, A., Duss, S.N., Zhang, R., Waag, R., Leimbacher, S., Sturman, O., Roessler, F.K., Heylen, A., Vermeiren, Y., Van Dam, D., De Deyn, P.P., Germain, P.-L., Bohacek, J., 2024. Noradrenaline release from the locus coeruleus shapes stress-induced hippocampal gene expression. eLife 12, RP88559. https://doi.org/10.7554/eLife.88559

Prut, L., Belzung, C., 2003. The open field as a paradigm to measure the effects of drugs on anxiety-like behaviors: a review. Eur. J. Pharmacol., Animal Models of Anxiety Disorders 463, 3–33. https://doi.org/10.1016/S0014-2999(03)01272-X

Rahman, M.F., McGowan, P.O., 2022. Cell-type-specific epigenetic effects of early life stress on the brain. Transl. Psychiatry 12, 326. https://doi.org/10.1038/s41398-022-02076-9

Rajput, N., Parikh, K., Kenney, J.W., 2022. Beyond bold versus shy: Zebrafish exploratory behavior falls into several behavioral clusters and is influenced by strain and sex. Biol. Open 11, bio059443. https://doi.org/10.1242/bio.059443

Ramsay, J.M., Feist, G.W., Varga, Z.M., Westerfield, M., Kent, M.L., Schreck, C.B., 2009. Whole-body cortisol response of zebrafish to acute net handling stress. Aquaculture 297, 157–162. https://doi.org/10.1016/j.aquaculture.2009.08.035

Randlett, O., Wee, C.L., Naumann, E.A., Nnaemeka, O., Schoppik, D., Fitzgerald, J.E., Portugues, R., Lacoste, A.M.B., Riegler, C., Engert, F., Schier, A.F., 2015. Whole-brain activity mapping onto a zebrafish brain atlas. Nat. Methods 12, 1039–1046. https://doi.org/10.1038/nmeth.3581

Ren, C., Komiyama, T., 2021. Characterizing Cortex-Wide Dynamics with Wide-Field Calcium Imaging. J. Neurosci. 41, 4160–4168. https://doi.org/10.1523/JNEUROSCI.3003-20.2021

Renier, N., Adams, E.L., Kirst, C., Wu, Z., Azevedo, R., Kohl, J., Autry, A.E., Kadiri, L., Umadevi Venkataraju, K., Zhou, Y., Wang, V.X., Tang, C.Y., Olsen, O., Dulac, C., Osten, P., Tessier-Lavigne, M., 2016. Mapping of Brain Activity by Automated Volume Analysis of Immediate Early Genes. Cell 165, 1789–1802. https://doi.org/10.1016/j.cell.2016.05.007

Rolls, E.T., 2017. The roles of the orbitofrontal cortex via the habenula in non-reward and depression, and in the responses of serotonin and dopamine neurons. Neurosci. Biobehav. Rev. 75, 331–334. https://doi.org/10.1016/j.neubiorev.2017.02.013

Russo, Scott J, Murrough, J.W., Han, M.-H., Charney, D.S., Nestler, E.J., 2012. Neurobiology of resilience. Nat. Neurosci. 15, 1475–1484. https://doi.org/10.1038/nn.3234

Russo, Scott J., Murrough, J.W., Han, M.-H., Charney, D.S., Nestler, E.J., 2012. Neurobiology of resilience. Nat. Neurosci. 15, 1475–1484. https://doi.org/10.1038/nn.3234

Rutter, M., 2012. Resilience as a dynamic concept. Dev. Psychopathol. 24, 335–344. https://doi.org/10.1017/S0954579412000028

S. de Abreu, M., Parker, M.O., Kalueff, A.V., 2024. Standardizing zebrafish laboratory husbandry to ensure replicability and reproducibility of data in neurobehavioral research. Lab Anim. 53, 189–190. https://doi.org/10.1038/s41684-024-01411-5

Seutin, V., Verbanck, P., Massotte, L., Dresse, A., 1989. Galanin decreases the activity of locus coeruleus neurons in vitro. Eur. J. Pharmacol. 164, 373–376. https://doi.org/10.1016/0014-2999(89)90481-0

Severi, K.E., Portugues, R., Marques, J.C., O'Malley, D.M., Orger, M.B., Engert, F., 2014. Neural Control and Modulation of Swimming Speed in the Larval Zebrafish. Neuron 83, 692–707. https://doi.org/10.1016/j.neuron.2014.06.032

Shvartsburd, Z., Vijayan, M.M., 2025. Corticotropin-releasing hormone receptor 1 mediates the enhanced locomotor activity and metabolic demands to an acute thermal stress in adult zebrafish. J. Neuroendocrinol. 37, e13497. https://doi.org/10.1111/jne.13497

Sial, O.K., Warren, B.L., Alcantara, L.F., Parise, E.M., Bolaños-Guzmán, C.A., 2016. Vicarious social defeat stress: Bridging the gap between physical and emotional stress. J. Neurosci. Methods 258, 94–103. https://doi.org/10.1016/j.jneumeth.2015.10.012

Sidrauski, C., Acosta-Alvear, D., Khoutorsky, A., Vedantham, P., Hearn, B.R., Li, H., Gamache, K., Gallagher, C.M., Ang, K.K.-H., Wilson, C., Okreglak, V., Ashkenazi, A., Hann, B., Nader, K., Arkin, M.R., Renslo, A.R., Sonenberg, N., Walter, P., 2013. Pharmacological brake-release of mRNA translation enhances cognitive memory. eLife 2, e00498. https://doi.org/10.7554/eLife.00498

Singh, C., Oikonomou, G., Prober, D.A., 2015. Norepinephrine is required to promote wakefulness and for hypocretin-induced arousal in zebrafish. eLife 4, e07000. https://doi.org/10.7554/eLife.07000

Southwick, S.M., Bonanno, G.A., Masten, A.S., Panter-Brick, C., Yehuda, R., 2014. Resilience definitions, theory, and challenges: interdisciplinary perspectives. Eur. J. Psychotraumatology 5, 10.3402/ejpt.v5.25338. https://doi.org/10.3402/ejpt.v5.25338

Speedie, N., Gerlai, R., 2008. Alarm substance induced behavioral responses in zebrafish (Danio rerio). Behav. Brain Res. 188, 168–177. https://doi.org/10.1016/j.bbr.2007.10.031

Stavreva, D.A., Wiench, M., John, S., Conway-Campbell, B.L., McKenna, M.A., Pooley, J.R., Johnson, T.A., Voss, T.C., Lightman, S.L., Hager, G.L., 2009. Ultradian hormone stimulation induces glucocorticoid receptor-mediated pulses of gene transcription. Nat. Cell Biol. 11, 1093–1102. https://doi.org/10.1038/ncb1922

Steimer, T., Driscoll, P., 2003. Divergent Stress Responses and Coping Styles in Psychogenetically Selected Roman High-(RHA) and Low-(RLA) Avoidance Rats: Behavioural, Neuroendocrine and Developmental Aspects. Stress 6, 87–100. https://doi.org/10.1080/1025389031000111320

Sterling, P., Eyer, J., 1988. Allostasis: A new paradigm to explain arousal pathology, in: Handbook of Life Stress, Cognition and Health. John Wiley & Sons, Oxford, England, pp. 629–649.

Stewart, A., Cachat, J., Wong, K., Gaikwad, S., Gilder, T., DiLeo, J., Chang, K., Utterback, E., Kalueff, A.V., 2010. Homebase behavior of zebrafish in novelty-based paradigms. Behav. Processes 85, 198–203. https://doi.org/10.1016/j.beproc.2010.07.009

Stewart, A., Gaikwad, S., Kyzar, E., Green, J., Roth, A., Kalueff, A.V., 2012. Modeling anxiety using adult zebrafish: A conceptual review. Neuropharmacology 62, 135–143. https://doi.org/10.1016/j.neuropharm.2011.07.037

Stewart, A.M., Gaikwad, S., Kyzar, E., Kalueff, A.V., 2012. Understanding spatio-temporal strategies of adult zebrafish exploration in the open field test. Brain Res. 1451, 44–52. https://doi.org/10.1016/j.brainres.2012.02.064

Swaminathan, A., Gliksberg, M., Anbalagan, S., Wigoda, N., Levkowitz, G., 2023. Stress resilience is established during development and is regulated by complement factors. Cell Rep. 42, 111973. https://doi.org/10.1016/j.celrep.2022.111973

Takahashi, H., Sakamoto, T., 2013. The role of 'mineralocorticoids' in teleost fish: Relative importance of glucocorticoid signaling in the osmoregulation and 'central' actions of mineralocorticoid receptor. Gen. Comp. Endocrinol., Combined Special Issues: CESP 2012 and 7th AOSCE Congress 181, 223–228. https://doi.org/10.1016/j.ygcen.2012.11.016

Terstege, D.J., Durante, I.M., Epp, J.R., 2022. Brain-wide neuronal activation and functional connectivity are modulated by prior exposure to repetitive learning episodes. Front. Behav. Neurosci. 16. https://doi.org/10.3389/fnbeh.2022.907707

Theodoridi, A., Dinarello, A., Badenetti, L., Pavlidis, M., Dalla Valle, L., Tsalafouta, A., 2021. Knockout of the hsd11b2 Gene Extends the Cortisol Stress Response in Both Zebrafish Larvae and Adults. Int. J. Mol. Sci. 22, 12525. https://doi.org/10.3390/ijms222212525

Thiele, T.R., Donovan, J.C., Baier, H., 2014. Descending control of swim posture by a midbrain nucleus in zebrafish. Neuron 83, 679–691. https://doi.org/10.1016/j.neuron.2014.04.018

Tillage, R.P., Wilson, G.E., Liles, L.C., Holmes, P.V., Weinshenker, D., 2020. Chronic Environmental or Genetic Elevation of Galanin in Noradrenergic Neurons Confers Stress Resilience in Mice. J. Neurosci. 40, 7464–7474. https://doi.org/10.1523/JNEUROSCI.0973-20.2020

Tovote, P., Esposito, M.S., Botta, P., Chaudun, F., Fadok, J.P., Markovic, M., Wolff, S.B.E., Ramakrishnan, C., Fenno, L., Deisseroth, K., Herry, C., Arber, S., Lüthi, A., 2016. Midbrain circuits for defensive behaviour. Nature 534, 206–212. https://doi.org/10.1038/nature17996

Tovote, P., Fadok, J.P., Lüthi, A., 2015. Neuronal circuits for fear and anxiety. Nat. Rev. Neurosci. 16, 317–331. https://doi.org/10.1038/nrn3945

Tudorache, C., ter Braake, A., Tromp, M., Slabbekoorn, H., Schaaf, M.J.M., 2015. Behavioral and physiological indicators of stress coping styles in larval zebrafish. Stress 18, 121–128. https://doi.org/10.3109/10253890.2014.989205

Turrigiano, G., 2012. Homeostatic Synaptic Plasticity: Local and Global Mechanisms for Stabilizing Neuronal Function. Cold Spring Harb. Perspect. Biol. 4, a005736–a005736. https://doi.org/10.1101/cshperspect.a005736

Tyssowski, K.M., DeStefino, N.R., Cho, J.-H., Dunn, C.J., Poston, R.G., Carty, C.E., Jones, R.D., Chang, S.M., Romeo, P., Wurzelmann, M.K., Ward, J.M., Andermann, M.L., Saha, R.N., Dudek, S.M., Gray, J.M., 2018. Different Neuronal Activity Patterns Induce Different Gene Expression Programs. Neuron 98, 530-546.e11. https://doi.org/10.1016/j.neuron.2018.04.001

Van Essen, D.C., Smith, S.M., Barch, D.M., Behrens, T.E.J., Yacoub, E., Ugurbil, K., 2013. The WU-Minn Human Connectome Project: An overview. NeuroImage, Mapping the Connectome 80, 62–79. https://doi.org/10.1016/j.neuroimage.2013.05.041

Varga, Z.K., Pejtsik, D., Biró, L., Zsigmond, Á., Varga, M., Tóth, B., Salamon, V., Annus, T., Mikics, É., Aliczki, M., 2020. Conserved Serotonergic Background of Experience-Dependent Behavioral Responsiveness in Zebrafish (Danio rerio). J. Neurosci. 40, 4551–4564. https://doi.org/10.1523/JNEUROSCI.2178-19.2020

Vecsey, C.G., Hawk, J.D., Lattal, K.M., Stein, J.M., Fabian, S.A., Attner, M.A., Cabrera, S.M., McDonough, C.B., Brindle, P.K., Abel, T., Wood, M.A., 2007. Histone deacetylase inhibitors enhance memory and synaptic plasticity via CREB:CBP-dependent transcriptional activation. J. Neurosci. Off. J. Soc. Neurosci. 27, 6128–6140. https://doi.org/10.1523/JNEUROSCI.0296-07.2007

Verbitsky, A., Dopfel, D., Zhang, N., 2020. Rodent models of post-traumatic stress disorder: behavioral assessment. Transl. Psychiatry 10, 132. https://doi.org/10.1038/s41398-020-0806-x

Vignet, C., Bégout, M.-L., Péan, S., Lyphout, L., Leguay, D., Cousin, X., 2013. Systematic Screening of Behavioral Responses in Two Zebrafish Strains. Zebrafish 10, 365–375. https://doi.org/10.1089/zeb.2013.0871

Vindas, M.A., Gorissen, M., Höglund, E., Flik, G., Tronci, V., Damsgård, B., Thörnqvist, P.-O., Nilsen, T.O., Winberg, S., Øverli, Ø., Ebbesson, L.O.E., 2017. How do individuals cope with stress? Behavioural, physiological and neuronal differences between proactive and reactive coping styles in fish. J. Exp. Biol. 220, 1524–1532. https://doi.org/10.1242/jeb.153213

Vladimirov, N., Mu, Y., Kawashima, T., Bennett, D.V., Yang, C.-T., Looger, L.L., Keller, P.J., Freeman, J., Ahrens, M.B., 2014. Light-sheet functional imaging in fictively behaving zebrafish. Nat. Methods 11, 883–884. https://doi.org/10.1038/nmeth.3040

Vom Berg-Maurer, C.M., Trivedi, C.A., Bollmann, J.H., De Marco, R.J., Ryu, S., 2016. The Severity of Acute Stress Is Represented by Increased Synchronous Activity and Recruitment of Hypothalamic CRH Neurons. J. Neurosci. Off. J. Soc. Neurosci. 36, 3350–3362. https://doi.org/10.1523/JNEUROSCI.3390-15.2016

Walker, C.-D., Bath, K.G., Joels, M., Korosi, A., Larauche, M., Lucassen, P.J., Morris, M.J., Raineki, C., Roth, T.L., Sullivan, R.M., Taché, Y., Baram, T.Z., 2017. Chronic early life stress induced by limited bedding and nesting (LBN) material in rodents: critical considerations of methodology, outcomes and translational potential. Stress Amst. Neth. 20, 421–448. https://doi.org/10.1080/10253890.2017.1343296

Wang, D., Levine, J.L.S., Avila-Quintero, V., Bloch, M., Kaffman, A., 2020. Systematic review and meta-analysis: effects of maternal separation on anxiety-like behavior in rodents. Transl. Psychiatry 10, 174. https://doi.org/10.1038/s41398-020-0856-0

Wang, M., Ramos, B.P., Paspalas, C.D., Shu, Y., Simen, A., Duque, A., Vijayraghavan, S., Brennan, A., Dudley, A., Nou, E., Mazer, J.A., McCormick, D.A., Arnsten, A.F.T., 2007. α2A-Adrenoceptors Strengthen Working Memory Networks by Inhibiting cAMP-HCN Channel Signaling in Prefrontal Cortex. Cell 129, 397–410. https://doi.org/10.1016/j.cell.2007.03.015

Wang, W., Liu, W., Duan, D., Bai, H., Wang, Z., Xing, Y., 2021. Chronic social defeat stress mouse model: Current view on its behavioral deficits and modifications. Behav. Neurosci. 135, 326–335. https://doi.org/10.1037/bne0000418

Warden, M.R., Selimbeyoglu, A., Mirzabekov, J.J., Lo, M., Thompson, K.R., Kim, S.-Y., Adhikari, A., Tye, K.M., Frank, L.M., Deisseroth, K., 2012. A prefrontal cortex–brainstem neuronal projection that controls response to behavioural challenge. Nature 492, 428–432. https://doi.org/10.1038/nature11617

Watanabe, K., Chiu, H., Anderson, D.J., 2024. HI-FISH: WHOLE BRAIN IN SITU MAPPING OF NEURONAL ACTIVATION IN DROSOPHILA DURING SOCIAL BEHAVIORS AND OPTOGENETIC STIMULATION. bioRxiv 2023.09.28.560045. https://doi.org/10.1101/2023.09.28.560045

Wee, C.L., Song, E.Y., Johnson, R.E., Ailani, D., Randlett, O., Kim, J.-Y., Nikitchenko, M., Bahl, A., Yang, C.-T., Ahrens, M.B., Kawakami, K., Engert, F., Kunes, S., 2019. A bidirectional network for appetite control in larval zebrafish. eLife 8, e43775. https://doi.org/10.7554/eLife.43775

Willmore, L., Cameron, C., Yang, J., Witten, I.B., Falkner, A.L., 2022. Behavioural and dopaminergic signatures of resilience. Nature 611, 124–132. https://doi.org/10.1038/s41586-022-05328-2

Willner, P., 2016. The chronic mild stress (CMS) model of depression: History, evaluation and usage. Neurobiol. Stress 6, 78–93. https://doi.org/10.1016/j.ynstr.2016.08.002

Winberg, S., Höglund, E., Øverli, Ø., 2016. 2 - Variation in the Neuroendocrine Stress Response, in: Schreck, C.B., Tort, L., Farrell, A.P., Brauner, C.J. (Eds.), Fish Physiology, Biology of Stress in Fish. Academic Press, pp. 35–74. https://doi.org/10.1016/B978-0-12-802728-8.00002-3

Winberg, S., Thörnqvist, P.-O., 2016. Role of brain serotonin in modulating fish behavior. Curr. Zool. 62, 317–323. https://doi.org/10.1093/cz/zow037

Wolf, A.B., Lintz, M.J., Costabile, J.D., Thompson, J.A., Stubblefield, E.A., Felsen, G., 2015. An integrative role for the superior colliculus in selecting targets for movements. J. Neurophysiol. 114, 2118–2131. https://doi.org/10.1152/jn.00262.2015

Wong, R.Y., French, J., Russ, J.B., 2019. Differences in stress reactivity between zebrafish with alternative stress coping styles. R. Soc. Open Sci. 6, 181797. https://doi.org/10.1098/rsos.181797

Wu, J., Yan, B., Bao, M., Shen, J., Zheng, P., Wu, D., Wang, J., Li, Z., Jiang, K., 2023. Early life exposure to chronic unpredictable stress induces anxiety-like behaviors and increases the excitability of cerebellar neurons in zebrafish. Behav. Brain Res. 437, 114160. https://doi.org/10.1016/j.bbr.2022.114160

Xu, X., Scott-Scheiern, T., Kempker, L., Simons, K., 2007. Active avoidance conditioning in zebrafish (*Danio rerio*). Neurobiol. Learn. Mem. 87, 72–77. https://doi.org/10.1016/j.nlm.2006.06.002

Yap, E.-L., Greenberg, M.E., 2018. Activity-Regulated Transcription: Bridging the Gap between Neural Activity and Behavior. Neuron 100, 330–348. https://doi.org/10.1016/j.neuron.2018.10.013

Yeh, C.-M., Glöck, M., Ryu, S., 2013. An Optimized Whole-Body Cortisol Quantification Method for Assessing Stress Levels in Larval Zebrafish. PLOS ONE 8, e79406. https://doi.org/10.1371/journal.pone.0079406

Yuan, M., Chen, Y., Huang, Y., Lu, W., 2018. Behavioral and Metabolic Phenotype Indicate Personality in Zebrafish (Danio rerio). Front. Physiol. 9. https://doi.org/10.3389/fphys.2018.00653

Zagrebelsky, M., Tacke, C., Korte, M., 2020. BDNF signaling during the lifetime of dendritic spines. Cell Tissue Res. 382, 185–199. https://doi.org/10.1007/s00441-020-03226-5

Zannas, A.S., Wiechmann, T., Gassen, N.C., Binder, E.B., 2016. Gene–Stress–Epigenetic Regulation of FKBP5: Clinical and Translational Implications. Neuropsychopharmacology 41, 261–274. https://doi.org/10.1038/npp.2015.235

Ziv, L., Muto, A., Schoonheim, P.J., Meijsing, S.H., Strasser, D., Ingraham, H.A., Schaaf, M.J.M., Yamamoto, K.R., Baier, H., 2013. An affective disorder in zebrafish with mutation of the glucocorticoid receptor. Mol. Psychiatry 18, 681–691. https://doi.org/10.1038/mp.2012.64

Zou, W.-J., Song, Y.-L., Wu, M.-Y., Chen, X.-T., You, Q.-L., Yang, Q., Luo, Z.-Y., Huang, L., Kong, Y., Feng, J., Fang, D.-X., Li, X.-W., Yang, J.-M., Mei, L., Gao, T.-M., 2020. A discrete serotonergic circuit regulates vulnerability to social stress. Nat. Commun. 11, 4218. https://doi.org/10.1038/s41467-020-18010-w

APPENDIX

Manuscript I

Quantifying Stress Resilience as Locomotor Rebound in Larval Zebrafish

João Campagnolo[1], Emel Ahmad[1], Raghavendra Selvan[2], Florence Kermen[1]

Affiliations:

[1] Department of Neuroscience, SUND, University of Copenhagen, Denmark

[2] Department of Computer Science, SCIENCE, University of Copenhagen, Denmark

ABSTRACT

Stress resilience, the ability to regain adaptive function after challenge, varies across individuals. We developed a behavioral assay in larval zebrafish that quantifies resilience by measuring locomotor rebound following acute stress. The resulting resilience score discriminates between two phenotypes, resilient and vulnerable, that diverge during recovery rather than during baseline or stressor exposure. The assay is robust across different transgenic lines and stressor types, and resilience decreases with increasing stressor strength. Resilience phenotypes showed limited stability between 1 and 2 weeks of age, but remained consistent from 1 week to 1 month of age. Together, these findings establish an accessible assay for standardized resilience phenotyping and longitudinal analysis in zebrafish.

INTRODUCTION

Stress responses help organisms maintain stability through change (allostasis). When prolonged or mismatched to context, the resulting allostatic load increases vulnerability to pathology (Charney 2004; McEwen 2007). Understanding the mechanisms that enable adaptive recovery offers leverage for preventing or alleviating stress-related disorders.

In modeling the variability of the behavioral stress responses in animal models, the concept of stress coping styles is especially relevant. Stress coping styles refer to a stable set of behavioral and physiological responses to stress (Koolhaas et al. 1999; Tudorache et al. 2015). Proactive individuals tend to display risk-taking behavior, high exploration of novel environments, and active avoidance strategies, while reactive individuals typically exhibit risk-avoidance and immobility. Several approaches have been developed to classify larval zebrafish according to their distinct stress coping styles, for example, using emergence latency from a dark shelter into a lit arena after netting stress (Tudorache et al. 2015), or control-indexed distance swam during recovery from a hyperosmotic stressor (Swaminathan et al. 2023).

A limitation of these approaches for assessing stress resilience or coping in larvae is that they rely on speed-based metrics to evaluate recovery after stress, without accounting for each larva's individual baseline activity. Yet, swimming activity in larval zebrafish is highly variable and depends on many developmental, internal, and external factors, such as genetic strain, swim bladder inflation, internal states, and time of day (Ingebretson and Masino 2013; Farrell et al. 2011; MacPhail et al. 2009; Andalman et al. 2019). Consequently, resilience metrics may be confounded by these sources of variability, which highlights the need for behavioral assays that can screen for stress resilience independently of initial locomotor activity.

Here, we establish a medium-throughput behavioral assay consisting of three consecutive phases: baseline, short-term stress, and recovery periods. Offline automated tracking of trajectories enables classification of larval zebrafish as stress resilient or stress vulnerable, based on their baseline-to-recovery locomotor dynamics following the challenge. We examine the stability of the resilience phenotypes in different transgenic lines, as well as in response to several stressor types and intensities. Finally, the stability of resilience scores throughout mid-larval and juvenile stages is also assessed.

RESULTS

Different resilience phenotypes based on locomotor recovery after stress exposure

Resilience was evaluated across multiple replicates of the same assay, each recording 24 larvae simultaneously, using a three-phase protocol comprising a 30-min baseline in artificial fish water, a 10-min exposure to 250 mM NaCl, and a 5-min recovery in renewed artificial fish water (Methods; Fig. 1A). At 6 days post-fertilization (dpf), larvae showed substantial individual variability in spontaneous locomotion during baseline (Fig. 1C). To ensure that these differences in spontaneous activity did not confound the measure of stress resilience during the recovery period, we defined the resilience score as the relative change in swimming speed from baseline to recovery, with negative values indicating suppressed swimming during recovery and values close to zero indicating rapid return to baseline activity (Methods).

To categorize individuals along the resilience-vulnerability axis, thresholds were set on the continuous score distribution. Visual and distributional analyses indicated multimodality, consistent with distinct behavioral subpopulations rather than a single continuum (Sup. Fig. 1). To maximize biological contrast while maintaining statistical power, we focused on the distributional extremes and adopted thresholds to label *vulnerable* (score ≤ -0.5) and *resilient* (score ≥ -0.1) fish. Representative trajectories illustrate the behavior of larvae within both phenotypic categories (Fig. 1B).

Across both resilient and vulnerable groups, locomotion speed decreased during the first part of the baseline period before stabilizing, which likely reflected habituation to the setup (Fig. 1C). Speed increased slightly on average during stressor exposure in both groups. Overall, no difference in speed was observed between resilient and vulnerable fish during the baseline and stress exposure periods. Resilient individuals exhibited a rapid return to pre-stress locomotor activity levels, characterized by a significant increase in average speed at the beginning of the recovery period (10 minutes post-stress; $p < 0.00001$), whereas vulnerable fish maintained reduced movement. This pattern held across additional behavioral metrics, including acceleration, angular velocity, angular acceleration, swim bursts, movement duration, idle time, total distance, and sharp turns. Contrastingly, distance to the well center remained similar between groups across all stages (Sup. Fig. 2A-B).

To assess how long stress-induced behavioral differences in resilience phenotypes persist after stress exposure, we conducted an additional experiment with a longer recovery period of 45 minutes (Sup. Fig. 3C-D). While swimming speed differed significantly between resilient and vulnerable zebrafish during the first 15 minutes post-stress, these differences did not persist thereafter, with both groups returning to comparable activity levels for the rest of the recovery period. These findings suggest that the distinction between resilience phenotypes is most apparent immediately following stressor removal. Additionally, the return of swimming speeds to similar levels in both groups indicates that these stress resilience phenotypes are not due to inherent differences in swimming ability, but rather to their acute reactivity shortly after stress exposure.

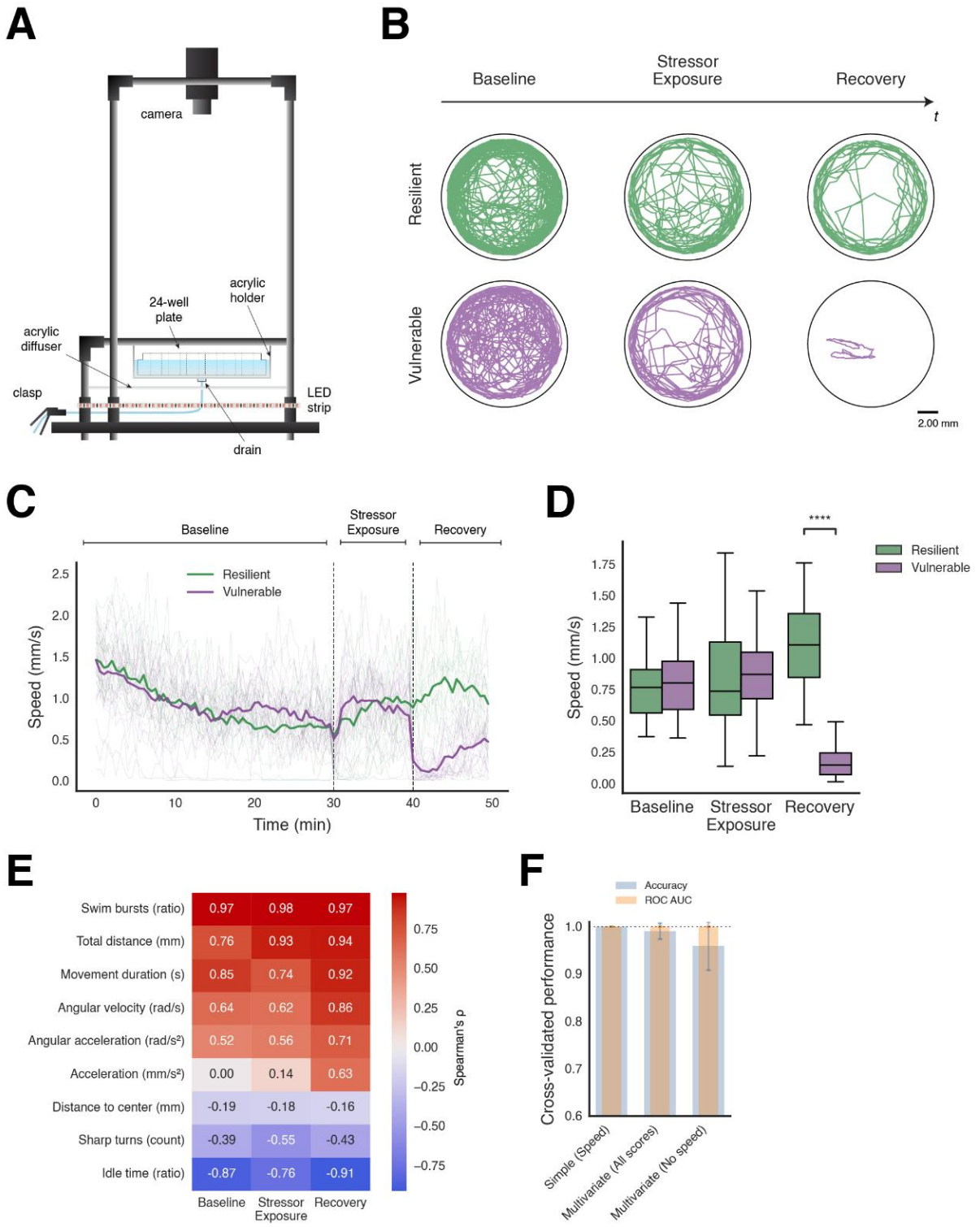

Figure 1. Stress-resilience assay design and behavioral readouts.

A. *Schematic of the custom arena: individual larvae in mesh-bottom wells of a modified 24-well plate.* ***B.*** *Example trajectories for larvae classified as resilient (R; green) or vulnerable (V; purple) across assay stages: baseline (0-30 min), stressor exposure (30-40 min; 250 mM NaCl), and recovery (≥40 min).* ***C.*** *Swimming speed (mm/s) during the assay for resilient (green) and vulnerable (purple); thin lines are individual larvae, thick lines are group means.* ***D.*** *Mean swimming speed (mm/s) per group within each stage (same animals as in C). Within-stage group differences: Welch's t-test at stressor exposure; Mann-Whitney U at baseline and recovery. Significance shown in the figure: **** p < 0.0001.* ***E.*** *Spearman correlations between swimming speed and other behavioral metrics across stages (baseline*

10-30 min, stressor 30-40 min, recovery 40-45 min; same animals as in C). ***F.*** *Cross-validated classification of resilient versus vulnerable from baseline-recovery behavioral scores. Shown are a single-feature reference model using Speed ("Simple: Speed") and two multivariate logistic models ("Multivariate: All scores" and "Multivariate: No speed"). Bars show mean balanced accuracy (blue) and ROC AUC (orange); error bars are SD across GroupKFold splits by assay. Sample sizes. R = 25; V = 52; total n = 77.*

To determine whether focusing solely on speed would forfeit behaviorally relevant variance or compromise discrimination of resilience labels, we conducted feature-redundancy analyses. Most of our metrics covaried with speed across all assay stages. Swim bursts, total distance, movement duration, and angular velocity were strongly and positively correlated with speed, whereas idle time was strongly negatively correlated with speed (Fig. 1E). Acceleration and distance to center had weak associations. A Principal Component Analysis yielded a first component explaining over 50% of the variance, with loadings aligned to these speed-related variables (Sup. Fig. 3A-B), indicating a shared locomotor-drive axis rather than independent dimensions.

To further assess this redundancy, we compared multivariate models derived from baseline-to-recovery resilience scores calculated using behavioral metrics other than speed and trained to predict the canonical speed-based resilience labels (Methods). The model using a combination of all behavioral measures generalized near-perfectly (balanced accuracy ≈ 0.99), and omitting speed produced only a modest decrease (balanced accuracy ≈ 0.96). This suggested that the non-speed measures largely reproduce the speed-derived classification rather than adding independent criterion variance (Fig. 1F). Therefore, we used speed as a concise summary of the principal recovery dimension, noting that additional metrics offer limited incremental discrimination.

Behavioral resilience assay is robust across genotypes and scales with stressor intensity

To evaluate the robustness of our behavioral resilience assay, we assessed resilience scores across two zebrafish lines with distinct transgenic histories (nacre or elavl3:GCaMP6s in a nacre background). Statistical analysis revealed no significant difference in average resilience scores or distribution across resilience categories between lines (Fig. 2A-B), indicating that the index reliably captures individual differences in stress recovery regardless of genetic background.

To investigate how the type and severity of stress influences behavioral resilience, we exposed zebrafish larvae to graded intensities of an acute low pH stressor (Yeh et al. 2013) and quantified their recovery. Our results reveal that the distribution of resilience scores changes significantly with stressor intensity. Under mild stress conditions (pH 5.5), the average resilience score and its distribution into resilience categories were similar to those measured after exposure to 250 mM saltwater. The average resilience scores decreased, and the proportion of vulnerable fish increased at higher stress intensities (pH < 5). Overall, resilience scores were strongly correlated with stressor intensity (Fig. 2E).

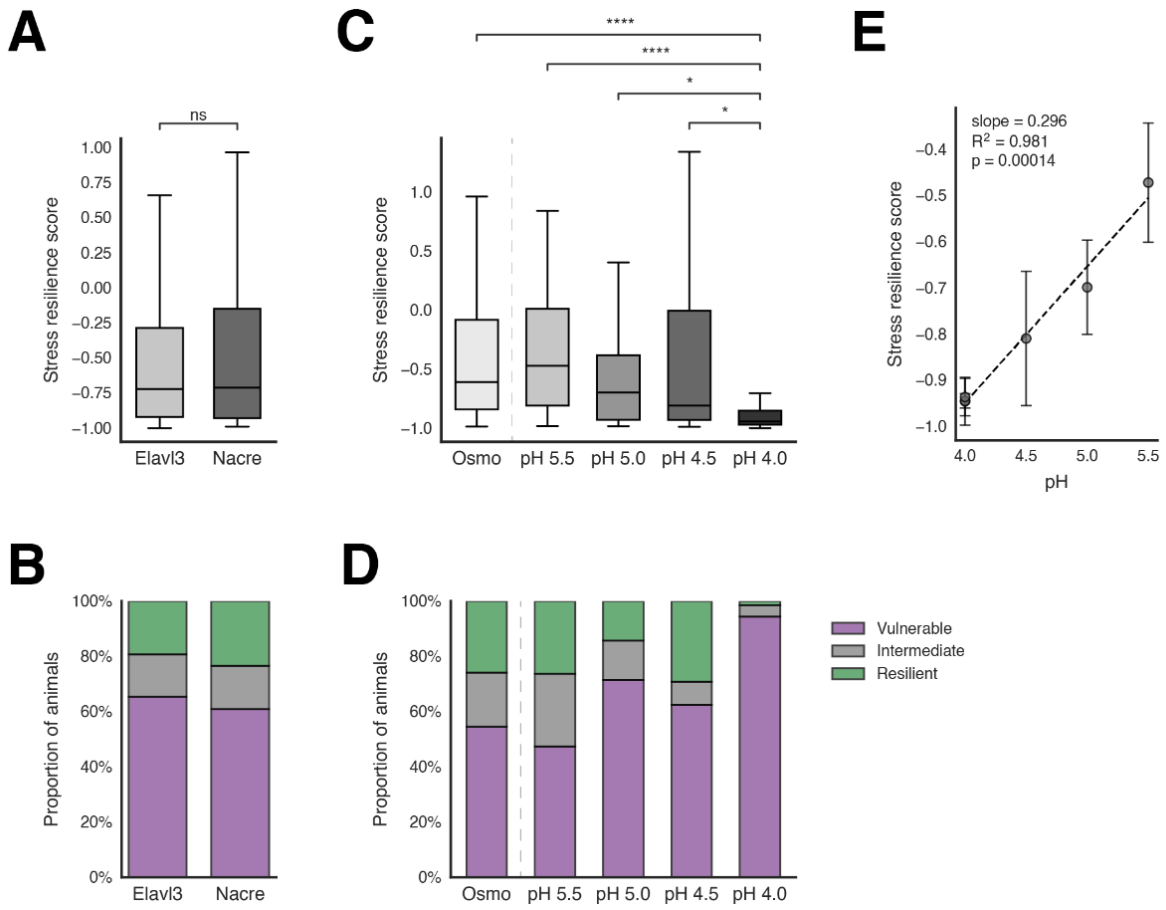

Figure 2. Consistency of the resilience score across zebrafish transgenic lines and stressors.

A. *Distribution of resilience scores by strain under an osmotic stressor (250 mM NaCl): Tg(elavl3:GCaMP6s) vs nacre. Mann-Whitney U with Holm correction; rank-biserial r reported.* ***B.*** *Proportions of vulnerable, intermediat, and resilient classifications by strain (totals as in A).* ***C.*** *Resilience scores in nacre under different stressors: osmotic (250 mM NaCl) and acid (pH 5.5, 5.0, 4.5, 4.0). Kruskal-Wallis omnibus; Dunn post-hoc with Holm adjustment (brackets show adjusted p). Significance shown in the figure: * $p < 0.05$; **** $p < 0.0001$.* ***D.*** *Proportions of vulnerable, intermediat, and resilient classifications by stressor (totals as in C).* ***E.*** *Resilience score vs pH (assay-level median ± SEM) with linear fit (slope, R^2, and p shown on plot). Sample sizes. Panels A-B: Tg(elavl3:GCaMP6s) n = 260; nacre n = 64. Panels C-D (nacre): Osmotic n = 189; pH 5.5 n = 19; pH 5.0 n = 21; pH 4.5 n = 24; pH 4.0 n = 71. Panel E: assay-level medians from the acid-stressor conditions in C-D.*

Resilience traits show partial stability during early larval development

To investigate the persistence of individual differences in stress resilience throughout larval development, we assessed resilience scores in the same cohort of zebrafish larvae at 6 dpf, and again at 14 dpf. At each time point, larvae were exposed to the same acute stressor (saltwater), and their resilience scores were calculated from locomotor activity during the first 5 minutes of the recovery period. To minimize potential stress from social isolation, larvae were reared in batches of 4-6 individuals grouped by their 6 dpf resilience scores (vulnerable or resilient). Consequently, results are reported at the batch level. Additionally, a control group of siblings, which had not undergone the resilience assay at 6 dpf, was raised under identical conditions and tested at 14 dpf to provide a baseline distribution of resilience scores at this developmental stage.

The average resilience scores decreased substantially from six to fourteen days in resilient batches, whereas those for vulnerable fish remained similar or increased slightly (Fig. 3B). In fact, the majority of individual larvae across all groups exhibited the vulnerable phenotype at 14 dpf (Fig. 3C; Sup. Fig. 4A). Although the range of resilience scores was compressed at 14 dpf compared to 6 dpf, the four batches with the highest scores at 14 dpf were resilient batches. Group-wise comparisons adjusted for multiple comparisons showed that resilient larvae scored significantly higher than controls (Mann-Whitney U; Holm-adjusted p = 0.016), and marginally higher than vulnerable larvae (one-sided Mann-Whitney U; Holm-adjusted p = 0.053; Sup. Fig. 4A). To account for the global age-dependent shift in behavior, we normalized the 14-dpf resilience scores to the control distribution. This analysis revealed that larvae from resilient batches maintained higher resilience scores at 14 dpf than those from vulnerable batches (one-sided Mann-Whitney U, p = 0.03; Figure 3D). Our results suggest that, while age-dependent factors influence individual resilience traits, they show some stability across development at the population level.

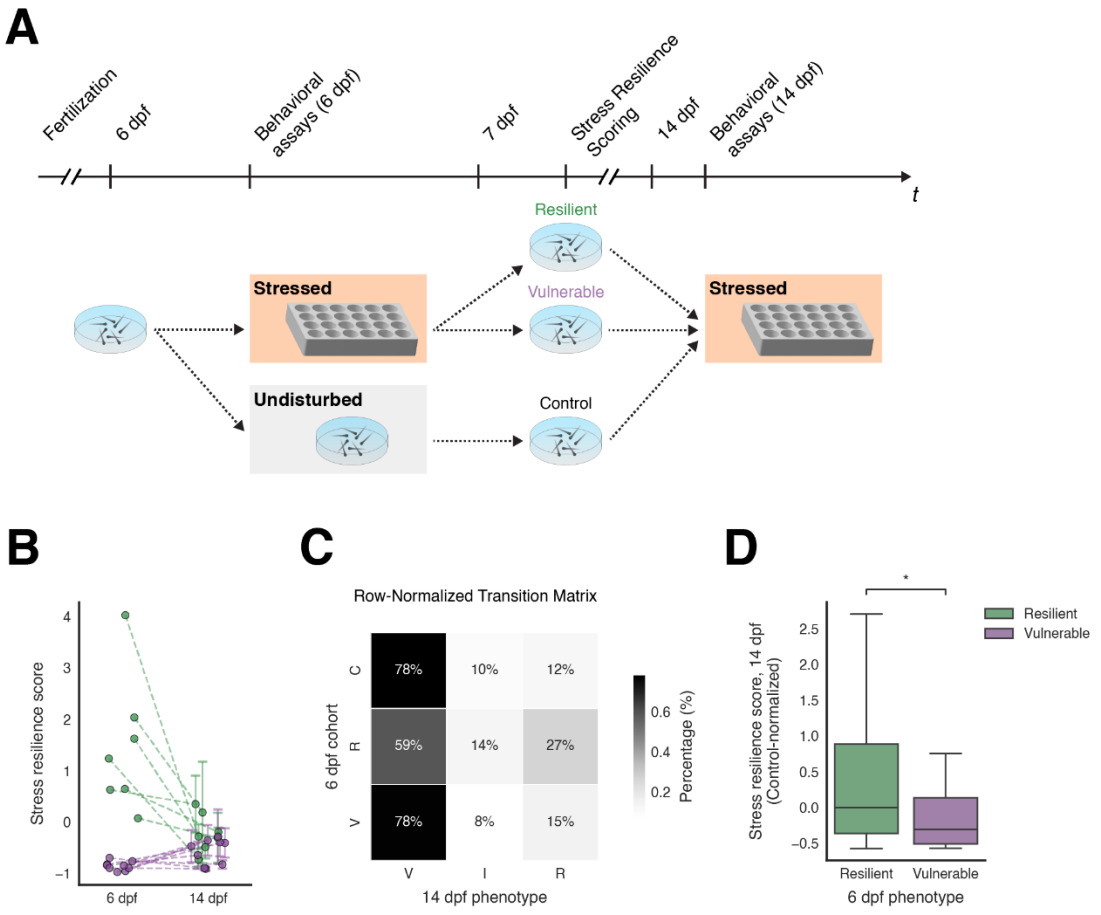

Figure 3. Consistency of stress resilience phenotypes during early larval development

A. *Experimental design. Larvae classified at 6 dpf as resilient (R), vulnerable (V), or undisturbed controls (C) were raised in Petri dishes and re-assayed at 14 dpf.* ***B.*** *Cohort-level stress-resilience scores from 6 to 14 dpf. Each line links one 6 dpf cohort to its 14 dpf outcome (R, green; V, purple). Left dots are 6 dpf cohort medians; right dots are 14 dpf cohort means ± SEM; slight horizontal jitter reduces overlap. Scores are z-scored to the 14 dpf control distribution.* ***C.*** *Transition matrix from 6 dpf cohorts (rows) to 14 dpf phenotypes: control (C), resilient (R), intermediate (I), vulnerable (V). Cells show row-normalized percentages.* ***D.*** *14 dpf resilience scores grouped by 6 dpf origin (z-scored to the 14 dpf*

*control distribution). Groups compared with one-sided Mann-Whitney U (R > V). Significance shown in the figure: * p < 0.05. Sample sizes. Panel B: R = 38, V = 40 (cohort pairs: R, k = 7; V, k = 9). Panels C-D: C = 93, R = 38, V = 40.*

Resilient fish exhibit higher stress-induced boldness at 1 month

To examine whether larval resilience phenotypes are reflected in juvenile behavior, we reared fish labeled at 6 dpf as resilient, vulnerable, or controls of the same age, to 1 month and assessed them in the novel tank test (NTT), .either under baseline conditions or directly following an acute stressor (10 min saltwater, Fig. 4A).

When tested in the NTT under baseline (unstressed) conditions, resilient and vulnerable groups showed comparable anxiety-like behavior, with similar mean vertical position and time in top and walls (Fig. 4C; Sup. Fig. 5). In contrast, following acute stress exposure, resilient juveniles explored higher regions of the tank than vulnerable peers, while control fihs displayed intermediate values (Fig. 4B-C). The time course indicates that this divergence in behavior across groups is largest during the first 5 min of the NTT assayand narrows over the session as vulnerable fish gradually ascend (Fig. 4B). Consistent with a bolder post-stress profile, resilient fish were closer to the water surface and swam farther from the walls than vulnerable fish (Sup. Fig. 5). Thus, baseline anxiety-like measures are similar across resilience phenotypes, whereas the 6 dpf resilience classification is associated with an enhanced challenge-evoked exploratory strategy at the juvenile stage.

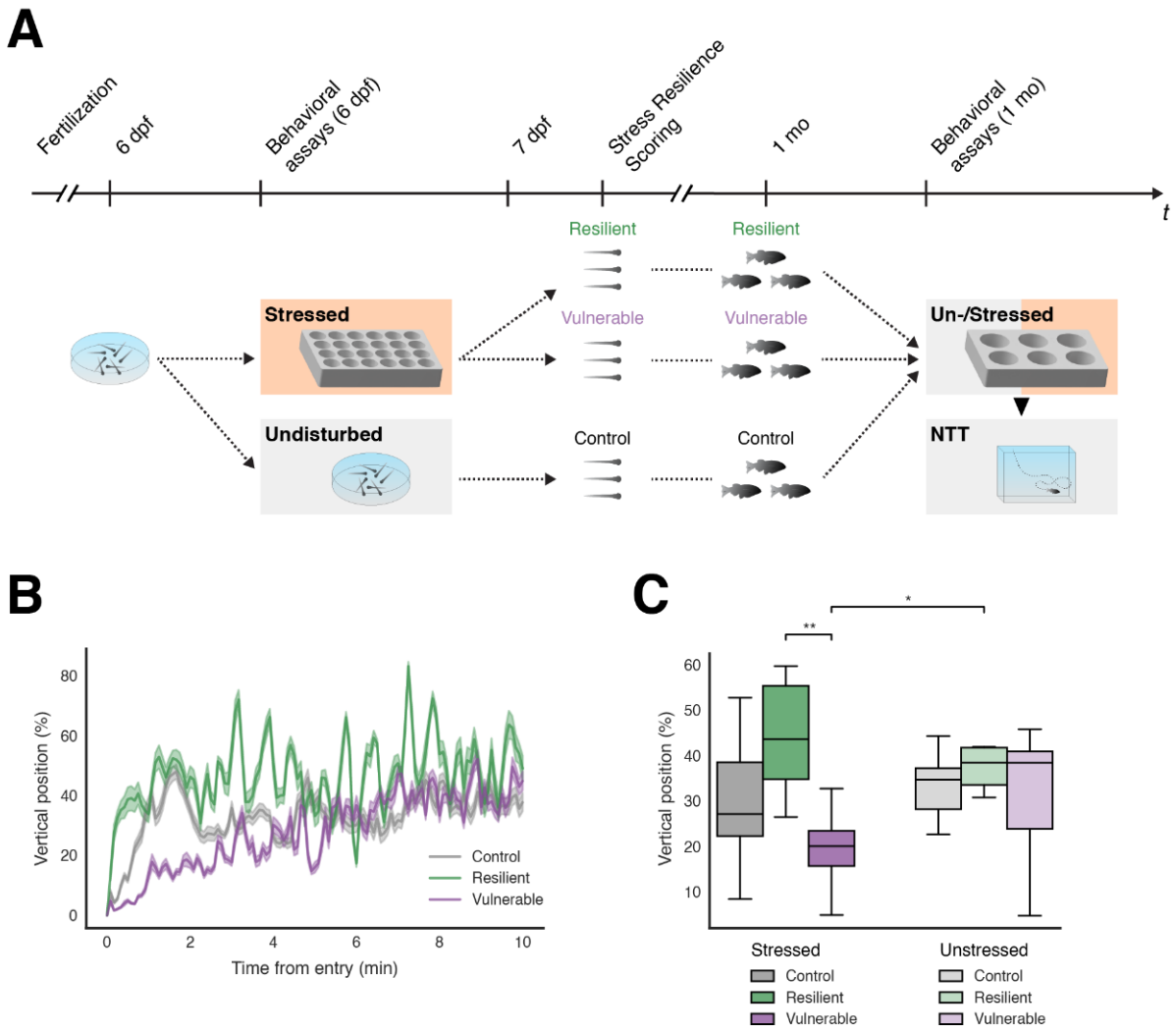

Figure 4. Anxiety-like responses of resilient and vulnerable groups in the novel tank test

A. *Experimental design. Larvae labelled at 6 dpf as control (C), resilient (R), or vulnerable (V) were reared ~1 month, assigned to stressed (S; 10-min 250 mM NaCl) or unstressed (U; 10-min AFW) cohorts, rested 5 min, and tested in the novel tank test.* ***B.*** *Vertical position (% tank height) over 0-10 min from entry for R and V fish; lines show group means ± SEM over 5 second bins.* ***C.*** *Vertical position (% tank height) per group, computed as each fish's mean over 0-6 min from its own tank entry, split by Stressed vs Unstressed conditions. Within-group differences used Kruskal-Wallis omnibus with Dunn post-hoc and Holm adjustment (brackets show adjusted p). Significance shown in the figure: * p < 0.05; ** p < 0.01. Sample sizes. S-C = 13, S-R = 6, S-V = 10, U-C = 13, U-R = 6, U-V = 9.*

DISCUSSION

Our approach builds on important previous studies that have used the recovery of baseline swimming speed to characterize coping styles or to distinguish between resilient and non-resilient fish. For example, Tudorache et al. (2015) found that fish emerging first from darkness to light after netting stress also recovered their baseline swimming speed the fastest. Swaminathan et al. (2023) categorized fish into resilient or susceptible labels by measuring post-stress swimming speed relative to controls. However, our approach differs in two ways. First, we use each larva's pre-stress baseline swimming speed to calculate resilience, thereby minimizing confounding effects from individual differences in locomotor activity. Second, we continuously monitor larval behavior in individual wells throughout baseline, stress, and recovery phases, eliminating the need for additional handling. This contrasts with the approach used by Swaminathan et al. (2023), where only the recovery phase was recorded after manually transferring 96 larvae into a well plate following stress exposure. Our method thus provides a medium-throughput, minimally disruptive assay conducted in a controlled environment, and is easily compatible with downstream analyses of brain activity or cortisol levels across different fish populations.

Conservative determination of resilience and vulnerable subsets

Many studies apply a single threshold to divide a stress-exposed population into two groups based on a threshold established on control, unstressed animals (Swaminathan et al. 2023; Krishnan et al. 2007; Golden et al. 2011; Willmore et al. 2022). In contrast, we focused on the extremes of the resilience score distribution, selecting only the most resilient (≈ 20%) and most vulnerable (≈ 65%) individuals. Two main considerations guided this decision. First, our modeling of the resilience score distribution indicated the presence of more than two distinct phenotypic subsets. Second, by focusing on these extreme subsets, which exhibit coherent behavior and reduced intra-group variability, we aim to investigate the neural correlates in future studies more effectively (Jacobs and Ryu 2023).

Factors influencing the consistency of the resilience score

Our results indicate that resilience scores do not differ significantly across transgenic lines in the nacre background. We did not assess pigmented zebrafish lines, as our assay is designed as a screening tool for subsequent whole-brain imaging of neural activity, which requires unpigmented larvae. Our results align with those reported by Swaminathan et al. (2023), who observed comparable resilience scores between wildtype AB and Tüpfel longfin strains. Strain-specific differences in stress sensitivity have been documented in zebrafish (Gorissen et al. 2015; Vignet et al. 2013) and might be expected to influence stress resilience. The lack of observed variation in our, and in the Swaminathan et al. (2023) study could be due to the relatively high intensity of the stressor used. Using lower stress intensities might help uncover inter-strain differences in resilience that are masked by the strong challenge in the current protocol.

Conversely, we found that both the resilience index and the proportion of resilient fish decreased as stressor intensity increased. This observation aligns with previous studies, which have shown that longer stressor duration or more severe stressors reduce resilience capacity (Cheng et al. 2022; Swaminathan et al. 2023). Furthermore, fish exhibited significantly lower resilience to the same stressor type and duration at 2 weeks of age compared to 1 week of age, suggesting increased sensitivity to stress during later larval developmental stages.

Collectively, our results validate the use of resilience scores to compare stress resilience across different genetic backgrounds and developmental stages in zebrafish larvae. However, longitudinal assessments of stress resilience should include control groups to account for the decline in absolute resilience scores over larval development.

Stability of resilience trait during development

Resiliience phenotypes exhibited moderate stability from 1 to 2 weeks of age. However, resilient larvae developed into juveniles that were clearly more risk-prone or proactive compared to vulnerable larvae. Therefore, vulnerability and resilience appear to be well-defined and consistent traits during early larval and juvenile stages, but less so at 2-week of age. This might be because the 2-week-old stage represents a period of behavioral transition, making phenotypic classification less clear. Previous studies support this interpretation, which have documented key behavioral changes in social interaction (Dreosti et al. 2015), as well as changes in dark-light preference and enhanced plasticity of responses to challenges (Varga et al. 2020), at that developmental period.

Limitations and future perspectives

We only used behavioral metrics to characterize the resilient and vulnerable populations. This could be complemented by assessing physiological and molecular markers. Specifically, we could measure cortisol levels, which vary in magnitude and temporal dynamics according to stress coping style (Wong et al. 2019), as well as the expression of genes encoding neuropeptides (such as neuropeptide Y, oxytocin, and vasopressin), which are upregulated in resilient individuals compared to vulnerable ones following stress (Swaminathan et al. 2023).

In addition, it would be valuable to investigate whether larval vulnerable phenotypes predispose to stress-induced diseases later in life. Research indicates that animals with reactive coping styles are more prone to maladaptive symptoms under stress (Albrechet-Souza and Gilpin 2019; McIlwrick et al. 2016; Tudorache et al. 2015; 2013). To test this, we plan to raise larvae identified as resilient or vulnerable, expose them to a chronic unpredictable stress protocol during juvenile stages (Golla et al. 2020; Varga et al. 2025), and compare their anxiety levels. We expect vulnerable fish to develop enhanced anxiety-like behaviors compared to resilient.

METHODS

Animals

Zebrafish (*Danio rerio*) were maintained under standard conditions. Adult breeders were housed in 3.5- or 8-L tanks on a recirculating system (Techniplast) at 28.4 °C, 400 µS cm^{-1} conductivity, pH 7.4, with a 14:10 h light/dark cycle. Embryos were obtained by natural spawning and raised at 28 °C in an incubator. For larval rearing, 40-60 embryos or larvae were kept per Petri dish containing 50 mL artificial fish water (AFW; 0.06 g L^{-1} marine salt in reverse-osmosis water), which was replaced daily. Larvae were fed once each morning starting at 5 dpf (shrimp larval diet, Royal Caviar, 5-50 µm).

Unless otherwise indicated, experiments used the nacre ($mitfa^{-/-}$) background (Lister et al. 1999). In a subset of assays, larvae from the Tg(elavl3:GCaMP6s) line in the nacre background were also used to assess assay robustness across lines with different transgenic backgrounds.

All experiments were conducted on 6-31 dpf larvae in compliance with European Directive 2010/63/EU on the protection of animals used for scientific purposes. Experimental protocols were approved by the Danish Animal Experiments Inspectorate (Dyreforsøgstilsynet) - license number 2023-15-0201-01493.

Experimental Design

Experiments were performed on 6 dpf larvae exposed to a standardized stress resilience assay. Fish were distributed into individual wells and divided into two main conditions: stressed (exposed to either 250 mM NaCl or acidified AFW at pH 5.5) and control (no stressor). To capture the temporal dynamics of neural activity, larvae were euthanized either 5 minutes or 10 minutes after the recovery phase.

Each experimental replicate refers to a single block of experiments conducted on the same day and sharing the same stressor type, recovery time point, and imaging session. Experimental replicates using the same stressor and recovery time point are considered biological replicates and are labeled accordingly (replicates 1, 2, and 3).

Stress Resilience Assay

Experiments were conducted in darkness between 13:00 and 18:00 inside a custom-built, lightproof enclosure where the temperature was maintained at 28 ± 0.5°C during experiments. Larvae were individually transferred using cut-tip pipettes into a modified 24-well plate (12.8 × 8.6 × 1.8 cm; Greiner Bio-One), rendered opaque with acetone and fitted with nylon mesh bottoms (300 µm pore size) to allow rapid fluid exchange. The plate was inserted into a custom acrylic holder (14.8 × 9.4 × 3.9 cm) equipped with a 6 mm silicone tubing drain system, enabling fast solution replacement within all wells (Figure 1A).

Each well was filled with artificial fish water to a depth of 1.2 cm. Larvae were allowed to acclimate for 5-10 minutes before recording. The assay consisted of three consecutive phases: a baseline period of 30 minutes in AFW; a stressor exposure period lasting 10 minutes; and a recovery period in AFW lasting 5 to 60 minutes, depending on the experiment. All solutions were pre-warmed to 28°C and introduced by draining and replacing the well contents manually via the tubing system.

Behavioral recordings were acquired using a Mako U-319B monochrome camera (Allied Vision), fitted with a 35 mm lens (Fujinon HF35SA-1) and positioned 69.7 cm above the multi-

well dish. Infrared illumination was delivered through a flexible infrared LED strip and an opaque acrylic diffuser positioned beneath the plate. Videos were captured at 10 fps using a custom Python script (Andreassen et al. 2022).

Scoring Stress Resilience

Following acquisition, 2 Hz videos were segmented into individual wells using a circular Hough transform. Zebrafish trajectories were extracted by tracking larval eyes with DeepLabCut (ResNet-50 trained on custom labels, Mathis et al. 2018). then post-processed to correct detection artefacts in a Python GUI.

Swimming speed was computed as inter-frame displacement divided by elapsed time. Cumulative distance was the running sum of displacements. Distance to center was the Euclidean distance of each point to the well's center. Angular velocity was the change in heading between consecutive displacement vectors per unit time, and angular acceleration was its per-sample first difference. Acceleration was the first derivative of speed. Freezing was defined as events in which displacement was below 0.075 mm for consecutive frames within a continuous 3 sec window, and was reported as the fraction of time spent freezing in a given interval (bin). Movement duration was the cumulative duration of swimming episodes (i.e., not freezing). Swim bursts were quantified as the percentage of recording time during which instantaneous speed exceeded 10 mm s^{-1}. Sharp turns were counted when the absolute change in heading between consecutive steps exceeded 90°.

To quantify stress resilience, for each fish we averaged speed over baseline 10-30 min ($Speed_{baseline}$) and recovery 0-5 min ($Speed_{recovery}$), and computed a relative-change score:

$$\text{Resilience Score} = \frac{\text{Speed}_{\text{recovery}} - \text{Speed}_{\text{baseline}}}{\text{Speed}_{\text{baseline}}} \quad (1)$$

To convert this continuous measure into categorical phenotypes, we examined the pooled score distribution and fit Gaussian mixture models with K = 2-10 components (McLachlan and Peel 2004). Model complexity was assessed with Akaike and Bayesian information criteria (AIC/BIC; lower is better; Schwarz 1978; Akaike 1974). The combined AIC/BIC profiles indicated an optimum around K = 5, with K = 7 a close alternative. Given the pronounced right tail beyond a resilience score of ~1.5, we adopted a 7-component GMM for density visualization to avoid underfitting the high-score tail, while noting that inferences were qualitatively similar for K = 5-7. Operational thresholds were then set to contrast the distribution's extremes while retaining adequate sample sizes: fish with scores ≤ -0.5 were labeled *vulnerable*, scores > -0.1 were labeled *resilient*, and intermediate values were left unclassified. Scores > 5 were flagged as outliers and excluded. Although necessarily heuristic, these cut points are empirically motivated by the observed multimodality and guided by formal model-selection diagnostics.

Multi-feature-based classification of stress resilience

To evaluate the predictive value of behavioral metrics for resilience labels, we quantified baseline-to-recovery change scores for each larva by averaging each behavioral metric during the baseline and recovery windows and expressing the difference as a relative change from baseline (Equation 1). Larvae classified as resilient or vulnerable were pooled across four stress resilience assays. Models were trained and evaluated using GroupKFold cross-validation, stratified by assay number to avoid data leakage.

Single-feature (i.e., behavioral metric) models were implemented as one-dimensional threshold classifiers, with thresholds optimized within each training fold. Multivariate models

were logistic regressions including all behavioral scores, or an ablation model excluding speed. To ensure fairness across models, we restricted evaluation to a common cohort of larvae with complete data across all behavioral metrics. Model performance was assessed using balanced accuracy and ROC AUC, reported as mean ± SD across folds.

Longitudinal experiments

SR re-assay (6-14 dpf)

Larvae were initially reared in 90-mm Petri dishes containing 30-40 animals per dish under identical conditions. At 6 dpf, a subset of dishes was used for the stress-resilience assay, while other dishes from the identical breeding batches were left entirely undisturbed to provide age-matched controls. Videos from the 6 dpf assays were processed overnight and stress resilience scores were computed as described above. By the next morning (7 dpf), stressed larvae were assigned to resilient or vulnerable groups based on the predefined scoring criteria, and controls were drawn in parallel from dishes that had not been assayed at 6dpf. Fish were housed by group (not individually) at 6/7 fish per 90-mm Petri dish in 50 mL AFW, under the same rearing conditions (28 °C; 14:10 h light/dark) for one week; group housing was used to conserve space and to avoid social isolation, which can itself induce stress in schooling species. At the start of longitudinal rearing, we housed resilient = 53 (9 dishes), vulnerable = 66 (10 dishes), and control = 210 (30 dishes) animals.

At 14 dpf, fish were re-assayed using the same apparatus and timing as at 6 dpf (30 min baseline, 10 min stressor exposure, 10 min recovery; solutions at 28 °C). Each assay run included approximately even distributions of control, resilient and vulnerable animals (typically ~24 total, ~8 per label) randomized across wells. Metric computation and resilience scoring followed the procedures in Scoring Stress Resilience.

Juvenile NTT after 6 dpf SR

Stress resilience assay at 6 dpf and rearing to one month

Larvae were initially reared in 90-mm Petri dishes containing 30-40 animals per dish under identical conditions. At six days post-fertilization, a subset of dishes was used for the stress-resilience assay, while other dishes from the same breeding batches were left entirely undisturbed to provide age-matched controls (control and stressed cohorts were never mixed). Assay videos were processed overnight and resilience scores computed as described above. By the next morning (seven days post-fertilization), assayed larvae were assigned to resilient or vulnerable groups according to predefined criteria, and controls were drawn in parallel from undisturbed dishes within the identical breeding batches. For longitudinal follow-up to one month of age, larvae were transferred directly at seven days post-fertilization into cohort tanks containing approximately 20-30 fish of the same group, to maintain a consistent social environment. These tanks remained in the incubator until ten days post-fertilization for monitoring and were then moved to the animal facility (as detailed in Animals) and reared to 30-31 days post-fertilization under standard conditions (28 °C; 14:10 h light/dark; artificial fish water with daily renewal).

Novel tank test apparatus

The experimental setup consisted of a rack (66 × 40 cm) holding six transparent tanks (each with dimensions: width, height, depth = 12 × 10 × 1.5 cm, along the camera's optical axis). Tanks were backlit by an LED circuit, with an opaque acrylic diffuser to provide uniform illumination and prevent direct exposure to the fish. Tanks were secured to the rack using magnets. Each tank was filled with 100 mL of artificial fish water for the duration of the

experiments. Videos were recorded at two frames per second with a Mako 319 (Allied Vision) camera controlled via Pylon Viewer.

Novel tank test procedure

On the day before testing, cohort tanks were moved to the experimentation room set at 28 °C to acclimate; on the experimental day, they were brought to the bench one hour before the assay. For each session, six fish were selected (two from each of the cohorts control, resilient, and vulnerable) and assigned to a Stressed or Unstressed sub-category. Stressed categories received a 10-minute exposure to an osmotic stressor (250 mM NaCl), while Unstressed ones were left in AFW. Subsequently, the six fish were transferred to 13 mL tubes containing 10 mL of artificial fish water, placed in a light-proof cabinet for five minutes, and then introduced into the tanks in randomized order, one by one, with no more than ten seconds between transfers. Each recording lasted twelve minutes to provide at least ten minutes of observation for each fish. After each recording, the tanks were refilled with fresh AFW before the next session began.

Behavioral analysis:

Assay videos were split per tank and processed in parallel with DeepLabCut (ResNet-50, custom labels; Mathis et al. 2018).

From each trajectory, we extracted per-frame metrics as follows. Speed (mm s^{-1}) was computed as inter-frame displacement divided by Δt. Distance to surface (mm) was the vertical distance to the annotated water line, and distance to wall (mm) was the minimum distance to the tank walls on the reference image. Vertical position (%) was expressed as normalized height from the bottom (0%) to the surface (100%). Freezing (ratio) was defined as periods in which speed remained below a low-speed threshold (0.5 mm) for ≥ 1.5 s and was reported as the fraction of frames. Swim bursts (ratio) were frames in which speed exceeded a pre-specified high-speed threshold. Time in the top third (ratio) was the fraction of frames with vertical position ≥ 33.3%, and time near wall (ratio) was the fraction of frames within 10 mm of a wall.

Statistical analysis.

All analyses were performed in Python (NumPy/Pandas, SciPy, statsmodels, scikit-posthocs). Continuous outcomes were compared between independent groups. For each analysis, missing values were dropped and, when pre-specified, extreme high-end outliers were truncated; groups with too few observations were excluded. Assumptions were checked per group using Shapiro-Wilk for normality and Levene's median-centered test for homogeneity of variances; a conservative rule required all groups with n ≥ 3 to pass normality to proceed with parametric tests.

For two groups, tests followed assumptions: Student's t (normal, equal variances), Welch's t (normal, unequal variances), or Mann-Whitney U (otherwise). Effect sizes accompanied pairwise results: Cohen's d (pooled SD) for Student's t, Hedges' g for Welch's t, and rank-biserial correlation for Mann-Whitney. All tests were two-sided, except for the test comparing resilient and vulnerable stress resilience scores at 14 dpf, which used a directional hypothesis (resilient > vulnerable; Fig. 3D; Sup. Fig. 4B).

For more than two groups, an omnibus test was run first: one-way ANOVA when normality and equal variances held (pairwise Tukey HSD); Welch's ANOVA for unequal variances (pairwise Games-Howell when available, otherwise Welch pairwise t-tests); or Kruskal-Wallis for non-normal data (pairwise Dunn when available, otherwise Mann-Whitney). Where post-

hoc procedures provide their own adjustment (Tukey/Games-Howell/Dunn), those adjusted p-values were reported; otherwise, pairwise p-values were corrected for multiple comparisons (default Holm).

SUPPLEMENTARY FIGURES

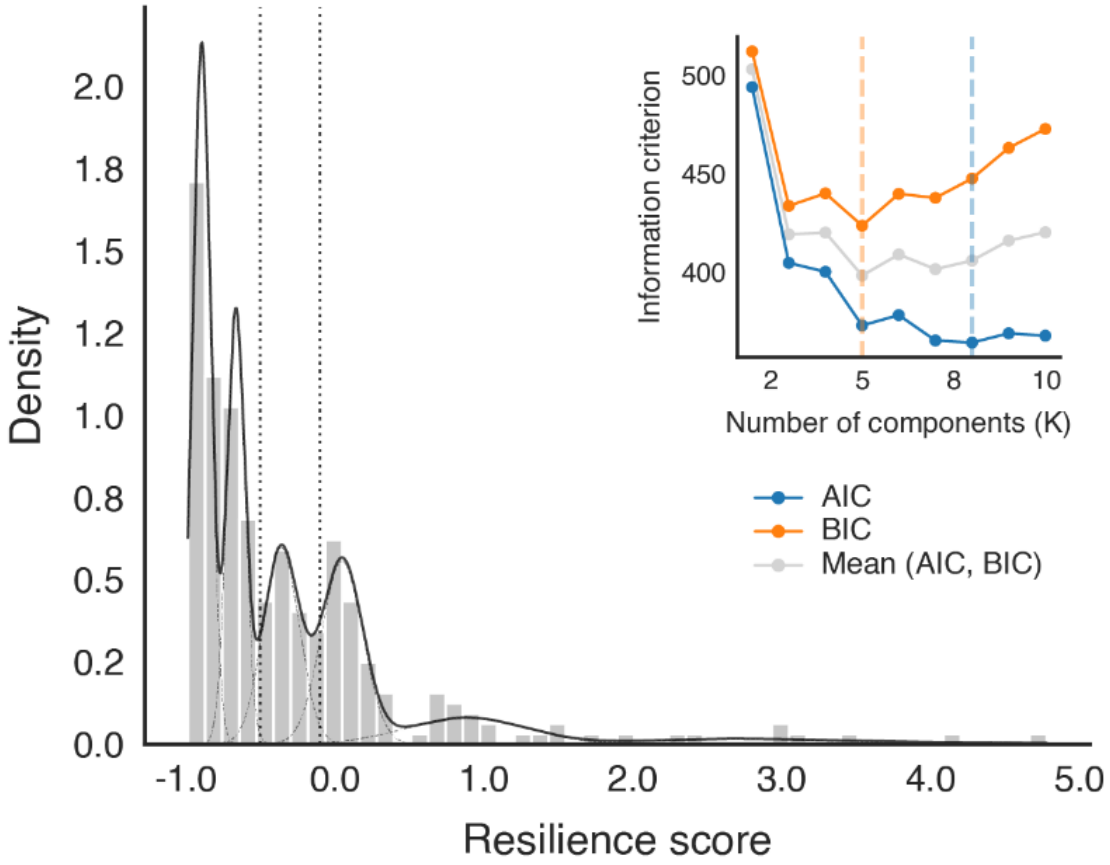

Supplementary Figure 1. Distribution of stress-resilience scores and model-selection diagnostics.

Histogram of pooled resilience scores from 14 behavioral assays (total N = 207 larvae). Vertical dotted lines mark the prespecified thresholds for assigning phenotypes: vulnerable (score ≤ -0.5) and resilient (score ≥ -0.1); intermediate otherwise (Methods). The solid black trace is the probability density from a 7-component Gaussian Mixture Model (GMM); dashed black traces show the individual Gaussian components. Inset: Akaike (AIC, blue) and Bayesian (BIC, orange) information criteria across candidate mixture sizes (K = 2-10; lower is better). The light-gray curve is the pointwise mean of AIC and BIC; vertical dashed lines indicate the K that minimizes each criterion.

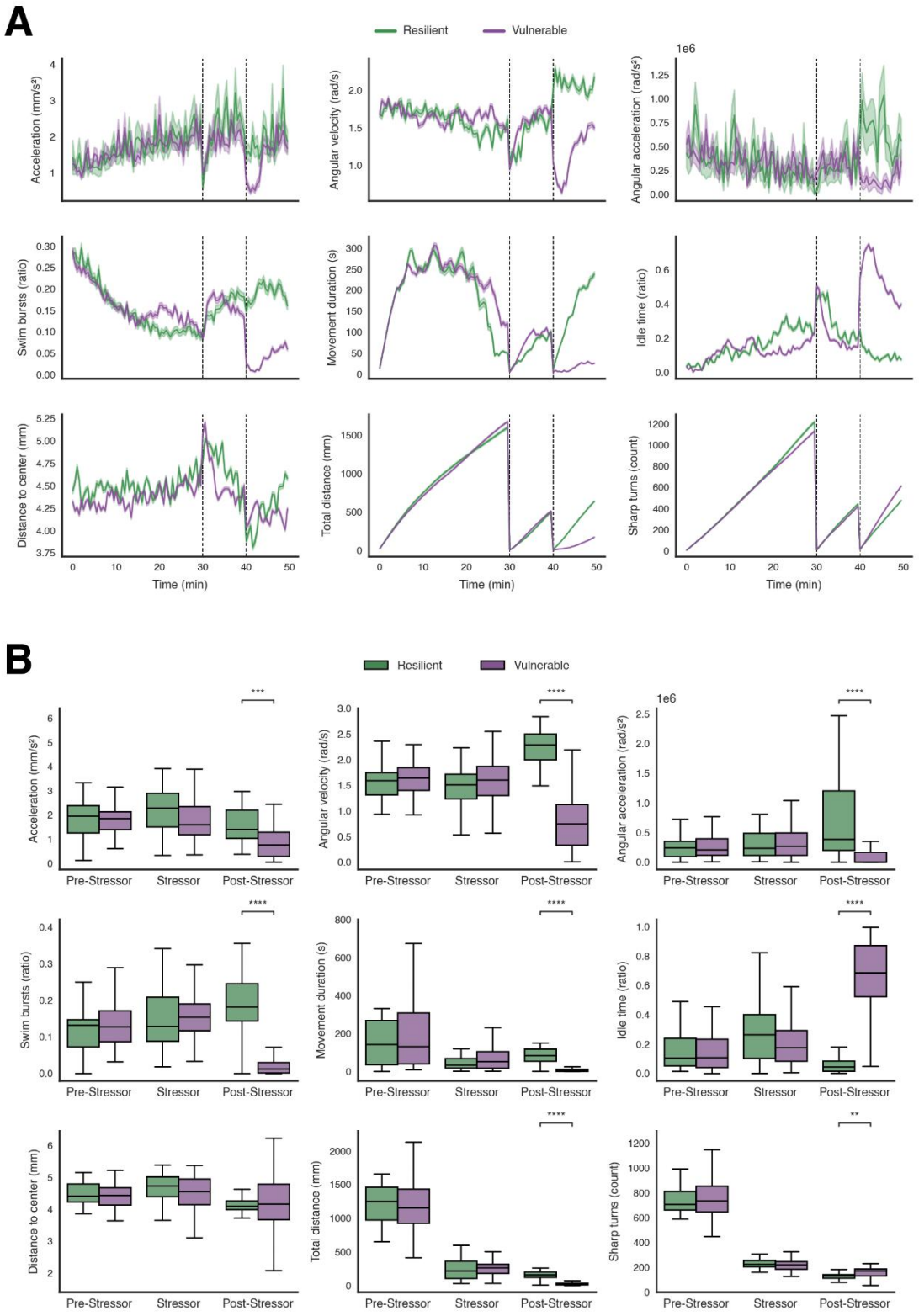

Supplementary Figure 2. Extended behavioral metrics across the stress resilience assay.

A. *Time courses of additional kinematic (acceleration [mm/s²], angular velocity [rad/s], angular acceleration [rad/s²], sharp turns [count], movement duration [s], idle time [ratio]) and spatial (distance to well center [mm], total distance [mm]) metrics for resilient (R; green) and vulnerable (V; purple) larvae across baseline, stressor exposure, and recovery. Thin lines show individual fish; thick lines show group*

means. Dashed lines mark stage transitions. ***B.*** *Boxplots of the same metrics, averaged per fish within baseline (10-30 min), stressor exposure (30-40 min), and recovery (40-45 min). Within-stage resilient versus vulnerable comparisons used two-sample tests selected per metric/stage (Student's t when normal with equal variances, Welch's t when variances were unequal, or Mann-Whitney U otherwise). Significance shown in the figure: ** p < 0.01; *** p < 0.001; **** p < 0.0001. Sample sizes. R = 25; V = 52; total n = 77.*

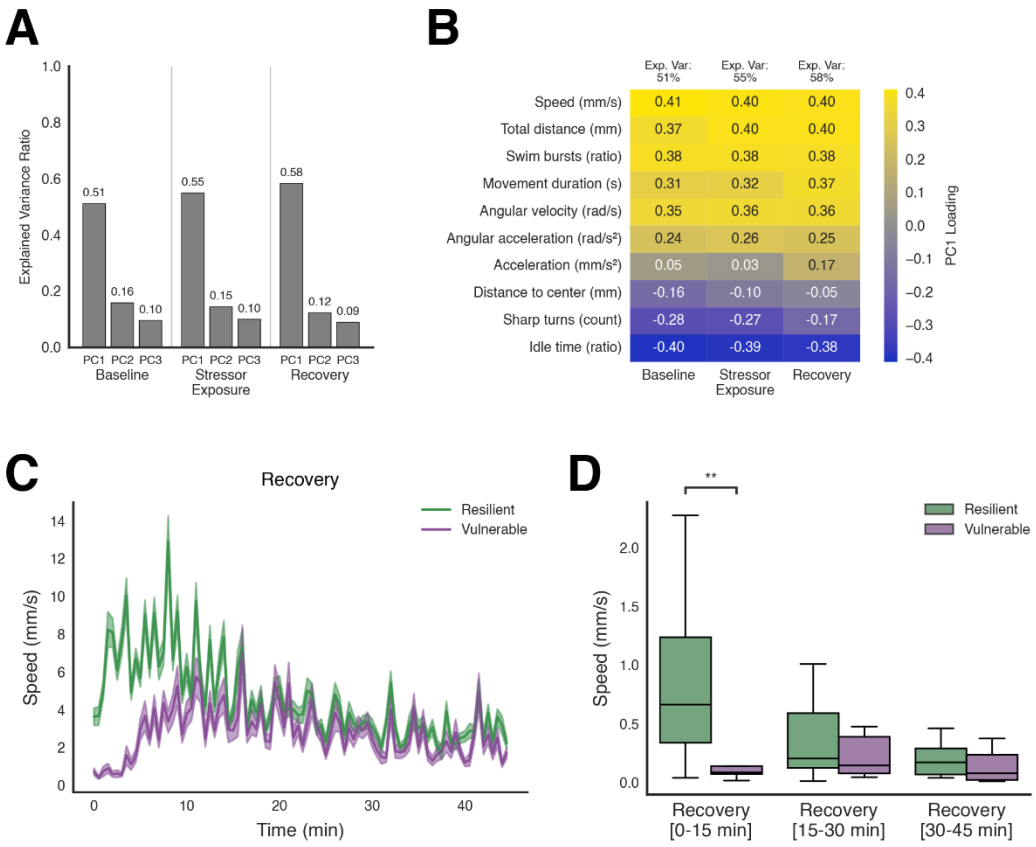

Supplementary Figure 3. Extended recovery dynamics and PCA summary.

A. *Explained variance ratios for PC1-PC3 at baseline, stressor exposure, and recovery (values above bars).* ***B.*** *PC1 loadings of behavioral metrics for each stage; column headers report the PC1 explained variance for that stage.* ***C.*** *Speed during the extended recovery (0-45 min) for resilient (R; green) and vulnerable (V; purple); mean ± SEM.* ***D.*** *Boxplots of per-fish mean speed across recovery windows (0-15, 15-30, 30-45 min). Within-window group differences tested with Student's t (0-15 min) and Mann-Whitney U (15-30 and 30-45 min). Significance shown in the figure: ** p < 0.01. Sample sizes. Panels A-B (same animals as Figure 1C-E): R = 25; V = 52; total = 77. Panels C-D: R = 28; V = 13.*

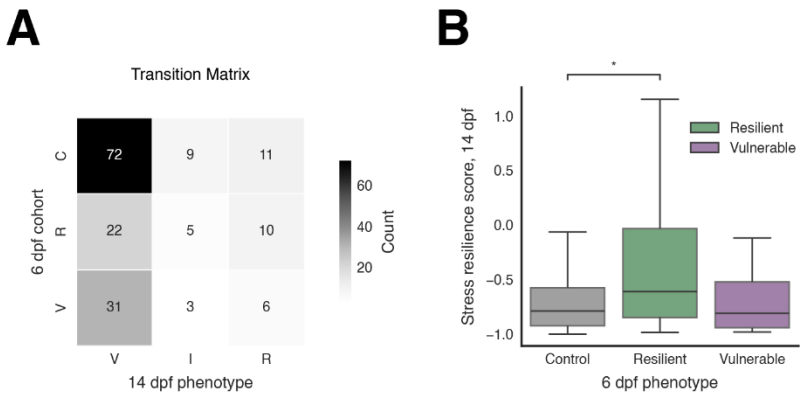

Supplementary Figure 4. 14 dpf resilience outcomes by 6 dpf cohort.

A. *Transition matrix from 6 dpf cohorts (rows) to 14 dpf phenotypes (columns: vulnerable, V; intermediat, I; resilient, R), shown as absolute counts.* ***B.*** *Resilience scores at 14 dpf grouped by 6 dpf origin (C, R, V). Groups compared with Kruskal-Wallis omnibus and Dunn post-hoc (one-sided for resilient > vulnerable, otherwise two-sided; Holm-adjusted). Significance shown in the figure: * $p < 0.05$. Sample sizes. C = 93, R = 38, V = 40.*

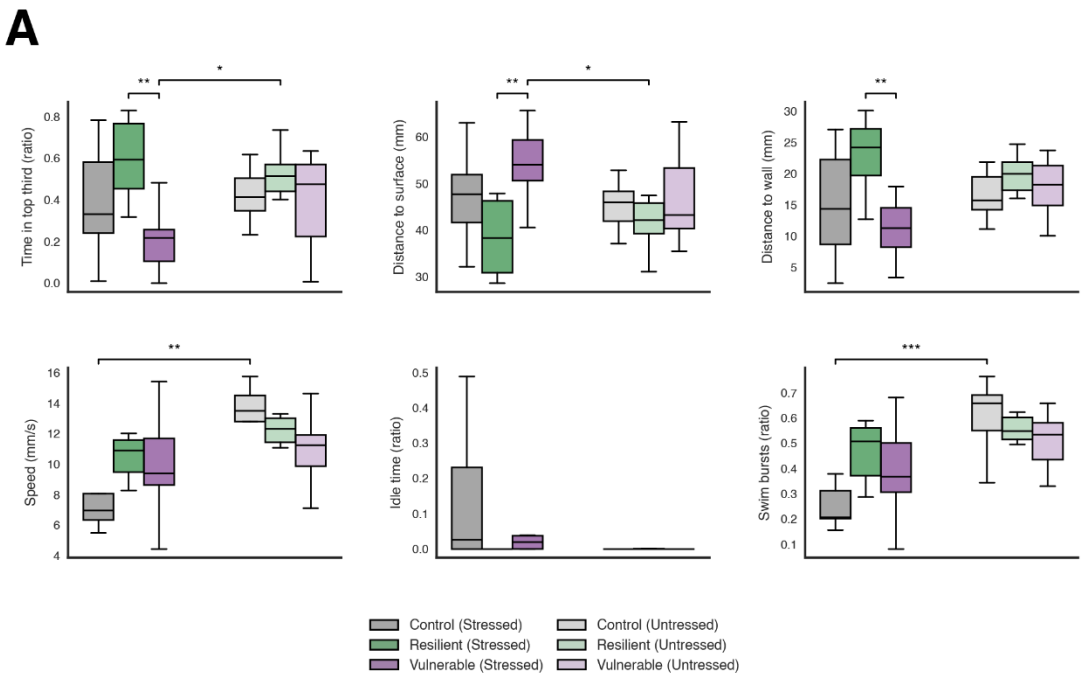

Supplementary Figure 5. Juvenile NTT behavioral metric profiles following 6 dpf stress resilience labeling.

*Boxplots summarize per-fish means over 0-6 min from tank entry for time in top third (ratio), distance to surface (mm), distance to wall (mm), speed (mm/s), idle time (ratio), and swim bursts (ratio) across groups Stressed-Control, Stressed-Resilient, Stressed-Vulnerable, Unstressed-Control, Unstressed-Resilient, and Unstressed-Vulnerable. Omnibus and post-hoc testing followed: Kruskal-Wallis per metric, with Dunn post-hoc and Holm adjustment; brackets show adjusted p. Significance shown in the figure: * p < 0.05; ** p < 0.01; *** p < 0.001. Sample sizes. S-C = 13, S-R = 6, S-V = 10, U-C = 13, U-R = 6, U-V = 9.*

REFERENCES

Akaike, H. 1974. “A New Look at the Statistical Model Identification.” *IEEE Transactions on Automatic Control* 19 (6): 716–23. https://doi.org/10.1109/TAC.1974.1100705.

Albrechet-Souza, Lucas, and Nicholas W. Gilpin. 2019. “The Predator Odor Avoidance Model of Post-Traumatic Stress Disorder in Rats.” *Behavioural Pharmacology* 30 (2 and 3-Spec Issue): 105–14. https://doi.org/10.1097/FBP.0000000000000460.

Andalman, Aaron S., Vanessa M. Burns, Matthew Lovett-Barron, et al. 2019. “Neuronal Dynamics Regulating Brain and Behavioral State Transitions.” *Cell* 177 (4): 970-985.e20. https://doi.org/10.1016/j.cell.2019.02.037.

Andreassen, Anna H., Petter Hall, Pouya Khatibzadeh, Fredrik Jutfelt, and Florence Kermen. 2022. “Brain Dysfunction during Warming Is Linked to Oxygen Limitation in Larval Zebrafish.” *Proceedings of the National Academy of Sciences* 119 (39): e2207052119. https://doi.org/10.1073/pnas.2207052119.

Charney, Dennis S. 2004. “Psychobiological Mechanisms of Resilience and Vulnerability: Implications for Successful Adaptation to Extreme Stress.” *American Journal of Psychiatry* 161 (2): 195–216. https://doi.org/10.1176/appi.ajp.161.2.195.

Cheng, Ruey-Kuang, Jazlynn Xiu Min Tan, Kai Xin Chua, Cheryl Jia Xin Tan, and Caroline Lei Wee. 2022. “Osmotic Stress Uncovers Correlations and Dissociations Between Larval Zebrafish Anxiety Endophenotypes.” *Frontiers in Molecular Neuroscience* 15 (June): 900223. https://doi.org/10.3389/fnmol.2022.900223.

Dreosti, Elena, Gonçalo Lopes, Adam R. Kampff, and Stephen W. Wilson. 2015. “Development of Social Behavior in Young Zebrafish.” *Frontiers in Neural Circuits* 9 (August): 39. https://doi.org/10.3389/fncir.2015.00039.

Farrell, Thomas C., Clinton L. Cario, Chiara Milanese, Andreas Vogt, Jong-Hyeon Jeong, and Edward A. Burton. 2011. “Evaluation of Spontaneous Propulsive Movement as a Screening Tool to Detect Rescue of Parkinsonism Phenotypes in Zebrafish Models.” *Neurobiology of Disease* 44 (1): 9–18. https://doi.org/10.1016/j.nbd.2011.05.016.

Golden, Sam A, Herbert E Covington, Olivier Berton, and Scott J Russo. 2011. “A Standardized Protocol for Repeated Social Defeat Stress in Mice.” *Nature Protocols* 6 (8): 1183–91. https://doi.org/10.1038/nprot.2011.361.

Golla, Archana, Henrik Østby, and Florence Kermen. 2020. “Chronic Unpredictable Stress Induces Anxiety-like Behaviors in Young Zebrafish.” *Scientific Reports* 10 (1): 10339. https://doi.org/10.1038/s41598-020-67182-4.

Gorissen, M., R. Manuel, T. N. M. Pelgrim, et al. 2015. “Differences in Inhibitory Avoidance, Cortisol and Brain Gene Expression in TL and AB Zebrafish.” *Genes, Brain, and Behavior* 14 (5): 428–38. https://doi.org/10.1111/gbb.12220.

Ingebretson, Justin J., and Mark A. Masino. 2013. “Quantification of Locomotor Activity in Larval Zebrafish: Considerations for the Design of High-Throughput Behavioral Studies.” *Frontiers in Neural Circuits* 7: 109. https://doi.org/10.3389/fncir.2013.00109.

Jacobs, Elina A. K., and Soojin Ryu. 2023. “Larval Zebrafish as a Model for Studying Individual Variability in Translational Neuroscience Research.” *Frontiers in Behavioral Neuroscience* 17 (June). https://doi.org/10.3389/fnbeh.2023.1143391.

Koolhaas, J. M, S. M Korte, S. F De Boer, et al. 1999. “Coping Styles in Animals: Current Status in Behavior and Stress-Physiology.” *Neuroscience & Biobehavioral Reviews* 23 (7): 925–35. https://doi.org/10.1016/S0149-7634(99)00026-3.

Krishnan, Vaishnav, Ming-Hu Han, Danielle L. Graham, et al. 2007. “Molecular Adaptations Underlying Susceptibility and Resistance to Social Defeat in Brain Reward Regions.” *Cell* 131 (2): 391–404. https://doi.org/10.1016/j.cell.2007.09.018.

Lister, J. A., C. P. Robertson, T. Lepage, S. L. Johnson, and D. W. Raible. 1999. “Nacre Encodes a Zebrafish Microphthalmia-Related Protein That Regulates Neural-Crest-Derived Pigment Cell Fate.” *Development (Cambridge, England)* 126 (17): 3757–67. https://doi.org/10.1242/dev.126.17.3757.

MacPhail, R.C., J. Brooks, D.L. Hunter, B. Padnos, T.D. Irons, and S. Padilla. 2009. “Locomotion in Larval Zebrafish: Influence of Time of Day, Lighting and Ethanol.” *NeuroToxicology* 30 (1): 52–58. https://doi.org/10.1016/j.neuro.2008.09.011.

Mathis, Alexander, Pranav Mamidanna, Kevin M. Cury, et al. 2018. “DeepLabCut: Markerless Pose Estimation of User-Defined Body Parts with Deep Learning.” *Nature Neuroscience* 21 (9): 1281–89. https://doi.org/10.1038/s41593-018-0209-y.

McEwen, Bruce S. 2007. “Physiology and Neurobiology of Stress and Adaptation: Central Role of the Brain.” *Physiological Reviews* 87 (3): 873–904. https://doi.org/10.1152/physrev.00041.2006.

McIlwrick, Silja, Alexandra Rechenberg, Mariana Matthes, et al. 2016. “Genetic Predisposition for High Stress Reactivity Amplifies Effects of Early-Life Adversity.” *Psychoneuroendocrinology* 70 (August): 85–97. https://doi.org/10.1016/j.psyneuen.2016.04.023.

McLachlan, Geoffrey J., and David Peel. 2004. *Finite Mixture Models*. John Wiley & Sons.

Schwarz, Gideon. 1978. “Estimating the Dimension of a Model.” *The Annals of Statistics* 6 (2): 461–64. https://doi.org/10.1214/aos/1176344136.

Swaminathan, Amrutha, Michael Gliksberg, Savani Anbalagan, Noa Wigoda, and Gil Levkowitz. 2023. “Stress Resilience Is Established during Development and Is Regulated by Complement Factors.” *Cell Reports* 42 (1): 111973. https://doi.org/10.1016/j.celrep.2022.111973.

Tudorache, Christian, Anique ter Braake, Mara Tromp, Hans Slabbekoorn, and Marcel J. M. Schaaf. 2015. “Behavioral and Physiological Indicators of Stress Coping Styles in Larval Zebrafish.” *Stress* 18 (1): 121–28. https://doi.org/10.3109/10253890.2014.989205.

Tudorache, Christian, Marcel J. M. Schaaf, and Hans Slabbekoorn. 2013. “Covariation between Behaviour and Physiology Indicators of Coping Style in Zebrafish (Danio Rerio).” Journal of Endocrinology. *Journal of Endocrinology* 219 (3): 251–58. https://doi.org/10.1530/JOE-13-0225.

Varga, Zoltan K., Archana Golla, and Florence Kermen. 2025. “Early Life Chronic Stress-Disrupted Activity of the Dorsal Raphe Nucleus Selectively Drives Behavioral Impairments.” Preprint, bioRxiv, August 6. https://doi.org/10.1101/2025.08.05.668669.

Varga, Zoltán K., Diána Pejtsik, László Biró, et al. 2020. “Conserved Serotonergic Background of Experience-Dependent Behavioral Responsiveness in Zebrafish (Danio Rerio).” *The Journal of Neuroscience* 40 (23): 4551–64. https://doi.org/10.1523/JNEUROSCI.2178-19.2020.

Vignet, Caroline, Marie-Laure Bégout, Samuel Péan, Laura Lyphout, Didier Leguay, and Xavier Cousin. 2013. “Systematic Screening of Behavioral Responses in Two Zebrafish Strains.” *Zebrafish* 10 (3): 365–75. https://doi.org/10.1089/zeb.2013.0871.

Willmore, Lindsay, Courtney Cameron, John Yang, Ilana B. Witten, and Annegret L. Falkner. 2022. “Behavioural and Dopaminergic Signatures of Resilience.” *Nature* 611 (7934): 124–32. https://doi.org/10.1038/s41586-022-05328-2.

Wong, Ryan Y., Jeffrey French, and Jacalyn B. Russ. 2019. “Differences in Stress Reactivity between Zebrafish with Alternative Stress Coping Styles.” *Royal Society Open Science* 6 (5): 181797. https://doi.org/10.1098/rsos.181797.

Yeh, Chen-Min, Mario Glöck, and Soojin Ryu. 2013. “An Optimized Whole-Body Cortisol Quantification Method for Assessing Stress Levels in Larval Zebrafish.” *PLoS ONE* 8 (11): e79406. https://doi.org/10.1371/journal.pone.0079406.

Manuscript II

Neural correlates of interindividual variability in rebound from acute stress in the zebrafish

João Campagnolo[1], Jonathan Luca Korn[1], Laia Pages Rigola[1], Raghavendra Selvan[2], Florence Kermen[1]

Affiliations:

[1] Department of Neuroscience, SUND, University of Copenhagen, Denmark

[2] Department of Computer Science, SCIENCE, University of Copenhagen, Denmark

ABSTRACT

Stress is a crucial contributing factor to neuropsychiatric disorders, yet individuals exhibit profound differences in their capacity for adaptive recovery, a process termed resilience. Understanding the neural circuits that mediate this individual variability requires brain-wide approaches in conserved vertebrate systems. We utilized the larval zebrafish, a model amenable to whole-brain imaging and possessing a highly conserved stress response, to map the neural signatures distinguishing resilient from vulnerable phenotypes following acute osmotic challenge. Individuals were categorized based on their locomotor rebound: Resilient larvae rapidly restored baseline swimming speed, reflecting active coping, while Vulnerable larvae exhibited prolonged immobility or freezing behavior. We quantified activity across the entire brain using phosphorylated extracellular signal-regulated kinase (pERK) immunohistochemistry at 5 and 10 minutes after stressor termination. We then employed Partial Least Squares Discriminant Analysis (PLS-DA) and network analysis to isolate the correlates of immediate recovery. Stress exposure induced widespread activation of sensory integration centers, the preoptic area, and the habenular/hypothalamic neuroendocrine axis. Crucially, brain-wide mapping revealed that stress resilience correlated with heightened activity in distinct dopaminergic clusters within the caudal hypothalamus and telencephalon, reminiscent of the mammalian mesolimbic dopamine system. Furthermore, resilient larvae uniquely engaged key brainstem premotor systems, including the nucleus of the medial longitudinal fasciculus and reticulospinal neuron clusters, providing a neuronal mechanism for their observed locomotor re-engagement. Functional network analysis indicated that while both phenotypes maintain small-world architecture, resilience is characterized by stronger coupling between these hypothalamic-monoaminergic hubs and premotor execution centers. These findings establish a quantifiable behavioral and anatomical framework in larval zebrafish, highlighting core hypothalamic and brainstem circuits that actively promote behavioral rebound from acute stress, thus providing novel targets for translational stress research.

INTRODUCTION

Stress is a pervasive physiological and behavioral response to real or perceived threats and is a significant contributing factor to neuropsychiatric disorders such as anxiety, depression, and post-traumatic stress disorder (Holsboer and Ising 2008; Lupien et al. 2009; McEwen 2007). While stress is an inevitable part of life, individuals exhibit profound differences in their responses, with some adapting efficiently (termed "resilient") and others proving susceptible to adverse outcomes (de Abreu et al. 2021). Stress resilience is an active process thought to result from the interaction of genetics, neural circuits, and the environment. (Cathomas et al. 2019; Southwick et al. 2014). Understanding the neurobiological mechanisms conferring resilience to stress, therefore, offers significant therapeutic opportunities and has been the focus of intense research in the past decades (Bonanno et al. 2011; Kalisch et al. 2017; Sapienza and Masten 2011).

To this end, several pre-clinical rodent models of stress resilience have been established through phenotypic selection following repeated exposure to an aggressive conspecific in the Chronic Social Defeat Stress (CSDS; Krishnan et al., 2007), or to inescapable electric foot shocks or restraint stress (Dong et al. 2023). Most stressed animals develop anhedonia (a core symptom of depression disorder) or avoidance of conspecifics. Critically, a restricted subset of animals, usually around 30%, is more resilient to maladaptive changes, thus matching the clinical observations associated with mental diseases in humans. These studies have tremendously advanced our understanding of distributed neural systems, which are affected differently in vulnerable versus resilient animals.

A key brain region differentially activated in stress-resilient versus stress-vulnerable animals is the prefrontal cortex, specifically its medial division (mPFC), which sends dense projections to the basolateral nucleus of the amygdala (Anastasiades and Carter 2021). Activity in the mPFC is decreased in mice exposed to CSDS, especially in vulnerable mice, in which optogenetic stimulation of the mPFC has an antidepressant effect (Covington et al. 2010). Similarly, in a rat model of posttraumatic stress disorder, mPFC activity is reduced in vulnerable individuals who show excessive fear generalization, and targeted manipulations increasing activity in the mPFC attenuate this vulnerable phenotype (Szente et al. 2025).

The mesolimbic dopamine system, composed chiefly of the ventral tegmental area (VTA) projections to the nucleus accumbens (NAc), also plays a crucial role in determining the resilience phenotype after stress exposure. This system modulates reward processing, motivation, and emotional regulation, which are critical processes for adaptive stress coping. Its original involvement in stress resilience came from the Nestler group, who found that viral-mediated upregulation of a resilience-associated gene in the VTA was sufficient to increase behavioral resilience in a mouse model of CSDS (Krishnan et al. 2007). Subsequent studies have since confirmed that activity within the VTA or the NAc differs in resilient and vulnerable animals (Chaudhury et al. 2013; Dong et al. 2023; Willmore et al. 2022). Moreover, pharmacological manipulations of dopaminergic signaling, or optogenetic manipulation of activity in the VTA, alters the stress-induced resilience phenotypes (Chaudhury et al. 2013; Dong et al. 2023; Friedman et al. 2014), thereby causally implicating dopaminergic signaling within the mesolimbic system in the behavioral outcome of chronic stress exposure.

While these studies provided detailed insights into the roles of specific cell types and projection-based circuits, brain-wide functional imaging of resilient and vulnerable animals is increasingly used to map the distributed neural responses to stress in an unbiased manner (Dai et al. 2025; Lupinsky et al. 2025; Szente et al. 2025). Most of this work is conducted in rodents, yet alternative vertebrate models such as the zebrafish also hold promise for

uncovering the brain-wide correlates of stress resilience (Jacobs and Ryu 2023). Zebrafish share high genetic homology with mammals (Howe et al. 2013), a conserved neuroendocrine stress response (Alsop and Vijayan 2008), and are particularly amenable to whole-brain imaging (Ahrens et al. 2013; Randlett et al. 2015). Interestingly, a few studies have modeled resilience following exposure to an acute stressor in zebrafish larvae, using behavioral metrics such as latency to explore a light compartment (Tudorache et al. 2015) or return of swimming speed to control levels (Swaminathan et al. 2023). While these studies provided valuable insights into the behavioral, physiological, and molecular mechanisms underlying stress resilience, the brain-wide neural signatures distinguishing resilience from vulnerable phenotypes in zebrafish remain unexplored.

In the present study, we leverage a stress resilience assay previously established in our group to separate resilient from vulnerable zebrafish larvae based on the recovery of baseline swimming speed after a short-term stressful challenge. Following this, we map whole-brain activity using phosphorylated extracellular signal-regulated kinase (pERK) and extract the network of brain regions differentially involved in resilient and vulnerable groups.

RESULTS

Locomotor response to acute stress exposure distinguishes between resilience types

To evaluate the stress recovery phenotype of individual larvae, we measured their displacement after exposure to 10 minutes of saltwater (250 mM NaCl; Sup. Fig. 1A, Fig. 1A), which serves as an aversive stimulus that triggers the stress response (Yeh et al. 2013). Larvae were classified as resilient or vulnerable based on their locomotor response during the first 5 minutes of the stress recovery phase (Methods). To control for possible habituation of locomotor activity over time, a control group remained in water throughout the entire assay. To verify the reproducibility of the behavioral responses and to ensure that enough larvae were available for subsequent pERK level analysis, these data were collected in two independent biological replicates (replicates 1 and 2; Fig. 1 A, C, D). To sample a later point along the recovery trajectory of neural activity, we also performed an otherwise identical experiment in which larvae were scored during the first 5 minutes but euthanized only after 10 minutes of recovery (replicate 3; Fig. 1E).

The swimming speed was overall similar across groups during the baseline and stressor exposure phases, except in the first replicate, where resilient fish swam significantly slower than controls during the baseline phase (Sup. Fig. 1B-C, Fig. 1C-D). By design, a pronounced divergence in swimming speed was observed between resilient and vulnerable fish during the recovery phases in both replicates (Fig. 1C-D). Resilient fish swam faster, and vulnerable fish swam slower than control fish during the recovery phase.

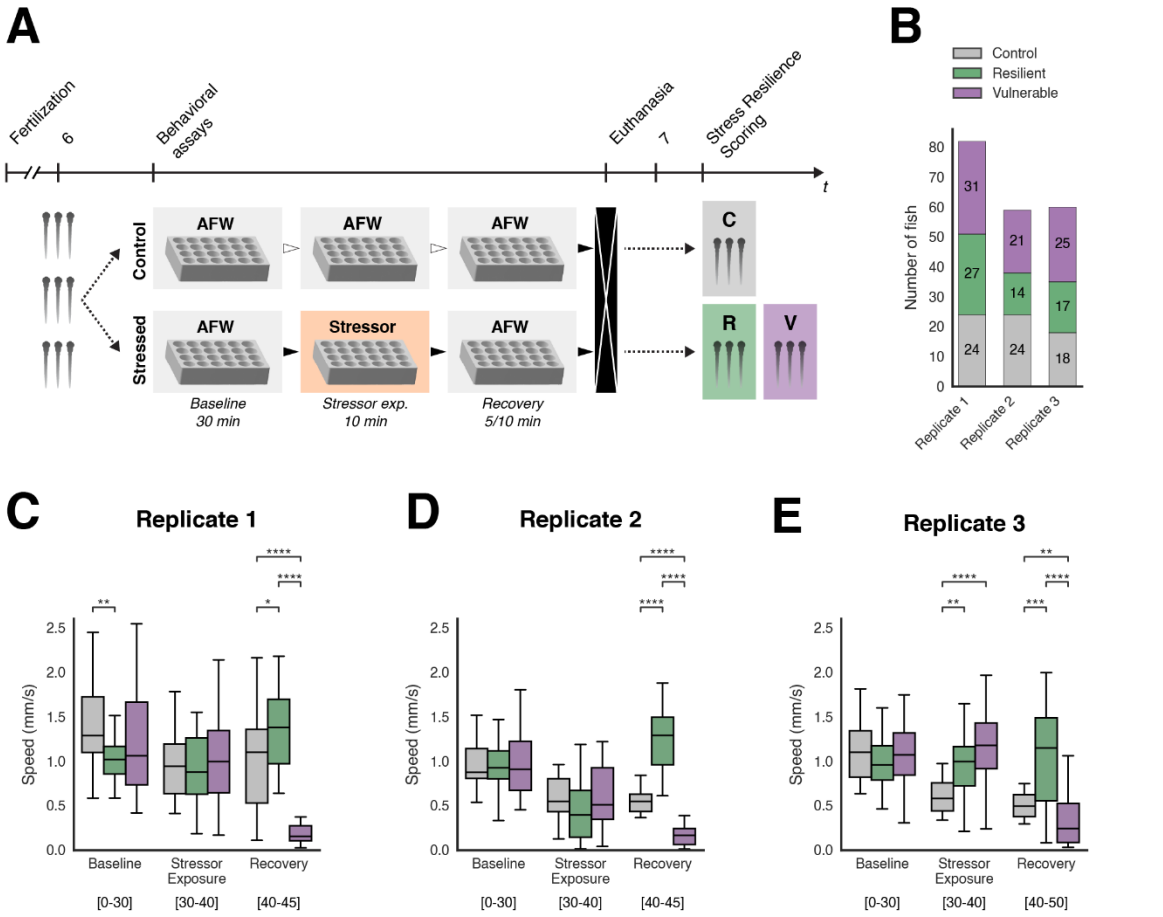

Figure 1: A stress recovery assay separates stress-resilient and -vulnerable zebrafish larvae.

A. *Experimental workflow. Larvae undergo a three-phase assay: Baseline (30 min in artificial freshwater, AFW), Stressor exposure (10 min in 250 mM NaCl), and Recovery (5 or 10 min in AFW). In parallel, control fish remain undisturbed in AFW for 45 min. After the assay, all fish are euthanized and the following morning, categorized as resilient or vulnerable based on locomotor rebound during recovery; brains are then processed for ex vivo pERK immunohistochemistry. Time in days post-fertilization (dpf).* ***B.*** *Numbers of animals per experimental replicate stacked by resilience class. Replicate 1: control, n=24; resilient, n=27; vulnerable, n=31; Replicate 2: control, n=24; resilient, n=14; vulnerable, n=21.* ***C-E.*** *Swimming speed (mm/s) across assay phases for each replicate is shown separately (C, Replicate 1; D, Replicate 2; E, Replicate 3). Within each phase, groups were compared with a Kruskal-Wallis test; when significant, pairwise Mann-Whitney U tests with Benjamini-Hochberg FDR correction were applied. Significance: *p < 0.05; **p < 0.01; ***p < 0.001; ***p < 0.0001.*

Comparison of brain-wide activity maps across resilience groups

To determine which brain regions are differentially activated across resilience classes, we performed immunohistochemistry against the marker of neuronal activity phosphorylated ERK (pERK; Randlett et al., 2015) and compared brain-wide neuronal activity patterns using voxel-wise statistics. We chose pERK because of its superior time resolution compared to c-Fos. Randlett and colleagues have shown that the pERK signal peaks in 2-5 min and returns to baseline within 30 min. Therefore, we reasoned that measuring brain activity in animals euthanized shortly after (5 or 10 min) the end of the stressor exposure period would capture activity levels in brain regions involved in the acute stress response, as well as in those activated during the stressor recovery period.

We first compared brain pERK levels between saltwater-exposed fish (resilient or vulnerable) and control fish to identify brain regions involved in the response to osmotic stress (Fig. 2A-B, Sup. Fig. 3A-B). Across both replicates, stressed fish showed increased neural activity in several telencephalic and diencephalic areas compared to controls. This included widespread activation of the olfactory bulbs and the posterior part of the dorsomedial pallium (Dm). Increased activity was also observed in the preoptic area and hypothalamic and habenular regions.

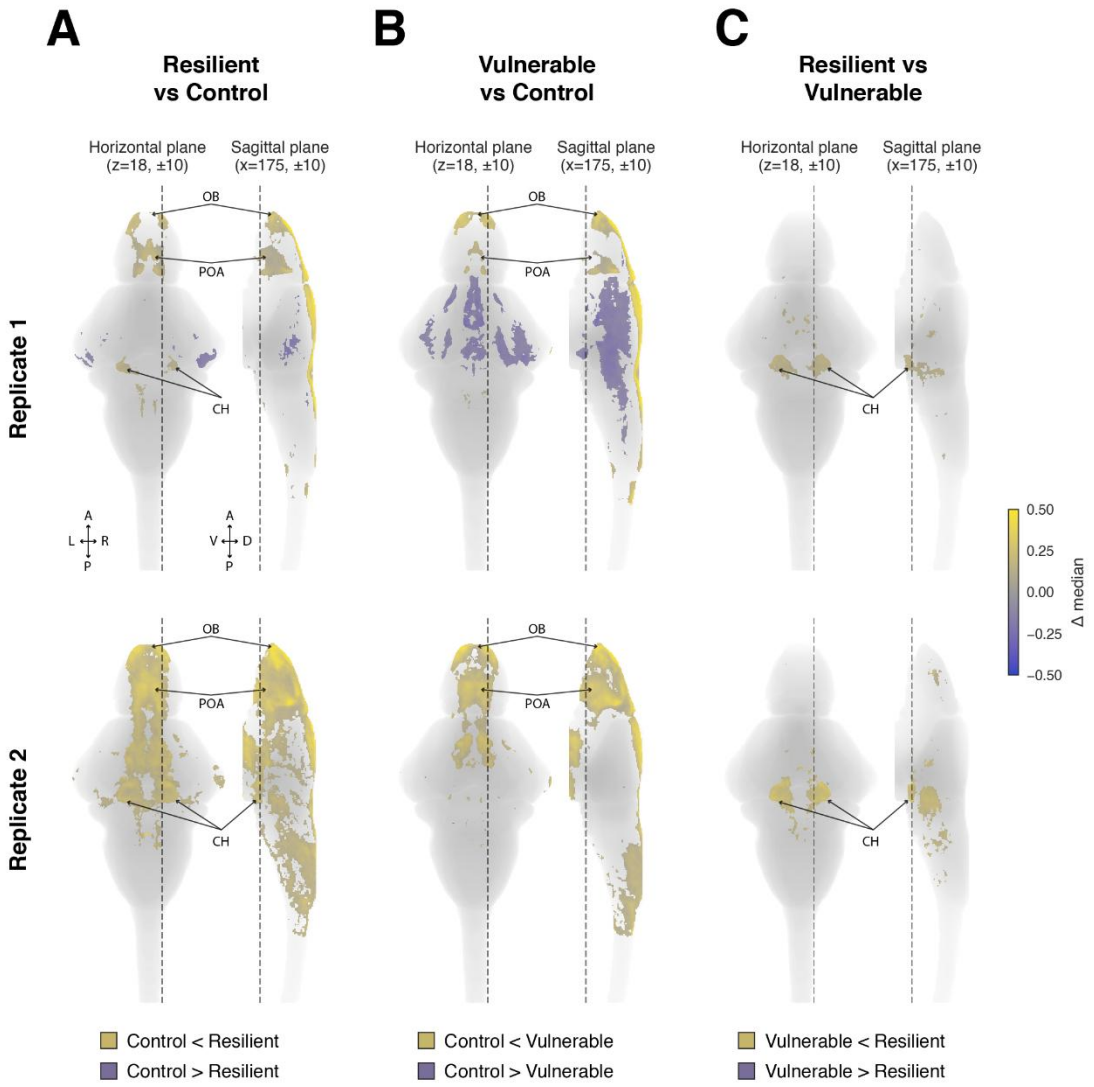

Figure 2: Brain-wide differences in neural activity between resilience groups

Maps of pairwise significant differences in pERK levels between resilience groups. Horizontal (left panels) and sagittal (right panels) projections are shown, with replicate 1 at the top and 2 at the bottom. ***A****. Significant differences between the resilient and control groups.* ***B****. Significant differences between vulnerable and control groups.* ***C****. Significant differences between resilient and vulnerable groups. Colors indicate the median difference between groups in each comparison. Slices are averaged over ±10 slices around the specified planes (horizontal: z=18; sagittal: x=175). OB: olfactory bulbs; POA: preoptic area; CH: caudal hypothalamus. Replicate 1 (control, n=21; resilient, n=22; vulnerable, n=31); replicate 2 (control, n=21; resilient, n=12; vulnerable, n=20).*

Next, we compared brain pERK levels between the resilient and vulnerable subpopulations to reveal the brain areas differentially implicated in post-stressor rebound (Fig. 2C). Compared ventrolateral stripe of serotonergic with the vulnerable group, resilient larvae showed stronger pERK signals in the caudal hypothalamus (CH). In the brainstem, increased activity was observed in the ventrolateral stripe of serotonergic neurons in the rhombencephalon, as well as in reticulospinal clusters (RoM1, RoV3, RoM2) and the nucleus of the medial longitudinal fasciculus (nMLF), which exhibited higher activity in resilient larvae. Resilient animals also displayed higher signals in hindbrain Gad1b+ and Glyt2+ inhibitory clusters.

Regional ERK Activity Patterns Distinguish Stress Resilience Classes

The voxel-wise statistical comparison used above enables the detection of even small, localized differences in brain activity that might be overlooked when averaging larger regions. The downside is that this results in numerous hits that are difficult to interpret. To complement this approach, we used Partial Least Squares Discriminant Analysis (PLS-DA) to identify multivariate patterns of regional ERK activity that separate control, resilient, and vulnerable fish. For each replicate, we fit PLS-DA to each replicate's regional ERK activity matrices after within-fish z-scoring (Sup. Fig. 2A, B, D, E), which emphasizes relative regional activity while minimizing global intensity differences. The resulting embeddings showed consistent structure: Component 1 separated stressed (resilient or vulnerable animals) from controls, and Component 2 separated resilient from vulnerable individuals (Fig. 3A-B). Both models achieved high cross-validated performance and explained substantial variance (balanced accuracy = 0.92 and 0.90; R^2 = 0.67 and 0.75 for replicates 1 and 2, respectively), whereas label-permutation nulls performed poorly (accuracy ≈ 0.61; < 11% variance explained), indicating that the observed separations were not attributable to chance.

To identify the brain areas that reproducibly contribute to each axis, we ranked regions by absolute loading for each component and replicate, selected the top 50 per replicate, and retained only regions that appeared in the top 50 for both replicates with the same loading sign. This yielded a consensus *stress exposure* set for Component 1 (21 regions; hereby termed the stress exposure network) and a consensus *stress resilience* set for Component 2 (25 regions; hereby termed the stress resilience network). Across-replicate overlaps among top contributors were 42% and 50%, respectively (Fig. 3C-D). These consensus sets provide anatomically interpretable, replicate-robust substrates for downstream network analyses.

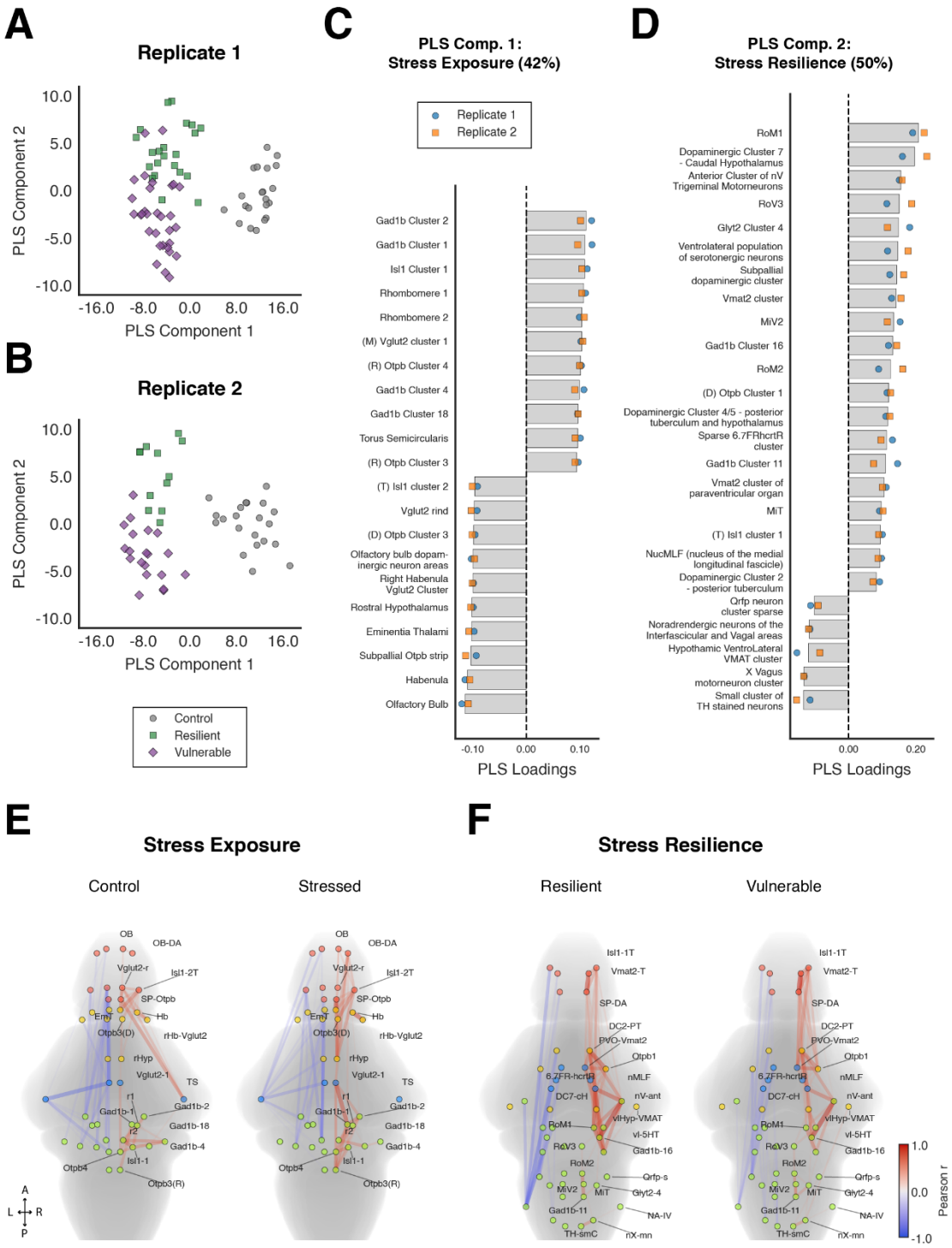

Figure 3: Partial Least Squares Discriminant Analysis (PLS-DA) embedding and region loadings across experimental replicates.

A-B. *PLS-DA embeddings by replicate using region-level ERK ratios across 218 filtered Z-Brain regions* (Randlett et al. 2015)*. A, Replicate 1. B, Replicate 2. Each point is a single fish, colored and shaped by group (control: gray circles; resilient: green squares; vulnerable: purple diamonds). Axes show PLS Components 1 and 2.* ***C-D.*** *Consensus region sets for each PLS component. For each replicate, the top 50 regions by absolute loading were identified for the component. Regions were retained only if they (i) appeared in the top-50 of both replicates and (ii) had the same loading sign in both replicates.*

C, PLS Component 1 - Stress Exposure (21 regions). D, PLS Component 2 - Stress Resilience (25 regions). Percentages above each panel indicate the proportion of overlapping regions between replicates out of the top 50 contributors. Bars show the average loading across both replicates for each overlapping region (dashed line at 0). Overlaid markers denote per-replicate loadings for the same region (Replicate 1: blue circles; Replicate 2: orange squares). ***E-F.*** *Anatomical projections of functional connectivity networks derived from the consensus region sets. E, Component 1 - Stress exposure network: correlations shown separately for control and stressed (resilient + vulnerable combined) groups. F, Component 2 - Stress resilience network: correlations shown separately for resilient and vulnerable groups. Each dot represents the centroid of a brain region. Edges represent strong functional connectivity between pairs of brain regions (only strong positive or negative Pearson correlations with $|r| \geq 0.40$ are displayed). Negative correlations are shown on the left half of the brain in blue; positive correlations are shown on the right in red. The thickness of edges is proportional to the $|r|$ value. Region abbreviations for E-F follow Supplementary Table 1. Replicate 1 (control, n=21; resilient, n=22; vulnerable, n=31); replicate 2 (control, n=21; resilient, n=12; vulnerable, n=20).*

The stress exposure network comprised sensory integration centers, hypothalamic neuroendocrine nuclei, and neuromodulatory regions spanning the telencephalon, diencephalon, mesencephalon, and rhombencephalon (Fig. 3C). Regions with negative loadings (showing higher relative activity in stressed fish, Sup. Fig. 3A) included the olfactory bulb, the habenulae (especially the right habenula), the rostral hypothalamus, as well as Otpb- and Vglut2-positive clusters within the preoptic and forebrain areas. In contrast, regions with positive loadings (showing higher relative activity in controls) were enriched for Gad1b-positive inhibitory clusters, Isl1-expressing motor and hypothalamic populations, rhombomeric segments, and midbrain sensory nuclei such as the torus semicircularis.

The stress resilience network mainly included posterior brainstem and hypothalamic regions, with additional involvement from telencephalic dopaminergic clusters (Fig. 3D; Sup. Fig. 3B). Most contributing regions showed positive loadings, indicating higher relative activity in resilient than in vulnerable fish along this axis. This involved regions of the reticulospinal system, such as the nMLF and several reticulospinal neurons (RoM1, RoM2, RoV3, MiT), as well as dopaminergic clusters in the CH (Cluster 7) and posterior tuberculum (Clusters 2 and 4/5), along with glycinergic and GABAergic cell groups (Glyt2 Cluster 4, Gad1b Clusters 11 and 16).

Connectivity architecture is conserved at global and primary division levels in stress exposure and stress resilience

To investigate whether resilience-related signatures extend beyond regional activation levels and into the structure of inter-regional connections, we examined functional connectivity within the stress-exposure and stress-resilience networks

described above. For each network and group, we computed connectivity matrices by correlating within-fish z-scored pERK/tERK values across all regions (Fig. 3E-F). As a sanity check on overall coupling patterns, we first inspected the full, unthresholded matrices (Fig. 4C-D) and compared the distributions of correlation coefficients between groups using Kolmogorov-Smirnov tests. These analyses revealed no significant differences in the global correlation distributions for either network (stress exposure: KS = 0.07, p = 0.714; stress resilience: KS = 0.09, p = 0.166; Sup. Fig. 4E-F). We then focused our primary analyses on the core of each network, retaining only edges with $|r| \geq 0.40$ to reduce weak or potentially spurious associations while preserving the strongest co-activation patterns.

At the level of the primary brain subdivisions (telencephalon, diencephalon, mesencephalon, rhombencephalon), both networks displayed similar organization. A Fisher-z difference map showed only modest differences between the stress exposure networks of control and

stressed animals: the stressed group had a somewhat stronger average coupling between mesencephalon and rhombencephalon, as well as between telencephalon and rhombencephalon, along with slightly weaker interactions between telencephalon and mesencephalon, and between diencephalon and rhombencephalon (all $|\Delta r| \leq 0.36$; Sup. Fig. 5A). Comparisons within the stress resilience network between resilient and vulnerable animals also revealed a common backbone but with a clearer reweighting of long-range connections in resilient animals, emphasizing a stronger coupling between the telencephalon and the rhombencephalon (all $|\Delta r| \leq 0.30$; Sup. Fig. 5B).

Stress exposure and stress resilience shift network modularity and hub centrality rank

Having established similar global and division-level coupling, we next asked whether the topology of the strong-edge backbone differs across groups. Across both the stress exposure and stress resilience networks, graph-theoretic analyses indicated a small-world-like organization. In each network, graph density and global efficiency were similar across the two groups (Sup. Fig. 6A, E), with pronounced modularity in the stressed and vulnerable graphs, respectively. We then compared bootstrap resamples of the empirical functional connectivity networks to degree-preserving random null networks obtained by repeated double-edge swaps of the empirical graphs. Clustering coefficients were consistently higher in the bootstrapped group networks, whereas global efficiency was of similar magnitude (Sup. Fig. 6B, F). Thus, at the $|r| \geq 0.40$ backbone threshold, control and stressed graphs, as well as resilient and vulnerable graphs, combined random-like global efficiency with elevated local clustering, consistent with small-world topology.

Within the stress-exposure network, the stressed group-level graph was slightly denser and more modular than control graphs, while global efficiency remained very similar between groups (Sup. Fig. 6A). Katz centrality highlighted changes in the identity of the most central nodes (Sup. Fig. 6C-D). In the control graph, the highest-centrality nodes included hindbrain Vglut2 and Gad1b stripes (e.g., Vglut2 rind, rhombomere 1, Gad1b cluster 2), a subpallial Otpb strip, and torus semicircularis. In the stressed graph, the torus semicircularis, the rostral hypothalamus, an Otpb3 hypothalamic cluster, the olfactory bulb, and a dopaminergic cluster within it occupied higher ranks, whereas telencephalic structures such as the Vglut2 rind and the habenulae, along with two Gad1b hindbrain nodes, dropped in relative centrality.

In the stress resilience network, resilient and vulnerable graphs showed nearly identical density and global efficiency. However, modularity was higher in vulnerable graphs (Sup. Fig. 6E). As in the stress exposure network, both phenotypes maintained small-world structure, with global efficiency close to their degree-preserving random counterparts and elevated clustering coefficients (Sup. Fig. 6F). Katz centrality profiles were highly similar between resilient and vulnerable groups (Sup. Fig. 6G-H): in both, the highest-centrality nodes were concentrated in neuromodulatory and hypothalamic regions, including diencephalic dopaminergic clusters, telencephalic dopaminergic/Vmat2 clusters, midbrain/brainstem nuclei such as the nMLF, and an Otpb-positive hypothalamic cluster. Differences between phenotypes were largely restricted to modest shifts in rank within this shared hub set.

Spatial patterns and regional hierarchy are preserved at 10 min but markedly attenuated

To determine how brain activity changes within the stress-exposure and stress-resilience networks as larvae recover further, we repeated the experiment and analysis on an independent cohort euthanized after 10 min of recovery (replicate 3).

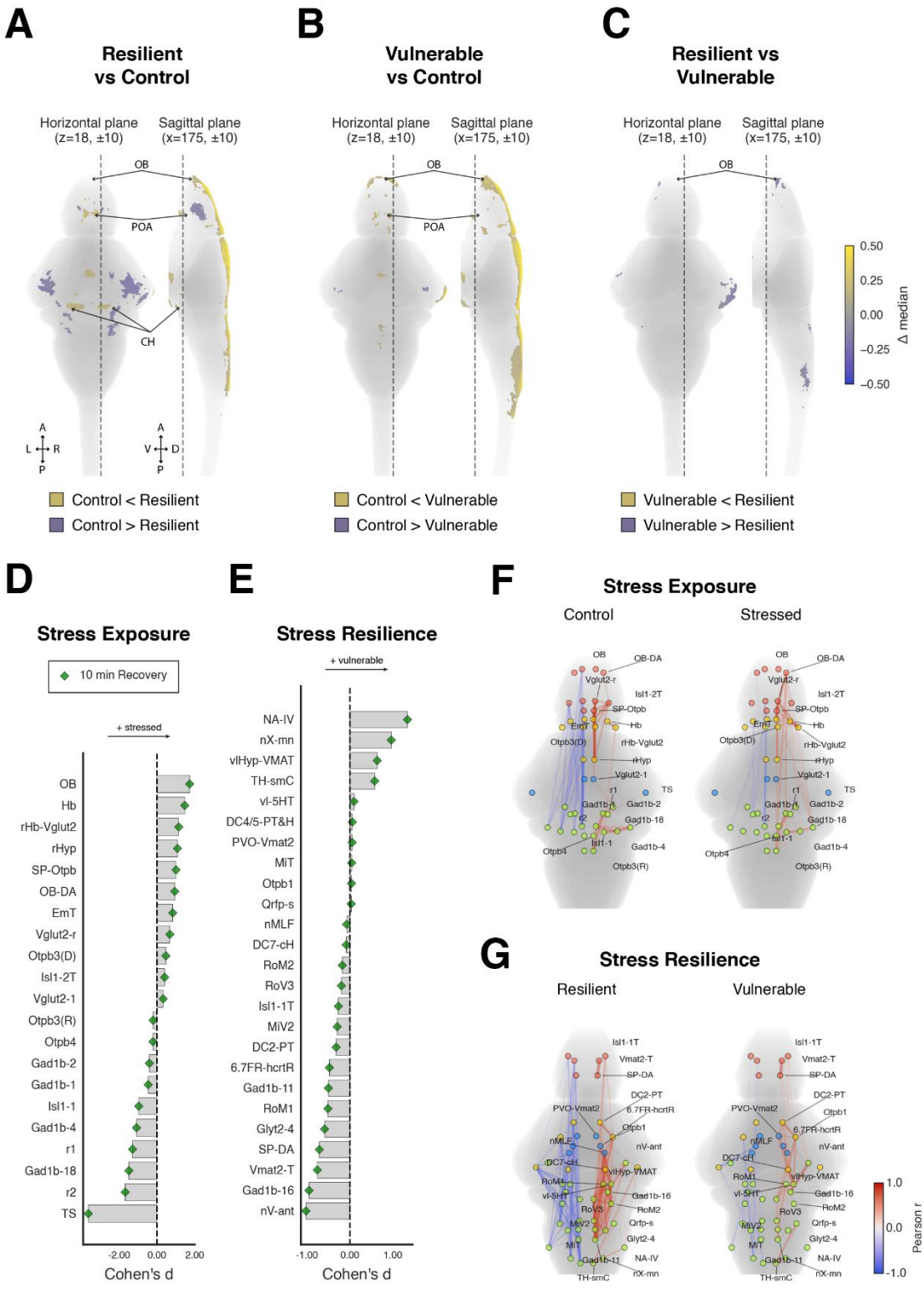

Figure 4. Brain-wide pERK/tERK maps, effect sizes, and connectivity for the 10 min recovery dataset.

A-C. *Projected maps of significant pERK/tERK differences for the 10 min recovery dataset are shown in two orthogonal views (horizontal and sagittal). Colors encode the median difference (Δ median) between the first and second group in each comparison (colorbar, yellow-blue): A, resilient (R) vs control*

(C; yellow: R > C; blue: C > R), B, vulnerable (V) vs control (yellow: V > C; blue: C > V), C, resilient vs vulnerable (yellow: R > V; blue: V > R). Only voxels that pass multiple-comparison correction are displayed (FDR, q ≤ 0.10). Slices are averaged over ±10 slices around the indicated planes (horizontal: z=18; sagittal: x=175). ***D-E.*** *Cohen's d effect sizes for the 10 min recovery dataset, computed for the PLS-DA region sets corresponding to each axis.* ***D****, Stress Exposure (PLS Comp. 1) compares control vs stressed with stressed, i.e., resilient + vulnerable combined (d < 0 ⇒ control > stressed; d > 0 ⇒ stressed > control). E, Stress Resilience (PLS Comp. 2) compares resilient vs vulnerable (d < 0 ⇒ resilient > vulnerable; d > 0 ⇒ vulnerable > resilient). Region abbreviations follow Supplementary Table 1. Markers show per-region effect sizes; dashed line at 0.* ***F-G.*** *Anatomical projections of functional connectivity for the 10 min recovery dataset, evaluated within the PLS-DA region sets for Stress Exposure (F, PLS Comp. 1) and Stress Resilience (G, PLS Comp. 2). For each network, correlations are shown for the relevant comparison: control and stressed (resilient + vulnerable combined) in* ***F****, and resilient and vulnerable in G. Nodes are Z-Brain region centroids* (Randlett et al. 2015)*; edges denote pairwise Pearson correlations between region-level ERK values and are colored by correlation. OB: olfactory bulbs; POA: preoptic area; CH: caudal hypothalamus. Region abbreviations for D-G follow Supplementary Table 1. 10 min recovery dataset (control, n=18; resilient, n=17; vulnerable, n=25).*

Behaviorally, replicate 3 recapitulated the key feature from replicates 1 and 2: resilient and vulnerable fish diverged only during the recovery phase, not during the baseline or exposure phases (Fig. 1C-E). During the initial 5 minutes of the recovery phase, vulnerable fish displayed an overwhelming freezing response, whereas resilient fish gradually increased their swimming speed, matching the observed speed at the beginning of the assay. After 5 minutes, this trend shifts: vulnerable fish gradually increase their swimming speed, while resilient fish decelerate (Sup. Fig. 1D).

Maps of pERK/tERK expression reflected this approximation in behavior: compared to the 5 min recovery references (Fig. 2A-C), replicate 3 maps displayed a similar biomarker pattern but with less extent and intensity (Fig. 4A-C). In both resilient-control and vulnerable-control comparisons, key foci remain in telencephalic regions such as OB, POA, Hb, and pineal VMAT clusters. At the regional level, per-fish pERK/tERK distributions confirmed this attenuation: signals in hypothalamic dopaminergic clusters (posterior tuberculum and caudal hypothalamus), hindbrain premotor/reticulospinal systems (nMLF, RoM/RoV), midbrain sensory relays (TS), and hindbrain inhibitory/glycinergic pools decreased at 10 min (Sup. Fig. 3; Sup. Fig. 7). Remaining differences at 10 min were mainly in anterior forebrain and epithalamic/diencephalic regions: telencephalic olfactory and pallial parts, a telencephalic Isl1 cluster (Isl1-2T), the preoptic/hypothalamic area, and the habenula/pineal VMAT axis.

Effect-size profiles calculated on the predefined PLS-DA sets showed that the 10 min regional ordering closely matched the 5 min pattern for the stress-exposure axis (Spearman $\rho = 0.82$). OB and Hb remained among the strongest stressed-higher nodes, including the right habenula Vglut2 subdivision. Most nodes decreased in magnitude (20/21; paired test on $|d|$: $t = -6.50$, $p = 2.5\times10^{-6}$; median $|\Delta d| = 1.83$). One region, Vglut2-1, reversed its sign between time points, and the torus semicircularis uniquely increased in the control-higher direction at 10 minutes. For the stress-resilience axis, the 10-minute ordering also followed the 5-minute profile, though more weakly (Spearman $\rho = 0.66$). Most nodes decreased (24/25; paired test on $|d|$: $t = -8.25$, $p < 10^{-6}$; median $|\Delta d| = 0.64$). The anterior trigeminal motor cluster (nV-ant) remained the top-ranked resilient-higher region at both time points, while the caudal-hypothalamic dopaminergic cluster (DC7-cH) showed a significant decrease.

DISCUSSION

We used a newly developed assay to separate stress-resilient and stress-vulnerable larvae based on the recovery of locomotion following exposure to saltwater, an aversive stimulus that disrupts the homeostasis of freshwater fish. *Ex vivo* whole-brain imaging of phosphorylated ERK levels during the early phases of post-stressor exposure enabled us to determine the brain-wide correlates of saltwater stimulation on the one hand and of post-stressor recovery phenotypes on the other.

Brain-wide correlates of saltwater exposure

Exposure of zebrafish to saltwater at concentrations comparable to those used in our study induces avoidance behaviors (Herrera et al. 2021; Vom Berg-Maurer et al. 2016) and elevates circulating cortisol levels (Yeh et al. 2013). In line with this, our results revealed that saltwater exposure strongly activated the preoptic area, which contains corticotropin-releasing hormone neurons that initiate the hypothalamic-pituitary-interrenal (HPI) axis response, leading to increased cortisol release. Moreover, we found that saltwater strongly activated the olfactory system (olfactory bulb, dorsal posterior part of the telencephalon) and areas recipient of olfactory bulb innervation in zebrafish, such as the right habenula (Kermen et al. 2013). Our findings, therefore, confirm a pioneering study that recently identified olfaction as the primary sense used for saltwater detection in the zebrafish (Herrera et al. 2021). The torus semicircularis was also a key contributing region in discriminating saltwater-exposed from control fish, with decreased activity levels in stressed fish. Located in the midbrain, the torus semicircularis integrates auditory information as well as inputs from the lateral line system in the zebrafish (Fame et al. 2006). While the decreased activity in the torus semicircularis may initially appear surprising, given that our saltwater exposure assay did not involve auditory or vibrational stimuli, this could be explained by the lateral line's additional role in saltwater sensing in zebrafish (Herrera et al. 2021).

Overall, the consistent activation of the olfactory and preoptic brain regions by saltwater across biological replicates in our study, as well as in previous research (Herrera et al. 2021; Randlett et al. 2015; Vom Berg-Maurer et al. 2016), underscores the reproducibility and robustness of our findings.

Brain-wide correlates of resilience versus vulnerable phenotypes

In line with the robust post-stressor locomotor rebound that defines the resilient phenotype in our assay, our analysis identified premotor regions (reticulospinal neurons and nucleus of the medial longitudinal fasciculus) as key determinants of the brain activity pattern in resilient animals. Reticulospinal neurons located in the reticular formation integrate information from diverse brain centers and directly project to the spinal cord to elicit movement. The set of reticulospinal neurons underlying the resilient phenotype in our study has been involved in the production of turns (RoV3 and MIV2; Huang et al., 2013), and of C-start escapes (Mauthner cells, Liu and Fetcho, 1999). The nucleus of the medial longitudinal fasciculus projects directly to the spinal cord, and its activation promotes swimming (Berg et al. 2023).

Our approach also revealed that resilient fish show increased activity in the caudal hypothalamus and paraventricular organ compared to vulnerable fish. These regions contain serotonergic, dopaminergic, and histaminergic cells, whose functions are still being explored in zebrafish. Caudal hypothalamus cells activity increases during aversive states (e.g., food deprivation; Wee et al., 2019) and in response to noxious stimuli (Ailani and Deepak 2017; Randlett et al. 2015). Moreover, recent studies suggest that monoaminergic clusters in the zebrafish hypothalamus play a role in gating spontaneous and stimulus-evoked locomotion.

Manipulating the activity of all dopaminergic neurons in the hypothalamus promotes swimming and modulates sound-evoked behaviors (Ailani and Deepak 2017; Barrios et al. 2020). Additionally, dopaminergic cells in the caudal hypothalamus enhance auditory-evoked escape responses (Mu et al. 2012) and populations of primarily serotonergic cells in the caudal, lateral hypothalamus and paraventricular organs modulate swimming bouts (Ailani and Deepak 2017). Collectively, our findings and previous studies point towards a possible role for monoaminergic neurons in the caudal hypothalamus and paraventricular organ in promoting locomotion to escape aversive internal states or environmental conditions threatening homeostasis.

Our PLS-DA analysis reveals that dopaminergic clusters in the telencephalon and diencephalon are among the most distinguishing features between resilient and vulnerable animals. In future experiments, we will use immunohistochemistry against pERK and markers of dopaminergic neurons (e.g., tyrosine hydroxylase and the dopamine transporter) to determine whether dopaminergic cells are indeed more activated in resilient than in vulnerable zebrafish. If confirmed, this would imply that heightened dopaminergic activity in these brain regions may contribute to stress resilience in the zebrafish, a finding that is reminiscent of the well-established role of the mammalian mesolimbic dopaminergic system, consisting of the midbrain ventral tegmental area (VTA) and nucleus accumbens (NAc), in mediating stress resilience (Cao et al. 2010; Chaudhury et al. 2013; Friedman et al. 2016; Krishnan et al. 2007). Given the different organization of the dopaminergic system in zebrafish, which lack midbrain dopaminergic neurons, identifying homologues to the VTA and NAc regions remains challenging. Nevertheless, clusters of dopaminergic cells in the ventral telencephalon and diencephalon have been suggested to serve analogous functions in social interaction (Geng and Peterson 2019). Overall, our finding that telencephalic and diencephalic dopaminergic regions in zebrafish are linked to stress resilience suggests that core functions of dopamine in coping with stress might be conserved across vertebrates.

Another finding of the PLS-DA analysis is the increased activity in the noradrenergic region of the medulla oblongata, in vulnerable compared to resilient fish (Fig. 3D). This region is known to respond robustly to aversive stimuli, such as repeated swim failures (Mu et al. 2019) or acoustic/vestibular stimuli (Orts-Del'Immagine et al. 2022), with noradrenergic neurons driving a shift toward behavioral suppression by activating adjacent radial glia (Chen et al. 2024; Mu et al. 2019). Our results suggest that the noradrenergic activation of medullary radial glia in vulnerable fish may underlie their prolonged immobility following saltwater exposure. To explore this further, future *in vivo* experiments will use head-embedded zebrafish to monitor Ca^{2+} signals in radial glia during saltwater exposure simultaneously, and the number of tail movements attempted during recovery will be used as a proxy for vulnerability or resilience.

Topological network properties of stress resilience

Here, network analysis complements the regional maps by showing that both the stress exposure and resilience graphs combine random-like global efficiency with elevated clustering, i.e., small-world organization. Exposure graphs were slightly denser and more modular than controls, and vulnerable graphs showed higher modularity than resilient graphs. This architecture is characteristic of activity-derived brain graphs and mirrors zebrafish networks that exhibit small-world, modular structure supporting rapid integration atop segregated sensory modules (Betzel 2020; Terstege et al. 2022). In our stress exposure network, Katz centrality shifted toward olfactory and hypothalamic nodes (plus torus semicircularis). In contrast, some telencephalic and hindbrain inhibitory nodes dropped in rank, consistent with sensory-biased modules coupling to the stress axis during exposure. In the Resilience network, centrality was shared across hypothalamic/monoaminergic clusters

and premotor brainstem nodes (nMLF/reticulospinal) with a reweighting of long-range telencephalon-rhombencephalon links. Together, these patterns suggest that resilience is supported by a conserved small-world scaffold whose hubs retune from sensory-neuroendocrine emphasis during exposure to hypothalamic/monoaminergic control coupled to premotor execution during recovery.

Possible confounds

Could the difference in swimming speed between resilient and vulnerable fish during recovery reflect differences in salt sensing, rather than resilience per se? In larvae, saltwater avoidance is mediated primarily by olfaction (Herrera et al. 2021), so a lower detection threshold in one subgroup could lead to more frequent freezing during the recovery period. In our data, however, olfactory bulb signals are similar between resilient and vulnerable fish, suggesting that both groups detect the stressor to the same extent.

METHODS

Animals

Zebrafish (*Danio rerio*) larvae used in this study were of the *nacre mitfa* background (Lister et al. 1999), and were raised at 28°C in artificial fish water (AFW; 0.06 g/L marine salt in purified water) under a 14:10 h light/dark cycle. Larvae were maintained in Petri dishes containing 40-60 animals in 50 mL of AFW, which was replaced daily. Dry feed (shrimp larval diet, Royal Caviar, 5-50 µm) was introduced at 5 days post-fertilization (dpf). All experiments were conducted on 6 dpf larvae in compliance with European Directive 2010/63/EU on the protection of animals used for scientific purposes. Experimental protocols were approved by the Danish Animal Experiments Inspectorate (license 2023-15-0201-01493).

Experimental Design

At 6 dpf, the fish were randomly assigned to two main treatment conditions during a stress resilience assay: stressed (exposed to 250 mM NaCl) and control (no stressor). To assess neural activity during the stress recovery period, larvae were euthanized either 5 minutes or 10 minutes after the termination of the stressor exposure and later processed for whole-brain analysis of phosphorylated ERK levels using immunohistochemistry and confocal microscopy. To assess the reproducibility of this method, the datasets for 5 min stress recovery were collected in two biological replicates performed by two different experimenters, months apart.

Stress Resilience Assay

Experiments were conducted between 13:00 and 18:00 inside a custom-built, lightproof enclosure, where the temperature was maintained at 28 ± 0.5 °C.

Larvae were individually transferred using cut-tip pipettes into a modified 24-well plate (12.8 x 8.6 x 1.8 cm; Greiner Bio-One), rendered opaque with acetone and fitted with nylon mesh bottoms to allow rapid fluid exchange. The plate was inserted into a custom acrylic holder (14.8 x 9.4 x 3.9 cm) equipped with a 6 mm silicone tubing drain system, enabling fast solution replacement within all wells. Each well was filled with artificial fish water to a depth of 1.2 cm. All solutions were pre-warmed to 28°C and introduced by draining and replacing the well contents manually via the tubing system.

Larvae were allowed to acclimate in darkness for 5-10 minutes before recording. The assay consisted of three consecutive phases: a baseline period of 30 min in AFW; a stressor exposure period of 10 min in salted water (250 mM NaCl) and a recovery period lasting 5 or 10 min. Behavioral recordings were acquired using a Mako U-319B monochrome camera (Allied Vision), fitted with a 35 mm lens (Fujinon HF35SA-1) and positioned above the multi-well dish. Infrared illumination was delivered through a flexible LED strip and an opaque acrylic diffuser positioned beneath the plate. Videos were captured at 10 fps using a custom Python script (Andreassen et al., 2022).

At the end of the experiment, larvae were euthanized by immersion in ice-cold water, fixed overnight at in 4°C in 10% formalin, rinsed three times in PBT (PBS with 0.25% Triton X-100), and stored in fresh PBT at 4°C until immunohistochemistry.

Video Analysis

Videos were downsampled to 2 Hz and segmented into individual wells using a circular Hough Transform. Zebrafish trajectories were extracted by tracking the eyes using DeepLabCut (Mathis et al. 2018), with a ResNet-50 architecture. Detection artefacts in output trajectories

were post-processed using interpolation and manual correction via a graphical user interface developed in-house.

Fish that failed to displace more than a minimum distance during baseline (< 385 mm) were excluded from analysis. To quantify stress resilience, the average swimming speed during the final 20 minutes of the baseline phase ($Speed_{pre}$) and the first 5 minutes of the recovery phase ($Speed_{post}$) were computed for each fish. A resilience score was then calculated as the relative change in speed across these two periods, as defined below:

$$\text{Resilience Score} = \frac{\text{Speed}_{\text{post}} - \text{Speed}_{\text{pre}}}{\text{Speed}_{\text{pre}}}$$

To categorize behavioral phenotypes, we applied fixed thresholds to this score: fish with values ≤ -0.5 were classified as Vulnerable, those > -0.1 as Resilient.

Statistical Analysis of Behavioral Features

Distributions were tested for normality using the Shapiro-Wilk test. Group-level comparisons of behavioral features (e.g., swimming speed) across assay stages and behavioral cohorts were conducted using non-parametric statistics. Kruskal-Wallis one-way ANOVA was used to assess overall group differences. Where significant, pairwise Mann-Whitney U tests were performed, and p-values were corrected for multiple comparisons using the Benjamini-Hochberg false discovery rate (FDR) method. All statistical analyses were conducted in Python (v3.12) using scipy, statsmodels, and pandas. A significance threshold of $p < 0.05$ was applied unless otherwise specified.

Immunohistochemistry

Whole-mount immunohistochemistry against phosphorylated extracellular signal-regulated kinase (pERK) and total ERK (tERK) was performed to visualize neural activity as previously published (Randlett et al., 2015). Samples were permeabilized in 0.05% EDTA-Trypsin on ice for 45 minutes, blocked in serum-containing buffer, and incubated at 4°C for 3 nights with primary antibodies (1:600; mouse anti-tERK and rabbit anti-pERK). After washing, larvae were incubated overnight at 4°C with secondary antibodies (1:600; Alexa Fluor 633 goat anti-mouse and Alexa Fluor 488 goat anti-rabbit). Following three washes in excess PBT, samples were stored in PBT at 4°C until imaging.

Confocal Imaging

Immunolabeled larvae were mounted upright in 2% low-melting-point agarose on glass slides equipped with silicone rings. Confocal scans were acquired using a Zeiss LSM 700 microscope with a 20x water-immersion objective. Image stacks were acquired with a spatial resolution of 0.33 x 0.33 x 1.00 µm (x, y, z) per voxel, capturing the full depth of the larval brain in two overlapping regions: an anterior stack spanning forebrain and midbrain, and a posterior stack covering hindbrain and anterior spinal cord. Channels corresponding to pERK and tERK were acquired under consistent acquisition settings within each experimental replicate.

Registration to Z-Brain

To enable voxel-wise comparisons of neural activity, all brains were spatially aligned to a common anatomical reference using intensity-based non-linear registration. The registration pipeline was based on the Computational Morphometry Toolkit (CMTK), adapted from the approach described by (Randlett et al. 2015), and included several optimizations to enhance anatomical precision.

Anterior and posterior image stacks were first stitched into a single 3D volume per sample using custom FIJI macros. These fused stacks were then resampled to isotropic voxel resolution and split into separate pERK and tERK channels in preparation for registration. The tERK channel was used as the anatomical reference for all registration steps due to its consistent structural contrast.

All scans were initially aligned to a Z-Brain reference brain using the Computational Morphometry Toolkit (CMTK), with the 'Cachero, Ostrovsky 2010' parameters preset, employing the following parameters: -T 16 -X 52 -C 8 -G 80 -R 3 -A '--accuracy 0.4' -W '--accuracy 1.6'. To improve registration performance, we implemented a second registration step: for each experimental replicate, a subset of scans exhibiting the best anatomical correspondence to the Z-Brain reference was selected and averaged voxel-wise to generate a refined template using SimpleITK (Lowekamp et al. 2013). These images were intensity-normalized (z-scored) prior to averaging, and the resulting template was rescaled to 16-bit resolution. The refined template was then used as the registration target for a second alignment of all scans in that replicate, applying the same transformation framework.

Voxel-wise Activity Mapping (MapMapping)

To visualize spatial patterns of brain-wide neural activity, we employed the MapMapping framework introduced by (Randlett et al. 2015), which enables voxel-wise comparison of pERK-to-tERK signal ratios across experimental groups. As a pre-processing step, registered 16-bit NRRD volumes were capped at an upper intensity limit determined independently for each experimental replicate. Specifically, the cap was set at the 99th percentile of voxel intensities across all scans for a given replicate, with an additional 5% safety margin. This normalization step helped to mitigate the influence of extreme outlier values while preserving dynamic range across animals.

Following intensity normalization, voxel-wise pERK to tERK signal ratios were computed and passed to the MapMapping MATLAB pipeline (https://github.com/owenrandlett/Z-Brain), which applies a Mann-Whitney U test to compare activity between groups on a per-voxel basis. Resulting p-values were corrected for multiple comparisons using the false discovery rate (FDR) method, with a significance threshold of $q < 0.00005$. Statistically significant voxels were visualized on a standardized brain template, yielding maps that highlight regions of differential neural activity across resilience classes.

Region-wise ERK Quantification and Statistical Profiling

To complement voxel-wise analyses, ERK activity was quantified within anatomically defined brain regions from the Z-Brain atlas. For each region and fish, the pERK to tERK signal ratio was computed, excluding background voxels (tERK = 0), and the median value was used to summarize activity within the region. Regions with insufficient signal coverage were excluded to ensure reliable quantification.

Prior to analysis, we derived a neuron-focused subset of Z-Brain regions without agglomeration. Starting from the atlas-derived full-region list (294 regions), we first removed peripheral ganglia, yielding 272 regions. We then applied rule-based text filters to exclude non-parenchymal or fiber-dominated compartments, removing entries whose names contained terms for fiber tracts or bundles, commissures or chiasmata, cranial nerves or roots, ventricles or luminal/meningeal/vascular structures, and neuropil or layer-only labels (e.g., 'tract,' 'fasciculus,' 'commissure,' 'nerve,' 'ventricle,' 'plexus,' 'vessel,' 'neuropil,' 'molecular layer'). This yielded 218 annotated brain regions, which were used in subsequent multivariate analyses (see Supplementary Data for the complete list).

To enable intersubject comparisons, regional activity values were normalized using z-scoring per fish. Group-level differences were assessed using Cohen's d effect sizes to identify regions showing significant between-group activation differences (see Supplementary Fig. 3).

Partial Least Squares analysis of pERK level correlation with behavior

We assessed whether regional ERK activity patterns could discriminate between experimental cohorts (resilient, vulnerable, control) using Partial Least Squares Discriminant Analysis (PLS-DA) (Barker and Rayens, 2003; Ståhle and Wold, 1987). Models were implemented in Python using scikit-learn's PLSRegression class. PLS-DA was performed separately for each experimental replicate using z-scored median pERK/tERK across brain regions as input features. The resulting component loadings were used to identify the regions that contributed most to group separation. For interpretability, we selected the 50 top-ranked regions per component based on the magnitude of their loadings and retained only those showing consistent directionality (sign) across experimental replicates.

Functional connectivity analysis

Matrices of median pERK/tERK values (fish x brain region) were assembled and z-scored within fish. Pairwise Pearson correlations were calculated across fish within a given group for all region pairs. To focus on robust connections, we thresholded the group-level matrices at $|r| \geq 0.40$, which is a commonly used heuristic range in graph-based functional connectivity analyses where no universally optimal threshold exists. This cut-off was chosen after inspecting the empirical correlation distributions (Sup. Fig. 4E-F): it removed the bulk of low-magnitude correlations while preserving a sparse but well-connected backbone, and nearby thresholds (0.35-0.45) produced qualitatively similar patterns. The same thresholded matrices were used for the mesoscale connectivity comparisons and all graph-theoretic analyses.

Mesoscale summaries of functional connectivity

Regions from each PLS-DA-derived set were assigned to four CNS macro-divisions (Telencephalon, Diencephalon, Mesencephalon, Rhombencephalon) using Z-Brain annotations. To summarize coupling at the mesoscale, within each cohort, we averaged correlations for each subdivision pair from the thresholded functional connectivity matrices using Fisher z-transformed means (atanh averaging, then tanh back-transform). A subdivision pair was summarized only if both cohorts contributing to a given comparison provided at least three retained edges. Group contrasts were defined as stressed versus control for the stress exposure network (Component 1) and resilient versus vulnerable for the stress resilience network (Component 2).

Graph-theoretic analysis

Thresholded functional connectivity matrices were interpreted as undirected, unweighted graphs, with nodes corresponding to Z-Brain regions and edges linking any pair of regions whose group-level correlation exceeded the threshold; isolated nodes were removed prior to analysis. For each group, we used NetworkX to compute graph density, global efficiency, modularity (Louvain community detection), and mean clustering coefficient.

Uncertainty in these metrics was estimated by non-parametric bootstrap resampling at the fish level: for each group, fish were sampled with replacement 1000 times, correlation matrices were recomputed from each resample, graphs were rebuilt, and metrics were recalculated; bootstrap distributions were summarized by their mean and 95% percentile intervals. Degree-matched null networks were generated from each empirical adjacency by repeated Maslov-Sneppen double-edge swaps, and the same global metrics were computed on these random

graphs. Node-level hub structure was quantified using Katz centrality on the single group-level graph for each condition (NetworkX implementation with default parameters), and regions were ranked by Katz score.

Statistics for comparing 5 versus 10 min regional hierarchies

We compared the regional effect-size profiles at 5 and 10 minutes after the start of the recovery phase within the predefined PLS-DA region sets (stress exposure network: control versus stressed groups; stress resilience network: resilient versus vulnerable groups). For each set, we first aligned regions by name and formed two vectors of per-region Cohen's *d* (5 min versus 10 min).

Similarity of the rank structure was quantified with Spearman's rank correlation (ρ) between the 5 min and 10 min *d* vectors. To assess the attenuation of effect magnitudes, we computed $\Delta|d| = |d_{10}| - |d_5|$ for each region. We tested whether magnitudes attenuated on average using a paired-samples t-test implemented as a one-sample t-test on Δ|d| against zero (df = $N_{regions} - 1$). We also report the median Δ|d| as a scale-robust summary and, as a robustness check, a Wilcoxon signed-rank test on Δ|d| (two-sided).

SUPPLEMENTARY INFORMATION

Full region name (Primary brain division, region name)	Abbreviation
Diencephalon, Dopaminergic Cluster 2, posterior tuberculum	DC2-PT
Diencephalon, Dopaminergic Cluster 4/5, posterior tuberculum and hypothalamus	DC4/5-PT&H
Diencephalon, Dopaminergic Cluster 7, Caudal Hypothalamus	DC7-cH
Diencephalon, Eminentia Thalami	EmT
Diencephalon, Habenula	Hb
Diencephalon, Hypothamic VentroLateral VMAT cluster	vlHyp-VMAT
Diencephalon, Otpb Cluster 1	Otpb1
Diencephalon, Otpb Cluster 3	Otpb3(D)
Diencephalon, Right Habenula Vglut2 Cluster	rHb-Vglut2
Diencephalon, Rostral Hypothalamus	rHyp
Mesencephalon, NucMLF (nucleus of the medial longitudinal fascicle)	nMLF
Mesencephalon, Sparse 6.7FRhcrtR cluster	6.7FR-hcrtR
Mesencephalon, Torus Semicircularis	TS
Mesencephalon, Vglut2 cluster 1	Vglut2-1
Mesencephalon, Vmat2 cluster of paraventricular organ	PVO-Vmat2
Rhombencephalon, Anterior Cluster of nV Trigeminal Motorneurons	nV-ant
Rhombencephalon, Gad1b Cluster 1	Gad1b-1
Rhombencephalon, Gad1b Cluster 11	Gad1b-11
Rhombencephalon, Gad1b Cluster 16	Gad1b-16
Rhombencephalon, Gad1b Cluster 18	Gad1b-18
Rhombencephalon, Gad1b Cluster 2	Gad1b-2
Rhombencephalon, Gad1b Cluster 4	Gad1b-4
Rhombencephalon, Glyt2 Cluster 4	Glyt2-4
Rhombencephalon, Isl1 Cluster 1	Isl1-1Rho
Rhombencephalon, MiT	MiT
Rhombencephalon, MiV2	MiV2
Rhombencephalon, Noradrendergic neurons of the Interfascicular and Vagal areas	NA-int-vagal
Rhombencephalon, Otpb Cluster 3	Otpb3(Rho)

Rhombencephalon, Otpb Cluster 4	Otpb4(Rho)
Rhombencephalon, Qrfp neuron cluster sparse	Qrfp-sparse
Rhombencephalon, Rhombomere 1	r1
Rhombencephalon, Rhombomere 2	r2
Rhombencephalon, RoM1	RoM1
Rhombencephalon, RoM2	RoM2
Rhombencephalon, RoV3	RoV3
Rhombencephalon, Small cluster of TH stained neurons	TH-smC
Rhombencephalon, Ventrolateral population of serotonergic neurons	vl-5HT
Rhombencephalon, X Vagus motorneuron cluster	nX-mn
Telencephalon, Isl1 cluster 1	Isl1-1T
Telencephalon, Isl1 cluster 2	Isl1-2T
Telencephalon, Olfactory Bulb	OB
Telencephalon, Olfactory bulb dopaminergic neuron areas	OB-DA
Telencephalon, Subpallial Otpb strip	SP-Otpb
Telencephalon, Subpallial dopaminergic cluster	SP-DA
Telencephalon, Vglut2 rind	Vglut2-r
Telencephalon, Vmat2 cluster	Vmat2-T

Supplementary Table 1. Z-Brain region abbreviations and full names (Randlett et al. 2015).

SUPPLEMENTARY FIGURES

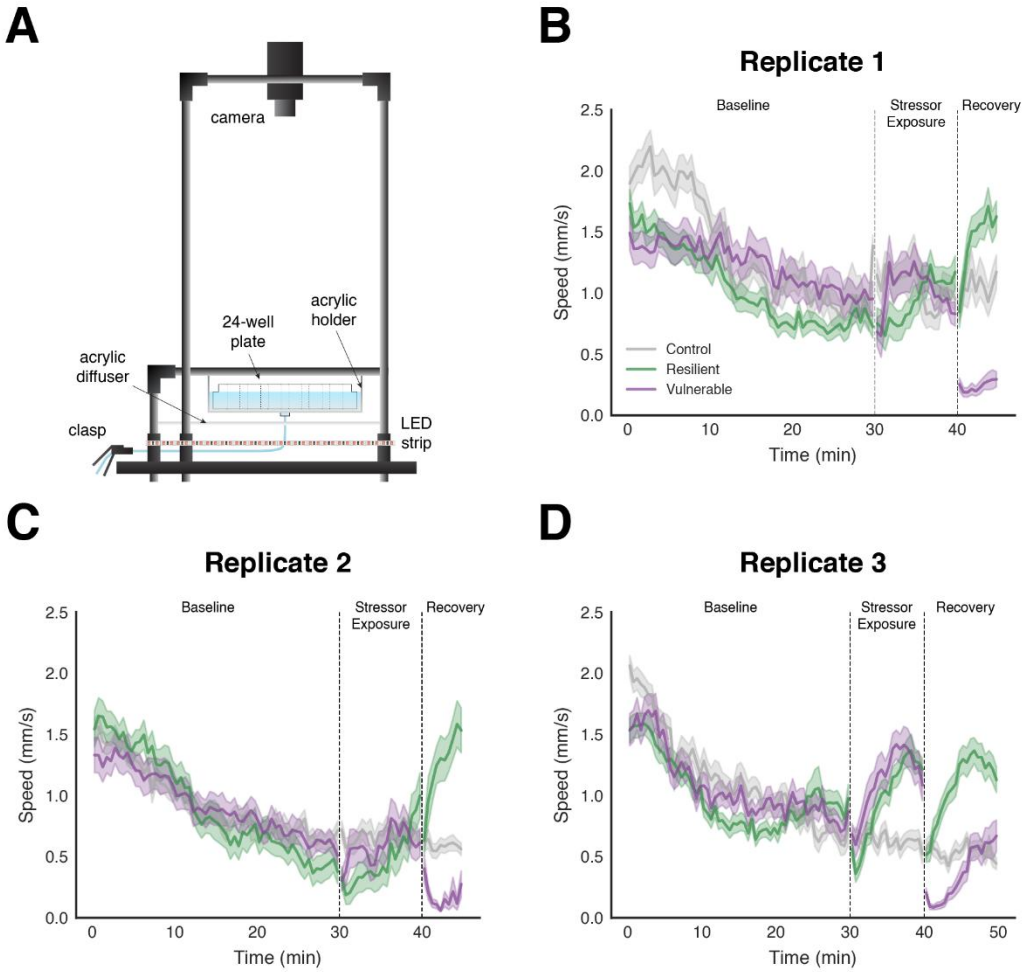

Supplementary Figure 1: Stress resilience assay design and behavioral readouts.

A. *Schematic of the custom behavioral arena used to assess stress resilience in zebrafish larvae. Individual larvae were housed in mesh-bottom wells of a modified 24-well plate, inserted into a custom acrylic holder. The arena was illuminated from below using an infrared LED strip and an opaque acrylic diffuser and imaged from above with a high-speed camera. A manual clasp allowed rapid draining and replacement of the medium without disturbing the plate, enabling fast transitions between assay phases.* ***B.*** *Time-binned average swimming speed (mm/s) across assay phases for replicate 1 (control, n=24; resilient, n=27; vulnerable, n=31). Vertical dashed lines mark the boundaries between the assay phases.* ***C****. Same as in B for replicate 2 (control, n=24; resilient, n=14; vulnerable, n=21).* ***D****. Same as in B-C for replicate 3 (control, n=18; resilient, n=17; vulnerable, n=25).*

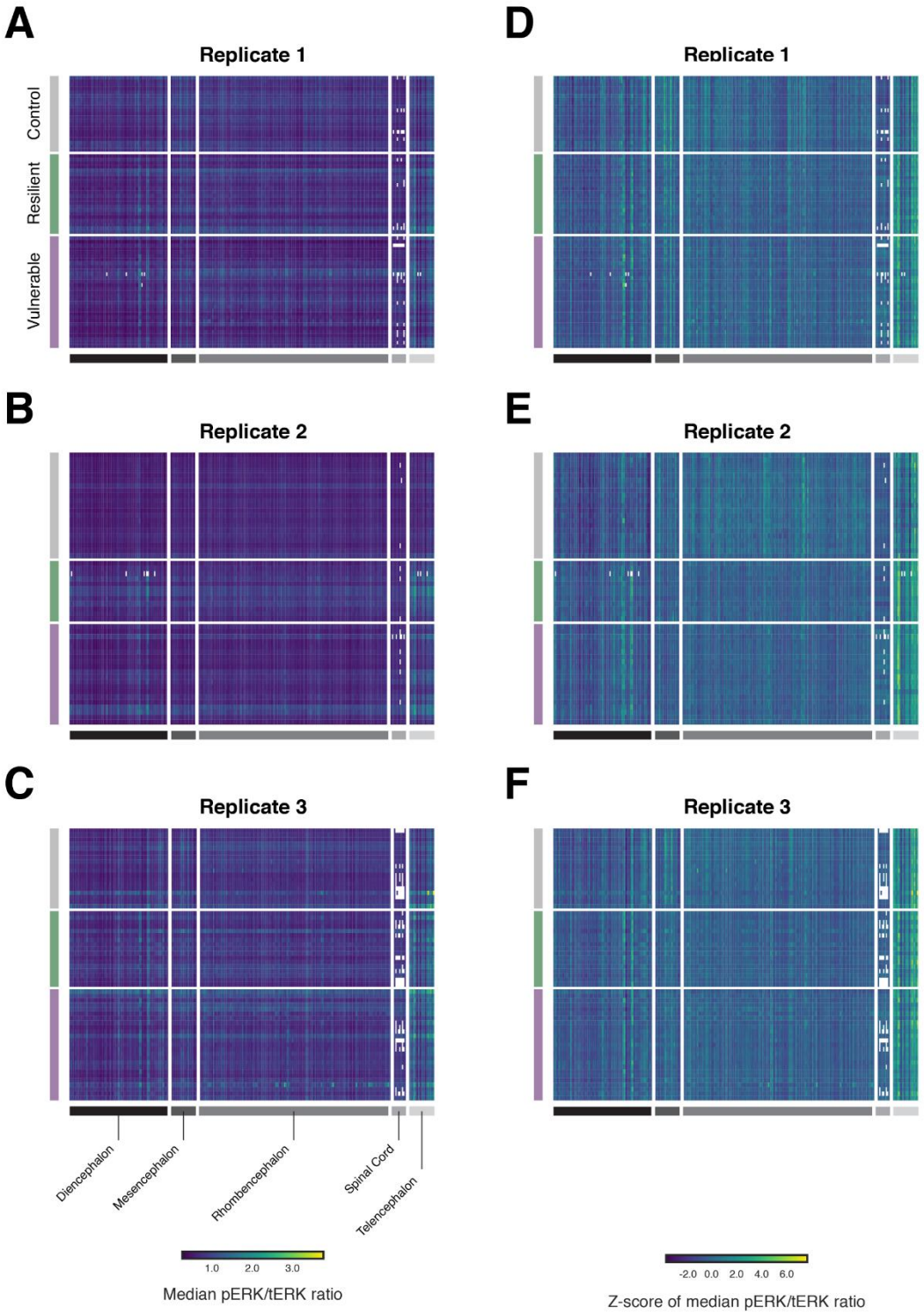

Supplementary Figure 2: Brain-wide regional ERK activity profiles across experimental replicates and resilience classes.

A-C. *Heatmaps of the median pERK/tERK ratio per region and fish before normalization for each replicate (A, Replicate 1; B, Replicate 2;* ***C****, Replicate 3). Rows are individual fish grouped by resilience class (control, resilient, vulnerable). Columns are 272 Z-Brain non-ganglia regions* (Randlett et al. 2015) *arranged by major subdivision (Diencephalon, Mesencephalon, Rhombencephalon, Spinal Cord, Telencephalon). White cells indicate regions with insufficient signal or missing values. Colorbar: median pERK/tERK ratio.* ***D-F.*** *The same data after within-fish z-scoring to emphasize relative regional activity*

while controlling for global intensity differences (D, Replicate 1; E, Replicate 2; F, Replicate 3). Colorbar: z-scored median pERK/tERK ratio. Replicate 1 (control, n=21; resilient, n=22; vulnerable, n=31); replicate 2 (control, n=21; resilient, n=12; vulnerable, n=20); replicate 3 (control, n=18; resilient, n=17; vulnerable, n=25).

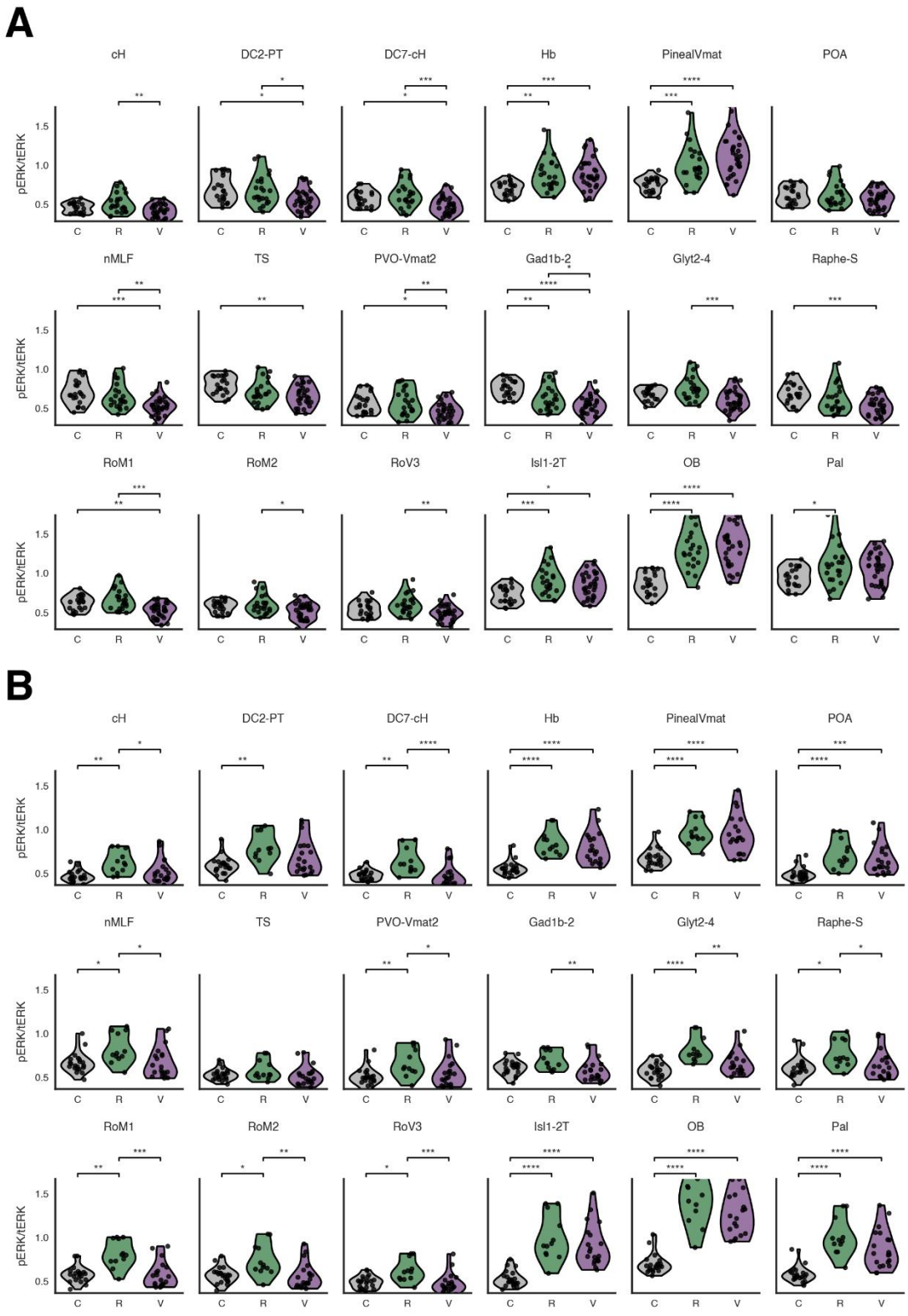

Supplementary Figure 3: Regional pERK/tERK differences across stress-resilience groups (5 minutes recovery).

A-B. *Violin plots show the distribution of the median pERK/tERK ratio per fish for selected Z-Brain regions in Replicate 1 (A) and Replicate 2 (B). Points are individual fish; violins depict kernel density. Groups: control (C, grey), resilient (R, green), vulnerable (V, purple). Horizontal brackets indicate*

*pairwise group comparisons with Holm-adjusted p values; asterisks denote significance (p < 0.05 *, < 0.01 **, < 0.001 ***, < 0.0001 ****). Included regions are: CH, caudal hypothalamus; DC2-PT, dopaminergic cluster 2 (posterior tuberculum); DC7-cH, dopaminergic cluster 7 (caudal hypothalamus); Hb, habenulae; PinealVmat, pineal Vmat2 cluster; POA, preoptic area; nMLF, nucleus of the medial longitudinal fasciculus; TS, torus semicircularis; PVO-Vmat2, paraventricular organ Vmat2 cluster; Gad1b-2, Gad1b cluster 2; Glyt2-4, Glyt2 cluster 4; Raphe-S, superior raphe; RoM1/2 and RoV3, reticulospinal neurons of medial (M) and ventral (V) nuclei; Isl1-2T, telencephalic Isl1 cluster 2; OB, olfactory bulb; Pal, pallium. Replicate 1 (control, n=21; resilient, n=22; vulnerable, n=31); replicate 2 (control, n=21; resilient, n=12; vulnerable, n=20); replicate 3 (control, n=18; resilient, n=17; vulnerable, n=25).*

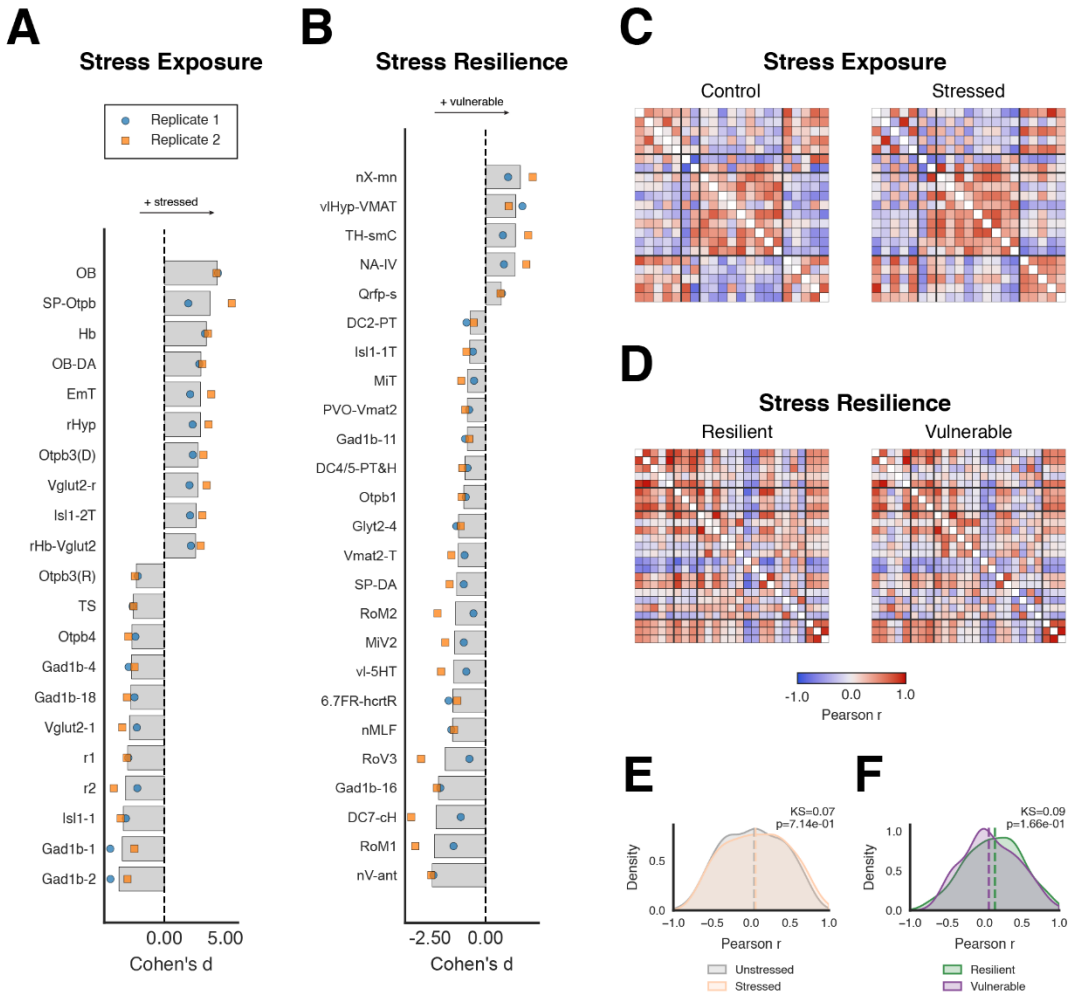

Supplementary Figure 4: Effect Size and Connectivity Structure for top PLS-DA contributing regions across replicates

A-B. *Mean effect sizes (Cohen's d) for the consistently selected top contributing regions for PLS-DA. A, PLS Component 1 - Stress Exposure. B, PLS Component 2 - Stress Resilience. Bars show the average Cohen's d across the two 5-minute recovery replicates; overlaid markers indicate per-replicate values (Replicate 1: blue circles; Replicate 2: orange squares). For Component 1, Cohen's d contrasts control vs stressed (resilient and vulnerable combined; d > 0 ⇒ stressed > control; d < 0 ⇒ control > stressed). For Component 2, Cohen's d compares resilient vs vulnerable (d > 0 ⇒ vulnerable > resilient; d < 0 ⇒ resilient > vulnerable). Region abbreviations follow Supplementary Table 1.* ***C-D.*** *Pearson correlation matrices for the PLS-DA-derived networks computed on the pooled 5 min recovery dataset. C, stress exposure network: matrices shown separately for control and stressed (resilient and vulnerable combined). D, stress resilience network: matrices shown for resilient and vulnerable groups. Entries are pairwise Pearson r between z-scored regional ERK values; the color scale is centered at 0.* ***E-F****. Edge-wise correlation distributions corresponding to the matrices in C-D. For each cohort, the upper-triangular off-diagonal entries of the square adjacency matrices were extracted and plotted as kernel density estimates. E, stress exposure network: control vs stressed. F, stress resilience network: resilient vs vulnerable. Dashed vertical lines mark medians; annotations report the two-sample Kolmogorov-Smirnov statistic (KS) and p value. Panels A-B: replicate 1 (control, n=21; resilient, n=22; vulnerable, n=31); replicate 2 (control, n=21; resilient, n=12; vulnerable, n=20). Panel C-F: pooled 5 min recovery dataset (control, n=42; stressed, n=85; resilient, n=34; vulnerable, n=51).*

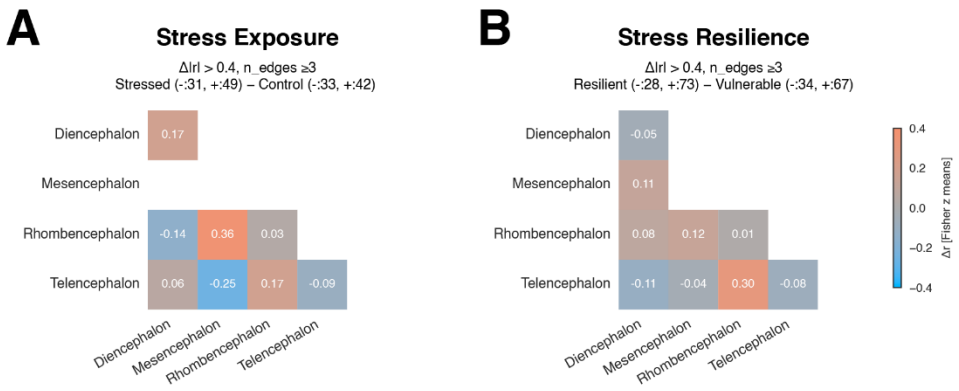

Supplementary Figure 5: Subdivision-level functional connectivity differences for the Stress-Exposure and Stress-Resilience sets.

A-B. *Block-level connectivity differences between the four major brain subdivisions (Telencephalon, Diencephalon, Mesencephalon, Rhombencephalon) for stress exposure (A) and stress resilience (B) networks. Values are Δr for the first minus the second group in each comparison, computed by Fisher-z averaging of surviving edges within each subdivision pair. A, Stress Exposure compares stressed (resilient + vulnerable combined) to control (warm colors indicate stressed > control, cool colors indicate control > stressed). B, Stress Resilience compares resilient to vulnerable (warm colors indicate resilient > vulnerable, cool colors indicate vulnerable > resilient). Edges were retained per group if |r| ≥ 0.40; cells are shown only when both groups contribute at least 3 edges; and the text above each matrix reports the number of surviving positive and negative edges in each group after thresholding. Sample sizes: stress exposure network (control, n=42, stressed, n=85); stress resilience network (resilient, n=34; vulnerable, n=51).*

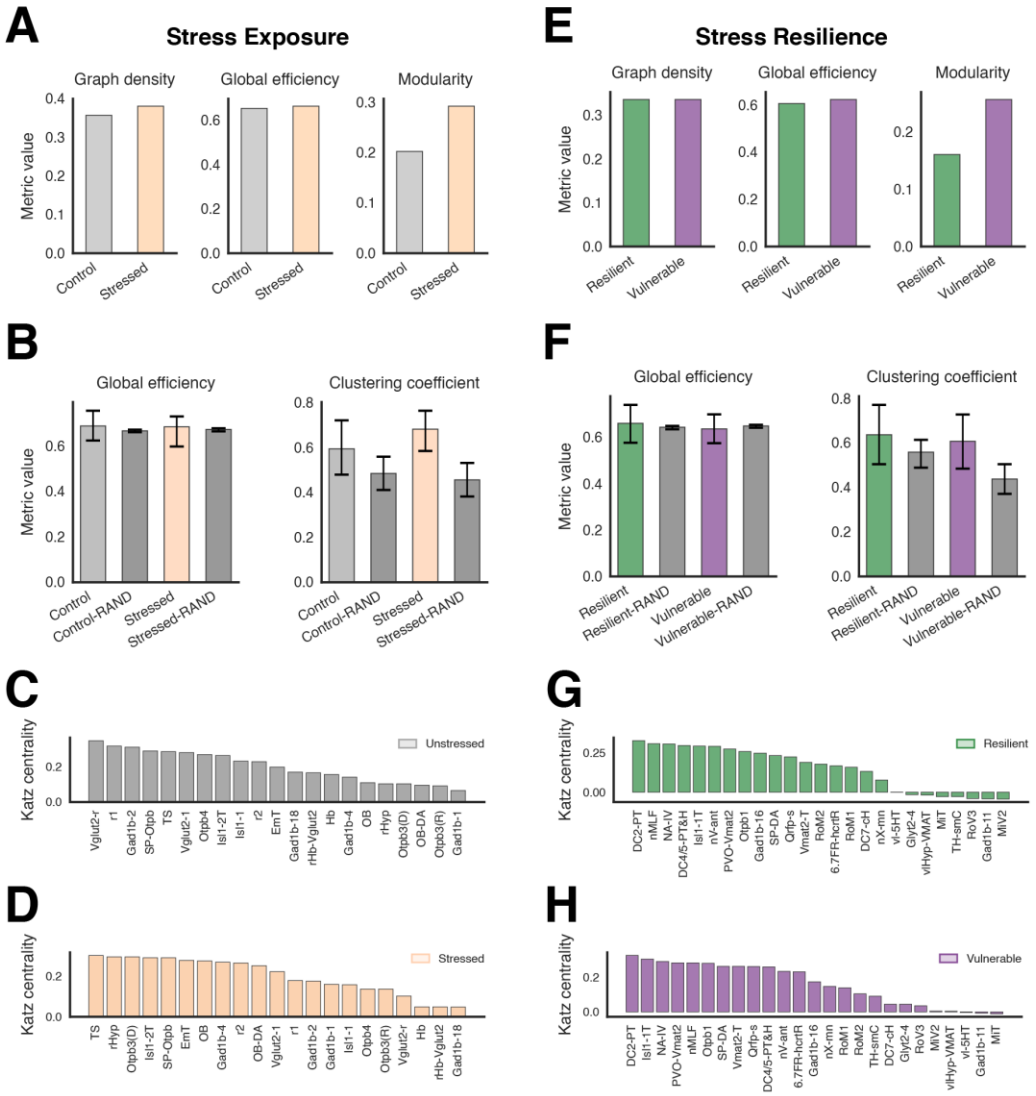

Supplementary Figure 6: Graph-theoretic organization and hub structure of stress exposure and stress resilience networks.

A,E. *Global graph metrics for empirical stress exposure (A) and stress resilience (E) networks. Bars show graph density, global efficiency, and modularity for the control and stressed group-level graphs.* ***B,F.*** *Small-worldness of the stress exposure network (B) and the stress resilience network (F). Bars show global efficiency (left) and mean clustering coefficient (right) for empirical network bootstraps and their degree-preserving random counterparts ("RAND") for each group. Random networks were generated by rewiring the empirical adjacency matrix while preserving the degree distribution; bars show means across randomizations with 95% confidence intervals.* ***C-D,G-H.*** *Katz centrality profiles for the stress exposure network. Bars show Katz centrality values for individual regions in the control (C) and stressed (D), resilient (G) and vulnerable (H) group-level graphs, ranked from highest to lowest within each group. Region labels follow the abbreviations in Supplementary Table 1. All networks were constructed from group-level Pearson correlation matrices of z-scored pERK/tERK values within the PLS-DA-defined stress exposure (Component 1) and stress resilience (Component 2) region sets (Fig. 3C-D). Adjacency matrices were thresholded at $|r| \geq 0.40$ and treated as undirected, unweighted graphs. Sample sizes: stress exposure network (control, n=42, stressed, n=85); stress resilience network (resilient, n=34; vulnerable, n=51).*

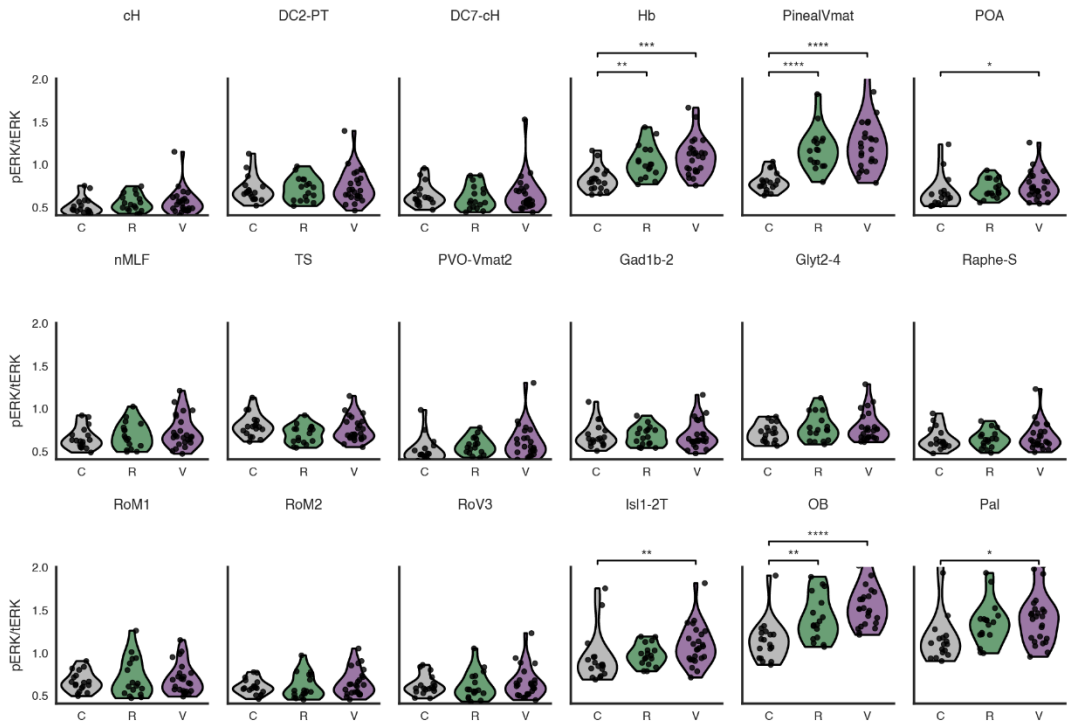

Supplementary Figure 7: Regional pERK/tERK differences across stress-resilience groups (10 minutes recovery).

*Violin plots show the distribution of the median pERK/tERK ratio per fish for selected Z-Brain regions in Replicate 3. Points are individual fish; violins depict kernel density. Groups: control (C, grey), resilient (R, green), vulnerable (V, purple). Horizontal brackets indicate pairwise group comparisons with Holm-adjusted p values; asterisks denote significance ($p < 0.05$ *, < 0.01 **, < 0.001 ***, < 0.0001 ****). Included regions are: cH, caudal hypothalamus; DC2-PT, dopaminergic cluster 2 (posterior tuberculum); DC7-cH, dopaminergic cluster 7 (caudal hypothalamus); Hb, habenulae; PinealVmat, pineal Vmat2 cluster; POA, preoptic area; nMLF, nucleus of the medial longitudinal fasciculus; TS, torus semicircularis; PVO-Vmat2, paraventricular organ Vmat2 cluster; Gad1b-2, Gad1b cluster 2; Glyt2-4, Glyt2 cluster 4; Raphe-S, superior raphe; RoM1/2 and RoV3, reticulospinal neurons of medial (M) and ventral (V) nuclei; Isl1-2T, telencephalic Isl1 cluster 2; OB, olfactory bulb; Pal, pallium. 10 min recovery dataset: (control, n=18; resilient, n=17; vulnerable, n=25).*

REFERENCES

Abreu, Murilo S. de, Konstantin A. Demin, Ana C. V. V. Giacomini, et al. 2021. “Understanding How Stress Responses and Stress-Related Behaviors Have Evolved in Zebrafish and Mammals.” *Neurobiology of Stress* 15 (November): 100405. https://doi.org/10.1016/j.ynstr.2021.100405.

Ahrens, Misha B., Michael B. Orger, Drew N. Robson, Jennifer M. Li, and Philipp J. Keller. 2013. “Whole-Brain Functional Imaging at Cellular Resolution Using Light-Sheet Microscopy.” *Nature Methods* 10 (5): 413–20. https://doi.org/10.1038/nmeth.2434.

Ailani, Deepak, and AILANI Deepak. 2017. “Genetic Studies on Hypothalamus Functions in Zebrafish.” *(No Title)*. https://ir.soken.ac.jp/?action=repository_action_common_download&item_id=5610&item_no=1&attribute_id=19&file_no=3.

Alsop, Derek, and Mathilakath M. Vijayan. 2008. “Development of the Corticosteroid Stress Axis and Receptor Expression in Zebrafish.” *American Journal of Physiology-Regulatory, Integrative and Comparative Physiology* 294 (3): R711–19. https://doi.org/10.1152/ajpregu.00671.2007.

Anastasiades, Paul G., and Adam G. Carter. 2021. “Circuit Organization of the Rodent Medial Prefrontal Cortex.” *Trends in Neurosciences* 44 (7): 550–63. https://doi.org/10.1016/j.tins.2021.03.006.

Barrios, Joshua P., Wei-Chun Wang, Roman England, Erica Reifenberg, and Adam D. Douglass. 2020. “Hypothalamic Dopamine Neurons Control Sensorimotor Behavior by Modulating Brainstem Premotor Nuclei in Zebrafish.” *Current Biology* 30 (23): 4606-4618.e4. https://doi.org/10.1016/j.cub.2020.09.002.

Berg, Eva M., Leander Mrowka, Maria Bertuzzi, David Madrid, Laurence D. Picton, and Abdeljabbar El Manira. 2023. “Brainstem Circuits Encoding Start, Speed, and Duration of Swimming in Adult Zebrafish.” *Neuron* 111 (3): 372-386.e4. https://doi.org/10.1016/j.neuron.2022.10.034.

Betzel, Richard F. 2020. “Organizing Principles of Whole-Brain Functional Connectivity in Zebrafish Larvae.” *Network Neuroscience* 4 (1): 234–56. https://doi.org/10.1162/netn_a_00121.

Bonanno, George A., Maren Westphal, and Anthony D. Mancini. 2011. “Resilience to Loss and Potential Trauma.” *Annual Review of Clinical Psychology* 7 (1): 511–35. https://doi.org/10.1146/annurev-clinpsy-032210-104526.

Cao, Jun-Li, Herbert E. Covington, Allyson K. Friedman, et al. 2010. “Mesolimbic Dopamine Neurons in the Brain Reward Circuit Mediate Susceptibility to Social Defeat and Antidepressant Action.” *The Journal of Neuroscience* 30 (49): 16453–58. https://doi.org/10.1523/JNEUROSCI.3177-10.2010.

Cathomas, Flurin, James W. Murrough, Eric J. Nestler, Ming-Hu Han, and Scott J. Russo. 2019. “Neurobiology of Resilience: Interface Between Mind and Body.” *Biological Psychiatry* 86 (6): 410–20. https://doi.org/10.1016/j.biopsych.2019.04.011.

Chaudhury, Dipesh, Jessica J. Walsh, Allyson K. Friedman, et al. 2013. “Rapid Regulation of Depression-Related Behaviours by Control of Midbrain Dopamine Neurons.” *Nature* 493 (7433): 532–36. https://doi.org/10.1038/nature11713.

Chen, Alex B., Marc Duque, Vickie M. Wang, et al. 2024. “Norepinephrine Changes Behavioral State via Astroglial Purinergic Signaling.” Preprint, bioRxiv, May 23. https://doi.org/10.1101/2024.05.23.595576.

Covington, Herbert E., Mary Kay Lobo, Ian Maze, et al. 2010. “Antidepressant Effect of Optogenetic Stimulation of the Medial Prefrontal Cortex.” Articles. *Journal of Neuroscience* 30 (48): 16082–90. https://doi.org/10.1523/JNEUROSCI.1731-10.2010.

Dai, Twain, Shannon Dee Algar, Michael Small, Andrew Zalesky, and Jennifer Rodger. 2025. “Identifying Neuroimaging Biomarkers of Resilience and Vulnerability to Chronic Stress in An Animal Model: An Exploratory Analysis.” Preprint, bioRxiv, August 6. https://doi.org/10.1101/2025.08.05.667822.

Dong, Yiyan, Yifei Li, Xinkuan Xiang, et al. 2023. “Stress Relief as a Natural Resilience Mechanism against Depression-like Behaviors.” *Neuron* 111 (23): 3789-3801.e6. https://doi.org/10.1016/j.neuron.2023.09.004.

Fame, Ryann M., Carole Brajon, and Alain Ghysen. 2006. “Second-Order Projection from the Posterior Lateral Line in the Early Zebrafish Brain.” *Neural Development* 1 (1): 4. https://doi.org/10.1186/1749-8104-1-4.

Friedman, Allyson K., Barbara Juarez, Stacy M. Ku, et al. 2016. “KCNQ Channel Openers Reverse Depressive Symptoms via an Active Resilience Mechanism.” *Nature Communications* 7 (1): 11671. https://doi.org/10.1038/ncomms11671.

Friedman, Allyson K., Jessica J. Walsh, Barbara Juarez, et al. 2014. “Enhancing Depression Mechanisms in Midbrain Dopamine Neurons Achieves Homeostatic Resilience.” *Science (New York, N.Y.)* 344 (6181): 313–19. https://doi.org/10.1126/science.1249240.

Geng, Yijie, and Randall T. Peterson. 2019. “The Zebrafish Subcortical Social Brain as a Model for Studying Social Behavior Disorders.” *Disease Models & Mechanisms* 12 (8): dmm039446. https://doi.org/10.1242/dmm.039446.

Herrera, Kristian J., Thomas Panier, Drago Guggiana-Nilo, and Florian Engert. 2021. “Larval Zebrafish Use Olfactory Detection of Sodium and Chloride to Avoid Salt Water.” *Current Biology* 31 (4): 782-793.e3. https://doi.org/10.1016/j.cub.2020.11.051.

Holsboer, Florian, and Marcus Ising. 2008. “Central CRH System in Depression and Anxiety — Evidence from Clinical Studies with CRH1 Receptor Antagonists.” *European Journal of Pharmacology*, Stress Hormone Actions in Brain, in Health and Disease, vol. 583 (2): 350–57. https://doi.org/10.1016/j.ejphar.2007.12.032.

Howe, Kerstin, Matthew D. Clark, Carlos F. Torroja, et al. 2013. “The Zebrafish Reference Genome Sequence and Its Relationship to the Human Genome.” *Nature* 496 (7446): 498–503. https://doi.org/10.1038/nature12111.

Huang, Kuo-Hua, Misha B. Ahrens, Timothy W. Dunn, and Florian Engert. 2013. “Spinal Projection Neurons Control Turning Behaviors in Zebrafish.” *Current Biology* 23 (16): 1566–73. https://doi.org/10.1016/j.cub.2013.06.044.

Jacobs, Elina A. K., and Soojin Ryu. 2023. “Larval Zebrafish as a Model for Studying Individual Variability in Translational Neuroscience Research.” *Frontiers in Behavioral Neuroscience* 17 (June). https://doi.org/10.3389/fnbeh.2023.1143391.

Kalisch, Raffael, Dewleen G. Baker, Ulrike Basten, et al. 2017. “The Resilience Framework as a Strategy to Combat Stress-Related Disorders.” *Nature Human Behaviour* 1 (11): 784–90. https://doi.org/10.1038/s41562-017-0200-8.

Kermen, Florence, Luis M. Franco, Cameron Wyatt, and Emre Yaksi. 2013. “Neural Circuits Mediating Olfactory-Driven Behavior in Fish.” *Frontiers in Neural Circuits* 7. https://doi.org/10.3389/fncir.2013.00062.

Krishnan, Vaishnav, Ming-Hu Han, Danielle L. Graham, et al. 2007. “Molecular Adaptations Underlying Susceptibility and Resistance to Social Defeat in Brain Reward Regions.” *Cell* 131 (2): 391–404. https://doi.org/10.1016/j.cell.2007.09.018.

Lister, J. A., C. P. Robertson, T. Lepage, S. L. Johnson, and D. W. Raible. 1999. “Nacre Encodes a Zebrafish Microphthalmia-Related Protein That Regulates Neural-Crest-Derived Pigment Cell Fate.” *Development (Cambridge, England)* 126 (17): 3757–67. https://doi.org/10.1242/dev.126.17.3757.

Liu, Katharine S, and Joseph R Fetcho. 1999. “Laser Ablations Reveal Functional Relationships of Segmental Hindbrain Neurons in Zebrafish.” *Neuron* 23 (2): 325–35. https://doi.org/10.1016/s0896-6273(00)80783-7.

Lowekamp, Bradley Christopher, David T. Chen, Luis Ibanez, and Daniel Blezek. 2013. “The Design of SimpleITK.” *Frontiers in Neuroinformatics* 7 (December). https://doi.org/10.3389/fninf.2013.00045.

Lupien, Sonia J., Bruce S. McEwen, Megan R. Gunnar, and Christine Heim. 2009. “Effects of Stress throughout the Lifespan on the Brain, Behaviour and Cognition.” *Nature Reviews Neuroscience* 10 (6): 434–45. https://doi.org/10.1038/nrn2639.

Lupinsky, Derek, Md Taufiq Nasseef, Carine Parent, et al. 2025. “Resting-State fMRI Reveals Altered Functional Connectivity Associated with Resilience and Susceptibility to Chronic Social Defeat Stress in Mouse Brain.” *Molecular Psychiatry* 30 (7): 2943–54. https://doi.org/10.1038/s41380-025-02897-2.

Mathis, Alexander, Pranav Mamidanna, Kevin M. Cury, et al. 2018. “DeepLabCut: Markerless Pose Estimation of User-Defined Body Parts with Deep Learning.” *Nature Neuroscience* 21 (9): 1281–89. https://doi.org/10.1038/s41593-018-0209-y.

McEwen, Bruce S. 2007. “Physiology and Neurobiology of Stress and Adaptation: Central Role of the Brain.” *Physiological Reviews* 87 (3): 873–904. https://doi.org/10.1152/physrev.00041.2006.

Mu, Yu, Davis V. Bennett, Mikail Rubinov, et al. 2019. “Glia Accumulate Evidence That Actions Are Futile and Suppress Unsuccessful Behavior.” *Cell* 178 (1): 27-43.e19. https://doi.org/10.1016/j.cell.2019.05.050.

Mu, Yu, Xiao-quan Li, Bo Zhang, and Jiu-lin Du. 2012. “Visual Input Modulates Audiomotor Function via Hypothalamic Dopaminergic Neurons through a Cooperative Mechanism.” *Neuron* 75 (4): 688–99. https://doi.org/10.1016/j.neuron.2012.05.035.

Orts-Del’Immagine, Adeline, Mahalakshmi Dhanasekar, François-Xavier Lejeune, Julian Roussel, and Claire Wyart. 2022. “A Norepinephrine-Dependent Glial Calcium Wave Travels in the Spinal Cord upon Acoustovestibular Stimuli.” *Glia* 70 (3): 491–507. https://doi.org/10.1002/glia.24118.

Randlett, Owen, Caroline L Wee, Eva A Naumann, et al. 2015. “Whole-Brain Activity Mapping onto a Zebrafish Brain Atlas.” *Nature Methods* 12 (11): 1039–46. https://doi.org/10.1038/nmeth.3581.

Sapienza, Julianna K., and Ann S. Masten. 2011. “Understanding and Promoting Resilience in Children and Youth.” *Current Opinion in Psychiatry* 24 (4): 267. https://doi.org/10.1097/YCO.0b013e32834776a8.

Southwick, Steven M., George A. Bonanno, Ann S. Masten, Catherine Panter-Brick, and Rachel Yehuda. 2014. “Resilience Definitions, Theory, and Challenges: Interdisciplinary Perspectives.” *European Journal of Psychotraumatology* 5 (October): 10.3402/ejpt.v5.25338. https://doi.org/10.3402/ejpt.v5.25338.

Swaminathan, Amrutha, Michael Gliksberg, Savani Anbalagan, Noa Wigoda, and Gil Levkowitz. 2023. “Stress Resilience Is Established during Development and Is Regulated by Complement Factors.” *Cell Reports* 42 (1): 111973. https://doi.org/10.1016/j.celrep.2022.111973.

Szente, László, Manó Aliczki, Gyula Y. Balla, et al. 2025. “Pre-Trauma Cognitive Traits Predict Fear Generalization and Associated Prefrontal Functioning in a Longitudinal Rodent Model.” *Neuropsychopharmacology*, November 4, 1–14. https://doi.org/10.1038/s41386-025-02263-4.

Terstege, Dylan J., Isabella M. Durante, and Jonathan R. Epp. 2022. “Brain-Wide Neuronal Activation and Functional Connectivity Are Modulated by Prior Exposure to Repetitive Learning Episodes.” *Frontiers in Behavioral Neuroscience* 16 (September). https://doi.org/10.3389/fnbeh.2022.907707.

Tudorache, Christian, Anique ter Braake, Mara Tromp, Hans Slabbekoorn, and Marcel J. M. Schaaf. 2015. “Behavioral and Physiological Indicators of Stress Coping Styles in Larval Zebrafish.” *Stress* 18 (1): 121–28. https://doi.org/10.3109/10253890.2014.989205.

Vom Berg-Maurer, Colette M., Chintan A. Trivedi, Johann H. Bollmann, Rodrigo J. De Marco, and Soojin Ryu. 2016. “The Severity of Acute Stress Is Represented by Increased Synchronous Activity and Recruitment of Hypothalamic CRH Neurons.” *The Journal of Neuroscience* 36 (11): 3350–62. https://doi.org/10.1523/JNEUROSCI.3390-15.2016.

Wee, Caroline Lei, Erin Yue Song, Robert Evan Johnson, et al. 2019. “A Bidirectional Network for Appetite Control in Larval Zebrafish.” *eLife* 8 (October): e43775. https://doi.org/10.7554/eLife.43775.

Willmore, Lindsay, Courtney Cameron, John Yang, Ilana B. Witten, and Annegret L. Falkner. 2022. “Behavioural and Dopaminergic Signatures of Resilience.” *Nature* 611 (7934): 124–32. https://doi.org/10.1038/s41586-022-05328-2.

Yeh, Chen-Min, Mario Glöck, and Soojin Ryu. 2013. “An Optimized Whole-Body Cortisol Quantification Method for Assessing Stress Levels in Larval Zebrafish.” *PLoS ONE* 8 (11): e79406. https://doi.org/10.1371/journal.pone.0079406.